

STELLINGEN

behorende bij het proefschrift

A CALCULATIONAL STUDY ON NEUTRON KINETICS AND THERMODYNAMICS OF A GASEOUS CORE FISSION REACTOR

1. De door Thubert en Kopp gegeven vierde-orde benadering voor het scheidend vermogen van een klassieke bundelvormer geeft een waarde voor dit scheidend vermogen, die ongeveer 20 % te groot is. Een zesde-orde benadering, volgens hetzelfde criterium, geeft een waarde voor het scheidend vermogen die binnen 2,5 % overeenkomt met het "werkelijke" scheidend vermogen van een klassieke bundelvormer.

Thubert, D. & Kopp, L. (1986), "Measurement accuracy and resolving power of high resolution passive methods", *Proc. EUSIPCO-86 Signal Processing III: Theory and Applications*, 1037 - 1040.

2. De bewering van Schwarz, dat de geïsoleerde hoofdlus van een "dirty beam" ongeschikt is als "clean beam", is niet van toepassing bij het gebruik van de "CLEAN" procedure bij het verwerken van passieve "towed-array" sonar data.

Schwarz, U.J. (1978), "Mathematical-statistical description of the iterative beam removing technique (method CLEAN)", *Astron. Astroph.*, Vol. 65, 345 - 356.

3. Uit de analogie tussen klassieke mechanica en geometrische optica enerzijds en quantummechanica en -scalaire- golfoptica anderzijds volgt dat de breedte van het intensiteitsprofiel in focuspunten goed is af te schatten uit de hoekspreiding van de lichtstralen met behulp van onzekerheidsrelaties, analoog aan die van Heisenberg.

Gloge, D. & Marcuse, D. (1969), "Formal quantum theory of light rays", *J. Opt. Soc. Am.*, Vol. 59, No. 12, 1629 - 1631.

4. De axiale warmtetransport-effecten in zogenoemde "natural engines" kunnen goed worden beschreven met behulp van storingstheorie, op dezelfde wijze als in dit proefschrift wordt toegepast bij het berekenen van de aangroeisnelheid van dichtheidsoscillaties in een gaskernreactor.

Wheatley, J. & Cox, A. (1985), "Natural engines", *Physics Today*, Vol. 38, 50 - 58.

5. De door Chapline *et. al.* gebruikte formule voor het berekenen van de benodigde magnetische veldsterkte in een "fission fragment rocket" is incorrect en levert een waarde voor de benodigde veldsterkte die ongeveer een factor 100 kleiner is dan wanneer deze zou zijn berekend met de correcte formule. De met de correcte formule berekende waarde voor de benodigde veldsterkte doet de haalbaarheid van het ontwerp teniet.

Chapline, G.F., Dickson, P.W. & Schitzler, B.G. (1988), "Fission fragment rockets - a potential breakthrough", *Proc. International Reactor Physics Conference*, September 18 - 22, Jackson Hole, Wyoming, USA.

6. Inhaber stelt "reverse Dutch auction" voor als methode voor het aanwijzen van bergplaatsen voor nucleair afval. Bij deze "veiling" verhoogt de centrale overheid telkens het bonusbedrag voor het beschikbaar stellen van een locatie voor een bergplaats, totdat een locale overheid voor het geboden bedrag een locatie ter beschikking stelt. Deze methode is echter niet geschikt voor toepassing in Nederland.

Inhaber, H. (1992), "How to solve nuclear siting problems", *Kerntechnik*, Vol. 57, No. 1, 69 - 71.

7. Een gaskernreactor biedt goede perspectieven als "actinide burner" en het verdient derhalve aanbeveling het onderzoek naar dit type reactoren te intensiveren.
8. Bij gaskernreactoren, zoals beschreven in dit proefschrift, bieden thermionische converters goede mogelijkheden voor het benutten van die fractie van de door kernsplijting geproduceerde energie, die in eerste instantie uit het reactorgas naar de wand wordt afgevoerd.
9. Het verdient aanbeveling om in de komende jaren de AOW-gerechtigde leeftijd te verhogen, teneinde een gezond evenwicht te behouden tussen het aantal AOW-premiebetalenden enerzijds en het aantal AOW-uitkeringsgerechtigden anderzijds.
10. Bij het bepalen of een potentieel ouderpaar al dan niet in aanmerking komt voor KI/IVF met donorzaad, dan wel voor adoptie, zouden dezelfde criteria met betrekking tot de geschiktheid als ouders moeten worden aangelegd.

Delft, 9 juni 1992

J.C. Kuijper

STELLINGEN

behorende bij het proefschrift

A CALCULATIONAL STUDY ON NEUTRON KINETICS AND THERMODYNAMICS OF A GASEOUS CORE FISSION REACTOR

1. De door Thubert en Kopp gegeven vierde-orde benadering voor het scheidend vermogen van een klassieke bundelvormer geeft een waarde voor dit scheidend vermogen, die ongeveer 20 % te groot is. Een zesde-orde benadering, volgens hetzelfde criterium, geeft een waarde voor het scheidend vermogen die binnen 2,5 % overeenkomt met het "werkelijke" scheidend vermogen van een klassieke bundelvormer.

Thubert, D. & Kopp, L. (1986), "Measurement accuracy and resolving power of high resolution passive methods", *Proc. EUSIPCO-86 Signal Processing III: Theory and Applications*, 1037 - 1040.

2. De bewering van Schwarz, dat de geïsoleerde hoofdlus van een "dirty beam" ongeschikt is als "clean beam", is niet van toepassing bij het gebruik van de "CLEAN" procedure bij het verwerken van passieve "towed-array" sonar data.

Schwarz, U.J. (1978), "Mathematical-statistical description of the iterative beam removing technique (method CLEAN)", *Astron. Astroph.*, Vol. 65, 345 - 356.

3. Uit de analogie tussen klassieke mechanica en geometrische optica enerzijds en quantummechanica en -scalair- golfoptica anderzijds volgt dat de breedte van het intensiteitsprofiel in focuspunten goed is af te schatten uit de hoekspreiding van de lichtstralen met behulp van onzekerheidsrelaties, analoog aan die van Heisenberg.

Gloge, D. & Marcuse, D. (1969), "Formal quantum theory of light rays", *J. Opt. Soc. Am.*, Vol. 59, No. 12, 1629 - 1631.

4. De axiale warmtetransport-effecten in zogenoemde "natural engines" kunnen goed worden beschreven met behulp van storingstheorie, op dezelfde wijze als in dit proefschrift wordt toegepast bij het berekenen van de aangroeiensnelheid van dichtheidsoscillaties in een gaskernreactor.

Wheatley, J. & Cox, A. (1985), "Natural engines", *Physics Today*, Vol. 38, 50 - 58.

5. De door Chapline *et. al.* gebruikte formule voor het berekenen van de benodigde magnetische veldsterkte in een "fission fragment rocket" is incorrect en levert een waarde voor de benodigde veldsterkte die ongeveer een factor 100 kleiner is dan wanneer deze zou zijn berekend met de correcte formule. De met de correcte formule berekende waarde voor de benodigde veldsterkte doet de haalbaarheid van het ontwerp teniet.

Chapline, G.F., Dickson, P.W. & Schitzler, B.G. (1988), "Fission fragment rockets - a potential breakthrough", *Proc. International Reactor Physics Conference*, September 18 - 22, Jackson Hole, Wyoming, USA.

6. Inhaber stelt "reverse Dutch auction" voor als methode voor het aanwijzen van bergplaatsen voor nucleair afval. Bij deze "veiling" verhoogt de centrale overheid telkens het bonusbedrag voor het beschikbaar stellen van een locatie voor een bergplaats, totdat een lokale overheid voor het geboden bedrag een locatie ter beschikking stelt. Deze methode is echter niet geschikt voor toepassing in Nederland.

Inhaber, H. (1992), "How to solve nuclear siting problems", *Kerntechnik*, Vol. 57, No. 1, 69 - 71.

7. Een gaskernreactor biedt goede perspectieven als "actinide burner" en het verdient derhalve aanbeveling het onderzoek naar dit type reactoren te intensiveren.
8. Bij gaskernreactoren, zoals beschreven in dit proefschrift, bieden thermionische converters goede mogelijkheden voor het benutten van die fractie van de door kernsplijting geproduceerde energie, die in eerste instantie uit het reactorgas naar de wand wordt afgevoerd.
9. Het verdient aanbeveling om in de komende jaren de AOW-gerechtigde leeftijd te verhogen, teneinde een gezond evenwicht te behouden tussen het aantal AOW-premiebetalenden enerzijds en het aantal AOW-uitkeringsgerechtigden anderzijds.
10. Bij het bepalen of een potentieel ouderpaar al dan niet in aanmerking komt voor KI/IVF met donorzaad, dan wel voor adoptie, zouden dezelfde criteria met betrekking tot de geschiktheid als ouders moeten worden aangelegd.

Delft, 9 juni 1992

J.C. Kuijper

TR diss
2067

550921
3172749
TR diss 2067

**A CALCULATIONAL STUDY ON
NEUTRON KINETICS AND THERMODYNAMICS OF
A GASEOUS CORE FISSION REACTOR**

J.C. KUIJPER



Interfacultair Reactor Instituut

Technische Universiteit Delft / Delft University of Technology

June 1992

Cover: Partially cut-away view of a -conceptual- gaseous core fission reactor with magneto-inductive energy extraction (by Jaap Hagenaar, 1992).

Copyright © 1992 by J.C. Kuijper.

CIP-GEGEVENS KONINKLIJKE BIBLIOTHEEK, DEN HAAG

Kuijper, James Cristian

A calculational study on neutron kinetics and thermodynamics of a gaseous core fission reactor / James Cristian Kuijper; [ill. van de auteur]. - Delft: Interfacultair Reactor Instituut van de Technische Universiteit Delft. - Ill. Proefschrift Technische Universiteit Delft. - Met lit. opg. - Met een samenvatting in het Nederlands.

ISBN 90-73861-06-3

NUGI 812

Trefw.: gaskernreactoren / neutronendynamica / thermodynamica.

**A CALCULATIONAL STUDY ON
NEUTRON KINETICS AND THERMODYNAMICS OF
A GASEOUS CORE FISSION REACTOR**

PROEFSCHRIFT

TER VERKRIJGING VAN DE GRAAD VAN DOCTOR AAN DE
TECHNISCHE UNIVERSITEIT DELFT, OP GEZAG VAN DE RECTOR
MAGNIFICUS, PROF. DRS. P.A. SCHENCK, IN HET OPENBAAR TE
VERDEDIGEN TEN OVERSTAAN VAN EEN COMMISSIE DOOR HET
COLLEGE VAN DEKANEN DAARTOE AANGEWEEZEN,
OP 9 JUNI 1992 TE 16.00 UUR

door

JAMES CRISTIAN KUIJPER

geboren te Hengelo (Ov.),
natuurkundig ingenieur

Dit proefschrift is goedgekeurd door de promotor:

Prof. Dr. Ir. H. van Dam

Toegevoegd promotor:

Dr. Ir. J.E. Hoogenboom

(plasma fission) reactor concept was 6500 K, which implies a sufficient degree of ionization for good conductivity of the plasma. Thanks to this conductivity it is possible to convert the thermal energy of the fissioning gas directly into electricity through interaction of the expanding plasma with a magnetic field. The authors state that "the estimated operating conditions look extreme but not impossible".

One of the major problems of such a proposal -and in fact of every high temperature GCFR- is the corrosive interaction between the fissioning gas and the surrounding container wall at the prevailing wall temperature of, say, 3500 K (in the design of Colgate and Aamodt). The solution of this problem was always sought in low working temperatures and/or a cold, hydrodynamically stable gas blanket between fissioning gas and surrounding vessel wall [Tho79]. A new principle was introduced by Kistemaker [Kis78a] with his proposal of using a reactor vessel that is in thermodynamic equilibrium with the gas and this idea was the starting point of the Dutch activities in GCFR research.

The central idea of the GCFR research in the Netherlands, which started in 1974 [Kis78a, Nie78], is a GCFR, consisting of a mixture of uranium and carbon fluorides in chemical and thermodynamical equilibrium with the surrounding graphite vessel wall. Carbon (graphite) seems to be a good wall material from the chemical, mechanical and reactor physical point of view as well: high sublimation point (4100 K), largest heat conductivity of all high temperature materials, high tensile strength and, last but not least, good neutron reflector/moderator properties [Dud76, Mas76]. The approach was shown to be feasible on the basis of an extensive study, carried out at the FOM-Institute for Atomic and Molecular Physics, Amsterdam, the Netherlands, of thermodynamic equilibria inside a graphite container with a ternary uranium-carbon-fluorine gas mixture over a broad range of temperatures (1000 to 4000 K) and pressures (0.01 to 100 bar) [Nie78, Kis78b]. The equilibrium gas mixture under the prevailing pressure conditions in a GCFR consists of approx. 70 % (molar) UF_4 and 30 % CF_4 at a wall temperature in the range of 2000 to 4000 K. This result was an incentive for further analysis in a broad area with emphasis on the heat transport from the fissioning gas to the vessel wall [Ker78] and neutronic aspects of a GCFR and led to a conceptual design for a GCFR with magneto-inductive electricity production [Kis78a].

Since 1978, the Dutch GCFR activities have been aimed towards gaining a more thorough understanding of subjects related to this conceptual design. A survey of these activities, up to the end of 1987, is given by Klein [Kle87]. The thermodynamical properties of the uranium-carbon-fluorine (UCF) gas and its interaction with the graphite wall were studied using better basic (chemical and thermodynamical) data and improved computer codes, leading to more accurate information on the (pressure- and temperature-dependent) equilibrium molecular composition of the gas (dissociation, ionization, recombination) and its Equation of State [Kis86, Kis87, Kle87, Boe89b, Boe90a, Boe90b].

A more fundamental study on neutron transport and heat transport, which are strongly related in a GCFR, was carried out for stationary, one-dimensional GCFR geometries by Uleman [Ule82] and van Dam and Hoogenboom [Dam83] at the Interuniversitair Reactor Instituut (nowadays Interfacultair Reactor Instituut), Delft, the Netherlands. They utilized the photon diffusion model of Kerkdijk and Kistemaker [Ker78] for the description of the heat transport from the fissioning gas (temperature at the centre approximately 10,000 K) to the wall (temperature at the interface approximately 2000 K), resulting in a very steep temperature gradient,



The research described in this thesis was performed within the Department of Reactor Physics of the Interfacultair Reactor Instituut, Delft University of Technology, Mekelweg 15, NL-2629 JB Delft, the Netherlands.

Financial support was obtained from the Netherlands Technology Foundation (Stichting Technische Wetenschappen), P.O. Box 3021, NL-3502 GA Utrecht, the Netherlands, under contract nos. FAM 66.0933, DRI 99.1662 and DRI 90.1662.

CONTENTS

Chapter 1	INTRODUCTION	1
1.1	General	1
1.2	Overview of the work	3
Chapter 2	NEUTRON STATICS	7
2.1	Introduction and overview	7
2.2	Static neutron transport models	10
2.2.1	Chord model	11
2.2.2	Multi-compartment models	12
2.3	Spherical GCFR	17
2.4	Cylindrical GCFR	33
Chapter 3	NEUTRON KINETICS	45
3.1	Point kinetics for solid piston GCFR model	45
3.2	Point kinetics for two-compartment GCFR model	47
3.3	Accuracy of point kinetics models	50
Chapter 4	REACTOR GAS THERMODYNAMICS	53
4.1	Reactor gas composition	53
4.2	Reactor gas properties	54
4.3	Heat transport	57
4.4	Modelium	61
4.5	Finite and infinitesimal thermodynamic cycles	63
Chapter 5	SOLID PISTON GCFR MODEL	67
5.1	Introduction	67
5.2	Model description	68
5.3	Finite cycle calculation results	70
5.4	Comparison with infinitesimal cycle	78
5.5	Conclusions	81
Chapter 6	GAS DYNAMICS	83
6.1	Introduction	83
6.2	Acoustic model	84
6.2.1	Adiabatic case	86
6.2.2	Non-adiabatic case	87
6.3	Two-compartment model	88
6.3.1	Adiabatic case	91
6.3.2	Non-adiabatic case	92
6.4	Energy extraction	94
Chapter 7	TWO-COMPARTMENT GCFR MODEL	97
7.1	Introduction	97
7.2	Model description	97
7.3	Constant flat flux approximation	102
7.4	Combined model calculation results	103

7.5	Influence of energy extraction	107
7.6	Conclusions	107
EPILOGUE		109
Appendix A	MULTI-COMPARTMENT NEUTRON TRANSPORT	111
Appendix B	NEUTRON GROUP CONSTANTS	115
Appendix C	TEMPERATURE INFLUENCE	121
Appendix D	TWO-COMPARTMENT NEUTRON KINETICS	125
REFERENCES		131
SUMMARY		137
SAMENVATTING		141
ACKNOWLEDGEMENT		145
CURRICULUM VITAE		147

Chapter 1

INTRODUCTION

1.1 General

In present day fission reactors for electricity production the conversion of nuclear energy into electricity is performed in an indirect way through the use of old-fashioned steam cycles. For a physicist it is rather frustrating to see how the very high kinetic energy of the electrically charged fission products is first degraded into -relatively- low temperature heat and eventually into mechanical energy and electricity. It is, however, not straightforward to obtain a more direct conversion: the fission products are strongly ionized and have high kinetic energy, but their directions of movement are uncorrelated. This implies that we have an inherently random movement of charges that should be converted into directed movement in as few stages as possible.

In the early 1950s it was realized that the use of gaseous nuclear fuel in a so-called Gaseous Core Fission Reactor (from now on to be designated as GCFR) offers the possibility of -very- high working temperatures and -therefore- more direct and efficient ways of converting nuclear fission energy into electricity (e.g. magneto-inductive (MI) or magneto-hydrodynamic (MHD) conversion [Col57, Tho79, Kle87]). Gaseous fuel also offers the advantages of its impossibility to melt (trivial but important!), homogeneous burn-up of the fuel and the possibility of continuous reprocessing [Kis78a, Kle87].

In the 1960s a considerable effort was spent in the United States (by the National Aeronautics and Space Administration) on the development of a nuclear reactor with a gaseous core, mainly for space propulsion applications [Sch75]. An excellent review of this development is given by Thom [Tho79], who also gives a complete survey of the potentialities of the GCFR, such as nuclear pumped lasers, and also commercial electricity production. In the same period also in the USSR research was carried out on the same subjects [Iye77], but in the beginning of the 1970s in both countries the programs were stopped, as the respective governments lost interest [Tho79]. However, a group at the University of Florida, led by Diaz, continued their work on GCFRs, still with a main interest in space applications [Dia80a, Dia80b, Dug88a, Dug88b, Pan88, Wel88, Pan91a, Pan91b]. At present also GCFR research is performed at other institutions, such as the Lawrence Livermore National Laboratory in the USA [Ale91]. Also there is classified research on this subject in both the USA and the USSR.

The GCFR offers the possibility of more efficient ways of converting nuclear energy into electricity, partly by increasing the temperatures of conventional indirect conversion processes and partly by introducing direct conversion processes. Direct conversion is possible because a high level of ionization can be realized in a fissioning gas (plasma core reactor), which opens the way to magneto-hydrodynamic (MHD) or magneto-inductive (MI) conversion of heat into electricity. A GCFR concept utilizing the latter, based on the use of highly enriched gaseous uranium in a heavy water reflected cylindrical configuration, was proposed by Colgate and Aamodt [Col57]. The design temperature of the fissioning gas in this

(plasma fission) reactor concept was 6500 K, which implies a sufficient degree of ionization for good conductivity of the plasma. Thanks to this conductivity it is possible to convert the thermal energy of the fissioning gas directly into electricity through interaction of the expanding plasma with a magnetic field. The authors state that "the estimated operating conditions look extreme but not impossible".

One of the major problems of such a proposal -and in fact of every high temperature GCFR- is the corrosive interaction between the fissioning gas and the surrounding container wall at the prevailing wall temperature of, say, 3500 K (in the design of Colgate and Aamodt). The solution of this problem was always sought in low working temperatures and/or a cold, hydrodynamically stable gas blanket between fissioning gas and surrounding vessel wall [Tho79]. A new principle was introduced by Kistemaker [Kis78a] with his proposal of using a reactor vessel that is in thermodynamic equilibrium with the gas and this idea was the starting point of the Dutch activities in GCFR research.

The central idea of the GCFR research in the Netherlands, which started in 1974 [Kis78a, Nie78], is a GCFR, consisting of a mixture of uranium and carbon fluorides in chemical and thermodynamical equilibrium with the surrounding graphite vessel wall. Carbon (graphite) seems to be a good wall material from the chemical, mechanical and reactor physical point of view as well: high sublimation point (4100 K), largest heat conductivity of all high temperature materials, high tensile strength and, last but not least, good neutron reflector/moderator properties [Dud76, Mas76]. The approach was shown to be feasible on the basis of an extensive study, carried out at the FOM-Institute for Atomic and Molecular Physics, Amsterdam, the Netherlands, of thermodynamic equilibria inside a graphite container with a ternary uranium-carbon-fluorine gas mixture over a broad range of temperatures (1000 to 4000 K) and pressures (0.01 to 100 bar) [Nie78, Kis78b]. The equilibrium gas mixture under the prevailing pressure conditions in a GCFR consists of approx. 70 % (molar) UF_4 and 30 % CF_4 at a wall temperature in the range of 2000 to 4000 K. This result was an incentive for further analysis in a broad area with emphasis on the heat transport from the fissioning gas to the vessel wall [Ker78] and neutronic aspects of a GCFR and led to a conceptual design for a GCFR with magneto-inductive electricity production [Kis78a].

Since 1978, the Dutch GCFR activities have been aimed towards gaining a more thorough understanding of subjects related to this conceptual design. A survey of these activities, up to the end of 1987, is given by Klein [Kle87]. The thermodynamical properties of the uranium-carbon-fluorine (UCF) gas and its interaction with the graphite wall were studied using better basic (chemical and thermodynamical) data and improved computer codes, leading to more accurate information on the (pressure- and temperature-dependent) equilibrium molecular composition of the gas (dissociation, ionization, recombination) and its Equation of State [Kis86, Kis87, Kle87, Boe89b, Boe90a, Boe90b].

A more fundamental study on neutron transport and heat transport, which are strongly related in a GCFR, was carried out for stationary, one-dimensional GCFR geometries by Uleman [Ule82] and van Dam and Hoogenboom [Dam83] at the Interuniversitair Reactor Instituut (nowadays Interfacultair Reactor Instituut), Delft, the Netherlands. They utilized the photon diffusion model of Kerkdijk and Kistemaker [Ker78] for the description of the heat transport from the fissioning gas (temperature at the centre approximately 10,000 K) to the wall (temperature at the interface approximately 2000 K), resulting in a very steep temperature gradient,

and therefore an increased density, of the gas near the wall: a dense gas layer protecting the wall [Kis78a]! Later the model was extended by taking into account the thermal conductivity and the dissociation/recombination behaviour of the gas [Kle87, Kis89, Hoo91, Boe91b], leading to somewhat different temperature profiles in the gas of the (stationary) GCFR.

Parallel to these investigations of the properties of a stationary GCFR a further step was taken towards a GCFR with magneto-inductive energy extraction. An initial investigation was carried out by van Dam [Dam88] of the neutron kinetics of a GCFR with oscillating fuel gas density. However, study of such a GCFR with magneto-inductive energy extraction calls for a calculational model combining (at least) neutron kinetics, reactor gas thermodynamics and gas dynamics. This thesis describes the development of such a combined model.

1.2 Overview of the work

The aim of our work was to investigate the static and dynamic properties of a GCFR with oscillating (moving) fuel gas. A simplified schematic diagram of such a GCFR, similar to the concept of Kistemaker [Kis78a], is shown in Figure 1.1. It consists of a graphite cylinder of, say, 2 m diameter and 10 m length, filled with a mixture of uranium and carbon fluorides (UCF) at high temperature in ionized state, in chemical and thermodynamical equilibrium with the graphite cylinder wall [Kis78a, Kis86, Kle87]. The cylindrical gas space is divided into an active "core" region, surrounded by an effective (thick) neutron reflector, and a so-called "expander" region, surrounded by a much less effective (thinner or with neutron poison) neutron reflector. In operation, part of the fuel gas oscillates back and forth between core and expander region. With homogeneously distributed fuel over core and expander, the reactor is approximately critical. As the fuel gas is ionized, and therefore electrically conductive, it can interact with the magnetic field, generated by a current in the coil surrounding the expander. In this way plasma dynamic compression of the fuel from the expander into the core (rendering the reactor supercritical) and magneto-inductive energy extraction are possible [Dam89, Kui89a, Kui89b, Kui90; Kui91a, Kui91b]. The investigation requires the study of neutron statics, neutron kinetics, reactor gas thermodynamics and gas dynamics, resulting in a combined calculational model, containing these aspects. In order to achieve this we followed a step-by-step approach.

In order to obtain more information of the influence of the density (distribution) of the fuel gas on the reactor physical properties of "our" GCFR, we performed static neutronics calculations for one-dimensional (sphere) and two-dimensional (finite cylinder) GCFR configurations. The results of these calculations, viz. the multiplication factor k_{eff} and other reactor physical quantities, are presented in Chapter 2. We found that the dependence of these quantities on the fuel gas density (distribution) can be adequately described by means of relatively simple functions, obtained from so-called "multi-compartment" GCFR models. These functions can be conveniently used in the neutron kinetics part (Chapter 3) of the combined GCFR models (Chapters 5 and 7).

In Chapter 3 we give a description of the neutron kinetics part of the combined GCFR models to be presented in Chapters 5 and 7. As mentioned, the necessary reactor physical quantities for these point kinetics models [Dud76] were

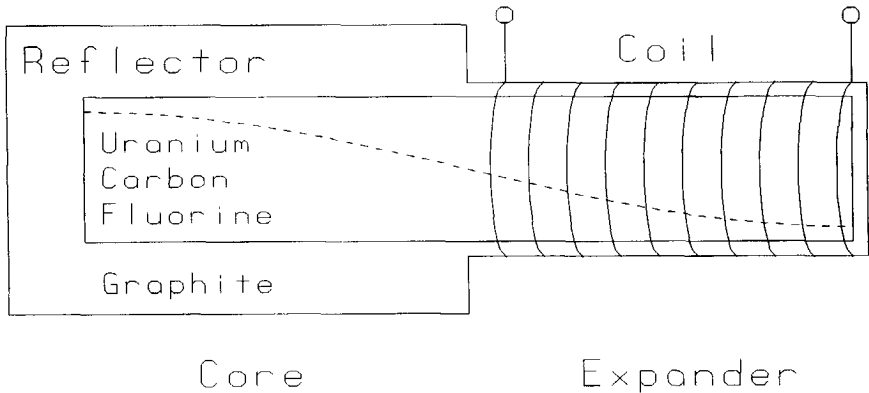


Figure 1.1 Conceptual design of a gaseous core fission reactor with magneto-inductive energy extraction (possible axial fuel gas density distribution is indicated by the dotted line).

obtained, in the form of relatively simple functions, from the static neutronic calculations described in Chapter 2.

Chapter 4 describes the thermodynamical properties of the UCF reactor gas. We introduce a model gas -"Modelium"- with an artificial, analytical Equation of State (EOS), as an approximation for the "real" EOS of the UCF gas. We also introduce the concept of a so-called "infinitesimal Otto cycle", by means of which the efficiency of a finite thermodynamic cycle can be estimated, with reasonable accuracy, from the thermodynamical properties of the working gas only [Kui91a].

In Chapter 5 we present the combined model of a so-called "solid piston" GCFR [Kui89a, Kui89b, Kui90, Kui91a, Dam89]. In this model the interaction of the ionized fuel gas with the magnetic field generated by the coil is represented by a solid piston, which controls the total volume occupied by the fuel gas. The extracted energy is then modelled as the mechanical work performed by the gas on the piston. The model combines neutron kinetics and thermodynamics. However, no gas dynamics is taken into account, as the fuel gas, occupying the space controlled by the piston, is assumed to be massless and homogeneous.

Chapter 6 introduces another element of the final combined model: gas dynamics. As the length of the cylindrical gas space is large compared with its diameter (about 5:1) we considered one-dimensional gas dynamics in axial direction only. In order to facilitate the use of gas dynamics in our combined "two-compartment" model (Chapter 7) we developed a so-called "Two-Compartment gas dynamics" Model ("TCM") for the GCFR [Kui91b]. The parameters governing this model are chosen such that the natural oscillation frequency and the momentary total kinetic energy of the gas in the system are the same as in the "Fundamental Acoustic Mode" ("FAM") description of the (one-dimensional) gas dynamics of the system.

A model for a GCFR with autonomously oscillating fuel gas, combining neutron kinetics, thermodynamics and gas dynamics is presented in Chapter 7. The

conditions will be shown under which, for the case of absence of an energy extraction mechanism, increasing density oscillations in the fuel gas will occur. These increasing oscillations are desired when the kinetic energy of the moving, ionized gas is to be directly extracted by magneto-inductive (MI) or magneto-hydrodynamic (MHD) means.

Chapter 2

NEUTRON STATICS

2.1 Introduction and overview

As a first step in the development of our combined GCFR models (to be presented in Chapters 5 and 7), and in order to obtain a better understanding of the influence of the density and the density distribution of the fuel gas on the reactor physical properties of our GCFR, we performed numerical static neutronics calculations for one-dimensional (sphere) and two-dimensional (finite cylinder) GCFR configurations. We investigated the influence of the fuel gas density and density distribution on the multiplication factor k_{eff} , the neutron generation time Λ and the core fission power fraction f_p (finite cylinder only). Information on this influence is necessary in the neutron (point-) kinetics part of our combined GCFR models, to be introduced in Chapter 3.

Other important quantities for these neutron kinetics models are the effective delayed neutron fractions $\beta_{eff,i}$ (delayed neutron precursor time group i ; $i = 1, \dots, 6$). Delayed neutrons are fission neutrons which are not released immediately as the fission process occurs, but which are emitted somewhat later by fission products, the so-called delayed neutron precursors [Bel70, Dud76, Mas76].

The most convenient way of representing the information concerning ρ , Λ and f_p mentioned above for use in the neutron kinetics models, is in the form of relatively simple fit functions, describing the behaviour of k_{eff} , Λ and f_p with the fuel gas density and density distribution, which can be fitted to the results obtained from the numerical static calculations mentioned above. In Section 2.2 we present two formal static neutron transport GCFR models: the so-called "chord model" (Section 2.2.1) and "multi-compartment models" (Section 2.2.2 and Appendix A). These formal models were developed and studied in order to obtain a better understanding of the numerical results and to provide for the functional form of the fit functions mentioned above.

In Section 2.3 we present the results of the (one-dimensional) static neutron transport and neutron diffusion calculations for a spherical GCFR. We investigated the influence of the (average) fuel gas density and the radial fuel gas density distribution on k_{eff} and Λ . We also compare the results, obtained from fine group neutron transport (187 or 123 energy groups), broad group neutron transport (4 energy groups) and broad group neutron diffusion calculations (4 energy groups). On the basis of this comparison, and in view of the explorative nature of our calculations, we decided to use 4-group neutron diffusion calculations for the investigation of the two-dimensional (finite cylinder) GCFR configuration, as this requires far less computing resources than -more accurate- fine group neutron transport calculations.

Results of two-dimensional static neutron diffusion calculations for a cylindrical GCFR are presented in Section 2.4. Like in the one-dimensional case, we investigated the influence of the (average) fuel gas density on k_{eff} , Λ and also on f_p . The emphasis of these calculations was, however, on the investigation of the influence of the axial fuel gas density distribution, in view of the use of this

information in the combined GCFR model calculations (Chapter 7).

An overview of the performed static neutronic calculations, for which we used a well-established set of computer codes, is shown in Figure 2.1. Data libraries are indicated by rounded boxes, codes by rectangular boxes. Basic nuclear data for our calculations, such as neutron point cross sections and resonance parameters, were taken from the ENDF/B-IV [Gar75] and JEF-1 [NEA85] data files. In Figure 2.1 three calculational routes are indicated.

The first route (indicated by "A"), starting from the ENDF/B-IV data file, was taken by Dveer [Dve88], using the codes XLACS [NEA73a] (data extraction from ENDF/B-IV; generation of a so-called AMPX-Master library, containing microscopic neutron cross section data in 123 fine energy groups and resolved resonance parameters), XSDRN [NEA73b] (one-dimensional fine group neutron transport calculation; generation of an ANISN-format library by condensing into 4 broad energy groups), ANISN(E) [NEA79] (one-dimensional broad group neutron transport calculations) and DAC-I [NEA72] (calculation of neutron generation time Λ and effective delayed neutron fractions $\beta_{eff,i}$). We used the ANISN-format library made by Dveer [Dve88] for our first one-dimensional broad group neutron transport calculations by ANISN(E) and DAC-I (Section 2.3; also see [Kui88]). From these calculations we obtained information on the influence of the fuel gas density on k_{eff} and Λ , which was used, in the form of fit functions, in the neutron kinetics part of the "solid piston" GCFR model (Chapter 5). From these calculations we also obtained information on $\beta_{eff,i}$.

For the second route (indicated by "B"), starting from the more up-to-date JEF-1 data file, we used a set of more modern codes, viz. the NSLINK system [Lee91] (data extraction from JEF-1; creation of an AMPX-Master library, containing neutron cross section data in 187 fine energy groups and resolved resonance parameters), NITAWL [NEA87] (creation of a 187-group AMPX-Working library) and XSDRNPM [NEA87] (improved version of XSDRN; one-dimensional fine group neutron transport calculations; creation of an AMPX-Weighted library by condensing into 4 broad energy groups). From the AMPX-Weighted library (which has the same format as an AMPX-Working library) we generated libraries for subsequent calculations. We used CONTAC [NEA78] for the generation of an ANISN-format library, to be used for one-dimensional broad group neutron transport calculations with ANISN [NEA86a] and DAC-I [NEA72] (Section 2.3), and OCTAGN [NEA78] for the generation of a CITATION-format library, to be used for one-dimensional (Section 2.3) and two-dimensional (Section 2.4) broad group neutron diffusion calculations with CITATION [NEA89]. From these two-dimensional calculations (route "B") we obtained information on the influence of the (average) fuel gas density and the (axial) fuel gas density distribution in the cylindrical GCFR on k_{eff} , Λ and f_p , and also information on $\beta_{eff,i}$, which was used, in the form of fit functions, in the neutron kinetics part of the "two-compartment" GCFR model (Chapter 7).

A third calculational route (indicated by "C") starts from the AMPX-Master library of route "A". This route uses COMET [NEA78] to convert the format of the AMPX-Master library, so that it can be used by the more modern codes also used in route "B". We followed this route in order to be able to make a good comparison between results, obtained with older data and older codes (route "A"), and those, obtained with more up-to-date data and more modern codes (route "B"; see Section 2.3). In Appendix B more information can be found on the generation of

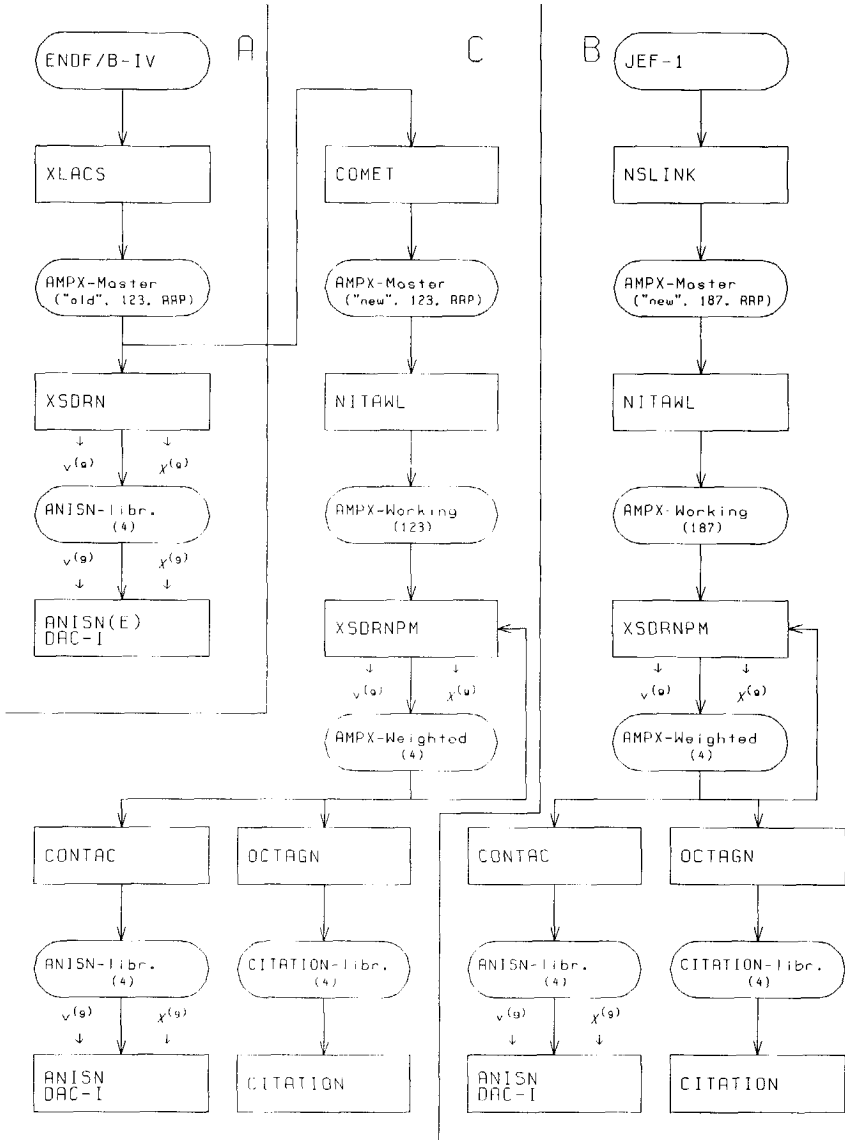


Figure 2.1 Overview of static neutronic calculations (rounded box indicates data library; number of groups and presence of Resolved Resonance Parameters ("RRP") indicated between brackets; rectangular box indicates code).

the fine group and broad group constants (neutron group cross sections, neutron group velocities, fission spectra, etc.).

2.2 Static neutron transport models

In general, the behaviour of neutrons in any medium (thus also in a fission reactor) can be described by the time-dependent Boltzmann transport equation [Wil66, Bel70, Dud76, Mas76], which for neutrons takes a linear form as neutrons do not interact with each other. In fact, the linear Boltzmann (or neutron transport) equation is a balance equation for the position- (\underline{r}), time- (t), energy- (E) and direction- ($\underline{\Omega}$) dependent neutron angular density $n(\underline{r}, E, \underline{\Omega}, t)$ (underline " $\underline{\quad}$ " denotes vector). The neutron angular flux density $\psi(\underline{r}, E, \underline{\Omega}, t)$ (from now on denoted by "angular flux") is then defined by:

$$\psi(\underline{r}, E, \underline{\Omega}, t) = v(E)n(\underline{r}, E, \underline{\Omega}, t) \quad (2.2.1)$$

(neutron velocity $v(E)$). The (total) neutron flux (density) $\varphi(\underline{r}, E, t)$ and the neutron current (density) $\underline{j}(\underline{r}, E, t)$ are defined by:

$$\varphi(\underline{r}, E, t) = \int_{4\pi} \psi(\underline{r}, E, \underline{\Omega}, t) d\Omega \quad (2.2.2)$$

and:

$$\underline{j}(\underline{r}, E, t) = \int_{4\pi} \underline{\Omega} \psi(\underline{r}, E, \underline{\Omega}, t) d\Omega \quad (2.2.3)$$

respectively (infinitesimal solid angle $d\Omega$ around direction $\underline{\Omega}$).

In order to obtain a time-independent form of the transport equation, the multiplication factor k_{eff} is introduced [Wil66, Bel70, Dud76, Mas76], which is the factor by which the (fission) neutron production term in the transport equation has to be reduced in order to bring it into balance with the neutron loss through absorption and leakage:

$$k_{eff} \equiv \frac{\text{fission neutron production rate}}{\text{neutron absorption rate} + \text{neutron leakage rate}} \quad (2.2.4)$$

Without external neutron sources (fission neutron sources only) the time-independent neutron transport equation is an eigenvalue equation with (fundamental, i.e. algebraically largest) eigenvalue k_{eff} and corresponding eigenfunction $\psi(\underline{r}, E, \underline{\Omega})$. The other possible solutions for the eigenfunction (the so-called "higher order" modes) correspond to algebraically smaller values of the eigenvalue. For a system in the fundamental neutronic mode the reactivity ρ is now defined by [Dud76]:

$$\rho \equiv \frac{k_{eff} - 1}{k_{eff}} \quad (2.2.5)$$

The codes XSDRNPM [NEA87] and ANISN [NEA86a] solve the time-independent neutron transport equation numerically, rendering the fundamental eigenfunction ψ (angular flux) and the corresponding eigenvalue k_{eff} for one-dimensional (sphere, infinite cylinder, infinite slab) geometries. The code CITATION [NEA89] solves, for one-, two- and three-dimensional geometries, the time-independent neutron

diffusion equation. This is an approximation to the neutron transport equation, in which it is assumed that the neutron current density \underline{j} is proportional to the spatial gradient of the total neutron flux φ [Bel70, Dud76, Mas76]. CITATION renders the fundamental eigenfunction φ (total flux) and the corresponding eigenvalue k_{eff} .

Formal static neutron transport GCFR models were developed and studied in order to obtain a better understanding of the numerical -static- neutron transport and neutron diffusion calculation results. Using these models, the functional relationships between several reactor physical properties can be derived. Also these models render -relatively simple- functions, describing the behaviour of k_{eff} , Λ and f_p with the fuel gas -average- density and density distribution, which can be fitted to the results obtained from the numerical static calculations. So, they can be conveniently used in the neutron (point-) kinetic models to be introduced in Chapter 3.

2.2.1 Chord model

The first formal GCFR static neutron transport model to be discussed here is the so-called "chord model", which was developed by Uleman [Ule82], van Dam and Hoogenboom [Dam83]. It is based on the assumptions that: (I) a fission neutron, born in the fuel gas core, travels directly (large mean free path for fast neutrons; Appendix B) to the surrounding reflector, and has a probability w_{TRC} (Thermalize and Return to Core) to return to the core as a thermal neutron; (II) a thermal neutron travels through the core in a straight line (i.e. very large scattering mean free path for thermal neutrons; see Appendix B) and is either absorbed in the gas (low, but nonzero absorption probability; each absorbed neutron produces η fission neutrons) or reaches again the reflector; (III) a thermal neutron entering the reflector, will be returned to the core gas with a probability, equal to the reflector albedo β . Under these assumptions the multiplication factor k_{eff} is given by [Dam83]:

$$k_{eff} = \eta w_{TRC} \frac{1 - \exp(-\Sigma_a \bar{a})}{1 - \beta \exp(-\Sigma_a \bar{a})} \quad (2.2.6)$$

For the GCFR core, which is a convex body, the mean chord length \bar{a} is given by [Cas53]:

$$\bar{a} = \frac{4V}{S} \quad (2.2.7)$$

(V = core volume; S = core surface). The reflector albedo β is close to unity, and $\Sigma_a \bar{a}$ is small compared to unity [Dam83], so Eq. (2.2.6) can be approximated by:

$$k_{eff} = \eta w_{TRC} \frac{1}{1 + \frac{1 - \beta}{\Sigma_a \bar{a}}} \quad (2.2.8)$$

In order to take into account the effect of variation of the gas density on the multiplication factor, the macroscopic absorption cross section Σ_a (which -by definition- is given at the reference gas density) may be multiplied by a dimensionless factor n_{rel} (the relative density). Applying Eq. (2.2.5) we then obtain for the reactivity (assuming that η , w_{TRC} and β are independent of n_{rel}):

$$\rho = \left[1 - \frac{1}{\eta w_{TRC}} \right] - \left[\frac{1 - \beta}{\eta w_{TRC} \Sigma_a \bar{a}} \right] (n_{rel})^{-1} \quad (2.2.9)$$

If we rewrite Eq. (2.2.9) in terms of the density, relative to the density at which the reactor is critical (n_{RCD} : Relative to the Critical Density), we obtain:

$$\rho = \left[1 - \frac{1}{\eta w_{TRC}} \right] - \left[1 - \frac{1}{\eta w_{TRC}} \right] (n_{RCD})^{-1} \quad (2.2.10)$$

Eq. (2.2.10) predicts that, in this case, both coefficients of the fitted function have the same value, which we -to a good approximation- indeed found to be the case in our numerical calculations (see Section 2.3).

Generally, the reflector albedo β depends upon material properties and dimensions. For a spherical GCFR, with core radius R_{core} , infinitely thick reflector, reflector (thermal) neutron diffusion coefficient D_{refl} and reflector (thermal) neutron diffusion length L_{refl} , we find [Gla60]:

$$\beta = \frac{1 - 2 D_{refl} \left[\frac{1}{L_{refl}} + \frac{1}{R_{core}} \right]}{1 + 2 D_{refl} \left[\frac{1}{L_{refl}} + \frac{1}{R_{core}} \right]} \quad (2.2.11)$$

For the graphite reflector of our spherical GCFR ($D_{refl} \approx 0.61$ cm, $L_{refl} \approx 76$ cm, $R_{core} = 100$ cm [Kui88]) we can approximate:

$$1 - \beta = 4 D_{refl} \left[\frac{1}{L_{refl}} + \frac{1}{R_{core}} \right] \quad (2.2.12)$$

We then find for the critical density of the fuel gas of a spherical GCFR (relative to the reference gas density, at which Σ_a is defined):

$$n_{rel,crit} = \frac{3 D_{refl}}{\Sigma_a (\eta w_{TRC} - 1)} \times \left[\frac{1}{R_{core} L_{refl}} + \frac{1}{(R_{core})^2} \right] \quad (2.2.13)$$

In Section 2.3 we will show that the variation of the critical density with the core radius indeed can be described by a function of the form of Eq. (2.2.13).

2.2.2 Multi-compartment models

In order to be able to derive fit functions for other reactor physical quantities than the reactivity only, we developed another type of formal (GCFR) static neutron transport models: the so-called "multi-compartment" models. Like in nodal methods (see eg. Ronen [Ron86]), in these models the reactor is considered to consist of M compartments (index $m = 1, \dots, M$; compartment volumes V_m), in each of which the volume-averaged neutron flux $\varphi_m^{(g)}$ (G energy groups; index $g = 1, \dots, G$; neutron group velocities $v^{(g)}$) is to be calculated. These volume-averaged neutron fluxes in all compartments and all energy groups are represented by the so-called flux vector $\underline{\varphi}$ with $(M \cdot G)$ elements. As is indicated in Appendix A, the multi-compartment representation for the time-independent neutron transport equation reads:

$$\underline{H} \cdot \underline{\psi} \equiv \left(\lambda \underline{F} \cdot \underline{V}_M + \underline{E} \cdot \underline{V}_M \right) \cdot \underline{\psi} = \underline{0} \quad (2.2.14)$$

(\underline{H} = system matrix ($(M \cdot G) \times (M \cdot G)$ elements); \underline{F} = fission matrix; \underline{E} = absorption-, scatter- and transport matrix, \underline{V}_M = volume matrix; \underline{H} , \underline{F} and \underline{E} are dependent upon the relative densities ($n_{rel,m}$) in the compartments and also on the scattering and absorption cross sections ($\Sigma_{s,m}^{(g \rightarrow g')}$ and $\Sigma_{a,m}^{(g)}$), the number of fission neutrons per absorbed neutron ($\eta_m^{(g)}$) and the compartment-to-compartment transport coefficients ($K_{m \rightarrow m'}^{(g)}$); see Appendix A). Eq. (2.2.14) is an eigenvalue equation with fundamental eigenvector $\underline{\psi}$ and corresponding eigenvalue λ ($= 1 / k_{eff} = 1 - \rho$). In Appendix A a more extensive description is presented of the multi-compartment models, including the (approximated) formal expressions for the reactivity ρ (or the multiplication factor k_{eff}), the neutron generation time Λ and the fission power fraction $f_{p,m}$ in compartment m . These expressions are rational algebraic functions of the relative densities $n_{rel,m}$. We will now discuss some examples of formal multi-compartment models.

• One-group/one-compartment model for spherical GCFR

The first model, which was also discussed by van Dam [Dam88], is the case of the one-group/one-compartment (also bare) spherical reactor. For this case we have: $M = 1$ (one compartment: the core; compartment index m omitted further on); $G = 1$ (one energy group; group index g omitted further on); $w_{1 \rightarrow 1}^{(1)} = 1$ (all fission neutrons appear in the core; $w_{1 \rightarrow 1}^{(1)}$ is the fraction of the fission neutrons, born in the core, which re-appear in the core in group 1; see Appendix A); $F = \eta \Sigma_a n_{rel}$ (1×1 matrix; group and compartment indices omitted); $E = -\Sigma_a n_{rel} - K_0$ (also 1×1 matrix; $K_{1 \rightarrow 0} = K_0$). We then find for the inverse of the multiplication factor:

$$\lambda = \frac{1}{\eta} + \frac{K_0}{\eta \Sigma_a} (n_{rel})^{-1} \quad (2.2.15)$$

The (relative) critical density is then given by:

$$n_{rel,crit} = \frac{K_0}{(\eta - 1) \Sigma_a} \quad (2.2.16)$$

And the reactivity can then be given in terms of the density, relative to the critical density ($n_{RCD} \equiv n_{rel} / n_{rel,crit}$):

$$\rho \equiv 1 - \lambda = \left[1 - \frac{1}{\eta} \right] - \left[1 - \frac{1}{\eta} \right] \cdot (n_{RCD})^{-1} \quad (2.2.17)$$

This is the same expression as we found with the "chord model" (Section 2.2.1; Eq. (2.2.10)), except that there is no factor w_{TRC} , as we only take into account thermal neutrons. The neutron generation time for this one-group/one-compartment model is given by:

$$\Lambda = \frac{(\eta - 1)}{\eta K_0 v} (n_{RCD})^{-1} \quad (2.2.18)$$

(neutron velocity v). Van Dam [Dam88] added an extra term to account for the time spent in the reflector. In the next model we will see this extra term appearing automatically, as we will take the reflector into account explicitly.

• Two-group/two-compartment model for spherical GCFR

The second multi-compartment model to be discussed is a two-group/two-compartment ($G = 2$: fast ($g = 1$) and thermal ($g = 2$); $M = 2$: core ($m = 1$) and (surrounding) reflector ($m = 2$)) model of a spherical GCFR. For this case we assume: $\Sigma_{s,2}^{(g)} = 0$ (no absorption in the reflector; only in the core), $\Sigma_{s,2}^{(1 \rightarrow 2)} > 0$ (no scattering in the core; only downscattering in the reflector), $n_{rel,1} = n_{rel}$ (variable relative density in the core), $n_{rel,2} = 1$ (fixed density in reflector), $\eta_1^{(2)} = \eta$ (no fission in reflector; only fission in core by thermal neutrons), $w_{1 \rightarrow 1}^{(1)} = \chi^{(1)} = 1$ (only fast fission neutrons, appearing in the core) and $K_{1 \rightarrow 0}^{(g)} = 0$ (core completely surrounded by reflector). For this case the \underline{F} and \underline{L} are 4×4 matrices. Following the procedure outlined in Appendix A, we obtain expressions for λ and Λ of the following forms (denoted by "new fit functions" in Section 2.3):

$$\lambda = C_{\lambda,1} n_{rel} + C_{\lambda,2} + C_{\lambda,3} (n_{rel})^{-1} \quad (2.2.19)$$

$$\Lambda = C_{\Lambda,1} n_{rel} + C_{\Lambda,2} + C_{\Lambda,3} (n_{rel})^{-1} \quad (2.2.20)$$

The first term (in both equations) becomes 0 if no absorption of fast neutrons in the core is taken into account (so if $\Sigma_{s,1}^{(1)} = 0$), and in that case the equations simplify to the forms used earlier [Dam88, Kui88] (hence denoted by "old fit functions" in Section 2.3; also see "chord model" and "one-group/one-compartment model"). If we now assume further that: $v^{(1)} \rightarrow \infty$ (very high velocity of fast neutrons), $\Sigma_{s,1}^{(1)} = 0$ (no absorption of fast neutrons in the core) and $K_{2 \rightarrow 0}^{(1)} = 0$ (no leakage of fast neutrons), we obtain:

$$\lambda = \frac{1}{\eta} \left[1 + \frac{K_{2 \rightarrow 0}^{(2)}}{K_{2 \rightarrow 1}^{(2)}} \right] + \frac{K_{2 \rightarrow 0}^{(2)} K_{1 \rightarrow 2}^{(2)}}{\eta \Sigma_{s,1}^{(2)} K_{2 \rightarrow 1}^{(2)}} \cdot (n_{rel})^{-1} \quad (2.2.21)$$

From this we can calculate the reactivity in terms of the density, relative to the critical density:

$$\rho = \left[1 - \frac{K_{2 \rightarrow 1}^{(2)} + K_{2 \rightarrow 0}^{(2)}}{\eta K_{2 \rightarrow 1}^{(2)}} \right] - \left[1 - \frac{K_{2 \rightarrow 1}^{(2)} + K_{2 \rightarrow 0}^{(2)}}{\eta K_{2 \rightarrow 1}^{(2)}} \right] \cdot (n_{RCD})^{-1} \quad (2.2.22)$$

This expression corresponds to Eq. (2.2.10), as the factor $K_{2 \rightarrow 1}^{(2)} \cdot [K_{2 \rightarrow 1}^{(2)} + K_{2 \rightarrow 0}^{(2)}]^{-1}$ actually is the fraction of the fission neutrons that thermalizes in the reflector and returns to the core (w_{TRC}), because we assumed no fast leakage and no absorption in the reflector. The expression for the neutron generation time reads:

$$\Lambda = \frac{1}{\eta K_{2 \rightarrow 1}^{(2)} v^{(2)}} + \frac{1}{K_{2 \rightarrow 0}^{(2)} v^{(2)}} \left[1 + \frac{V_1}{V_2} \left[1 + \frac{K_{2 \rightarrow 0}^{(2)}}{K_{2 \rightarrow 1}^{(2)}} \right] \right] \left[1 - \frac{K_{2 \rightarrow 1}^{(2)} + K_{2 \rightarrow 0}^{(2)}}{\eta K_{2 \rightarrow 1}^{(2)}} \right] \cdot (n_{RCD})^{-1} \quad (2.2.23)$$

The first term represents the time that a neutron remains in the reflector after

thermalization, before returning to the core.

● **One-and-a-half-group/two-compartment model for spherical GCFR 1**

In the next model we attempt to reduce the size of the matrices, while retaining the effect of fast and thermal neutrons, in the so-called one-and-a-half-group/two-compartment model. The geometry ($M = 2$) is the same as in the previous model, but only the thermal flux is explicitly calculated (so $G = 1$; group index g omitted further on). The effect of the thermalization of fast (fission) neutrons in the reflector is taken into account by means of $w_{m' \rightarrow m}$: $w_{1 \rightarrow 2} = 1$ (fission neutrons, born in the core ($m' = 1$), re-appear in the reflector ($m = 2$) as thermal neutrons; no fast leakage; group index omitted). Now \underline{F} and \underline{E} are 2×2 matrices, which are much more manageable than 4×4 ones. If we then also keep the remaining assumptions the same as in the previous model, the expressions for λ , ρ and Λ turn out to be the same as the expressions found with the two-group/two-compartment model (Eqs. (2.2.21), (2.2.22) and (2.2.23), respectively; group index omitted). So the one-and-a-half group approximation seems to be sufficient. In Section 2.3 we will show that functions of the form(s) given above (one-group/one-compartment-, two-group/two-compartment- and one-and-a-half-group/two-compartment models; "old" and "new" functions) indeed describe quite well the dependence of reactivity and neutron generation time on the fuel gas density of the (one-dimensional, spherical) GCFR.

● **One-and-a-half-group/two-compartment model for spherical GCFR 2**

The next model is also a one-and-a-half-group/two-compartment model, but this time we want to describe the effect of fuel (gas) distribution between a core centre and a (surrounding) core edge (between core centre and reflector [Kui88]). This time the flux in the reflector is not explicitly calculated (there is no explicit reflector compartment in the model), but the effect of thermalization of (fission) neutrons in the reflector and their (possible) return to the core is again taken into account by means of $w_{m' \rightarrow m}$ (group index omitted): $w_{m' \rightarrow 2} = w_{TRC}$ (fission neutrons, born in the core centre ($m' = 1$) or core edge ($m' = 2$) have a probability w_{TRC} of thermalizing in the reflector and returning to the adjacent core edge). The leakage of thermal neutrons from the reflector is simulated by leakage from the core edge ($K_{2 \rightarrow 0} > 0$; group index omitted). The -relative- densities in core centre and core edge are related to the average core relative density n_{rel} by:

$$n_{rel,1} = n_{rel} \left(1 - \varepsilon \frac{V_2}{V_1} \right) \quad (2.2.24)$$

$$n_{rel,2} = n_{rel} (1 + \varepsilon) \quad (2.2.25)$$

The variable ε describes the density distribution over core centre and core edge ($\varepsilon = 0$ means equal densities in core centre and core edge). In we furthermore assume that $w_{TRC} = 1$ (i.e. all fission neutron are thermalized in the reflector and return to the core edge first; no fast leakage and no absorption in the reflector) and that there exists a strong coupling between core centre and core edge (i.e. $(K_{1 \rightarrow 2} V_1) / (K_{2 \rightarrow 0} V_2) = K_{2 \rightarrow 1} / K_{2 \rightarrow 0} \equiv z^{-1} \rightarrow \infty$), then we can approximate the rational algebraic expressions for λ and Λ by a Taylor expansion to first order in z from

$z = 0$, obtaining for the reactivity:

$$\rho = \left[1 - \frac{1}{\eta} \right] - \frac{K_{2 \rightarrow 0} V_2}{\eta \Sigma_a (V_1 + V_2)} (n_{rel})^{-1} - \frac{K_{2 \rightarrow 0}}{\eta K_{2 \rightarrow 1}} \left[\frac{\varepsilon V_2 - V_1}{V_1 + V_2} \right]^2 \quad (2.2.26)$$

(n_{rel} = average relative core fuel gas density). The fuel distribution variable ε can attain values between -1 (all fuel in core centre) and V_1 / V_2 (all fuel in core edge). From Eq. (2.2.26) we can expect that the reactivity increases as fuel is moved from core centre to core edge. A maximum reactivity is expected for $\varepsilon = V_1 / V_2$, which is also the maximum value for ε . In Section 2.3 we will show that the reactivity change, caused by fuel redistribution between core centre and core edge indeed can be described adequately by a function of the form of Eq. (2.2.26). Following the same procedure, we can obtain a function, describing the dependence of the neutron generation time Λ on ε (and n_{rel}). Like Eq. (2.2.26), this function contains terms with ε and ε^2 . However, the function does not contain a term describing the time spent in the reflector after thermalization, before returning to the core. This can be expected, as in this model (like in the one-group/one-compartment model) the reflector is not taken into account as an actual compartment. For an extremely strong coupling between core edge and core centre (i.e. $z \rightarrow 0$) the influence of fuel distribution disappears and the expressions for ρ (Eq. (2.2.26)) and Λ from this model simplify to the corresponding one-group/one-compartment expressions (Eqs. (2.2.17) and (2.2.18)).

● One-and-a-half-group/two-compartment model for cylindrical GCFR

The final formal model to be presented is a one-and-a-half-group/two-compartment ($G = 1$; group index omitted further on; $M = 2$) model of a cylindrical GCFR (like the one in Figure 1.1) consisting of a "core"- ($m = 1$) and an "expander"-compartment ($m = 2$) of equal volume ($V_1 = V_2 = 0.5 V_{tot}$; so $K_{1 \rightarrow 2} = K_{2 \rightarrow 1}$; see Appendix A), both containing fuel gas. In this case we are interested in the reactivity ρ , the neutron generation time Λ and the core fission power fraction f_p ($= f_{p,1}$) as function of the average relative density (core plus expander) n_{rel} and the fuel gas distribution over core and expander. The latter is described by the density distribution variable ε . The relative densities in core and expander are given by:

$$n_{rel,1} = n_{rel} (1 + \varepsilon) \quad (2.2.27)$$

$$n_{rel,2} = n_{rel} (1 - \varepsilon) \quad (2.2.28)$$

As core and expander have equal volumes, the density distribution variable can attain values between -1 and 1 ($\varepsilon = 0$ denotes a flat density distribution). Like in the previous model, there is no explicit reflector compartment in this model, but like in that model the effect of thermalization of fast (fission) neutrons in the reflector and their (possible) return to the core or expander is taken into account by means of -again- $w_{m' \rightarrow m}$: it is assumed that all fission neutrons, born in the core or expander, thermalize in the reflector and return to either the core or the reflector (no fast leakage and no absorption in the reflector):

$$w_{m' \rightarrow m} = \delta_{m',m} w_{TRS} + (1 - \delta_{m',m}) (1 - w_{TRS}) \quad (2.2.29)$$

w_{TRS} is the probability that a fission neutron, born in core or expander, after Thermalization in the reflector, Returns to the Same compartment (as a thermal neutron). The leakage (of thermal neutrons) from the reflector is simulated by leakage from the core ($K_{1 \rightarrow 0} > 0$) and expander ($K_{2 \rightarrow 0} > 0$). In general, the (thermal) leakage from the reflector part surrounding the core is different from the leakage from the reflector part surrounding the expander. This is taken into account by means of a factor δ_{th} , assuming:

$$V_2 K_{2 \rightarrow 0} = V_1 K_{1 \rightarrow 0} (1 + \delta_{th}) \quad (2.2.30)$$

For $\delta_{th} = 0$ we have the so-called symmetric case. For $\delta_{th} > 0$ we have the situation of a core, surrounded by an efficient reflector, and an expander, surrounded by a less effective reflector. Following the procedure outlined in Appendix A, using the algebraic manipulation code package REDUCE [Ray87], we were able to obtain expressions for ρ , Λ and f_p in terms of rational functions of the average relative density n_{rel} and the density distribution variable ϵ . These expressions, however, are much too complicated to be useful as fit functions for the numerical calculation results to be presented in Section 2.4. Therefore, we approximated these expressions in a way, similar to the way we followed for the previous model, obtaining expressions of the following forms:

$$\rho = C_{\rho,1} n_{rel} + C_{\rho,2} + C_{\rho,3} (n_{rel})^{-1} + C_{\rho,4} \epsilon^2 + C_{\rho,5} \epsilon \quad (2.2.31)$$

$$\Lambda = C_{\Lambda,1} n_{rel} + C_{\Lambda,2} + C_{\Lambda,3} (n_{rel})^{-1} + C_{\Lambda,4} \epsilon^2 + C_{\Lambda,5} \epsilon \quad (2.2.32)$$

$$f_p = C_{f,1} + C_{f,2} (n_{rel})^{-1} + C_{f,3} (n_{rel})^{-2} + C_{f,4} \epsilon^2 + C_{f,5} \epsilon \quad (2.2.33)$$

Note that we have added a term to the expression for the neutron generation time to take into account the time spent in the reflector after thermalization, before returning to the core ($C_{\Lambda,2}$). In the expressions for both ρ and Λ we also added a term describing fast absorption in the fuel gas (like in the two-group/two-compartment model for the spherical GCFR) ($C_{\rho,1}$ and $C_{\Lambda,1}$). For the so-called symmetric case ($\delta_{th} = 0$) we can expect that, for symmetry reasons: $C_{\rho,5} = 0$, $C_{\Lambda,5} = 0$, $C_{f,1} = 0.5$ and $C_{f,2} = C_{f,3} = C_{f,4} = 0$. In Section 2.4 we will show that the results from two-dimensional numerical calculations (concerning the influence of the average fuel gas density and the axial fuel gas density distribution in a cylindrical GCFR) can be described quite well by functions of the form of Eqs. (2.2.31), (2.2.32) and (2.2.33).

2.3 Spherical GCFR

Using the computer codes XSDRNPM [NEA87], ANISN(E) [NEA79], ANISN [NEA86a], DAC-I [NEA72] and CITATION [NEA89], we performed one-dimensional numerical neutron transport and neutron diffusion calculations for a spherical GCFR, investigating the influence of several parameters on its static neutronic behaviour. As a central "point of reference" for these calculations we now introduce our "Reference Spherical GCFR" (from now on to be designated as RSG).

Figure 2.2 presents the characteristics of this reactor. The nuclide densities in the gas originate from an ANISN(E) critical density search calculation (for RSG geometry), using the ANISN-format neutron group cross section library of route "A" (see Figure 2.1), made by Dveer [Dve88, Kui88]. These nuclide densities are based on an enrichment of 50 % in ^{235}U and the molecular composition of UCF gas in thermodynamical and chemical equilibrium with a graphite wall at 2000 K, according to Klein [Kle87]: 20.5 % CF_4 , 25.0 % UF_4 , 54.5 % UF_5 (also see Section 4.1). The same nuclide composition of the fuel gas was assumed for all our static neutronic calculations (also for our two-dimensional calculations: Section 2.4). The total mass of the fuel gas in the RSG is then $m_{\text{tot}} = 40 \text{ kg}$ (i.e. a mass density of $\rho_m = 9.55 \cdot 10^{-3} \text{ g cm}^{-3}$) and the total mass of the ^{235}U is $m_{25} = 13.4 \text{ kg}$. Also in all our calculations the nuclide density in the graphite reflector was chosen to be $8.55 \cdot 10^{22} \text{ cm}^{-3}$, which corresponds to 1.70 g cm^{-3} . This is based on the density of CS-312 graphite [UNI59] at a temperature of 1000 K [UIe82]. The bulk temperature of the graphite reflector was assumed to be 1000 K, because the high-temperature region (1000 - 2000 K) will be limited to a small layer near the gas core boundary (which is assumed to be at 2000 K), due to heat removal by reflector cooling [Dam83].

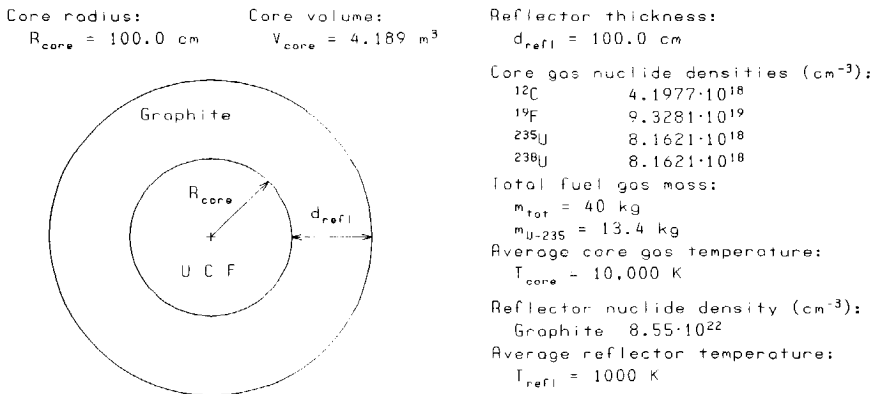


Figure 2.2 Reference Spherical GCFR ("RSG"): reference geometry for one-dimensional fine- and broad-group neutron transport and neutron diffusion calculations.

In the calculations presented in this section, the temperature of the -bulk of the- fuel gas in the core was assumed to be $T_{\text{core}} = 10,000 \text{ K}$. However, the temperatures of the fuel gas and the reflector influence the group cross sections in the core and the reflector, and therefore the reactor physical behaviour of the GCFR. More information on the influence of the temperature can be found in Appendix C.

The codes XSDRNPM [NEA87], ANISN [NEA86a] and ANISN(E) [NEA79] solve the Boltzmann transport equation numerically (rendering the fundamental eigenfunction ψ and corresponding eigenvalue for one-dimensional geometries (sphere, infinite cylinder, infinite slab; sphere in our calculations), assuming: (I) a

Table 2.1 Main parameters for fine group static neutron transport and cross section condensation calculations by XSDRNPM (routes "B" and "C").

General			
Calculation type	k_{eff} -calculation & cross section condensation to broad groups		
Geometry	Sphere (one-dimensional)		
Quadrature order	S_4		
Scattering Legendre order	P_3		
Left boundary condition	Reflective (centre of sphere)		
Right boundary condition	Vacuum (outer boundary)		
Number of zones	2		
Number of spatial intervals	84		
Overall convergence criterion	$1 \cdot 10^{-5} - 1 \cdot 10^{-4}$		
Point convergence criterion	$1 \cdot 10^{-4}$		
Nuclide composition	As in RSG		
Group condensation weighting option	Zone weighting		
Spatial structure			
Zone	1 (core)	2 (reflector)	
Spatial interval range	1 - 34	35 - 84	
Coordinate range (cm)	0.0 - 100.0	100.0 - 200.0	
Interval size (cm)	0.5 - 10.0	0.5 - 5.0	
Broad group structure			
Basic data	Energy range (eV)	Fine groups	Broad group index
JEF-1 (route "B") (LANL 187 fine groups)	$2.0 \cdot 10^7 - 1.11 \cdot 10^5$	1 - 49	1
	$1.11 \cdot 10^5 - 4.31 \cdot 10^3$	50 - 76	2
	$4.31 \cdot 10^3 - 2.38$	77 - 137	3
	$2.38 - 1 \cdot 10^{-5}$	138 - 187	4
ENDF/B-IV (route "C") (GAM-THERMOS 123 fine groups)	$14.9 \cdot 10^6 - 1.11 \cdot 10^5$	1 - 49	1
	$1.11 \cdot 10^5 - 4.31 \cdot 10^3$	50 - 62	2
	$4.31 \cdot 10^3 - 2.38$	63 - 92	3
	$2.38 - 5.0 \cdot 10^{-3}$	93 - 123	4

multi-group approach (i.e. using group cross sections and angular group fluxes; the angular group flux of an energy group is the angular flux integrated over that energy group [Mas76, Dud76]; (II) numerical discretization of the directional dependence, replacing integrals over the solid angle by a weighted sum over a finite number of directions (S_N -method [Bel70, Mas76, Dud76]; S_4 in our calculations), (III) a finite number of terms of the Legendre (P_l) expansion of the scattering cross section, necessary for the description of the scattering anisotropy

([Bel70, Mas76]; P_3 in our XSDRNPM calculations, P_1 in our ANISN(E) and ANISN calculations), and (IV) a spatial discretization (i.e. a finite number of spatial intervals). The main parameters for our one-dimensional neutron transport calculations can be found in Table 2.1 (123- and 187-group XSDRNPM) and Table 2.2 (4-group ANISN and ANISN(E)), respectively.

Table 2.2 Main parameters for broad group static neutron transport calculations by ANISN(E) (route "A") and ANISN (routes "B" and "C").

General			
Calculation type	k_{eff} -calculation, density search		
Geometry	Sphere		
Quadrature order	S_4		
Scattering Legendre order	P_1		
Left boundary condition	Reflective (centre of sphere)		
Right boundary condition	Vacuum (outer boundary)		
Number of zones	2 or 3 (see below)		
Number of spatial intervals	84		
Eigenvalue and upscatter convergence criterion	$5 \cdot 10^{-5} - 1 \cdot 10^{-4}$		
Point convergence criterion	$1 \cdot 10^{-4}$		
Core nuclide composition	As in RSG (relative density as specified)		
Reflector nuclide density (cm^{-3})	$8.55 \cdot 10^{22}$ (as in RSG)		
Spatial structure (RSG)			
Zone	1 (core)	2 (reflector)	
Spatial interval range	1 - 34	35 - 84	
Coordinate range (cm)	0.0 - 100.0	100.0 - 200.0	
Interval size (cm)	0.5 - 10.0	0.5 - 5.0	
Spatial structure (influence of radial fuel gas density distribution; route "A")			
Zone	1 (core centre)	2 (core edge)	3 (reflector)
Spatial interval range	1 - 29	30 - 34	35 - 84
Coordinate range (cm)	0.0 - 97.5	97.5 - 100.0	100.0 - 200.0
Interval size (cm)	0.5 - 10.0	0.5	0.5 - 5.0

The code CITATION [NEA89] solves the neutron diffusion equation numerically (rendering the fundamental eigenfunction ψ and the corresponding eigenvalue) for one-, two- and three-dimensional geometries (one-dimensional sphere in the calculations presented in this section), also assuming: (I) a multi-group approach (4 groups in our calculations) and (II) a spatial discretization. The main parameters for our one-dimensional neutron diffusion calculations by CITATION are listed in Table 2.3.

In Figure 2.3 the neutron spectrum (i.e. the spatially averaged neutron flux)

Table 2.3 Main parameters for one-dimensional broad group static neutron diffusion calculations by CITATION.

General		
Calculation type	k_{eff} -calculation, calculation of neutron generation time and effective delayed neutron fraction	
Geometry	Sphere	
Left boundary condition	Reflective (centre of sphere)	
Right boundary condition	Extrapolated (outer boundary)	
Number of zones	2	
Number of spatial intervals	110	
Flux convergence criterion	$1 \cdot 10^{-5}$	
Eigenvalue convergence criterion	$1 \cdot 10^{-6}$	
Total fission power (flux normalization) (MW_{th})	100.0	
Core nuclide composition	As in RSG (relative density as specified)	
Reflector nuclide density (cm^{-3})	$8.55 \cdot 10^{22}$ (as in RSG)	
Spatial structure		
Zone	1 (core)	2 (reflector)
Spatial interval range	1 - 50	51 - 110
Coordinate range (cm)	0.0 - 100.0	100.0 - 200.0

in core gas and reflector of the RSG is shown (187-group XSDRNPM calculation; route "B"; see Table 2.1). Clearly, the neutron spectrum in the core gas is much "harder" (higher average energy) than the spectrum in the reflector. This can be seen more quantitatively from the "fast flux-to-thermal flux-ratio" ("FTR"; energy boundary between fast and thermal neutrons set at 2.38 eV). In the core this ratio is $FTR(2.38 \text{ eV}) = 1.76$, whereas in the reflector this ratio is $FTR(2.38 \text{ eV}) = 0.187$. This behaviour can be explained by the fact that the source of high energy neutrons -fission- is located in the core, whereas the source of low energy neutrons -moderation- is located in the reflector. However, in both spectra still the fission spectrum part (high energies) and the thermal spectrum part (low energies) can be recognized easily.

A demonstration of the moderating and reflecting properties of the graphite reflector (in the RSG) is given in Figure 2.4 (187-group XSDRNPM calculation; route "B"; see Table 2.1). We see neutrons of high energies going from the core to the reflector and neutrons of low (thermal) energies going back into the core. However, at these low energies almost as many neutrons leak out of the reflector, as the (RSG) reflector is only 1.0 m, i.e. 1.3 thermal neutron diffusion lengths, thick. A temperature increase of the reflector also causes an increase of the average energy with which the neutrons return to the core (or leak out of the reflector).

The code XSDRNPM was also used to generate the 4-group neutron cross

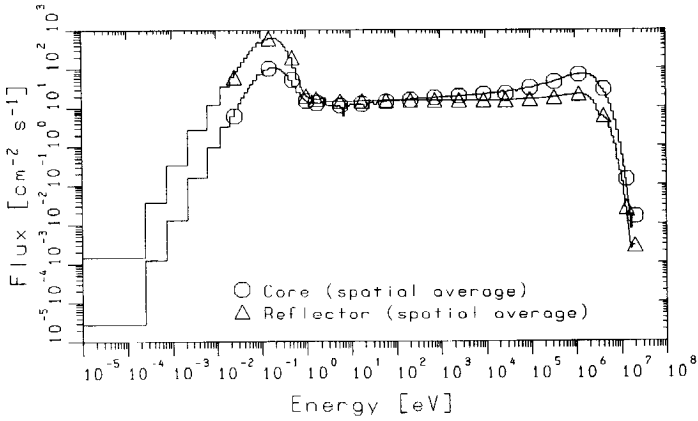


Figure 2.3 Neutron spectrum (neutron flux per unit lethargy) in core and reflector of the RSG (187-group neutron transport calculation by XSDRNPM, route "B").

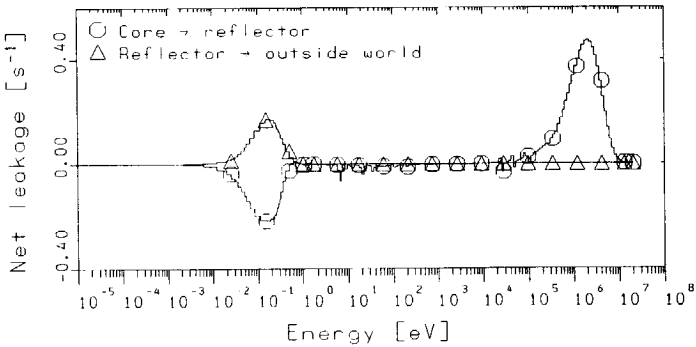


Figure 2.4 Reflecting and moderating properties of the graphite reflector in the RSG (net neutron leakage per unit lethargy; 187-group neutron transport calculation by XSRNPM, route "B").

section libraries (see Figure 2.1 and Table 2.1; routes "B" and "C"; also see Appendix B), necessary for subsequent broad group neutron transport and neutron diffusion calculations by ANISN and CITATION, respectively. In Figure 2.5 (A) we show, for the RSG, the four composite broad group fluxes from the 187 to 4 group cross section condensation calculation by XSDRNPM (route "B"; S_4P_3). Note that XSDRNPM normalizes the flux in such a way that the total fission neutron production rate is 1 s^{-1} . For all energy groups the neutron flux in the core part is almost spatially flat, which was expected in view of the large (total and absorption) mean free path of neutrons in the core gas (10 - 100 metres for neutron energies

above approximately 1 eV; see Appendix B). This mean free path is -much- larger than the dimensions of the gas space in the RSG, which means that criticality is based upon multiple reflections of neutrons by the graphite wall. This requires a high reflection coefficient (or albedo β ; e.g. see Eqs. (2.2.11) and (2.2.12)) of that wall. In the reflector part, the (broad) group 4 reflector peak is clearly visible. This peak is due to thermalization of neutrons with higher energies (groups 1, 2, 3) in the reflector.

For a comparison we also show the results of a 4-group neutron transport calculation (S_4P_1 ; route "B"; see Table 2.2) by ANISN (Figure 2.5 (B)) and a 4-group neutron diffusion calculation (route "B"; see Table 2.3) by CITATION (Figure 2.5 (C)). ANISN, like XSDRNPM, normalizes the flux in such a way that the total fission neutron production rate is 1 s^{-1} , whereas CITATION normalizes the flux in such a way that the total fission power has a preset value (100 MW in all our calculations). Note that, also for these broad group calculations, the neutron flux in the core is almost spatially flat for all groups, which was expected in view of the large (broad group) mean free path and diffusion length for neutrons in the core gas (see Appendix B, Table B.3). The flux profiles obtained from 187-group (S_4P_3) neutron transport calculation (XSDRNPM), the 4-group (S_4P_1) neutron transport calculation (ANISN) and the 4-group neutron diffusion calculation (CITATION) agree quite well. Only the group 1 flux (fast flux) in the core, as calculated by CITATION, is about 18 % lower, and is also more spatially flat, than is calculated by the transport codes.

We investigated the influence of the core radius R_{core} and the reflector thickness d_{refl} on the critical density of the spherical GCFR. We used the density search option of the code ANISN (route "C") to calculate the critical density $n_{RRS,crit}$ (i.e. the critical density, Relative to the RSG gas density) for various combinations of R_{core} and d_{refl} . We varied R_{core} and d_{refl} by "stretching" or "squeezing" zone 1 (core) and/or zone 2 (reflector), starting from the spatial structure used in the ANISN RSG calculations (Table 2.2), retaining the number of spatial intervals in each zone. The results of these calculations are shown in Figure 2.6. Note that a reduction of a factor of approximately 1.3 in critical density can be achieved by increasing the reflector thickness from 1 m to 2 m (due to less leakage of thermal neutrons through the reflector). Also an increase of R_{core} reduces the density, necessary for achieving criticality. E.g. changing R_{core} from 1 m to 2 m reduces the critical density by a factor of approximately 3.4. This can be explained from the fact that the mean chord length \bar{a} in the core increases proportionally with the core radius R_{core} , and a larger chord length results in a higher k_{eff} at the same density (Section 2.2.1: "chord model"; Eq. (2.2.8); constant η , β and w_{TRC} assumed). We attempted to fit two types of functions to these numerical $n_{RRS,crit}(R_{core})$ -data. The first function is the one we derived in Section 2.2.1 ("chord model"), viz. Eq. (2.2.13). The second one is a power function, also used earlier by Kuijper [Kui88]. The results of these fitting procedures are listed in Table 2.4 and the corresponding graphs of the fit functions are shown in Figure 2.6 as well. For each of the four curves the quantity Δ is also given, which is defined by:

$$\Delta \equiv \left[\frac{\sum_i (y_i - y(x_i))^2}{\sum_i (y_i - \bar{y})^2} \right]^{1/2} \quad (2.3.1)$$

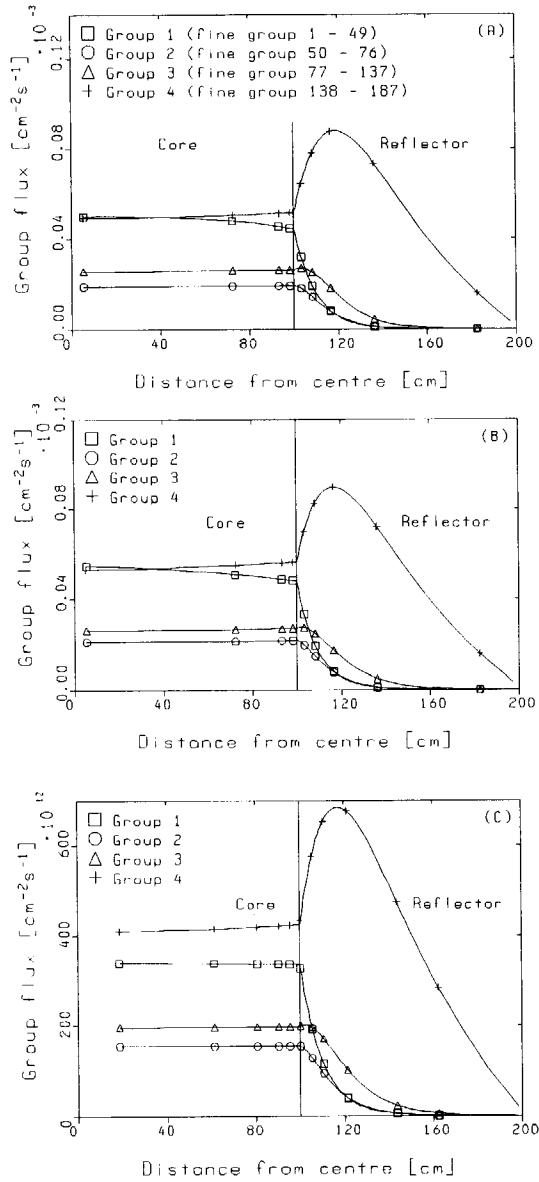


Figure 2.5 Comparison of broad group flux profiles in the RSG (route "B"), calculated by: (A) XSDRNPM (composite 4-group fluxes from 187→4 condensation), (B) ANISN and (C) CITATION.

Table 2.4 Influence of cores radius R_{core} and d_{refl} on the critical fuel gas density of the spherical GCFR.

d_{refl} (m)	Fit function for $n_{RRS,crit}(R_{core})$	Δ	Remarks
1.00	$0.841(66) \cdot R_{core}^{-2} + 0.116(57) \cdot R_{core}^{-1}$	0.026	Eq. (2.2.13)
	$0.945(25) \cdot R_{core}^{-1.788(57)}$	0.035	[Kui88]
2.00	$0.629(40) \cdot R_{core}^{-2} + 0.112(35) \cdot R_{core}^{-1}$	0.022	Eq. (2.2.13)
	$0.733(17) \cdot R_{core}^{-1.760(51)}$	0.032	[Kui88]

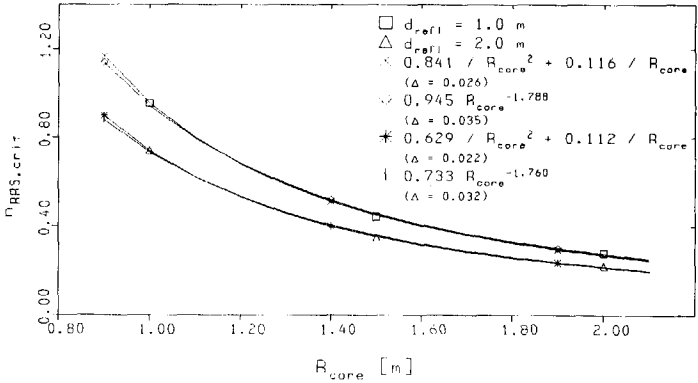


Figure 2.6 Influence of core radius R_{core} and reflector thickness d_{refl} on the critical fuel gas density $n_{RRS,crit}$ of a spherical GCFR.

(i = index of data point (x_i, y_i) ; y_i = value of dependent variable of data point i ($n_{RRS,crit}$ in this case); x_i = value of independent variable of data point i (R_{core} in this case); $y(x_i)$ = value of fit function at $x = x_i$; \bar{y} = average value of dependent variable of data points). The small values of Δ (compared to 1) indicate that both function types describe quite well the variation of the critical density with the core radius.

The main part of our calculations on the spherical GCFR concerned the influence of the core gas density on the reactivity ρ and the neutron generation time Λ of this reactor. We also calculated the effective delayed neutron fractions $\beta_{eff,i}$ (delayed neutron precursor time group i ; $i = 1, \dots, 6$; sum β_{eff}), using the codes DAC-I [NEA72] (neutron transport) and CITATION [NEA79] (neutron diffusion). As mentioned in Section 2.1, these quantities are important in the neutron (point-) kinetics models [Bel70, Dud76, Mas76] to be introduced in Chapter 3.

In order to calculate the neutron generation time Λ , the codes DAC-I and CITATION require an adjoint function, which is the (fundamental) eigenfunction of the adjoint transport or adjoint diffusion equation, respectively [Lew65, Bel70, Mas76]. The adjoint function for DAC-I is calculated by ANISN (routes "B" and "C") or ANISN(E) (route "A"). The adjoint function for CITATION is calculated by

CITATION itself (routes "B" and "C"; same geometry and nuclide densities as for the "forward" calculation). Furthermore the (broad) group neutron velocities $v^{(g)}$ ($g = 1, \dots, 4$) are required [Lew65, Bel70, Mas76] (see Appendix B, Table B.2).

For the calculation of the effective delayed neutron fractions $\beta_{eff,i}$ (and their sum β_{eff} , the total effective delayed neutron fraction) it is necessary to supply the spectrum $\chi_d^{(g)}$ of the delayed neutrons, the delayed neutron fractions β_i (sum: β_{tot}) and the delayed neutron precursor time constants λ_i (delayed group $i = 1, \dots, 6$) [Bel70, Mas76] (see Appendix B, Table B.4). The spectrum of delayed group 2 was assumed for all of the six delayed groups, as is often done [Mas76].

For all cases presented (also for our two-dimensional calculations, to be presented in the next section), we found $\beta_{eff} = 0.00652(5)$ ($\beta_{eff,i} / \beta_{eff} = \beta_i / \beta_{tot}$, because we assumed the same delayed neutron spectrum for all delayed groups), fairly independent of the density (distribution). This is very close to the value of β_{tot} (= 0.0065; see Appendix B, Table B.4), which can be explained by the fact that the leakage of fast neutrons is very small (see Figure 2.4) and the fact that the 4-group delayed neutron spectrum does not differ too much from the 4-group prompt neutron spectrum (see Appendix B, Tables B.2 and B.4). A "harder" delayed neutron spectrum would yield a lower value for β_{eff} (e.g. $\chi_d^{(1)} = 1.0$ renders $\beta_{eff} = 0.00647$; CITATION, RSG, route "B"), whereas a "softer" delayed neutron spectrum leads to a higher value (e.g. $\chi_d^{(2)} = 1.0$ renders $\beta_{eff} = 0.00724$; CITATION, RSG, route "B").

In Section 2.2 we derived ("old" and "new") fit functions to describe the dependence of the reactivity ρ and the neutron generation time Λ on the (relative) core fuel gas density n_{rel} (see Eqs. (2.2.19) and (2.2.20)). The general form of these functions is:

$$\rho = C_{\rho,1} n_{RRS} + C_{\rho,2} + C_{\rho,3} (n_{RRS})^{-1} \quad (2.3.2)$$

$$\Lambda = C_{\Lambda,1} n_{RRS} + C_{\Lambda,2} + C_{\Lambda,3} (n_{RRS})^{-1} \quad (2.3.3)$$

(n_{RRS} = density, Relative to the RSG gas density). Putting $C_{\rho,1}$ and $C_{\Lambda,1}$ to zero renders the "old" functions, already used by van Dam [Dam88] and Kuijper [Kui88].

A comparison is made in Figure 2.7 between the results of fine group XSDRNPM calculations using 123 group ENDF/B-IV data (route "C") and 187 group JEF-1 data (route "B"). The reactivity ρ is shown as a function of the relative gas density n_{RRS} . The solid lines are functions, fitted to the calculated $\rho(n_{RRS})$ -data using the code RRGRAPH [Rea88]. We used the form of the "old" fit functions, obtained from the "chord" and "multi-compartment" GCFR models (see Section 2.2). These models predict that both coefficients of the function have the same value, provided that the density variable is taken relatively to the actual critical density: n_{RCD} . This is -to a good approximation- indeed the case (also see Table 2.5). Clearly, the JEF-1 results for ρ are somewhat higher (0.010 - 0.015) than the ENDF/B-IV results. This is in agreement with the differences found more generally, when comparing ENDF/B-IV and JEF-1 results of k_{eff} -calculations [Lee90]. However, the functional form of the fit functions seems appropriate and there is a good agreement between the coefficients of the terms of the fit functions, describing the variation of ρ with n_{RRS} , obtained from calculations with ENDF/B-IV and JEF-1 data.

Using Eq. (2.2.9) (Section 2.2.1: "chord model") we can calculate the value of w_{TRC} from the first coefficient of the fit function, for the 187-group case. With $\eta = 2.041$ (broad group 4; calculated by the XSDRNPM 187 to 4 group

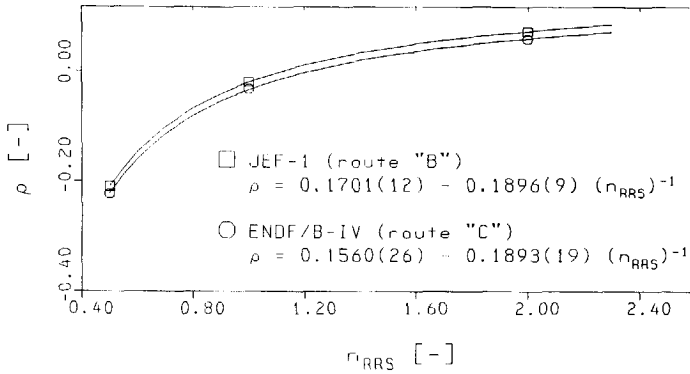


Figure 2.7 Comparison of 123-group and 187-group XSDRNPM neutron transport calculations for RSG geometry: influence of the fuel gas density on the reactivity.

condensation; route "B"), we find: $w_{TRC} = 0.59$. This means that 41 % of the produced fission neutrons do not even return to the core at least once.

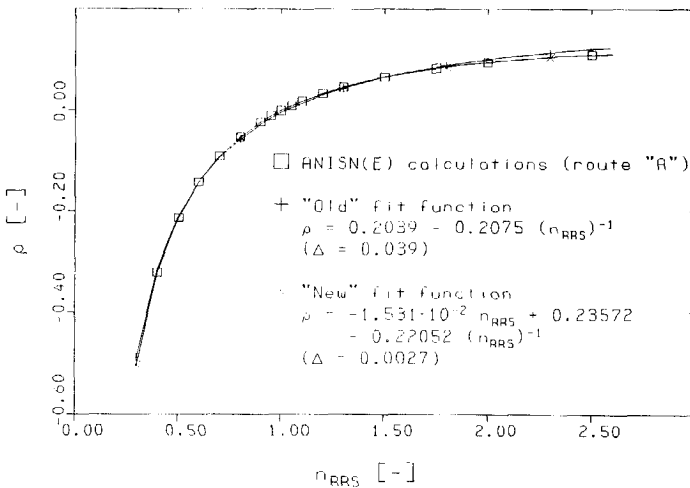


Figure 2.8 Comparison of "old" and "new" fit function for the reactivity as function of the fuel gas density (GCFR in RSG geometry; calculations by ANISN(E), route "A").

In Figure 2.8 we compare the accuracy of the "old" ($C_{\rho,1} = 0$) and the "new" ($C_{\rho,1} \neq 0$) fit function for the reactivity ρ . The $\rho(n_{RRS})$ -data (gas density Relative to the gas density in the RSG) were obtained from 4-group S_4P_1 neutron

Table 2.5 Influence of the fuel gas density and radial fuel gas density distribution on the reactivity of a GCFR in RSG geometry ("old" and "new" fit functions).

Influence of (relative) density n_{RRS}		
Calc. route Code (# groups)	Fit function for $\rho(n_{RRS})$	Remarks
"A"	$0.2039(26) - 0.2075(21) \cdot n_{RRS}^{-1}$	"old"
ANISN(E) (4)	$-0.01531(30) \cdot n_{RRS} + 0.23572(64) - 0.22052(30) \cdot n_{RRS}^{-1}$	"new"
"B"	$0.1701(12) - 0.18963(93) \cdot n_{RRS}^{-1}$	"old"
XSDRNPM (187)	$-2.5046 \cdot 10^{-3} \cdot n_{RRS} + 0.17573 - 0.19195 \cdot n_{RRS}^{-1}$	"new"
"B"	$0.2252(63) - 0.2079(48) \cdot n_{RRS}^{-1}$	"old"
XSDRNPM (4)	$-1.2830 \cdot 10^{-2} \cdot n_{RRS} + 0.25408 - 0.21986 \cdot n_{RRS}^{-1}$	"new"
"B"	$0.2152(66) - 0.2104(50) \cdot n_{RRS}^{-1}$	"old"
CITATION (4)	$-1.3418 \cdot 10^{-2} \cdot n_{RRS} + 0.24532 - 0.22286 \cdot n_{RRS}^{-1}$	"new"
"C"	$0.1560(26) - 0.1893(19) \cdot n_{RRS}^{-1}$	"old"
XSDRNPM (123)	$5.2133 \cdot 10^{-3} \cdot n_{RRS} + 0.16776 - 0.19418 \cdot n_{RRS}^{-1}$	"new"
"C"	$0.2167(65) - 0.2111(49) \cdot n_{RRS}^{-1}$	"old"
XSDRNPM (4)	$-1.3203 \cdot 10^{-2} \cdot n_{RRS} + 0.24644 - 0.22335 \cdot n_{RRS}^{-1}$	"new"
Influence of radial density distribution ϵ		
Calc. route Code (# groups)	Fit function for $\rho(\epsilon)$	Remarks
"A"	$3.4(26) \cdot 10^{-5} + 1.895(19) \cdot 10^{-3} \cdot \epsilon - 1.228(21) \cdot 10^{-4} \cdot \epsilon^2$	fit $-0.5 \leq \epsilon \leq 9.0$
ANISN(E) (4)	$2.9(34) \cdot 10^{-5} + 1.920(67) \cdot 10^{-3} \cdot \epsilon - 1.25(40) \cdot 10^{-4} \cdot \epsilon^2$	fit $-0.5 \leq \epsilon \leq 2.0$

transport calculations for the RSG by ANISN(E) (route "A"). Clearly, both the "old" and the "new" fit function describe the dependence of ρ on n_{RRS} quite well, but the "new" fit function is slightly better at higher densities. This is also demonstrated by the values of Δ (Eq. (2.3.1)); in this case $y_i = \rho$ and $x_i = n_{RRS}$. For both curves the value of Δ is small (compared to 1), but the value for the "new" fit function is slightly smaller, which indicates a slightly better fit.

In Figure 2.9 we make the same comparison for the neutron generation time Λ (data from the same calculations). Again both functions ("old" and "new") can be fitted to the numerical data quite well (small values for Δ). The "old" and the "new" functions almost produce identical graphs (in the investigated density range), as the fitted coefficient $C_{\Lambda,1}$ is very small.

The coefficients of the fit functions can be found in Table 2.5 (reactivity) and Table 2.6 (neutron generation time). Kuijper [Kui88] also performed these

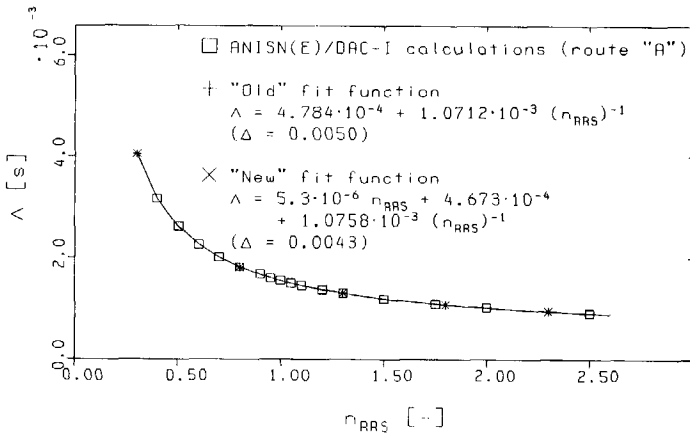


Figure 2.9 Comparison of "old" and "new" fit function for the neutron generation time as function of the fuel gas density (calculations by ANISN(E) and DAC-I, route "A").

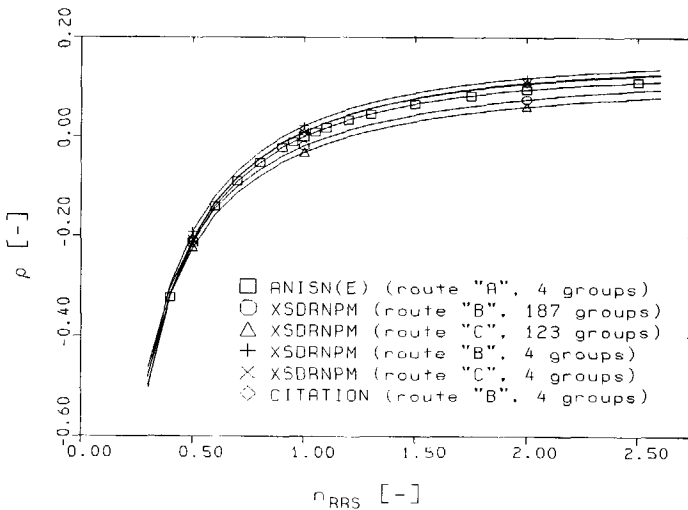


Figure 2.10 Comparison of reactivity calculation results (reactivity as function of fuel gas density in RSG geometry).

calculations for other core sizes ($R_{core} = 2$ m) and other geometries (infinite and pseudo-finite cylinders) and found that also in those cases the dependence of ρ and Λ on the core gas density can be described very well by similar fit functions.

In Figure 2.10 we compare the results of reactivity calculations for RSG-

Table 2.6 Influence of the fuel gas density and the radial fuel gas density distribution on the neutron generation time of a GCFR in RSG geometry ("old" and "new" fit functions).

Influence of (relative) density n_{RSG}		
Calc. route Code(s) (# groups)	Fit function for $\Lambda(n_{RSG})$ (s)	Remarks
"A"	$4.784(18) \cdot 10^{-4} + 1.0712(14) \cdot 10^{-3} \cdot n_{RSG}^{-1}$	"old"
ANISN(E)/DAC-I (4)	$5.3(25) \cdot 10^{-6} \cdot n_{RSG} + 4.673(53) \cdot 10^{-4} - 1.0785(25) \cdot 10^{-3} \cdot n_{RSG}^{-1}$	"new"
"B"	$6.8450(59) \cdot 10^{-4} + 1.59509(45) \cdot 10^{-3} \cdot n_{RSG}^{-1}$	"old"
CITATION (4)	$1.2000 \cdot 10^{-6} \cdot n_{RSG} + 6.818 \cdot 10^{-4} - 1.5962 \cdot 10^{-3} \cdot n_{RSG}^{-1}$	"new"
Influence of radial density distribution ϵ		
Calc. route Code(s) (# groups)	Fit function for $\Lambda(\epsilon)$ (s)	Remarks
"A"	$1.548610(79) \cdot 10^{-3} - 6.268(58) \cdot 10^{-6} \cdot \epsilon + 3.918(64) \cdot 10^{-7} \cdot \epsilon^2$	fit $-0.5 \leq \epsilon \leq 9.0$
ANISN(E)/DAC-I (4)	$1.548599(61) \cdot 10^{-3} - 6.45(12) \cdot 10^{-6} \cdot \epsilon + 4.68(71) \cdot 10^{-7} \cdot \epsilon^2$	fit $-0.5 \leq \epsilon \leq 2.0$

geometry of different codes and different calculational routes (see Figure 2.1): ANISN(E) (4-group S_4P_1 neutron transport; route "A"), XSDRNPM (4-group S_4P_3 neutron transport; routes "B" and "C") and CITATION (4-group neutron diffusion; route "B"). We also included the results of the 187-group (route "B") and 123-group (route "C") S_4P_3 neutron transport calculations by XSDRNPM reported earlier. In the figure also the corresponding fit functions ("new") are plotted and in Table 2.5 these fit functions are listed. Apart from the differences to be expected when comparing ENDF/B-IV and JEF-1 results [Lee90], we see that, in general, broad group calculations render a higher value for the reactivity than fine group calculations (better description of leakage by fine groups). Also P_3 -calculations render a somewhat lower value than P_1 -calculations, although the difference is small: less than 0.001. This was found by comparing the results of 4-group S_4P_1 ANISN calculations (routes "B" and "C"; not shown in Figure 2.10) with those of the 4-group S_4P_3 XSDRNPM calculations. The values found by the broad group diffusion calculations (CITATION, route "B") are approximately 0.01 lower than the corresponding values from the broad group transport calculations (XSDRNPM, route "B"). This difference may seem small, but it leads to a prediction of the actual critical density (at which $\rho = 0$ exactly), which is 6 % higher for the CITATION calculations. However, the differences are small compared to the differences imposed by the expected variation of the average density of the fuel gas.

We make a similar comparison for the neutron generation time Λ (no fine group results) in Figure 2.11. The corresponding fit functions are also shown in the graph ("new" only) and are listed in Table 2.6. Clearly, both the results from the

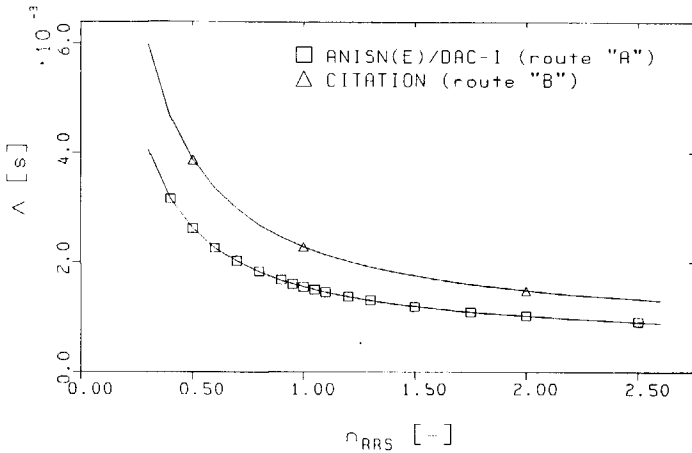


Figure 2.11 Comparison of neutron generation time calculation results (neutron generation time as function of fuel gas density).

S_4P_1 neutron transport calculation by ANISN(E)/DAC-I (route "A") and the results from the neutron diffusion calculation by CITATION (route "B") can be described quite well by both the "old" and the "new" fit function. However, the values rendered by the ANISN(E)/DAC-I calculations (route "A") are too low by a factor of approximately 1.5. This was expected in view of the differences in the neutron group velocities $v^{(3)}$ and $v^{(4)}$, resulting from the group condensation calculation by XSDRN (route "A") and XSDRNPM (route "B"; see Appendix B, Table B.2). Unfortunately, we used these Λ -values (or rather the corresponding fit function) for the neutron kinetics part of our "solid piston" GCFR model (Chapter 5), as they were the only data available at that time. We also calculated the neutron generation time (for the RSG) by ANISN/DAC-I and CITATION, using data originating from JEF-1 (route "B") and ENDF/B-IV (route "C") and using the correct broad group neutron velocities (Appendix B, Table B.2). We found $\Lambda = 2.29 \cdot 10^{-3}$ s in all of the four cases. This is in line with the values, calculated by van Dam [Dam87], for the time required for neutrons to thermalize in the graphite reflector and to return to the core.

We have seen that, for the cases presented here, viz. the RSG broad group neutron flux shape and the dependence of ρ and Λ on the fuel gas density, the results of broad group neutron diffusion calculations approximate quite well the results of broad and fine group neutron transport calculations. Therefore, and in view of the explorative nature of our calculations, we decided to use the neutron diffusion code CITATION also for our static neutronic investigations of a cylindrical (also two-dimensional) GCFR (Section 2.4). This is also favourable from the point of view of the requirement of computing resources. A typical CPU-time (DEC VAXstation 3100 Model 76) required for the iterations in an XSDRNPM 187-group S_4P_3 calculation (see Table 2.1 for calculational parameters) for the RSG is 170 minutes. For a XSDRNPM 4-group S_4P_3 calculation for the same system the

required CPU-time is already much less, viz. 2.4 seconds. A 4-group CITATION calculation for the same system (see Table 2.3) requires even less CPU-time: $8.9 \cdot 10^{-2}$ seconds. If we then consider that a typical CPU-time required for the two-dimensional CITATION calculations (Section 2.4) is 100 minutes, then it is clear that two-dimensional 187-group neutron transport calculations, which are certainly more accurate than 4-group neutron diffusion calculations, would be extremely time-consuming indeed.

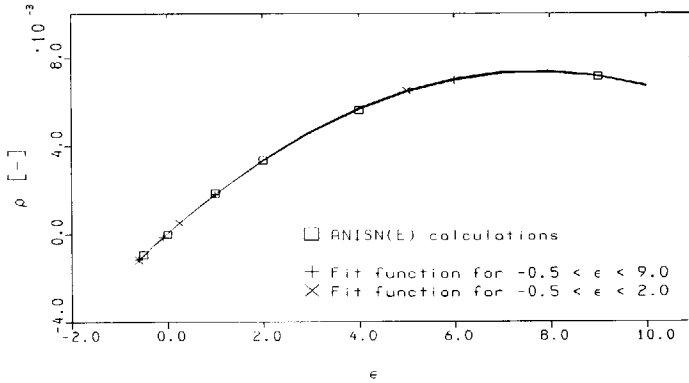


Figure 2.12 Influence of the radial fuel gas density distribution on the reactivity of a GCFR in RSG geometry (ANISN(E) calculations, route "A").

A final item in these one-dimensional calculations is the influence of the radial fuel gas density distribution on the reactivity and the neutron generation time. We investigated this influence in a two-zone core geometry (see Table 2.2). In Figure 2.12 we show the influence of the radial fuel gas density distribution (specified by the density distribution variable ϵ ; Eqs. (2.2.24) and (2.2.25)) on the reactivity ρ (calculations by ANISN(E); route "A"). Obviously, the effect of fuel gas displacement from the core centre to the core edge is a -small- increase of the reactivity. Uleman [Ule82], van Dam and Hoogenboom [Dam83] also report these small reactivity effects. In Section 2.2.2 we derived a function to describe this effect, viz. Eq. (2.2.26). This function predicts a maximum reactivity for the maximum possible value of ϵ , viz. $\epsilon = V_{centre} / V_{edge} \approx 12.7$ (also at empty core centre). The actual maximum is found, however, at $\epsilon = 7.7$. However, the effect is quite well described by a function of the form of Eq. (2.2.26), viz. a second order polynomial in ϵ , as is also demonstrated in Figure 2.12 by the second graph line. This is the graph of a fit function of the same form, but only fitted to data points for which $-0.5 \leq \epsilon \leq 2.0$. Clearly, the reactivity at $\epsilon = 9.0$ is predicted quite well by this function. Both fit functions are listed in Table 2.5.

The fit function mentioned above (Eq. (2.2.26)), was derived in Section 2.2.2 using a one-and-a-half-group/two-compartment model for a spherical GCFR. It is also possible to understand the behaviour of the reactivity with ϵ from the point of view of the "chord model" (Section 2.2.1), as was already done by Uleman [Ule82], van Dam and Hoogenboom [Dam83]. The governing parameter is the average "optical" path length for thermal neutrons crossing the core. The

optical path length is the path length measured in units of mean free path, thus a dimensionless quantity. For a homogenous core, the average optical path length is given by $\Sigma_a \bar{a}$, neglecting scattering events. In curved geometries a piling up of fuel near the wall gives a decrease of optical path length for neutrons flying through the central core region and an increase of optical path length for neutrons moving along short chords. On the basis of a classical analysis of chord length distributions it can be shown that the latter effect more than compensates for the first effect; i.e. on the average, the neutrons "see" a higher fuel density. This implies that the average optical path length increases due to fuel pileup near the wall, giving rise to a positive reactivity effect (see Eqs. (2.2.6) and (2.2.8)). Details of an analytical treatment based on chord length distributions are given by Uleman [Ule82].

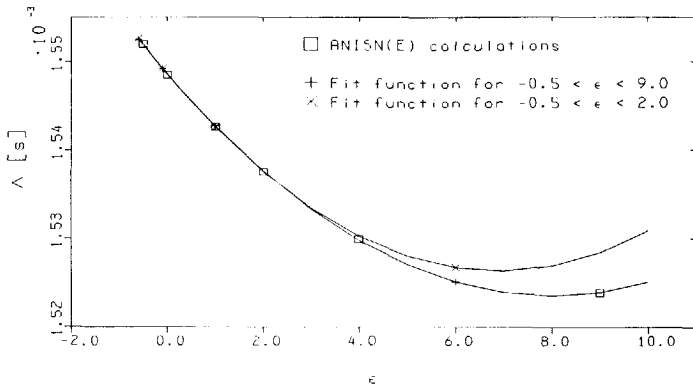


Figure 2.13 Influence of the radial fuel gas density distribution on the neutron generation time of a GCFR in RSG geometry (ANISN(E)/DAC-I calculations, route "A").

In Figure 2.13 we demonstrate the influence of the radial fuel gas density distribution on the neutron generation time Λ (calculations by ANISN(E) and DAC-I; route "A"). The influence of fuel gas displacement from the core centre to the core edge on Λ is small but negative. We also fitted a function of the form of Eq. (2.2.26), viz. a second order polynomial in ϵ , to the data points. Clearly, $\Lambda(\epsilon)$ is reproduced quite well by this function. We again tried to fit a function of the same form to only those data points, for which $-0.5 \leq \epsilon \leq 2.0$, but this second function predicts a value for Λ at $\epsilon = 9.0$, which is approximately $5 \cdot 10^{-5}$ s too high. Both fit functions are listed in Table 2.6. However, the variations in ρ and Λ , caused by radial fuel re-distribution, are quite small compared to the variations caused by the expected variations of the average core fuel density.

2.4 Cylindrical GCFR

We investigated the influence of the average fuel gas density and the axial fuel gas density distribution on the static neutronic behaviour of a cylindrical GCFR by two-

dimensional neutron diffusion calculations using the one-, two- and three-dimensional diffusion code CITATION [NEA79], with broad group cross sections originating from JEF-1 (route "B"). As indicated in Figure 2.14, the GCFR configuration studied here consists of a cylindrical gas space (length $L_{gas} = 10.0$ m; radius $R_{gas} = 1.0$ m), surrounded by a reflector (zone 11). This gas space is divided into a "core" section (zones 1 - 5) and an "expander" section (zones 6 - 10) of equal volume ($V_{core} = V_{exp} = 0.5 V_{core}$). Three different (reflector) geometries were studied: (I) "symmetric" (reflector thickness around expander $d_{refl,exp} =$ reflector thickness around core $d_{refl,core} = 1.0$ m), (II) "slightly asymmetric" ($d_{refl,exp} = 0.60$ m) and (III) "asymmetric" ($d_{refl,exp} = 0.20$ m). The main parameters for these calculations are listed in Table 2.7. The reduction of $d_{refl,exp}$ for the asymmetric cases was achieved by replacing part of the reflector by a "black absorber" (zone 12) (also indicated in Figure 2.14). We only investigated the effect of the axial density distribution, as we expect the influence of the radial distribution to be relatively small (see Section 2.3). Furthermore, in the calculations presented in this section we assumed a value of 10,000 K for the temperature of the fuel gas and 1000 K for the temperature of the reflector (like in the RSG; see Section 2.3).

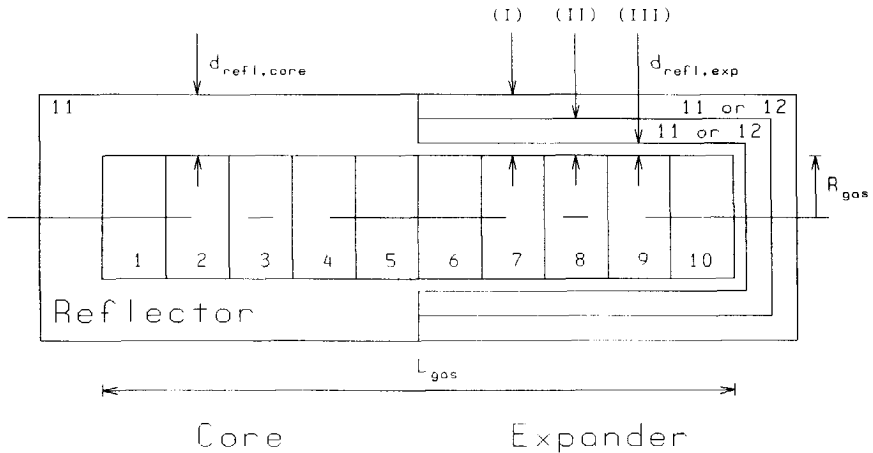


Figure 2.14 Structure of the cylindrical GCFR model for two-dimensional neutron diffusion calculations by CITATION.

Using the CITATION density search option, we calculated the critical density $n_{RRS,crit}$ (Relative to RSG gas density), for a flat density distribution of the fuel gas (also the same $n_{rel,m}$ for $m = 1, \dots, 10$) in the configurations ("I", "II" and "III") mentioned above. The results of these calculations are listed in Table 2.8. Note that for case "I" ("symmetric") and case "II" ("slightly asymmetric") the critical density is smaller than for the RSG, whereas for case "III" ("asymmetric") the critical density is much larger. This can be explained by the enormous neutron leakage through the part of the reflector, surrounding the expander. This reflector part is only 20 cm thick, i.e. 1/4 thermal neutron diffusion length. Note that,

Table 2.7 Main parameters for two-dimensional broad group static neutron diffusion calculations by CITATION.

General				
Calculation type	K_{eff} -calculation, density search, calculation of Λ and $\beta_{eff,i}$			
Geometry	Cylinder: radial (R), axial (Z)			
Left boundary condition (R)	Reflective (cylinder axis)			
Right boundary condition (R)	Extrapolated (outer boundary)			
Top boundary condition (Z)	Extrapolated (outer boundary: core end)			
Bottom boundary condition (Z)	Extrapolated (outer boundary: expander end)			
Number of zones	11 or 12 (see below)			
Flux convergence criterion	$1 \cdot 10^{-5}$			
Eigenvalue convergence criterion	$1 \cdot 10^{-5}$			
Total fission power (flux normalization) (MW _{th})	100.0			
Fuel gas nuclide composition	As in RSG			
Reflector nuclide density (cm ⁻³)	$8.55 \cdot 10^{22}$ (as in RSG)			
Spatial structure				
Zone	Radial interval range	Radial coordinate range (cm)	Axial interval range	Axial coordinate range (cm)
1 (core gas)	1 - 27	0 - 100	33 - 59	100 - 200
2 (core gas)	1 - 27	0 - 100	60 - 69	200 - 300
3 (core gas)	1 - 27	0 - 100	70 - 79	300 - 400
4 (core gas)	1 - 27	0 - 100	80 - 89	400 - 500
5 (core gas)	1 - 27	0 - 100	90 - 99	500 - 600
6 (expander gas)	1 - 27	0 - 100	100 - 109	600 - 700
7 (expander gas)	1 - 27	0 - 100	110 - 119	700 - 800
8 (expander gas)	1 - 27	0 - 100	120 - 129	800 - 900
9 (expander gas)	1 - 27	0 - 100	130 - 139	900 - 1000
10 (expander gas)	1 - 27	0 - 100	140 - 166	1000 - 1100
11/12 (reflector; zone 12 is black absorber)	1 - 59 28 - 59 1 - 59	0 - 200 100 - 200 0 - 200	1 - 32 33 - 166 167 - 198	0 - 100 100 - 1100 1100 - 1200

because the mean free path and the diffusion length are proportional to the inverse of the nuclide density, the mean free path and the diffusion length in the gas for case "III" will be much smaller (for a critical reactor) than for case "I", case "II" or even the RSG (see Appendix B).

In Figure 2.15 (A) the broad group axial flux profiles are shown for the

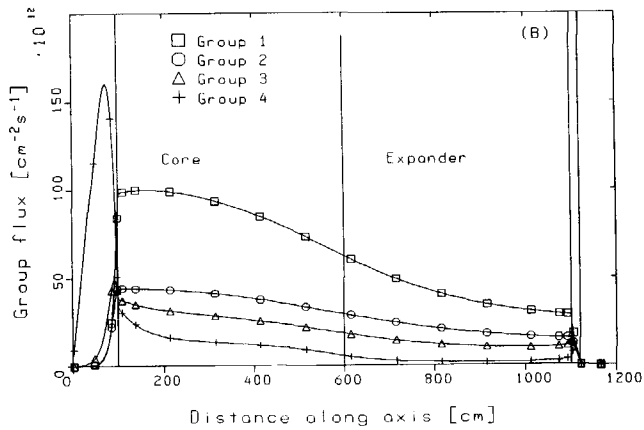
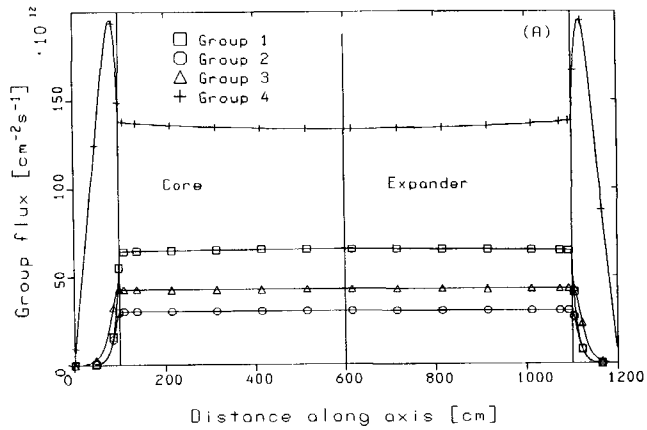


Figure 2.15 Broad group fluxes along the axis of cylindrical GCFRs with "flat" fuel gas density distribution: (A) "symmetric" GCFR (case "I") and (B) "asymmetric" GCFR (case "III").

symmetric case ("I") with flat fuel gas density distribution. Note that the neutron flux (all groups) in the gas is almost spatially flat, which was expected in view of the large mean free path and diffusion length for this case. For a comparison in Figure 2.15 (B) the broad group axial flux profiles are shown for the asymmetric case ("III"), also with flat fuel gas density distribution. Note that all group fluxes drop off quickly by going from the core part to the expander part. This is due to the very large leakage of neutrons through the thin reflector surrounding the expander. In this case the neutron diffusion lengths (in the gas) for group 1 and 2 are of the same order of magnitude as the length of the gas space, whereas the diffusion lengths for group 3 and 4 are (much) smaller. The radial flux profiles are

similar to the profiles in the spherical GCFR (see Section 2.3).

The main part of our two-dimensional neutron diffusion calculations was dedicated to the investigation of the influence of the average fuel gas density and the axial fuel gas density distribution on the reactivity ρ , the neutron generation time Λ and the core (zones 1 - 5) fission power fraction f_p . In view of the large mean free paths and diffusion lengths (especially in cases "I" and "II") we can expect that small scale (spatial) density variations within the core or expander part will not have a large influence on these quantities. We therefore describe the fuel density distribution over the core and the expander zones in terms of a single fuel density distribution variable ε , which is given by:

$$\varepsilon \equiv \frac{m_{core} V_{tot}}{V_{core} m_{tot}} - 1 = 2 \frac{m_{core}}{m_{tot}} - 1 \quad (2.4.1)$$

(m_{core} = mass of the fuel gas in the core part (zones 1 - 5); m_{tot} = total mass of the fuel gas; $V_{core} = V_{exp} = 0.5 V_{tot}$). This definition is consistent with Eqs. (2.2.27) and (2.2.28). This "two-compartment" description of the fuel gas density distribution agrees with the "two-compartment" cylindrical GCFR model introduced in Section 2.2.2 and is also favourable in view of the coupling with gas dynamics in the combined "two-compartment" GCFR model to be presented in Chapter 7. In fact, the description of the distribution of the fuel gas in terms of ε is an approximation of the (axial) Fundamental Acoustic Mode ("FAM").

Bearing this in mind, we expect that the influence of the axial fuel gas density distribution (ε) and the variation of the average fuel gas density (n_{rel}) on the reactor physical quantities ρ , Λ and f_p can be described by the fit functions, derived from the one-and-a-half-group/two-compartment model for the cylindrical GCFR (Section 2.2.2), viz. Eqs. (2.2.31), (2.2.32) and (2.2.33). In these equations the influences of n_{rel} and ε are independent. This means that for the determination of the coefficients it is sufficient to perform CITATION calculations for varying average fuel gas density n_{rel} (or n_{RCD} : the spatially averaged density, Relative to the Critical Density; $n_{RCD} \equiv n_{rel} / n_{rel,crit}$) at flat density distribution ($\varepsilon = 0$) and for varying axial density distribution ε at average critical density ($n_{RCD} = 1$).

Table 2.8 Critical fuel gas densities and critical total fuel gas mass for cylindrical GCFRs with homogeneous ("flat") fuel gas density distribution.

GCFR geometry	$n_{RCD,crit}$	$m_{tot,crit}$ (kg)
"symmetric" ("I")	0.42038	125.1
"slightly asymmetric" ("II")	0.58429	173.9
"asymmetric" ("III")	4.04503	1204

In order to verify the validity of the description of the axial fuel gas density distribution by a single variable ε , we performed these calculations for two different types of axial density distributions, both consistent with Eq. (2.4.1). The first type is the so-called "rectangular distribution", for which the (relative) densities in the gas zones (Figure 2.14) are given by:

$$n_{rel,m} = \begin{cases} (1 + \varepsilon) n_{rel} & m = 1, \dots, 5 \\ (1 - \varepsilon) n_{rel} & m = 6, \dots, 10 \end{cases} \quad (2.4.2)$$

(also see Eqs. (2.2.27) and (2.2.28)). The second type is the so-called "triangular distribution", for which the relative densities in the gas zones are given by:

$$n_{rel,m} = \left[1 + \frac{1}{5}(11 - 2m)\varepsilon \right] n_{rel} \quad m = 1, \dots, 10 \quad (2.4.3)$$

Table 2.9 Influence of the fuel gas density and axial fuel gas density distribution on the reactivity, the neutron generation time and the core fission power fraction of the symmetric cylindrical GCFR (case "I").

Quantity	Fit function	Remarks
$\rho(\varepsilon, n_{RCD})$	$-1.0466 \cdot 10^{-2} \cdot n_{RCD} + 0.30551 - 0.29345 \cdot n_{RCD}^{-1} - 5.063(58) \cdot 10^{-2} \cdot \varepsilon^2$	rectangular distribution
	$-1.0466 \cdot 10^{-2} \cdot n_{RCD} + 0.30551 - 0.29345 \cdot n_{RCD}^{-1} - 7.7617 \cdot 10^{-2} \cdot \varepsilon^2$	triangular distribution
$\Lambda(\varepsilon, n_{RCD})$	$2.2733 \cdot 10^{-5} \cdot n_{RCD} + 6.0107 \cdot 10^{-4} + 3.0004 \cdot 10^{-3} \cdot n_{RCD}^{-1} + 4.556(45) \cdot 10^{-4} \cdot \varepsilon^2$	rectangular distribution
	$2.2733 \cdot 10^{-5} \cdot n_{RCD} + 6.0107 \cdot 10^{-4} + 3.0004 \cdot 10^{-3} \cdot n_{RCD}^{-1} + 7.680 \cdot 10^{-4} \cdot \varepsilon^2$	triangular distribution
$f_p(\varepsilon, n_{RCD})$	$0.5000 + 0.459(16) \cdot \varepsilon$	rectangular distribution
	$0.5000 + 0.3988 \cdot \varepsilon$	triangular distribution

These two density distributions are both approximations to the FAM (axial) density distribution (at a certain moment in time), which can be described by a sine-function (see Section 6.2.1).

So, we performed two-dimensional broad group neutron diffusion calculations with CITATION (route "B") for the three reflector configurations and for both axial density distribution types mentioned above, varying n_{rel} and ε . We then determined the coefficients of the fit functions, Eqs. (2.2.31), (2.2.32) and (2.2.33) for ρ , Λ and f_p , respectively, using the code RRGRAPH [Rea88]. The results are listed in Tables 2.9, 2.10 and 2.11. Note that for the symmetric case ("I"), for symmetry reasons, the functions for ρ and Λ only contain an ε^2 -term and the function for f_p only contains an ε -term to describe the influence of ε -variation.

In Figure 2.16 we make a graphical comparison, for the three reflector configurations, between the "rectangular" and "triangular" CITATION calculation results for the reactivity ρ (for varying ε and $n_{RCD} = 1$). In Figure 2.17 and Figure 2.18 we do the same for the neutron generation time Λ and the core power fraction f_p , respectively. Also the graphical representations of the corresponding fit functions are shown and in Figure 2.18 also the variation of f_p with ε is shown for the case of a spatially flat neutron flux distribution, which is given by:

Table 2.10 Influence of the fuel gas density and axial density distribution on the reactivity, the neutron generation time and the core fission power fraction of the "slightly asymmetric" cylindrical GCFR (case "II").

Quantity	Fit function	Remarks
$\rho(\varepsilon, n_{RCD})$	$-1.3257 \cdot 10^{-2} \cdot n_{RCD} + 0.26374 - 0.24977 \cdot n_{RCD}^{-1} + 6.184(87) \cdot 10^{-3} \cdot \varepsilon - 6.804(30) \cdot 10^{-2} \cdot \varepsilon^2$	rectangular distribution
	$-1.3257 \cdot 10^{-2} \cdot n_{RCD} + 0.26374 - 0.24977 \cdot n_{RCD}^{-1} + 7.2702 \cdot 10^{-3} \cdot \varepsilon - 9.7642 \cdot 10^{-2} \cdot \varepsilon^2$	triangular distribution
$\Lambda(\varepsilon, n_{RCD})$	$6.5284 \cdot 10^{-6} \cdot n_{RCD} + 5.3224 \cdot 10^{-4} + 2.1052 \cdot 10^{-3} \cdot n_{RCD}^{-1} - 8.73(94) \cdot 10^{-5} \cdot \varepsilon + 4.01(22) \cdot 10^{-4} \cdot \varepsilon^2$	rectangular distribution
	$6.5284 \cdot 10^{-6} \cdot n_{RCD} + 5.3224 \cdot 10^{-4} + 2.1052 \cdot 10^{-3} \cdot n_{RCD}^{-1} - 1.0600 \cdot 10^{-4} \cdot \varepsilon + 7.4400 \cdot 10^{-4} \cdot \varepsilon^2$	triangular distribution
$f_p(\varepsilon, n_{RCD})$	$0.54112 - 3.0583 \cdot 10^{-2} \cdot n_{RCD}^{-1} + 7.4611 \cdot 10^{-3} \cdot n_{RCD}^{-2} + 0.424(11) \cdot \varepsilon - 0.016(25) \cdot \varepsilon^2$	rectangular distribution
	$0.54112 - 3.0583 \cdot 10^{-2} \cdot n_{RCD}^{-1} + 7.4611 \cdot 10^{-3} \cdot n_{RCD}^{-2} + 0.34940 \cdot \varepsilon - 0.0408 \cdot \varepsilon^2$	triangular distribution

$$f_p = \frac{1}{2} (1 + \varepsilon) \quad (2.4.4)$$

For the other cases the variation of f_p with ε is always smaller, due to thermal flux depression in the compartment with the larger fuel density. Obviously, the effect of an ε -variation in the "rectangular" density distribution is not exactly the same as in the "triangular" density distribution. However, the effects are of the same sign and the same order of magnitude. We can also conclude that a single variable ε gives a fair description of the influence of the (axial) fuel gas density distribution on the reactivity ρ , the neutron generation time Λ and the core power fraction f_p . We used this results (in the form of the fit functions; Table 2.9; "rectangular") in our combined "two-compartment" GCFR model, to be presented in Chapter 7.

For the asymmetric case ("III") the core fission power fraction f_p is relatively close to 1 and fairly independent of the fuel gas distribution over core and expander ($0.76 \leq f_p \leq 0.87$ for $-0.4 \leq \varepsilon \leq 0.4$; "rectangular" distribution; $n_{RCD} = 1$), as can be concluded from Figure 2.18 and Table 2.11. This means that almost only the fuel gas in the core takes part in the fission chain reaction. Furthermore, there exists a strong resemblance between the graphs describing the influence of the axial fuel gas density distribution variable ε on ρ and Λ for the cylindrical GCFR (Figures 2.16 and 2.17) and the graphs describing this influence of the core fuel gas density in the spherical GCFR (Section 2.3; Figures 2.8 and 2.9). Therefore, we also attempted to use the fit functions for the one-dimensional case (Section 2.3; Eqs. (2.3.2) and (2.3.3); "old" fit functions; substitute: $n_{RRS} = (1 + \varepsilon)$) for the description of the effect of the axial fuel gas density distribution in the asymmetric cylindrical GCFR (case "III"). The results of the fitting procedures, which are also listed in Table 2.11 ("1-dim. form."), show the feasibility of this approach, which in fact treats the cylindrical GCFR as if only the fuel gas in the core takes part in the fission chain reaction and, therefore, has influence on the reactivity and the neutron generation time. We made use of this

Table 2.11 Influence of fuel gas density and axial fuel gas density distribution on the reactivity, the neutron generation time and the core fission power fraction of the asymmetric cylindrical GCFR (case "III").

Quantity	Fit function	Remarks
$\rho(\epsilon, n_{RCD})$	$0.022(11) \cdot n_{RCD} + 0.074(48) - 0.099(15) \cdot n_{RCD}^{-1} + 0.0441(19) \cdot \epsilon - 0.0333(42) \cdot \epsilon^2$	rectangular distribution
	$0.022(11) \cdot n_{RCD} + 0.074(48) - 0.099(15) \cdot n_{RCD}^{-1} + 0.0408(13) \cdot \epsilon - 0.0573(87) \cdot \epsilon^2$	triangular distribution
$\rho(\epsilon)$ ($n_{RCD} = 1$)	$0.0308(12) - 0.03012(65) \cdot (1 + \epsilon)^{-1}$	rect. distr. (1-dim. form.)
	$0.0383(14) - 0.0389(14) \cdot (1 + \epsilon)^{-1}$	triang. distr. (1-dim. form.)
$\Lambda(\epsilon, n_{RCD})$	$-3.628(87) \cdot 10^{-5} \cdot n_{RCD} + 7.651(37) \cdot 10^{-4} + 4.023(12) \cdot 10^{-4} \cdot n_{RCD}^{-1} - 3.64(17) \cdot 10^{-4} \cdot \epsilon + 3.03(39) \cdot 10^{-4} \cdot \epsilon^2$	rectangular distribution
	$-3.628(87) \cdot 10^{-5} \cdot n_{RCD} + 7.651(37) \cdot 10^{-4} + 4.023(12) \cdot 10^{-4} \cdot n_{RCD}^{-1} - 4.172(95) \cdot 10^{-4} \cdot \epsilon + 5.63(64) \cdot 10^{-4} \cdot \epsilon^2$	triangular distribution
$\Lambda(\epsilon)$ ($n_{RCD} = 1$)	$8.91(11) \cdot 10^{-4} + 2.432(58) \cdot 10^{-4} \cdot (1 + \epsilon)^{-1}$	rect. distr. (1-dim. form.)
	$7.39(12) \cdot 10^{-4} + 3.98(11) \cdot 10^{-4} \cdot (1 + \epsilon)^{-1}$	triang. distr. (1-dim. form.)
$f_p(\epsilon, n_{RCD})$	$0.9457(41) - 0.1527(68) \cdot n_{RCD}^{-1} + 0.0220(16) \cdot n_{RCD}^{-2} + 0.1336(72) \cdot \epsilon - 0.021(16) \cdot \epsilon^2$	rectangular distribution
	$0.9457(41) - 0.1527(68) \cdot n_{RCD}^{-1} + 0.0220(16) \cdot n_{RCD}^{-2} + 0.0809(10) \cdot \epsilon - 0.0160(69) \cdot \epsilon^2$	triangular distribution

approach, utilizing the results of the one-dimensional neutron transport calculations by ANISN(E) and DAC-I (route "A"; see Tables 2.5 and 2.6) in the neutron kinetics part of our combined "solid piston" GCFR model, to be presented in Chapter 5.

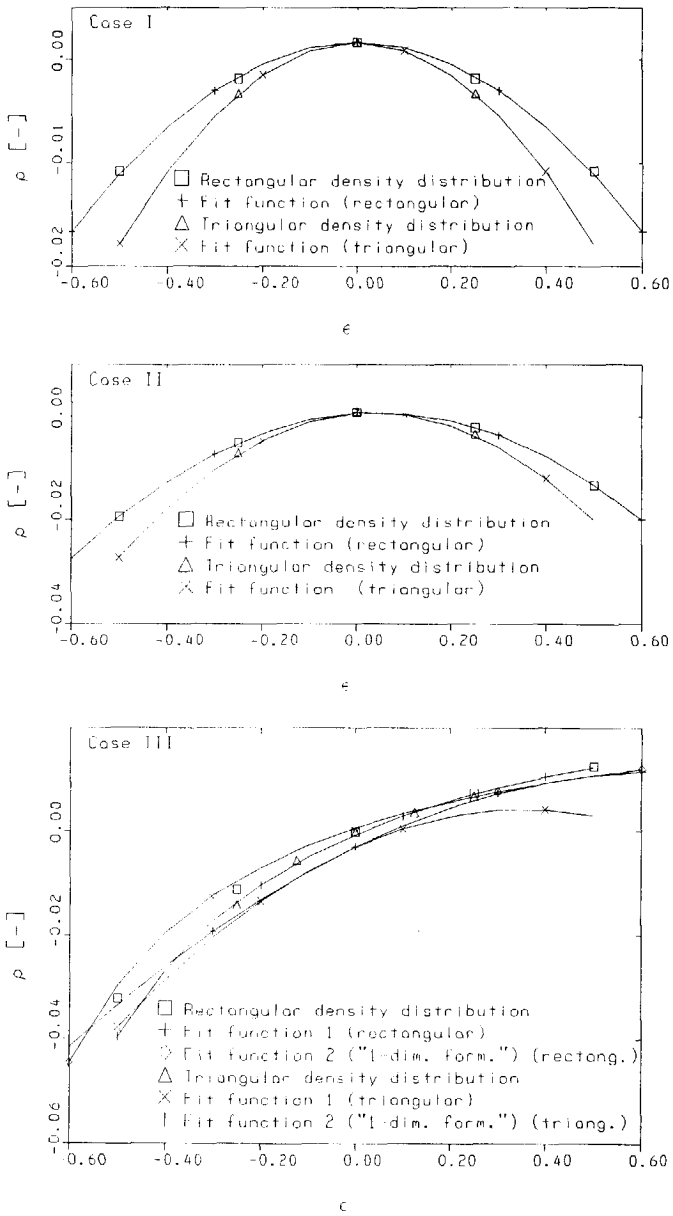


Figure 2.16 Influence of the axial fuel gas density distribution on the reactivity of the cylindrical GCFRs (cases "I", "II" and "III"; $n_{RCD} = 1$).

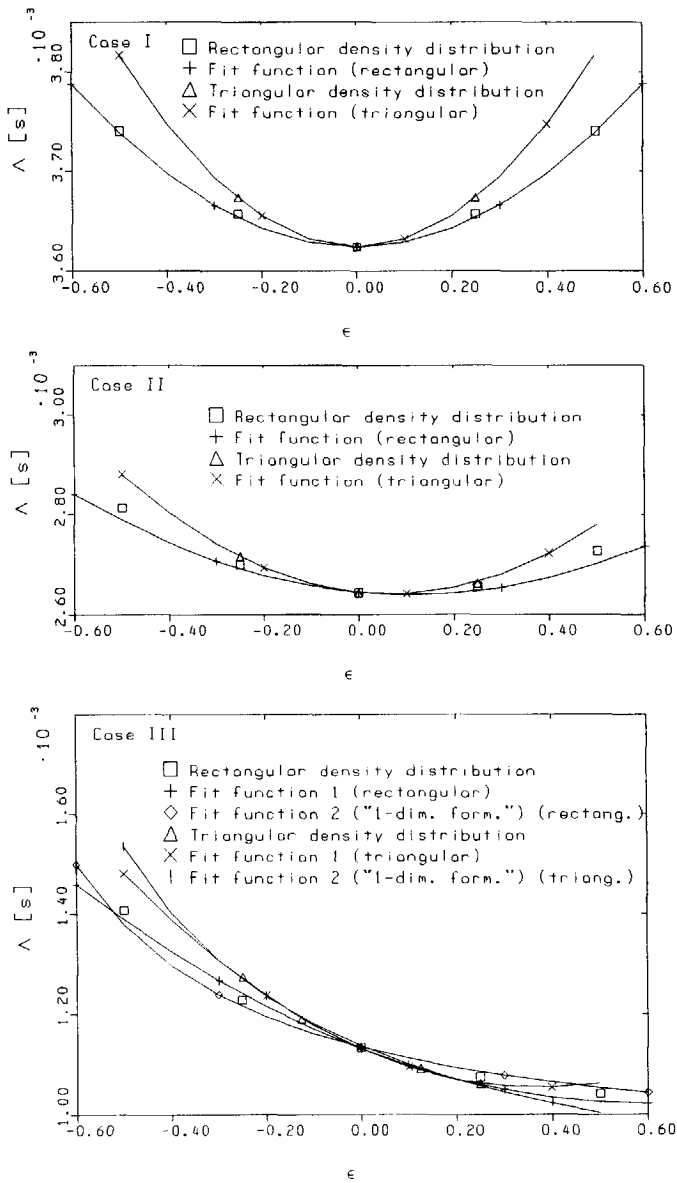


Figure 2.17 Influence of the axial fuel gas density distribution on the neutron generation time of the cylindrical GCFRs (cases "I", "II" and "III"; $n_{RCD} = 1$).

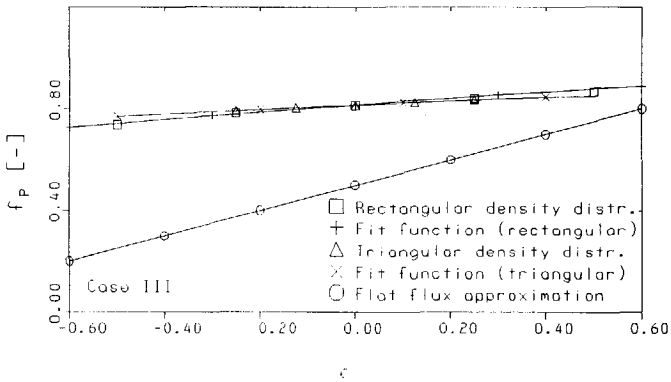
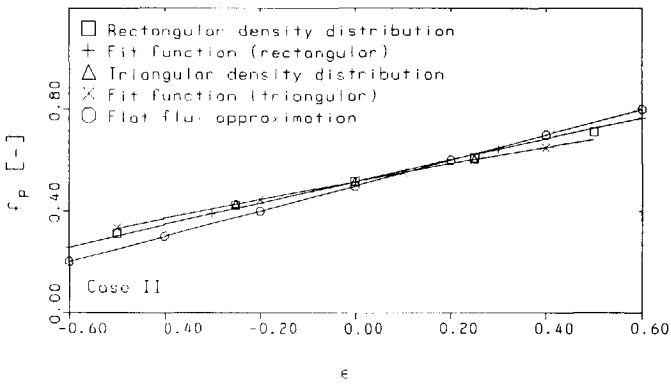
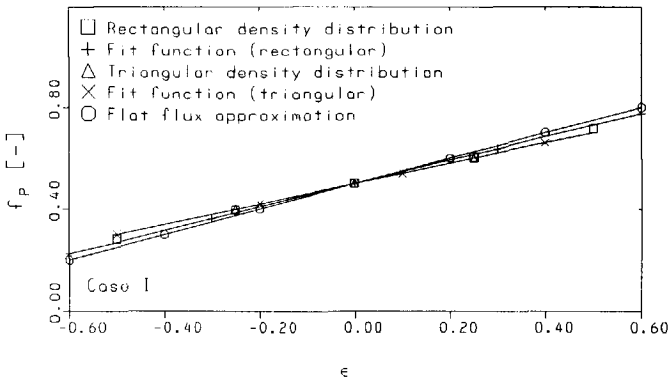


Figure 2.18 Influence of the axial fuel gas density distribution on the core fission power fraction of the cylindrical GCFRs (cases "I", "II" and "III"; $n_{RCD} = 1$).

Chapter 3

NEUTRON KINETICS

3.1 Point kinetics for solid piston GCFR model

In the "solid piston" model, to be presented in Chapter 5, we assume the GCFR to be asymmetric (see Section 2.4: case "III"). This means that almost all the fission power P_{fiss} is produced in the core part, because almost only the fuel in the core takes part in the fission chain reaction. For the derivation of the neutron kinetics model, we go one step further and assume that only the fuel in the core takes part in the fission chain reaction. Consequently, all the fission power P_{fiss} is produced in the core and the reactivity ρ and the neutron generation time Λ are assumed to depend only on the fuel gas density in the core. As was shown in Section 2.4, this dependence can be described by the fit functions used for the one-dimensional (spherical) case:

$$\rho = C_{\rho,2} + C_{\rho,3}(n_{rel})^{-1} \quad (3.1.1)$$

$$\Lambda = C_{\Lambda,2} + C_{\Lambda,3}(n_{rel})^{-1} \quad (3.1.2)$$

(n_{rel} = relative density of the gas in the core; "old" fit functions).

In the "solid piston" GCFR model (Chapter 5) the interaction between the ionized gas and the magnetic field, generated by the current in the coil surrounding the expander (see Figure 1.1), is represented by a solid piston, which moves in the expander and -externally- controls the volume $V_{fuel}(t)$ occupied by the fuel gas. It is assumed that:

$$V_{core} \leq \frac{V_{tot}}{K} \leq V_{fuel}(t) \leq V_{tot} \quad (3.1.3)$$

(V_{core} = core volume; V_{tot} = maximum volume of fuel gas; K = compression ratio).

Following van Dam [Dam88], we will derive the one-group/one-compartment neutron kinetics equation for the "solid piston" GCFR. First of all we assume a homogeneous density distribution of the fuel gas over the momentary gas volume V_{fuel} . This means that gas dynamical effects are not taken into account. The relative density of the gas (in both core and -part of- the expander) is then given by:

$$n_{rel}(t) = n_{rel,0} \frac{V_{tot}}{V_{fuel}(t)} \quad (3.1.4)$$

($n_{rel,0}$ = relative density of the fuel gas at maximum fuel gas volume $V_{fuel} = V_{tot}$; $n_{rel,0}$ is proportional to the total mass m_{tot} of the fuel gas). The fuel gas volume V_{fuel} and consequently n_{rel} is assumed to be a periodical function of time (period τ ; frequency $f = 1 / \tau$).

In one-group/one-compartment approximation the time-dependent multi-compartment neutron transport equation (see Appendix A, Eq. (A.4) and Appendix D, Eq. (D.1)) for the core reads, including delayed neutrons (see e.g. [Dud76]):

$$v^{-1} \frac{d\varphi}{dt} = (1 - \beta_{eff}) \eta \Sigma_a n_{rel} \varphi - \Sigma_a n_{rel} \varphi - K_0 \varphi + S_d \quad (3.1.5)$$

(φ = average -thermal- neutron flux in the core; v = velocity of -thermal- neutrons; β_{eff} = effective delayed neutron fraction; η = average number of fission neutrons produced per absorbed neutron in the fuel gas; K_0 = leakage coefficient = $K_{1 \rightarrow 0}$ (see Appendix A); S_d = delayed neutron source density in the fuel gas). Using the one-group/one-compartment expressions for the reactivity ρ and the neutron generation time Λ (see Appendix A, Eqs. (A.16) and (A.17)), this can also be written as:

$$\frac{d\varphi}{dt} = \frac{\rho - \beta_{eff}}{\Lambda} \varphi + v S_d \quad (3.1.6)$$

The envisaged oscillation frequency f of the fuel volume sequence $V_{fuel}(t)$ (and, consequently, of n_{rel}) is so high (≈ 50 Hz) that the oscillation period τ is much shorter than the half-life of the shortest living delayed neutron precursor (≈ 0.23 s; see Appendix B, Table B.4). It seems physically reasonable that in this period of a few oscillations the delayed neutron precursors (which are generated in the core) will be homogeneously distributed over the entire fuel gas volume [Dam88, Kui89a, Kui89b], which means that the -homogeneous- delayed neutron source density is given by:

$$S_d = \frac{1}{V_{fuel}} \sum_{i=1}^6 \lambda_i C_i \quad (3.1.7)$$

(C_i = number of delayed neutron precursors of delayed group i ; λ_i = decay constant of delayed neutron precursors of delayed group i ; see Table B.4). The balance equation of the delayed neutron precursors of delayed group i reads:

$$\frac{dC_i}{dt} = \beta_{eff,i} \eta \Sigma_a n_{rel} V_{core} \varphi - \lambda_i C_i \quad (3.1.8)$$

($\beta_{eff,i}$ = effective delayed neutron fraction for delayed neutron precursors of delayed group i ; delayed neutron precursors are generated in the core, hence V_{core}). According to Eq. (A.12) (Appendix A), the total fission power is given by:

$$P_{fiss}(t) = \frac{Q_f}{v_f} \eta \Sigma_a n_{rel}(t) V_{core} \varphi(t) \quad (3.1.9)$$

(v_f = average number of neutrons released per fission event; Q_f = average thermal energy produced per fission event; only fuel gas in the core takes part in the fission chain reaction, hence V_{core}). Using Eqs. (3.1.6), (3.1.7), (3.1.8) and (3.1.9), we derive:

$$\frac{dP_{fiss}}{dt} = \left[\frac{\rho - \beta_{eff}}{\Lambda} + \frac{1}{n_{rel}} \frac{dn_{rel}}{dt} \right] P_{fiss} + \frac{Q_f V_{core}}{v_f V_{fuel} \Lambda} \sum_{i=1}^6 \lambda_i C_i \quad (3.1.10)$$

And:

$$\frac{dC_i}{dt} = \frac{v_f \beta_{eff,i}}{Q_f} P_{fiss} - \lambda_i C_i \quad i = 1, \dots, 6 \quad (3.1.11)$$

It is also possible to derive these equations, starting from a more general one-

group/two-compartment description of the neutron kinetics. This is shown in Appendix D.

Following van Dam [Dam88], we assume that the fission power P_{fiss} and the number of delayed neutron precursors C_i can be written as a product of a periodic component ($P'(t)$ and $C_i'(t)$), respectively; period τ) and a trend component ($e^{\omega t}$):

$$P_{fiss}(t) = P'(t) e^{\omega t} \quad (3.1.12)$$

And:

$$C_i(t) = C_i'(t) e^{\omega t} \quad i = 1, \dots, 6 \quad (3.1.13)$$

($\omega = 1 / T$; $T =$ reactor period). Combining Eqs. (3.1.11), (3.1.12) and (3.1.13) and averaging over an oscillation period τ renders:

$$\langle C_i' \rangle_\tau = \frac{v_i \beta_{eff,i}}{Q_i} \frac{\langle P' \rangle_\tau}{\omega + \lambda_i} \quad i = 1, \dots, 6 \quad (3.1.14)$$

($\langle \dots \rangle_\tau =$ average over oscillation period τ). Because of the high oscillation frequency, the number of delayed neutron precursors will not follow the oscillations. We therefore can approximate [Dam88]: $C_i' \approx \langle C_i' \rangle_\tau$. Applying this approximation, we can derive a single equation for the oscillatory component P' of the fission power P_{fiss} :

$$\frac{dP'}{dt} = \left[\frac{\rho - \beta_{eff}}{\Lambda} - \frac{1}{V_{fuel}} \frac{dV_{fuel}}{dt} - \omega \right] P' + \frac{V_{core} \langle P' \rangle_\tau}{V_{fuel} \Lambda} \sum_{i=1}^6 \frac{\beta_{eff,i} \lambda_i}{\omega + \lambda_i} \quad (3.1.15)$$

For a given value of ω (or the desired reactor period $T = 1 / \omega$), and a given, periodic, fuel volume sequence $V_{fuel}(t)$ ($V_{fuel}(\tau) = V_{fuel}(0)$), the total fuel gas mass m_{tot} , which is proportional to $n_{rel,0}$, is adjusted iteratively, until $P'(\tau) = P'(0)$. The fission power P_{fiss} is then known as a function of time [Kui89a, Kui89b]. Examples of the solution of P_{fiss} for several pumping schemes $V_{fuel}(t)$ will be shown in Chapter 5. It is also possible to solve Eqs. (3.1.10) and (3.1.11) directly by numerical integration, as was done by Stekelenburg in his GCFR simulators [Stek88, Stek90].

3.2 Point kinetics for two-compartment GCFR model

In the "two-compartment" GCFR model, to be presented in Chapter 7, we assume the cylindrical gas space of the GCFR (total volume V_{tot}) to consist of two compartments of equal volume: the core (V_{core}) and the expander (V_{exp}):

$$V_{core} = V_{exp} = V_1 = V_2 = \frac{1}{2} V_{tot} \quad (3.2.1)$$

Like in the final example treated in Section 2.2.2, for a given average relative density n_{rel} of the fuel gas, which is proportional to the total mass m_{tot} of the fuel gas, the relative densities in core and expander are given by:

$$n_{rel,1} = n_{rel}(1 + \varepsilon) \quad (3.2.2a)$$

$$n_{rel,2} = n_{rel}(1 - \varepsilon) \quad (3.2.2b)$$

(ε = density distribution variable; also see Eqs. (2.2.27) and (2.2.28)).

In one-group/two-compartment approximation the time-dependent multi-compartment neutron transport equation for this system reads, including delayed neutrons (see Appendix A, Eq. (A.4) and Appendix D, Eq. (D.1)):

$$\underline{V}_M \cdot \frac{1}{v} \frac{d\boldsymbol{\varphi}}{dt} = (1 - \beta_{eff}) \underline{F}(\varepsilon) \cdot \underline{V}_M \cdot \boldsymbol{\varphi} + \underline{E}(\varepsilon) \cdot \underline{V}_M \cdot \boldsymbol{\varphi} + \underline{V}_M \cdot \underline{f}_d(\varepsilon) S_d \quad (3.2.3)$$

(v = neutron velocity; \underline{F} = fission matrix; \underline{E} = absorption-, scatter- and transport matrix; $\boldsymbol{\varphi} \equiv (\varphi_1, \varphi_2)^T$ = time-dependent neutron flux vector; S_d = average delayed neutron source density; \underline{f}_d = distribution of delayed neutron sources over core and expander; dimensionless; superscript "T" denotes transposed vector or matrix). The -average- delayed neutron source density is given by:

$$S_d = \frac{1}{V_{tot}} \sum_{i=1}^6 \lambda_i C_i \quad (3.2.4)$$

(C_i = number of delayed neutron precursors of delayed group i ; λ_i = decay constant of delayed neutron precursors of delayed group i ; 6 delayed neutron precursor time groups; see Appendix B, Table B.4). From Eq. (3.2.3) the corresponding time-independent one-group/two-compartment neutron transport and adjoint equations can be derived (see Appendix A, Eqs. (A.8) and (A.15), and Appendix D, Eq. (D.4)), with -fundamental- eigenvectors $\boldsymbol{\varphi}_0 \equiv (\varphi_{0,1}, \varphi_{0,2})^T$ (static neutron flux vector) and $\boldsymbol{\varphi}_0^+ \equiv (\varphi_{0,1}^+, \varphi_{0,2}^+)^T$ (adjoint function vector), respectively.

We assume that, at any moment, the higher order neutronic mode components in the neutron flux are negligible compared to the fundamental mode (see Section 3.3), so that the time-dependent neutron flux can be written as:

$$\boldsymbol{\varphi} = \boldsymbol{\varphi}_0 \Omega(t) \quad (3.2.5)$$

(Ω = dimensionless function of time). Assuming that both the static neutron flux vector $\boldsymbol{\varphi}_0$ and the adjoint function vector $\boldsymbol{\varphi}_0^+$ are strictly time-independent (see Appendix D), we can write:

$$\frac{d\boldsymbol{\varphi}}{dt} = \boldsymbol{\varphi}_0 \frac{d\Omega}{dt} \quad (3.2.6)$$

By multiplying both sides of Eq. (3.2.3) by $(\boldsymbol{\varphi}_0^+)^T$, substituting the expressions for the reactivity ρ and the neutron generation time Λ from Appendix A (Eqs. (A.16) and (A.17); fundamental eigenvectors $\boldsymbol{\varphi}_0$ and $\boldsymbol{\varphi}_0^+$) and applying Eq. (3.2.6) we obtain:

$$\frac{d\Omega}{dt} = \frac{\rho - \beta_{eff}}{\Lambda} \Omega + \frac{1}{\Lambda} \frac{(\boldsymbol{\varphi}_0^+)^T \cdot \underline{V}_M \cdot \underline{f}_d}{(\boldsymbol{\varphi}_0^+)^T \cdot \underline{E} \cdot \underline{V}_M \cdot \boldsymbol{\varphi}_0} S_d \quad (3.2.7)$$

According to Eq. (A.12) the total fission power generated in this system is given by:

$$P_{fiss}(t) = \frac{Q_f}{v_f} \eta \sum_a [n_{rel,1}(\varepsilon) V_1 \varphi_{0,1} + n_{rel,2}(\varepsilon) V_2 \varphi_{0,2}] \Omega(t) \quad (3.2.8)$$

(Q_f = average thermal energy produced per fission event; v_f = average number of neutrons released per fission event). The normalization of the static flux vector is assumed to be chosen in such a way that the term between square brackets ("[...]") is independent of the density distribution variable ε . This means that, in the static calculation, the total fission neutron production rate in the system is assumed to be constant. This is e.g. the case in the numerical static neutronic calculations by XSDRNPM, ANISN(E), ANISN and CITATION, presented in Chapter 2.

We now assume that, at any moment, the relative source strength distributions of prompt and delayed neutrons are equal, so that:

$$\frac{1}{V_{tot}} \underline{V}_M \cdot \underline{f}_d = \frac{\underline{F} \cdot \underline{V}_M \cdot \underline{\varphi}_0}{\eta \sum_a n_{rel} [(1 + \varepsilon) V_1 \varphi_{0,1} + (1 - \varepsilon) V_2 \varphi_{0,2}]} \quad (3.2.9)$$

For a spatially flat flux (i.e. $\varphi_{0,1} = \varphi_{0,2}$) this is equivalent to the assumption of homogeneously mixed delayed neutron precursors. This is physically reasonable in the application of this neutron kinetics model in the combined "two-compartment" GCFR model (Chapter 7), as the envisaged oscillation frequency of ε is so high (≈ 30 Hz) that the oscillation period τ is much shorter than the half-life of the shortest living delayed neutron precursor (≈ 0.23 s; see Appendix B, Table B.4). However, even in the case of the symmetric cylindrical GCFR (Section 2.4, case "1", and Chapter 7) the neutron flux is not exactly spatially flat, and therefore Eq. (3.2.9) is not fulfilled exactly, not even with homogeneously mixed delayed neutron precursors. For our GCFR models we expect, however, that the assumption of homogeneously mixed delayed neutron precursors still provides a good approximation for the requirement stated in Eq. (3.2.9).

Therefore, using Eqs. (3.2.7), (3.2.8) and (3.2.9), we can derive the following equation for the produced fission power as a function of time:

$$\frac{dP_{fiss}}{dt} = \frac{\rho - \beta_{eff}}{\Lambda} P_{fiss} + \frac{Q_f}{v_f \Lambda} \sum_{i=1}^6 \lambda_i C_i \quad (3.2.10)$$

And the balance equations for the delayed neutron precursors read (like Eq. (3.1.11)):

$$\frac{dC_i}{dt} = \frac{v_f \beta_{eff,i}}{Q_f} P_{fiss} - \lambda_i C_i \quad i = 1, \dots, 6 \quad (3.2.11)$$

It is also possible to derive these equations, starting from a somewhat more general description of one-group/two-compartment neutron kinetics. This is shown in Appendix D.

According to Eq. (A.13) (Appendix A), the fission power generated in the core (P_{core}) and expander (P_{exp}) are given by, respectively:

$$P_{core}(t) = f_p(\varepsilon) P_{fiss}(t) \quad (3.2.12a)$$

$$P_{exp}(t) = [1 - f_p(\varepsilon)] P_{fiss}(t) \quad (3.2.12b)$$

(f_p = core fission power fraction; see Section 2.2.2).

In the "two-compartment" GCFR model (Chapter 7), Eqs. (3.2.10), (3.2.11), (3.2.12a) and (3.2.12b) are combined with equations describing the gas dynamical behaviour of the system (density distribution variable $\varepsilon(t)$; fixed value of n_{rel} , which is proportional to the total mass of the fuel gas m_{tot}). In the application of this neutron kinetics model in the combined "two-compartment" GCFR model, the delayed neutron contribution (Eq. (3.2.11)) is assumed to depend on the cycle-averaged total fission power $\langle P_{fiss} \rangle_\tau$ (oscillation period $\tau = 1/\eta$ only, as the envisaged oscillation period ($\tau \approx 0.02$ s) is much shorter than the half-life of the shortest living delayed neutron precursors ($T_{1/2} = 0.23$ s; see Appendix B, Table B.4).

3.3 Accuracy of point kinetics models

In Section 3.2 we assumed that, at any moment, the higher order mode components of the neutron flux are negligible compared to the fundamental mode. This means that the rate constants of the higher order modes (ω_i ; $i > 0$) must be -algebraically- small compared to the rate constant of the fundamental neutronic mode (ω_0) and that the difference in rate constant between the fundamental mode and the higher order modes must be large, compared to the frequency of the density oscillations in the fuel gas. In this section we will estimate the difference in rate constant between the fundamental mode and the first higher order mode (modes of higher order have -algebraically- smaller rate constants: $\omega_{i+1} < \omega_i$ for a cylindrical GCFR (in one-group/two-compartment approximation).

Like in the one-group/two-compartment GCFR kinetics model treated in Section 3.2, we assume that the cylindrical gas space (volume V_{tot} ; length L_{gas} ; cross sectional area $S_{gas} = \pi R_{gas}^2$; radius R_{gas}) consists of two compartments of equal volume ($V_1 = V_2 = 0.5 V_{tot}$, so $K_{1 \rightarrow 2} = K_{2 \rightarrow 1} = K_c$; length $L_{gas}/2$). We further assume: (I) a spatially flat fuel gas density distribution ($n_{rel,1} = n_{rel,2} = n_{rel}$); (II) a symmetrical or asymmetrical GCFR (see Section 2.2: $K_{1 \rightarrow 0} = K_0$; $K_{2 \rightarrow 0} = K_0(1 + \delta_{th})$); (III) prompt fission neutrons only; (IV) separability of the neutron flux in time and "position":

$$\underline{\varphi}(t) = (\varphi_1, \varphi_2)^T e^{\omega t} \quad (3.3.1)$$

The one-group/two-compartment time-dependent neutron transport equation (Appendix A, Eq. (A.4)) for this system can then be written as:

$$\frac{\omega}{v} \varphi_1 = [(\eta - 1) \Sigma_a n_{rel} - K_0 - K_c] \varphi_1 + K_c \varphi_2 \quad (3.3.2a)$$

$$\frac{\omega}{v} \varphi_2 = [(\eta - 1) \Sigma_a n_{rel} - K_0(1 + \delta_{th}) - K_c] \varphi_2 + K_c \varphi_1 \quad (3.3.2b)$$

In order for this system of equations to have a non-trivial solution, the following requirement (on ω) must be met:

$$\left[(\eta - 1) \Sigma_a n_{rel} - K_0 - K_c - \frac{\omega}{v} \right] \left[(\eta - 1) \Sigma_a n_{rel} - K_0(1 + \delta_{th}) - K_c - \frac{\omega}{v} \right] - [K_c]^2 = 0 \quad (3.3.3)$$

Solving Eq. (3.3.3) renders two possible values for the rate constant (or time eigenvalue) ω , corresponding to the fundamental neutronic mode (ω_0 ; $\varphi_1, \varphi_2 > 0$) and the first higher order mode (ω_1 ; φ_1 and φ_2 have opposite sign), respectively:

$$\omega_0 = \nu \left[(\eta - 1) \Sigma_a n_{ref} - K_0 \left(1 + \frac{1}{2} \delta_{th} \right) - K_c + \frac{1}{2} \sqrt{\delta_{th}^2 K_0^2 + 4 K_c^2} \right] \quad (3.3.4a)$$

$$\omega_1 = \nu \left[(\eta - 1) \Sigma_a n_{ref} - K_0 \left(1 + \frac{1}{2} \delta_{th} \right) - K_c - \frac{1}{2} \sqrt{\delta_{th}^2 K_0^2 + 4 K_c^2} \right] \quad (3.3.4b)$$

The difference in rate constant between the fundamental mode and the first higher order mode is then given by:

$$\Delta \omega \equiv \omega_0 - \omega_1 = \nu \sqrt{\delta_{th}^2 K_0^2 + 4 K_c^2} \quad (3.3.5)$$

In the following we assume a symmetric GCFR (so $\delta_{th} = 0$). For a numerical value of $\Delta \omega$, we must estimate K_c . In the one-group diffusion approximation (see e.g. [Dud76]) the net neutron current from compartment 1 ("core") to compartment 2 ("expander") is given by:

$$J = -D \frac{\partial \varphi}{\partial x} \quad (3.3.6)$$

(D = thermal neutron diffusion coefficient in the gas; φ = neutron flux; x = axial coordinate). The flux gradient at the interface between the compartments can be approximated by:

$$\frac{\partial \varphi}{\partial x} \approx \frac{\varphi_2 - \varphi_1}{\frac{1}{2} L_{gas}} \quad (3.3.7)$$

In the two-compartment description, the net neutron transport from compartment 1 ("core") to compartment 2 ("expander") is given by:

$$J S_{gas} = V_1 K_{1 \rightarrow 2} \varphi_1 - V_2 K_{2 \rightarrow 1} \varphi_2 = V_1 K_c (\varphi_1 - \varphi_2) \quad (3.3.8)$$

(see Appendix A). We can now derive an approximated-expression for K_c in terms of the thermal neutron diffusion coefficient D and the length of the cylindrical gas space L_{gas} :

$$K_c \approx \frac{4D}{L_{gas}^2} \quad (3.3.9)$$

For the symmetrical GCFR in critical state (with spatially flat fuel gas distribution), for which (see Chapter 2 and Appendix B): $\nu = 4761 \text{ m s}^{-1}$ (thermal group velocity), $L_{gas} = 10 \text{ m}$ and $D = 2.86 \text{ m}$, we find: $\Delta \omega = 1090 \text{ s}^{-1}$. This is an order of magnitude larger than the characteristic density oscillation frequency in our GCFR (approximately 30 Hz), which is an indication that we may neglect the influence of the higher order neutronic modes in the neutron kinetics model for our GCFR, at least in the symmetric case ("I"). For the ("slightly") asymmetric GCFRs (cases "II" and "III") the value for $\Delta \omega$ will be smaller, because D will be smaller due to the necessary increase in n_{ref} to achieve criticality. But in those cases also δ_{th} will be > 0 , because the wall around the expander is assumed to be thinner, and therefore less effective as a neutron reflector, than the wall around the core. This again causes an increase in $\Delta \omega$, according to Eq. (3.3.5).

Chapter 4

REACTOR GAS THERMODYNAMICS

4.1 Reactor gas composition

One of the main characteristics of our GCFR is that the graphite reflector wall is part of the chemical system. This means that this wall, in order to stay intact (at least on average), must be in chemical and thermodynamical equilibrium with the reactor gas mixture, which consists of uranium, carbon and fluorine (UCF). This chemical solid-gas system was thoroughly investigated by Klein [Kle87, Boe90a], using the computer codes SOLGASMIX and SAGE (calculation method: Gibbs free energy minimization [Eri75, Eri89]). It was found that a graphite wall at 2000 K will be in equilibrium with a gas mixture, consisting of 20.5 % CF_4 , 54.5 % UF_5 and 25 % UF_4 (molar) at a pressure of 25 bar. This composition is, at a temperature of 2000 K, not sensitively dependent upon the pressure [Kle87] and corresponds to a ratio of atomic densities in the gas of $[\text{U}]:[\text{C}]:[\text{F}] = 0.70 : 0.18 : 4.00$. If the wall temperature increases, the relative amount of carbon in the equilibrium gas mixture increases as well, which means corrosion of the wall [Kle87, Boe90a]. So, in all of our investigations we assumed the temperature at the gas-solid interface to be kept constant at 2000 K (and the reflector bulk temperature at $T_{refl} = 1000$ K: RSG conditions; see Chapter 2), and the ratio of atomic densities in the fuel gas to be as specified above. At 2000 K and 25 bar (the reference conditions for the UCF gas) the molar mass of the UCF gas is then $M_0 = 0.277$ kg.

In our GCFR, where the envisaged bulk temperature of the gas is much higher than 2000 K (RSG: $T_{core} = 10,000$ K), this is the situation within a few mm off the wall, as a strong temperature gradient exists in the gas close to the wall [Kle87, Hoo91], and an increase of temperature causes dissociation of UF_5 , UF_4 and CF_4 into lower valent uranium- and carbon fluorides [Kle87, Boe89b, Boe90b]. Keeping the ratio of atomic densities at the value specified above, Klein calculated, using the computer codes SOLGASMIX and SAGE, the (molecular) composition of the fuel gas for various temperatures (between 2000 and 10,000 K) and pressures (between 1 and 100 bar) [Kle87]. In Figure 4.1 (major components) and Figure 4.2 (minor components, ions and electrons) the equilibrium molecular composition of the UCF gas is shown as function of the temperature for a pressure of 10 bar. Note that, for increasing temperature, first dissociation of UF_5 and CF_4 occurs, causing an initial increase in the amount of UF_4 . When the temperature increases further, also the UF_4 dissociates. At higher temperatures (above approximately 5000 K) we also see ions and free electrons becoming part of the equilibrium mixture, which increases the electrical conductivity of the gas [Kle87, Boe89b]. This is favourable in view of the envisaged magneto-hydrodynamical (MHD) or magneto-inductive (MI) energy extraction from a GCFR in oscillatory operation.

In a GCFR in oscillatory operation, the -bulk- temperature and the pressure of the fuel gas change with time. Consequently, the equilibrium composition of the gas also must change with time. However, at the envisaged reactor gas temperatures the necessary chemical reactions take place extremely rapidly (half-

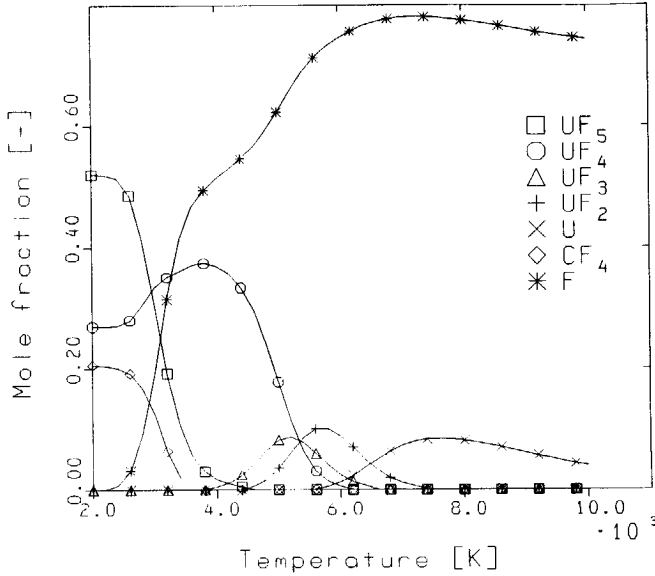


Figure 4.1 Equilibrium composition of UCF gas at a pressure of 10 bar (major components).

life 10^{-7} to 10^{-9} s [Kle87, Boe90a]). So, in view of the envisaged time scale of the pressure- and temperature variations in our GCFR (about 0.02 s), we may consider the equilibrium molecular composition of the gas to be attained instantaneously.

4.2 Reactor gas properties

As we have seen in Section 4.1, the composition of the UCF fuel gas mixture changes with temperature T and pressure p , due to dissociation, recombination and ionization. As a consequence, the total amount of gas particles (molecules, ions, electrons) $N(p, T)$ (mole) also changes with temperature and pressure. From the calculations of the equilibrium compositions [Kle87] the total number of particles at given temperature and pressure can be calculated easily (given the amount of gas N_0 (mole) at the reference temperature, 2000 K, and pressure, 25 bar; $N_0 = 1$ ("original") mole corresponds to $m_{tot} = M_0$). The Equation Of State ("EOS") of the UCF gas is then given by [Kle87, Kui89a, Kui89b, Kui91a]:

(gas volume V ; universal gas constant $R = 8.3144 \text{ J K}^{-1} \text{ mole}^{-1}$). In Figure 4.3 the so-called dissociation function g of the UCF gas is given as a function of the temperature T at pressures of 1, 10 and 100 bar. Contrary to the case of a perfect gas (for which $g \equiv 1$), the pressure increases more than proportionally with the temperature (at constant volume), e.g. by going from 2000 to 10,000 K, the

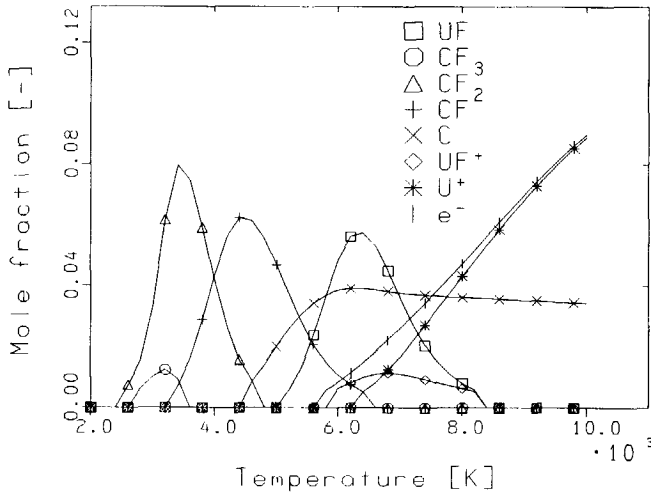


Figure 4.2 Equilibrium composition of UCF gas at a pressure of 10 bar (minor components, ions and electrons).

pressure increases from 3 to 100 bar. In Figure 4.3 also the dissociation function of "Modelium" is shown. "Modelium" is a model gas, which is an intermediate step between non-dissociating perfect gas and UCF gas (see Section 4.4).

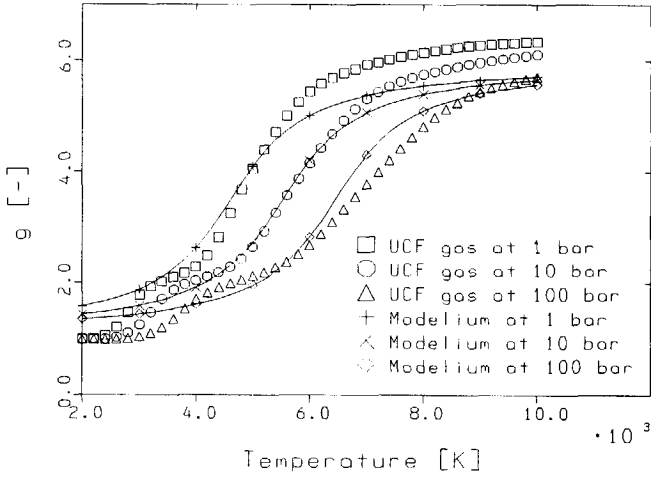


Figure 4.3 Dissociation functions g (i.e. $N(p, T) / N_0$) of UCF gas and Modelium at pressures of 1, 10 and 100 bar.

As can be seen in Figure 4.3, UCF exhibits two major dissociation regions

when its temperature is increased from 2000 to 10,000 K. For $p = 1$ bar, the first region (dissociation of UF_5 and CF_4 ; see Figure 4.1) occurs at approximately 3000 K and the second one (dissociation of UF_4 and lower valent uranium- and carbon fluorides) at approximately 5000 K. These regions shift towards higher temperatures if the pressure is increased, i.e. increasing pressure suppresses dissociation.

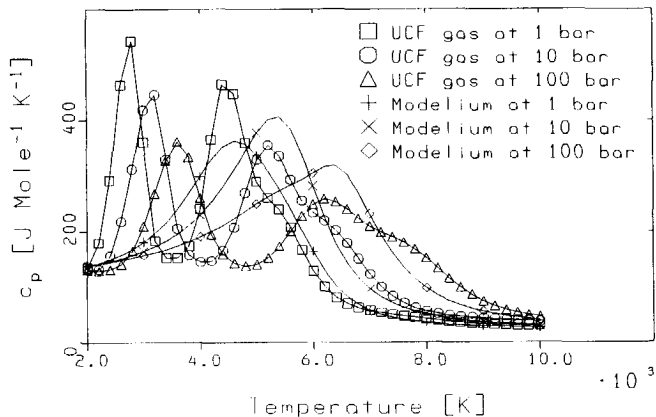


Figure 4.4 Specific heat at constant pressure c_p for UCF and Modelium as function of temperature at pressures of 1, 10 and 100 bar.

The thermodynamical complexity of the UCF gas is also reflected in the internal energy U and the specific heats of the gas at constant volume, c_v , and pressure, c_p . These quantities also resulted from the calculations by SOLGASMIX and SAGE [Kle87, Boe89a, Boe90b]. In Figures 4.4 and 4.5 the specific heat at constant pressure c_p and the c_p/c_v -ratio κ of UCF gas (and Modelium) are shown as a function of the temperature T at pressures of 1, 10 and 100 bar. Note that these curves exhibit local maxima in the neighbourhood of the dissociation regions mentioned above. At high temperatures (fully dissociated state) c_p and κ approach the values for a monatomic perfect gas (i.e. $c_p = (5/2)R$ and $\kappa = (5/3)$, respectively).

Klein also calculated many other parameters of the UCF gas, such as degree of ionization, electrical conductivity, thermal conductivity and viscosity, which are of importance for GCFR operation [Kle87, Boe89b, Boe91a, Boe91b]. For pressures between 1 and 100 bar, the dynamic viscosity varies between $0.75 \cdot 10^{-4}$ (for $T = 2000$ K) and $1.6 \cdot 10^{-4} \text{ kg m}^{-1} \text{ s}^{-1}$ (for $T = 6000$ K). The thermal conductivity λ_{th} (including translational, reactive and internal contributions [Boe91a, Boe91b]) varies between 0.05 and $1 \text{ W m}^{-1} \text{ K}^{-1}$. Like the specific heats c_p and c_v , the thermal conductivity λ_{th} (as function of T) exhibits local maxima in the vicinity of the dissociation regions mentioned above.

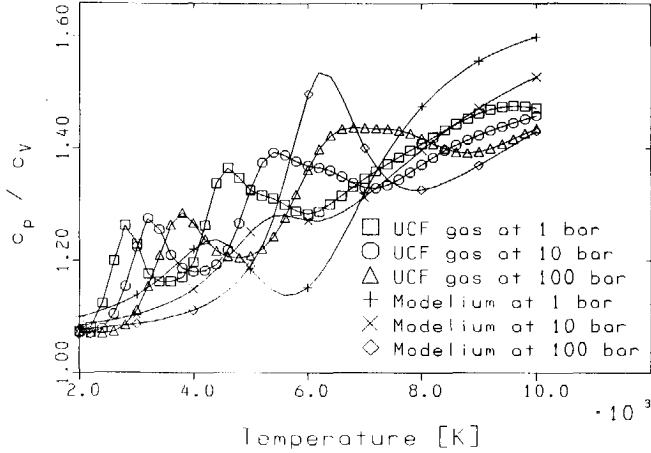


Figure 4.5 Ratio of specific heats $\kappa \equiv c_p / c_v$ of UCF and Modelium as function of temperature at pressures of 1, 10 and 100 bar.

4.3 Heat transport

In a GCFR, all the heat that is produced in the gas by nuclear fissions, and that is not extracted by "direct" means (such as MHD and MI), will be transported to the wall, surrounding the gas, and can subsequently be used as "input" for a more conventional energy conversion system (such as a steam cycle or -possibly- a thermionic converter [Wol90]). Van Dam and Hoogenboom [Dam83] elaborated a model, developed by Kerkdijk and Kistemaker [Ker78], for the description of this heat transport (radiative transport by photon diffusion) from the fissioning gas to the wall in a stationary GCFR.

The basic equations for radiative transport by photon diffusion read [Ker78, Dam83]:

$$\underline{j}_{q,rad}(\underline{r}) = -D_{ph}(\underline{r}) \nabla u(\underline{r}) \quad (4.3.1a)$$

with:

$$u(\underline{r}) = \frac{4 \sigma_{SB}}{c_{ph}} T^4(\underline{r}) \quad (4.3.1b)$$

and:

$$D_{ph}(\underline{r}) = \frac{c_{ph} \lambda_{ph}(\underline{r})}{3} = \frac{c_{ph}}{3 \sigma_{ph} N_A n(\underline{r})} \quad (4.3.1c)$$

($\underline{j}_{q,rad}(\underline{r})$ = radiative heat flux density vector (dimension: [W m⁻²]) at position \underline{r} ;
 $D_{ph}(\underline{r})$ = radiative diffusion coefficient (dimension: [m² s⁻¹]); $u(\underline{r})$ = radiation density (dimension: [J m⁻³]); c_{ph} = velocity of light (= 299,792,458 m s⁻¹); σ_{SB} = Stefan-Boltzmann's constant (= 5.67 · 10⁻⁸ W m⁻² K⁻⁴); $\lambda_{ph}(\underline{r})$ = photon mean free path;
 σ_{ph} = average photon absorption cross section for white light (= 2.5 · 10⁻²¹ m²)

[Par68]); N_A = Avogadro's number (= $6.022 \cdot 10^{23}$ mole⁻¹); $n(r)$ = gas density (dimension: [mole m⁻³]).

In the model they assumed: (I) a stationary GCFR (i.e. the total produced fission power P_{fis} is equal to the radiative heat transport P_{rad} to the wall), (II) a one-dimensional GCFR geometry (i.e. sphere, infinite cylinder or infinite slab; geometry parameter $q = 2, 1$ or 0 , respectively), (III) a perfect gas (dissociation function $g \equiv 1$ in Eq. (4.2.1)), (IV) a uniform pressure p (and consequently a gas density $n(r)$ varying with the temperature $T(r)$), and (V) a spatially flat neutron flux (so that the fission power density $Q_{fis}(r) \sim n(r)$), and arrived at the following equation for the temperature profile in the fissioning gas:

$$4 T^4 \left[\frac{dT}{dz} \right] + T^5 \left[\frac{d^2T}{dz^2} + \frac{q}{z} \frac{dT}{dz} \right] = - \frac{3 \sigma_{ph}}{16 k^2 \sigma_{SB} N_A} \times \frac{P_{fis} R_{core}^2 p^2}{N} \equiv -\alpha \quad (4.3.2a)$$

($z = r / R_{core}$ = reduced coordinate; R_{core} = radius of sphere ($q = 2$) or cylinder ($q = 1$), or slab halfwidth ($q = 0$); k = Boltzmann's constant = $1.38 \cdot 10^{-23}$ J K⁻¹; N = total amount of gas (mole)). The boundary conditions for this equation are:

$$T(z=1) = T_{wall} \quad (4.3.2b)$$

(fixed wall temperature)

$$\frac{dT}{dz}(z=0) = 0 \quad (4.3.2c)$$

(symmetry)

Eq. (4.3.2a) was solved numerically by Uleman, van Dam and Hoogenboom [Ule82, Dam83], rendering the temperature profile $T(r)$ for given values of the total fission power P_{fis} and the amount of gas N . The solutions show a rather flat temperature distribution over a large part of the core gas and a steep temperature gradient, and therefore an increased density, close to the wall: a dense gas layer protecting the wall [Kis78a]!

An approximative analytical solution, which was also given by van Dam and Hoogenboom [Dam83], can be obtained by changing the coefficient of the first term of Eq. (4.3.1) to 5, resulting in:

$$T^6(z) = \frac{3\alpha}{q+1} + T_{wall}^6 \quad (4.3.3)$$

This, however, is not an explicit expression for the temperature, because the parameter α contains the square of the pressure, which is temperature dependent.

In view of the development of our combined GCFR models we are interested in the radiative heat transfer in terms of the bulk temperature of the gas. Therefore, following van Dam and Hoogenboom [Dam83], we introduce an effective temperature T_{eff} , which is the hypothetical uniform core gas temperature which would give the correct pressure for a given N (also the bulk temperature). So:

$$pV = NRT_{eff} \quad (4.3.4)$$

(V = core gas volume). For "normal" (high enough) power densities the centre temperature T_0 (at $z = 0$) can be approximated by:

$$T_0 = \left[\frac{3\alpha}{q+1} \right]^{1/6} \quad (4.3.5)$$

According to van Dam and Hoogenboom [Dam83], the ratio $\Theta \equiv T_{eff} / T_0$ only varies in a limited range. For an infinite cylinder, Θ varies from 5/6 (for very high α) to 1 (for $\alpha = 0$: $T_{eff} = T(r) = T_{wall}$). We can now derive an expression for the radiative energy transport to the wall of a stationary one-dimensional GCFR, in terms of the effective temperature of the fuel gas [Stek88]:

$$P_{rad} = P_{fiss} = \frac{16 \sigma_{SB} (q+1)}{9 \sigma_{ph} N_A \Theta^6 R_{core}^2} \frac{V^2 T_{eff}^4}{N} \quad (4.3.6)$$

This expression was used by Stekelenburg [Stek88] to describe the radiative energy transport to the wall in his GCFR simulator. Because the core in that simulator model (and also in our "solid piston" model; see Chapter 5) is a finite cylinder, the numerical values for q and Θ were assumed to be between those of a sphere and an infinite cylinder, also $q = 1.5$ and $\Theta = 0.8130$ [Stek88, Dam83]. Eq. (4.3.6) can then be written as:

$$P_{rad} = C_{rad} \frac{V^2 T_{eff}^4}{N} \quad (4.3.7)$$

With $C_{rad} = 5.80 \cdot 10^{-10} \text{ W mole m}^6 \text{ K}^{-4}$ ($R_{core} = 1 \text{ m}$). We also used this in our "solid piston" GCFR model (Chapter 5).

Later the stationary heat transfer model was extended by taking into account the thermal conductivity (translational, reactive and internal components), (free) convection (by multiplying the thermal conductivity by a "convection factor" C) and the dissociation/recombination behaviour of the gas [Kle87, Kis89, Hoo91, Boe91b], leading to somewhat different temperature profiles (at the same total fission power), with lower values for T_0 and T_{eff} for a given value of P_{fiss} . However, for the sake of simplicity, in our combined GCFR models (see Chapters 5 and 7) we only assumed radiative heat transfer, which can be described by formulas like Eq. (4.3.7).

In the stationary heat transport model described above, the pressure p is assumed to be uniformly distributed (Uniform Pressure Diffusion Model, "UPDM" [Ker78]). A somewhat more simple approach, which was taken by Kerkdijk and Kistemaker as well [Ker78], is to assume a uniform gas density $n(r) = n$ (Uniform Density Diffusion Model, "UDDM"). Assuming a uniform density $n (= N / V)$, and retaining the other assumptions of the UPDM (I, II and III; see above), the following equation for the temperature profile in the fissioning gas of an infinite cylindrical GCFR ($q = 1$) can be derived:

$$3 T^2 \frac{dT}{dz} + T^3 \left[\frac{d^2 T}{dz^2} + \frac{1}{z} \frac{dT}{dz} \right] = - \frac{3 \sigma_{ph} N_A}{16 \sigma_{SB}} \times \frac{P_{fiss} R_{core}^2 N}{V^2} \quad (4.3.8)$$

Assuming the same boundary conditions (Eqs. (4.3.2b) and (4.3.2c)) as in the UPDM model, we find for the temperature profile:

$$\left(\frac{T(z)}{T_0}\right)^4 = 1 - z^2 \left[1 - \left(\frac{T_{wall}}{T_0}\right)^4\right] \quad (4.3.9)$$

The effective (in this case the volume-averaged) temperature is then given by:

$$T_{eff} = \frac{4}{5} \frac{T_0^5 - T_{wall}^5}{T_0^4 - T_{wall}^4} \quad (4.3.10)$$

So, for high T_0 we obtain: $T_{eff} / T_0 \equiv \Theta = 4/5$. For high T_0 the radiative heat transport from the gas to the wall is then given by:

$$P_{rad} = \frac{16 \sigma_{SB}}{3 \sigma_{ph} N_A \Theta^4 R_{core}^2} \frac{V \left(\frac{1}{2} R_{core} S_{out}\right) T_{eff}^4}{N} = C_{rad} \frac{V \left(\frac{1}{2} R_{core} S_{out}\right) T_{eff}^4}{N} \quad (4.3.11)$$

(S_{out} = area of the wall surrounding the gas). For a long cylinder, we have: $V \approx 0.5 (R_{core} S_{out})$, so in that case Eq. (4.3.11) reduces to Eq. (4.3.7), but with a different value of C_{rad} , viz. $4.90 \cdot 10^{-10} \text{ W mole}^{-1} \text{ m}^{-6} \text{ K}^{-4}$ ($R_{core} = 1 \text{ m}$). However, the values of C_{rad} found with the UPDM and UDDM radiative transport models differ by less than 20 %. We used the UDDM radiative transport model, viz. Eq. (4.3.11), in our combined "two-compartment" GCFR model (Chapter 7).

Besides the radial radiative heat transport, treated above, in the "two-compartment" combined GCFR model (cylindrical GCFR; see Chapter 7) also the axial heat transport P_{1-2} from core (compartment 1) to expander (compartment 2) is taken into account. In the combined "two-compartment" GCFR model the axial heat transport consists of two contributions: heat conduction and photon diffusion. Convection is not taken into account in the axial heat transport, because in the "two-compartment" description of the GCFR gas dynamics the fuel gas is assumed not to go through the movable "imaginary wall" (see Section 6.3) between the compartments. Applying the same description for the photon diffusion process as was used for the radial radiative heat transport (see [Ker78, Ule82, Dam83]), we can derive the following expression for the axial heat flux density:

$$J_{q,axial} = - \frac{4 \sigma_{SB}}{3 n N_A \sigma_{ph}} \frac{dT^4}{dx} - \lambda_{th} \frac{dT}{dx} \quad (4.3.12)$$

($J_{q,axial}$ = axial heat flux density; n = (average) gas density; λ_{th} = thermal conductivity; x = axial coordinate; derivatives with respect to x are taken at the interface of compartments 1 and 2). For a cylinder with length L_{gas} we can approximate:

$$\frac{dT^i}{dx} \approx \frac{T_2^i - T_1^i}{\frac{1}{2} L_{gas}} \quad (4.3.13)$$

($i = 1$ for heat conduction; $i = 4$ for photon diffusion). The axial heat transport from compartment 1 to compartment 2 can now be approximated by:

$$P_{1-2} = \frac{2 S_{gas}}{L_{gas}} \left[C_{rad,axial} (T_1^4 - T_2^4) + \lambda_{th} (T_1 - T_2) \right] \quad (4.3.14)$$

(S_{gas} = cross sectional area of the cylindrical gas space = $\pi R_{gas}^2 = \pi R_{core}^2$). If we assume that the average density is given by $n = N / V_{tot}$ (V_{tot} = total volume of the gas space = $S_{gas} L_{gas}$), then the constant $C_{rad,axial}$ can be written as:

$$C_{rad,axial} = \frac{4 V_{tot} \sigma_{SB}}{3 N N_A \sigma_{ph}} \quad (4.3.15)$$

If we further assume that the temperature and the pressure in both compartments are not too far from the mean temperature T and the mean pressure p of the entire gas space, we can approximate:

$$C_{rad,axial} = \frac{4 k \sigma_{SB} T}{3 \sigma_{ph} p} \quad (4.3.16)$$

E.g. $T = 10,000$ K and $p = 50$ bar renders: $C_{rad,axial} = 8.35 \cdot 10^{-13} \text{ W m}^{-1} \text{ K}^{-4}$.

4.4 Modelium

In Sections 4.1 and 4.2 we have seen that the UCF reactor gas exhibits a quite complicated thermodynamical behaviour, for which a description is only available in tabular form [Kle87, Boe89a]. We therefore developed the model gas "Modelium", which is an intermediate step between the non-dissociating perfect gas and the UCF gas [Kui89a, Kui89b, Kui91a]. As is the case with a perfect gas, its behaviour can be described by analytical functions. Contrary to UCF gas, which exhibits a "step-wise" dissociation behaviour in two dissociation regions, Modelium was designed to exhibit a smooth dissociation behaviour. Its dissociation function $g(p, T)$ is defined by [Kui89a, Kui89b, Kui91a]:

$$g(p, T) = C_1 + C_2 \arctan \left(\frac{T - C_4 \ln \frac{p}{p_{unit}}}{C_3} \right) \quad (4.4.1)$$

($p_{unit} = 1$ Pa). The values of the constants C_1, \dots, C_4 have been determined by fitting to the dissociation behaviour of UCF gas (see Table 4.1). As is shown in Figure 4.3 the dissociation behaviour of UCF gas is approximated quite accurately by Modelium, especially at intermediate temperatures and pressures.

Table 4.1 Modelium parameters.

C_1	3.50
C_2	1.59
C_3	1000 K
C_4	400 K
p_0	$2.5 \cdot 10^6$ Pa (25 bar)

A general thermodynamic relationship reads [Cal60]:

$$c_p - c_v = \frac{T}{N} \left(\frac{\partial p}{\partial T} \right)_v \left(\frac{\partial V}{\partial T} \right)_p = - \frac{T \left(\frac{\partial V}{\partial T} \right)_p^2}{N \left(\frac{\partial V}{\partial p} \right)_T} \quad (4.4.2)$$

The specific heats at constant pressure (c_p) and volume (c_v) are given by, respectively:

$$c_p = \frac{1}{N} \left(\frac{\partial H}{\partial T} \right)_p \quad (4.4.3a)$$

$$c_v = \frac{1}{N} \left(\frac{\partial U}{\partial T} \right)_v \quad (4.4.3b)$$

(H = enthalpy; U = internal energy = $H - pV$; $N = N_0 g(p, T)$; specific heat per "actual" mole). From this it can be derived that, for a general, dissociating gas:

$$\begin{aligned} N(c_p - c_v) &= \left(\frac{\partial V}{\partial T} \right)_p \left[\left(\frac{\partial U}{\partial p} \right)_T + p \left(\frac{\partial V}{\partial p} \right)_T \right] \left(\frac{\partial V}{\partial p} \right)_T^{-1} \\ &= \left(\frac{\partial V}{\partial T} \right)_p \left[\left(\frac{\partial H}{\partial p} \right)_T - V \right] \left(\frac{\partial V}{\partial p} \right)_T^{-1} \end{aligned} \quad (4.4.4)$$

The combination of Eqs. (4.4.2) and (4.4.4) renders:

$$\left(\frac{\partial H}{\partial p} \right)_T = V - T \left(\frac{\partial V}{\partial T} \right)_p \quad (4.4.5)$$

Combining Eq. (4.4.5) with Eqs. (4.2.1) and (4.4.1), we find for Modelium [Kui89a, Kui91a]:

$$\left(\frac{\partial H}{\partial p} \right)_T = - \frac{N_0 R T^2}{p} \left(\frac{\partial g}{\partial T} \right)_p = - \frac{N_0 R T^2}{C_4} \left(\frac{\partial g}{\partial p} \right)_T \quad (4.4.6)$$

From this an expression can be derived for the enthalpy H of an amount of N_0 "original" (i.e. non-dissociated) moles of Modelium:

$$H(p, T) = H_0(T) + \frac{N_0 R T^2}{C_4} [g(p, T) - g(p_0, T)] \quad (4.4.7)$$

As mentioned in Section 4.2, the curves for c_p and κ as function of T for UCF gas (Figures 4.4 and 4.5) exhibit local maxima in the vicinity of the dissociation regions. The enthalpy $H_0(T)$ at the reference pressure p_0 was chosen such that Modelium shows a similar behaviour, including the correct limits for high temperatures (fully dissociated state) [Kui89a, Kui89b, Kui91a]:

$$H_0(T) = 15 N_0 R T + N_0 R C_4 \left[\ln \frac{p_0}{p_{unit}} \right]^2 [g(p_0, T) - C_1] \quad (4.4.8)$$

In Figures 4.4 and 4.5 the behaviour of c_p and κ of Modelium as a function of the temperature T is shown for pressures of 1, 10 and 100 bar.

From Eqs. (4.4.7) and (4.4.8) analytical expressions for other thermodynamic variables can be derived in a straightforward manner. The internal energy of an amount of N_0 "original" moles of Modelium is e.g. given by:

$$U(\rho, T) = H(\rho, T) - N_0 R T g(\rho, T) \quad (4.4.9)$$

And the volume of the same amount of Modelium (i.e. its EOS) is given by:

$$V(\rho, T) = \frac{N_0 R T g(\rho, T)}{\rho} \quad (4.4.10)$$

Expressions for the specific heats c_v , c_p and the ratio of specific heats κ , which can be obtained by applying Eqs. (4.4.3a) and (4.4.3b), will be given in Section 4.5.

For a non-dissociating, perfect gas (dissociation function $g \equiv 1$) the expressions for the thermodynamic variables are much simpler, e.g.:

$$U(\rho, T) = U_0 + N_0 c_v T \quad (4.4.11)$$

(U_0 = internal energy at zero temperature; constant c_v).

4.5 Finite and infinitesimal thermodynamic cycles

With our "solid piston" GCFR model (Chapter 5) we performed thermodynamic cycle calculations for a predetermined volume sequence (or compression scheme) $V(t)$ (time t). In this section we will discuss some features of thermodynamic cycles. One of the compression schemes to be studied is a pseudo "Otto" scheme. An ideal Otto cycle consists of adiabatic compression, isochoric heating (i.e. heating of the working medium -the gas- at constant volume), adiabatic expansion and isochoric cooling in order to return to the initial state [Cal60]. The Otto scheme is the most efficient scheme for a system cycling between two preset volumes (V_{min} and V_{max}). In case of such an ideal Otto cycle, applied with a perfect (i.e. non-dissociating) gas, the work fraction (or efficiency) η is given by [Cal60]:

$$\eta = 1 - \left[\frac{1}{K} \right]^{\kappa-1} = 1 - \left[\frac{1}{K} \right]^{R/c_v} \quad (4.5.1)$$

($K = V_{max} / V_{min} =$ compression ratio). This is also an upper bound for the efficiencies that can be attained by non-ideal (Otto) cycles (for perfect- or non-perfect gases), such as in our "solid piston" GCFR model.

For non-perfect, dissociating gases there is no such simple expression for the work fraction of a finite (Otto) cycle. However, in order to gain a better understanding of our finite cycle calculation results with our "solid piston" GCFR model (with perfect and non-perfect gases), especially of the influence of the thermodynamic properties of the gas, we studied the so-called "infinitesimal Otto cycle" [Kui91a]. As shown in Figure 4.6, an infinitesimal Otto cycle is an Otto cycle in which variations of volume ΔV , pressure Δp and temperature ΔT are small, compared to the volume V , the pressure p and the temperature T at the Beginning Of the Cycle ("BOC"). The compression ratio K approaches 1 and the adiabatic compression and expansion phases can be approximated by straight lines in the $p(V)$ -diagram. The work fraction $\Delta\eta$ for such an infinitesimal cycle is then given by [Kui91a]:

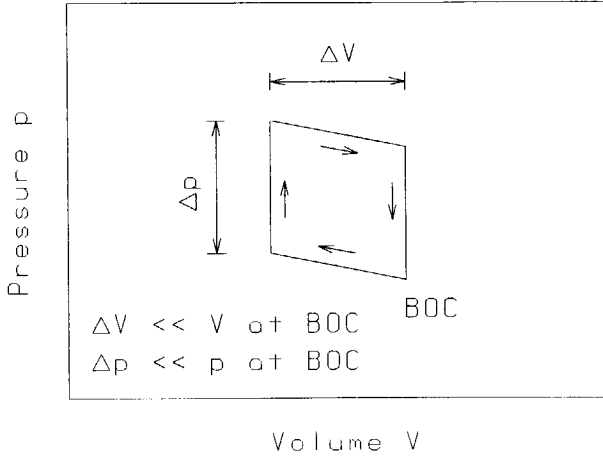


Figure 4.6 Pressure as function of volume for the infinitesimal Otto cycle.

$$\Delta\eta = -\frac{A_V(\rho, T) \Delta V}{D(\rho, T)} \quad (4.5.2)$$

with:

$$D(\rho, T) \equiv A_U(\rho, T) B_V(\rho, T) - B_U(\rho, T) A_V(\rho, T) \quad (4.5.3)$$

and:

$$\begin{aligned} A_V(\rho, T) &\equiv \left[\frac{\partial V}{\partial T} \right]_{\rho} & B_V(\rho, T) &\equiv \left[\frac{\partial V}{\partial \rho} \right]_T \\ A_U(\rho, T) &\equiv \left[\frac{\partial U}{\partial T} \right]_{\rho} & B_U(\rho, T) &\equiv \left[\frac{\partial U}{\partial \rho} \right]_T \end{aligned} \quad (4.5.4)$$

For Modelium, the derivatives A_U , A_V , B_U and B_V can be calculated in a straightforward manner from the expressions for $U(\rho, T)$ and $V(\rho, T)$ (Eqs. (4.4.9) and (4.4.10), respectively), for given values of the pressure ρ and the temperature T .

The so-called "infinitesimal efficiency factor" ζ of an infinitesimal Otto cycle is now defined as [Kui91a]:

$$\zeta \equiv \lim_{\Delta V \rightarrow 0} V \frac{\Delta\eta}{\Delta V} = \lim_{K \rightarrow 1} \Delta\eta(K) \frac{K}{K-1} \quad (4.5.5)$$

(compression ratio $K = V / (V - \Delta V)$). With Eq. (4.5.2), this can also be written as:

$$\zeta = -\frac{A_V(\rho, T) V(\rho, T)}{D(\rho, T)} \quad (4.5.6)$$

(EOS: $V(\rho, T)$). So, ζ is completely determined by the properties (EOS and $U(\rho, T)$) of the gas.

Applying Eqs. (4.4.3a) and (4.4.3b), we can write the specific heats c_p and c_v , and the c_p/c_v -ratio κ , for a dissociating gas in terms of the derivatives defined in Eqs. (4.5.3) and (4.5.4):

$$c_p = \frac{1}{g N_0} (A_U + p A_V) \quad (4.5.7a)$$

$$c_v = \frac{1}{g N_0} \left(A_U - \frac{B_U A_V}{B_V} \right) \quad (4.5.7b)$$

$$\kappa \equiv \frac{c_p}{c_v} = \frac{B_V (A_U + p A_V)}{D} \quad (4.5.7c)$$

Furthermore, from Eq. (4.4.5) the following expression can be derived, using Eq. (4.5.4):

$$B_U = -T A_V - p B_V \quad (4.5.8)$$

Using these expressions, the infinitesimal efficiency factor ζ can also be written as:

$$\zeta = \frac{V}{T A_V} (\kappa - 1) = - \frac{V A_V}{g N_0 B_V c_v} \quad (4.5.9)$$

For a (non-dissociating) perfect gas (constant c_v and κ) this simplifies to:

$$\zeta = \kappa - 1 = \frac{R}{c_v} \quad (4.5.10)$$

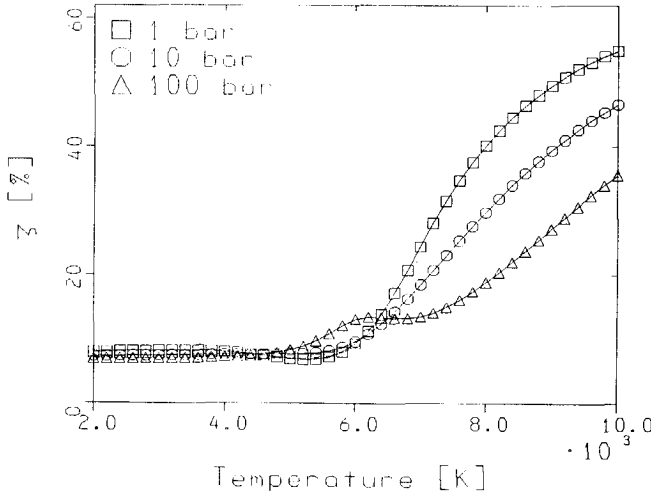


Figure 4.7 Infinitesimal efficiency factor ζ for Modelium as function of temperature at pressures of 1, 10 and 100 bar.

For Modelium it is also possible to derive a -quite complicated- analytical expression for ζ , e.g. using Eq. (4.5.9). In Figure 4.7 the infinitesimal efficiency factor for

Modelium is shown as function of temperature for pressures of 1, 10 and 100 bar. Note that below $T \approx 5000$ K, ζ is almost independent of temperature and pressure.

In Chapter 5, where we present our finite thermodynamic cycle calculations with the "solid piston" GCFR model, we will demonstrate that the infinitesimal efficiency factor ζ , which is completely determined by the gas only, provides a reasonable estimation η^* of the attainable work fraction η of a (finite) Otto cycle, according to:

$$\eta^* = \zeta \frac{K - 1}{K} \quad (4.5.11)$$

This also means that the infinitesimal efficiency factor ζ can be used to estimate those BOC conditions (temperature and pressure), where a finite cycle can be expected to render a maximal work fraction.

Chapter 5

SOLID PISTON GCFR MODEL

5.1 Introduction

The first combined model to be presented is the so-called "solid piston" GCFR model. The origin of this model is the asymmetric GCFR with magneto-inductive (MI) energy extraction, as is shown in Figure 1.1. The description of the interaction between the -(partly) ionized- fuel gas and the magnetic field, generated by the current in the coil, surrounding the expander, is quite complicated and requires -in principle- the full set of magneto-hydrodynamical equations (see e.g. [Cra73]). However, when the density of free electrons in the gas is sufficient ($T > 5000$ K, see [Kle87]), the magnetic field basically acts like a piston: when the magnetic pressure (which is proportional to the square of the magnetic field strength) is larger than the kinetic pressure of the gas, the gas will be compressed and pushed out of the expander into the core (a magnetic field of 1 Tesla will be in equilibrium with a gas/plasma at a pressure of approximately 4 bar [Kle87]); but when the kinetic pressure is larger than the magnetic pressure, the gas/plasma will expand against the magnetic field in the expander, thereby performing work on that magnetic field [Kle87], and reducing the field strength.

The -envisaged- operation of this GCFR is now as follows (see [Kis78a, Kle87, Kui89a, Kui89b, Kui90, Kui91a]). In fully expanded state of the fuel gas/plasma the reactor is subcritical. An increase of the magnetic field will then compress the fuel gas and push it into the core, thereby driving the reactor highly supercritical. The increasing fission power will also cause an increase of the fuel gas temperature and, therefore, of its kinetic pressure. This will lead to expansion of the fuel gas/plasma into the expander. The work done on the magnetic field during this expansion appears as electrical energy in a resonant "LC"-circuit, which consists of the coil, surrounding the expander, and a capacitor bank (not indicated in Figure 1.1). In this way, part of the kinetic energy of the plasma is extracted in a purely inductive manner. This energy can be extracted from the "LC"-circuit by a load over the capacitor bank. However, a -large- part of the energy has to be stored in the "LC"-circuit, to provide for the increase of the magnetic field in the expander, necessary for compression of the gas in the next "stroke".

In our "solid piston" model of this GCFR, we simulate the interaction between the fuel gas/plasma and the coil ("LC"-) system by a solid piston, which moves in the expander and -externally- controls the volume V_{fuel} , occupied by the fuel gas, as is indicated in Figure 5.1. The extracted energy is then modelled as the mechanical work performed by the gas on the piston. Certainly, this approximation is quite crude, but for the moment we are primarily interested in the neutron kinetical and thermodynamical behaviour of the system. Therefore, we also did not take gas dynamics into account in this model and assumed the fuel gas to be homogeneous and massless.

We investigated the influence of several parameters (such as fuel gas type (dissociating or non-dissociating), fuel gas -initial- temperature T_{BOC} ("Beginning Of Cycle"), pumping frequency f , compression ratio K , cycle-averaged fission power

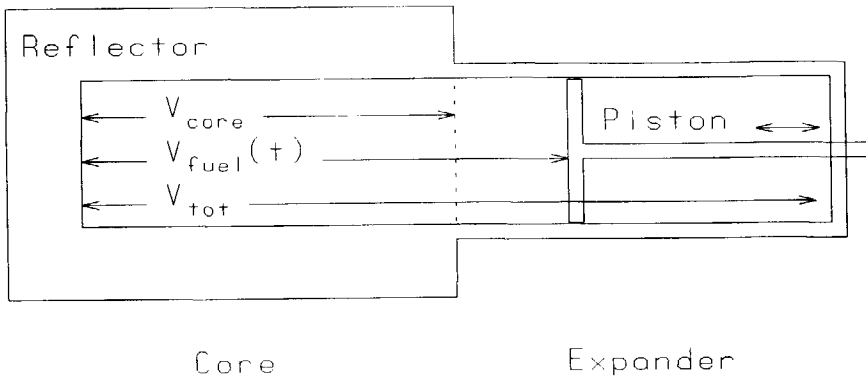


Figure 5.1 Solid piston GCFR model.

$\langle P_{fiss} \rangle_{\tau}$ (oscillation period $\tau = 1 / f$) on the neutron kinetical and thermodynamical behaviour of the system, and especially on the attainable work fraction (or conversion efficiency) η , which is defined by:

$$\eta \equiv \frac{\text{net extracted energy in one cycle}}{\text{produced fission energy in one cycle}} \quad (5.1.1)$$

We also investigated several types of fuel volume sequences (or pumping schemes) $V_{fuel}(t)$, such as a harmonic scheme or a -pseudo- Otto scheme (anharmonic scheme) [Kui89a, Kui89b, Kui90, Kui91a]. This, however, does not imply that these sequences are necessarily feasible with magnetic pumping.

5.2 Model description

Two major components of the "solid piston" GCFR model are neutron kinetics and thermodynamics. The neutron kinetics part is essentially a one-group zero power point kinetics model [Dam88], which was introduced in Section 3.1. For a given (periodical) fuel volume sequence $V_{fuel}(t)$, a given value of the reactor period T ($\equiv 1 / \omega$; Eqs. (3.1.12), (3.1.13)) and a given value of the cycle-averaged fission power $\langle P_{fiss} \rangle_{\tau}$, it calculates the total fission power P_{fiss} as a function of time, and also the total mass m_{tot} and the total amount $N_0 = m_{tot} / M_0$ ("original" mole) of the fuel gas, necessary to maintain the requested value of ω . As the GCFR is asymmetric, we assumed that the reactivity ρ and the neutron generation time Λ only depend on the fuel gas density in the core (see Sections 2.4 and 3.1). We further assumed that this dependence can be described by the "old" formulas used for the one-dimensional spherical GCFR (see Chapter 2, Tables 2.5 and 2.6; route "A"):

$$\begin{aligned} \rho &= 0.2039 - 0.2075 n_{RRS}^{-1} \\ \Lambda &= 4.784 \cdot 10^{-4} + 1.0713 \cdot 10^{-3} n_{RRS}^{-1} \end{aligned} \quad (5.2.1)$$

(n_{RGS} = density, relative to the RSG gas density; see Section 2.3). Note that, as already mentioned in Section 2.3, the values of Λ rendered by Eq. (5.2.1) are too low by a factor of approximately 1.5. However, we used these ("old") fit functions in our "solid piston" GCFR model, as they were the only ones available at that time. The main characteristics of the "solid piston" GCFR model are listed in Table 5.1.

Table 5.1 General parameters of the "solid piston" GCFR model.

Core radius R_{core}	1.0 m (RSG)
Core volume V_{core}	4.189 m ³ (RSG)
Total volume V_{tot}	12.57 m ³
Fuel gas composition (molar) (at 2000 K, 25 bar)	25.0 % UF ₄ 54.5 % UF ₅ 20.5 % CF ₄ (RSG)
Enrichment	50 % ²³⁵ U (RSG)
Critical core nuclide densities (RSG)	4.1977·10 ¹⁸ cm ⁻³ ¹² C 93.281·10 ¹⁸ cm ⁻³ ¹⁹ F 8.1621·10 ¹⁸ cm ⁻³ ²³⁵ U 8.1621·10 ¹⁸ cm ⁻³ ²³⁸ U
Reflector material	graphite
Reflector nuclide density (RSG)	8.55·10 ²² cm ⁻³ C
Reflector thickness (around core) d_{refl}	1.0 m (RSG)
Average reflector temperature T_{refl}	1000 K (RSG)

We investigated two different volume sequences $V_{fuel}(t)$, viz.: (I) a harmonic cycle, for which:

$$V_{fuel}(t) = V_{tot} \left[\frac{K+1}{2K} + \frac{K-1}{2K} \cos(2\pi ft) \right] \quad (5.2.2)$$

(V_{tot} = maximum volume of fuel gas; K = compression ratio; f = pumping frequency), and (II) a -pseudo- Otto cycle, consisting of a fast (approximately adiabatic) compression phase, an compressed isochoric phase, a fast (approximately adiabatic) expansion phase and an expanded isochoric phase (see [Kui89a, Kui89b, Kui90, Kui91a] and Section 4.5). Examples of these cycles are shown in Figure 5.2.

For the thermodynamics part of the model it is assumed that the system only passes through stable equilibrium states [Cal60, Hat79]. Under this assumption the internal energy (U) balance of the fuel gas is given by:

$$\frac{dU}{dt} = P_{fiss}(t) - P_{red}(t) - p(U, V_{fuel}) \times \frac{dV_{fuel}}{dt} \quad (5.2.3)$$

The momentary total fission power P_{fiss} is supplied by the neutron kinetics part of the model. The momentary heat transport P_{red} from the gas to the wall is given by Eq. (4.3.7) (Section 4.3; substitute $V = V_{fuel}$ and $T_{eff} = T$). The final term on the right hand side of Eq. (5.2.3) represents the momentary mechanical working-power

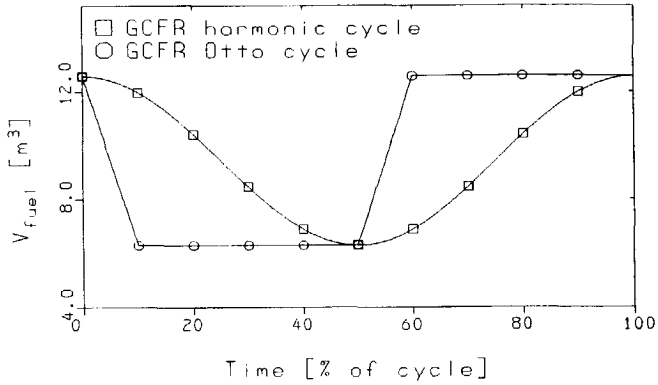


Figure 5.2 Volume sequences for GCFR harmonic and Otto cycles (compression ratio $K = 2$ in these examples).

P_{work} on the piston, which represents the directly convertible energy by magneto-inductive (MI) means [Kui91a]. The cycle averaged value of P_{work} should be positive in order to get net work (i.e. directly converted energy by MI) out of the system.

In order to integrate Eq. (5.2.3), the pressure p , the temperature T and the total amount of gas N must be known as functions of the internal energy U and the momentary fuel volume V_{fuel} . These relationships can be obtained from the "original" (non-dissociated) amount of fuel gas N_0 , the dissociation function $g(p, T)$, the Equation Of State $V_{fuel}(p, T)$ and the internal energy function $U(p, T)$ of the fuel gas under investigation. We performed calculations, considering a perfect gas (several values of κ), a Modelium-type gas and a "real" UCF gas.

Numerical integration of Eq. (5.2.3) over one pumping cycle renders, among other things, the totally produced fission energy W_{fiss} ($= P_{fiss}$ integrated over one cycle), the total heat loss W_{rad} (P_{rad} integrated over one cycle), the net amount of mechanical work W (P_{work} integrated over one cycle) and the internal energy U_{EOC} at the End Of the Cycle ($= U_{BOC} + \text{integral of } (dU / dt) \text{ over the cycle}$). The work fraction η ($= W / W_{fiss}$; see Eq. (5.1.1)) can then be calculated. In general, U_{EOC} is not equal to U_{BOC} , so there exists a (positive or negative energy) "gap" (calculated by integration of (dU / dt) over the cycle), which still has to be closed in order to return to the original BOC state [Kui89a, Kui89b, Kui90, Stek88, Stek90]. This "cycle closure" can be achieved by applying e.g. magneto-hydrodynamical (MHD) energy extraction after the magneto-inductive (MI) one.

5.3 Finite cycle calculation results

Some results of the finite (i.e. compression ratio $K > 1$) GCFR neutronic and thermodynamic cycle calculations are given below. In Figure 5.3 some examples of $P_{fiss}(t)$ are presented, for the volume sequences (harmonic and Otto) shown in Figure 5.2 ($f = 10$ Hz; $K = 2.0$). For the Otto cycle the -approximately-exponential power increase in the compressed (isochoric) phase (between 10 and

50 % of the cycle), due to neutron multiplication, is clearly demonstrated, as is the -approximately- exponential power decrease during the expanded (isochoric) phase (between 60 and 100 % of the cycle). This effect is less important for higher pumping frequencies [Dam89]. In case of the Otto cycle, the fission power $P_{fiss}(t)$ is also non-zero during other cycle-phases than the compressed isochoric heating one, which causes the work fraction η to be smaller than in the case of an ideal Otto cycle (Eq. (4.5.1)). A comparison with Figure 5.2 shows the existence of a time lag between the moments of maximum compression and maximum power. This time lag also decreases with increasing pumping frequency (see Figure 5.4).

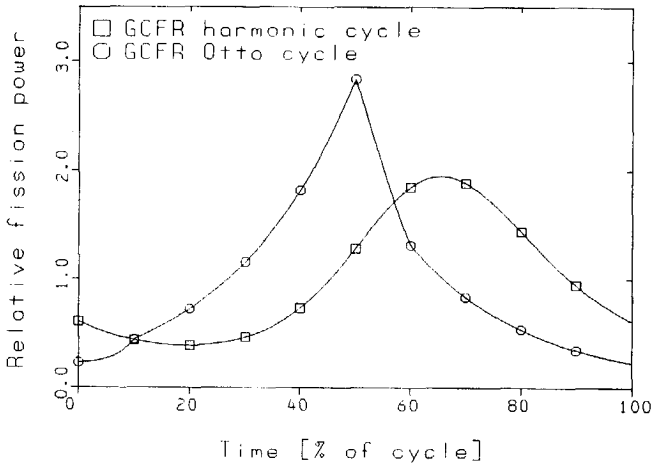


Figure 5.3 Fission power (relative to the cycle-averaged fission power) as function of time for harmonic and Otto cycle ($f = 10$ Hz; $K = 2.0$).

In Figure 5.4 the influence of the pumping frequency on the power history $P_{fiss}(t)$ is shown for the harmonic cycle ($K = 2.0$). At lower frequencies the neutron population gets more time to increase in an exponential-like manner, so the power excursions are more pronounced than for higher pumping frequencies, where the neutron population is more constant, so that the fuel volume sequence $V_{fuel}(t)$ and the power history $P_{fiss}(t)$ will be in anti-phase.

As already mentioned earlier (Sections 2.3 and 5.2) the values of Λ used in these calculations are too low by a factor of approximately 1.5, which means that the influence of the $(\rho - \beta_{eff})/\Lambda$ -term in Eq. (3.1.10) is overestimated in the calculations presented here. Using the "correct" values for Λ will cause the variations in the fission power not to be as pronounced as is shown here. However, for higher pumping frequencies (30 - 50 Hz), at which we performed most of the following calculations, the influence of the $(\rho - \beta_{eff})/\Lambda$ -term on the power history will be small, as, at these frequencies, the neutron population is almost constant already.

In Figures 5.3 and 5.4 the non-linearity of the neutron kinetics is clearly demonstrated. This non-linearity is already known from studies on strong reactivity oscillations in reactors with stationary fuel mass [Akc58, Smi65]. It is, however,

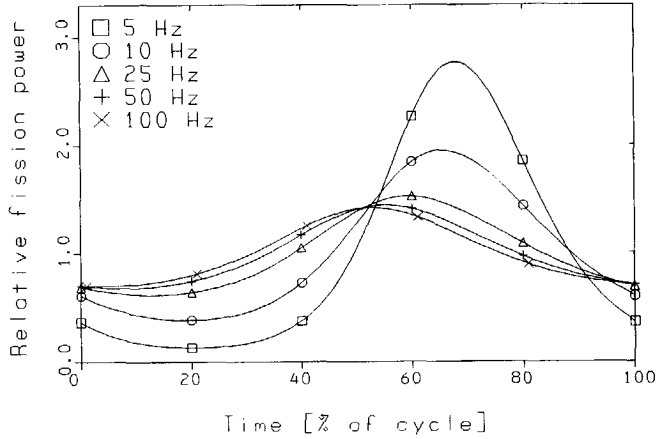


Figure 5.4 Fission power (relative to the cycle-averaged fission power) as function of time for several pumping frequencies (harmonic cycle; $K = 2.0$).

more pronounced in a system with oscillating fuel mass because of the synchronic but in anti-phase oscillation of the neutron generation time [Dam88, Kui90]. Another consequence of the non-linearity is shown in Figure 5.5, where the cycle-averaged prompt reactivity $\langle \rho_p \rangle_\tau$ is shown as function of the compression ratio K for "stationary" (i.e. $\omega = 0$) pumped operation. The prompt reactivity ρ_p is defined as [Dam88]:

$$\rho_p \equiv 1 - \frac{1}{k_{eff}(1-\beta_{eff})} = \frac{\rho - \beta_{eff}}{1 - \beta_{eff}} \quad (5.3.1)$$

As can be seen in the figure, the cycle-averaged prompt reactivity is negative and decreases with increasing compression ratio K . For $K \rightarrow 1$ (i.e. $V_{fuel} \rightarrow V_{tot}$; no pumping) the value of the cycle-averaged prompt reactivity becomes:

$$\langle \rho_p \rangle_\tau \rightarrow - \frac{V_{core}}{V_{tot}} \frac{\beta_{eff}}{1 - \beta_{eff}} \quad (5.3.2)$$

(see Eqs. (3.1.10) and (3.1.11); zero time-derivatives). The factor (V_{core} / V_{tot}) follows from the "complete mixing" assumption for the delayed neutron precursors, stated in Eq. (3.1.7). For the case presented here this implies that the effective delayed neutron fraction β_{eff} will be reduced by a factor of 3 (at $K \rightarrow 1$), because of the total-to-core volume ratio (V_{tot} / V_{core}) of 3 (see Table 5.1).

In Figure 5.6 the necessary total fuel mass m_{tot} , necessary for maintaining the specified value of ω (0.0 and 1.0 s^{-1} , respectively), is shown as function of the compression ratio K (harmonic cycle, $f = 30 \text{ Hz}$). It is clear that, in order to increase the average fission power $\langle P_{fiss} \rangle_\tau$ (i.e. $\omega > 0$), either the compression ratio K or the total mass of the fuel gas m_{tot} has to be increased. It should also be noted that stopping of pumping (i.e. $K \rightarrow 1$) will lead to an immediate and strong power decrease (negative ω ; see [Dam89, Kui89a, Kui89b]).

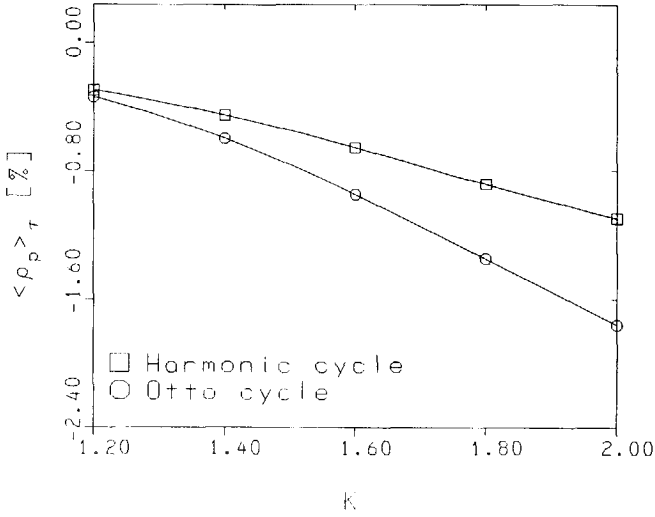


Figure 5.5 Cycle-averaged prompt reactivity $\langle \rho_p \rangle_r$ as function of compression ratio K for harmonic and Otto cycle ($f = 50$ Hz).

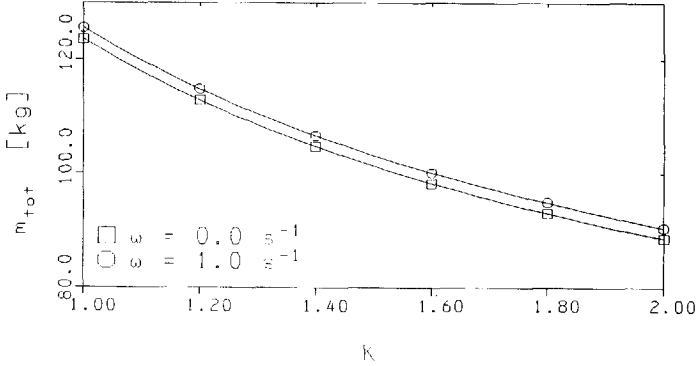


Figure 5.6 Necessary total fuel mass m_{tot} to maintain specified inverse reactor period ω as function of compression ratio K (harmonic cycle; $f = 30$ Hz).

The pressure versus volume ($p(V_{fuel})$ -) diagrams for the harmonic and Otto cycle are shown in Figure 5.7 (the volume sequence $V_{fuel}(t)$ is shown in Figure 5.2; $\langle P_{fis} \rangle_r = 100$ MW; perfect gas; $\kappa = 1.40$; $T_{BOC} = 3000$ K; radiative heat transfer "switched off": $C_{rad} = 0$). Note the compressed isochoric heating phase in the Otto cycle. Also the existence of a cycle "closure gap" (see Section 5.2) is clearly demonstrated, as the pressure at EOC (hence the temperature and the

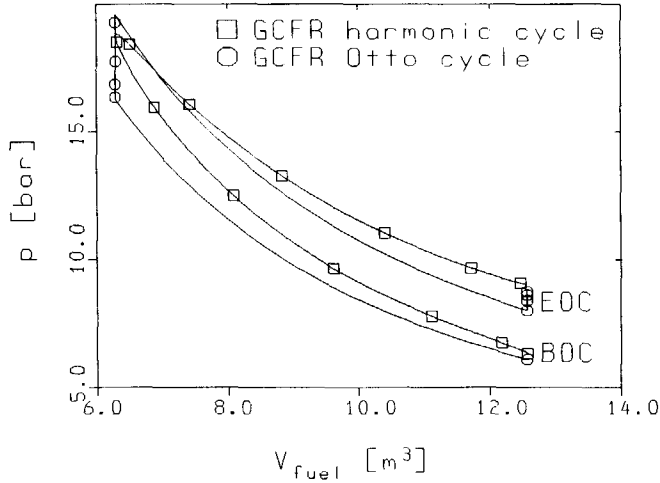


Figure 5.7 Pressure as function of volume for harmonic and Otto cycle (perfect gas; $\kappa = 1.40$; $T_{BOC} = 3000$ K; $C_{rad} = 0$; $\langle P_{fiss} \rangle \tau = 100$ MW).

internal energy) is not equal to the pressure at BOC. The total amount of -mechanical- work W produced in one cycle is given by the area of the $p(V_{fuel})$ -diagram. For equal compression ratio, this area is larger for the Otto cycle than for the harmonic cycle, so the Otto cycle renders a larger work fraction η than the harmonic cycle. If Modelium or UCF gas is used instead of non-dissociating perfect gas, W (hence η) will become smaller, because of the "damping" influence of dissociation and recombination on the pressure- and temperature variations and hence on the area of the $p(V_{fuel})$ -diagram [Kui89a].

The starting point of the following parametric study is the so-called "basic cycle", the parameters of which are listed in Table 5.2. In each of the following cases one of the parameters was varied, whereas the others were kept fixed on the values in the "basic cycle" (unless stated otherwise).

For the first cases we "switch off" the radiative heat transfer from the gas to the surrounding wall (Eq. (4.3.7): $C_{rad} = 0$). In Figure 5.8 the effect is shown of variation of the compression ratio K on the work fraction η . At higher compression ratios the work fraction is also higher. Furthermore the Otto cycle seems to be more efficient than the harmonic cycle (also see Figure 5.7). In the same figure also the work fraction η for an ideal Otto cycle is shown, calculated using Eq. (4.5.1). The work fraction for the GCFR Otto cycle is lower than in the ideal case because in the GCFR Otto cycle the volume changes are not adiabatic. Furthermore, an increase in the c_p/c_v -ratio κ also causes an increase in η , which can also be expected from Eq. (4.5.1) (also see [Kui89a]).

The temperature at the beginning of the cycle T_{BOC} also influences the attainable work fraction η in the case of the dissociating gases Modelium and UCF, as is shown in Figure 5.9. In absence of heat transfer from the gas to the wall ($C_{rad} = 0.0$) the work fraction increases with increasing T_{BOC} , except for the

Table 5.2 "Basic cycle" parameters.

Gas type	non-dissociating, perfect
c_p/c_v -ratio κ	1.40
Pumping scheme $V_{fuel}(t)$	harmonic (Eq. (5.2.2))
Pumping frequency f	50 Hz
Compression ratio K	2.0
Gas temperature at BOC T_{BOC}	5000 K
Cycle-averaged fission power $\langle P_{fiss} \rangle_\tau$	100 MW
Inverse reactor period ω	0.0 s ⁻¹
Radiation constant (Eq. (4.3.7)) C_{rad}	5.80 · 10 ⁻¹⁰ W mole ⁻¹ m ³ K ⁻⁴

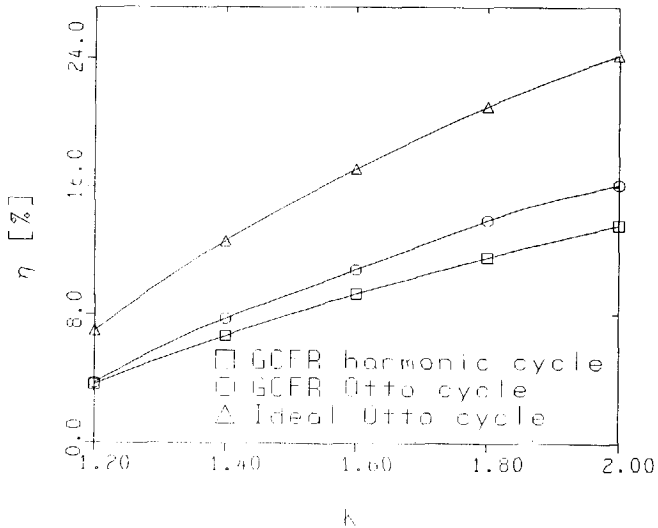


Figure 5.8 Work fraction η as function of the compression ratio K for ideal Otto cycle, GCFR harmonic cycle and GCFR Otto cycle (perfect gas).

"hump" in the UCF curve at $T_{BOC} \approx 4000$ K, which is related to the first dissociation step (Chapter 4, Figure 4.3). In Figure 5.9 it is furthermore demonstrated that, also in the case of dissociating gases, the GCFR Otto cycle is more efficient than the GCFR harmonic cycle. The attainable work fraction, however, is much lower than in the case of a perfect gas (compare with Figure 5.8). Furthermore, Figure 5.9 gives an indication that Modelium approximates the behaviour of UCF gas quite well, especially at high temperatures.

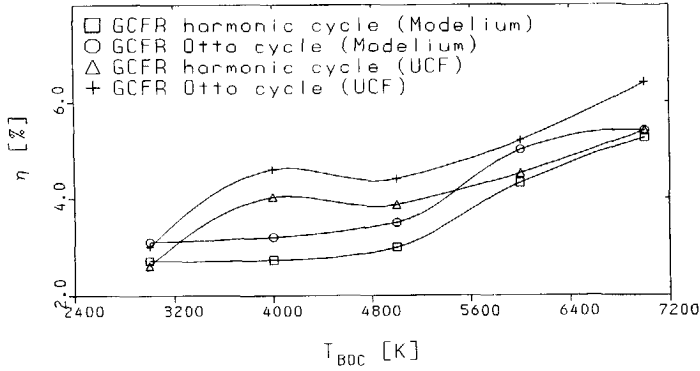


Figure 5.9 Work fraction η as function of T_{BOC} for GCFR harmonic and Otto cycle with Modelium and UCF gas.

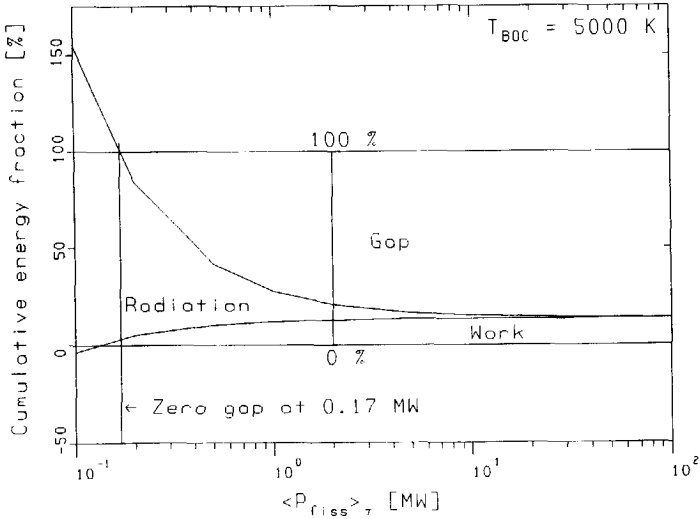


Figure 5.10 Cumulative energy fractions as function of average fission power $\langle P_{fiss} \rangle_{\tau}$ for the "basic cycle" ($T_{BOC} = 5000$ K).

For the remaining cases the radiative heat transfer from the gas to the wall is "switched on" again (Eq. (4.3.7): $C_{rad} = 5.80 \cdot 10^{-10} \text{ W mole}^{-1} \text{ m}^{-2} \text{ K}^{-4}$). In Figure 5.10 the energy balance of a pumped GCFR is shown as function of the average fission power $\langle P_{fiss} \rangle_{\tau}$. In the vertical direction the cumulative energy fractions for work (direct MI conversion), radiative transfer to the reactor wall and "closure gap" of the thermodynamic cycle are indicated. For $\langle P_{fiss} \rangle_{\tau}$ below

approximately 0.14 MW (for $T_{BOC} = 5000$ K) the reactor cools down due to the intense heat radiation at 5000 K, the work fraction is negative and so is the closure gap. With increasing $\langle P_{fiss} \rangle_{\tau}$, the work fraction becomes positive and increases, whereas the radiative fraction (i.e. the radiated energy relative to the produced fission energy) decreases strongly, which means that there is an increasing cycle closure gap. At high powers, where the radiative fraction becomes very small, the work fraction approximates the value of 13.6 %, which was calculated for the case of absence of radiative heat transfer (see Figure 5.8: harmonic cycle, $K = 2.0$). At an average fission power of 0.17 MW a peculiar situation arises: there is a positive work fraction of approximately 3 % and an exact closure of the cycle. This means that the $p(V_{fuel})$ -diagram has a small positive area, but the cooling down during the expansion phase due to heat radiation is just sufficient to return to the BOC state.

In Figure 5.11, which shows the cumulative energy fractions as function of T_{BOC} , the average fission power $\langle P_{fiss} \rangle_{\tau}$ is kept constant at 1.0 MW. At relatively low temperatures there is a large positive cycle closure gap: the reactor heats up until it reaches an equilibrium temperature of approximately 7845 K, at which the closure gap is zero. At this temperature the work fraction is again a few percent, and the remaining part of the produced fission energy is radiated to the wall. This part can be converted into electricity by more conventional means (like a steam cycle or -possibly- a thermionic converter).

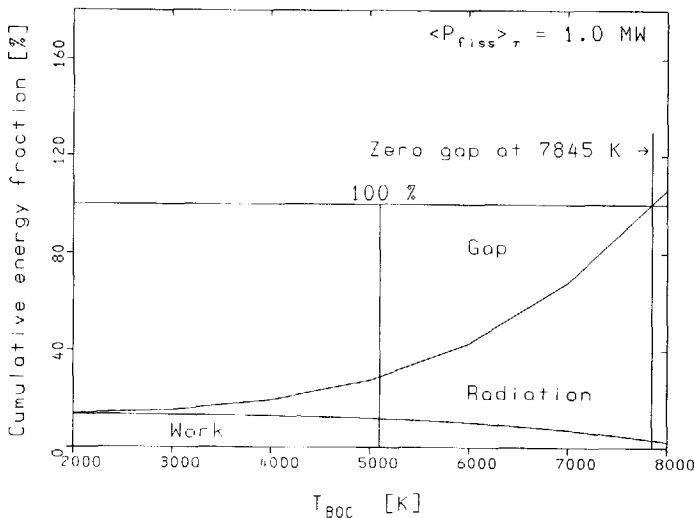


Figure 5.11 Cumulative energy fractions as function of the temperature at BOC for the "basic cycle" ($\langle P_{fiss} \rangle_{\tau} = 1.0$ MW).

Further cycle calculations (see [Kui89a]) show, among other things, that Otto cycles (and Diesel cycles [Stek88, Dam89]) render a larger work fraction than the harmonic ones, but that for dissociating (Modelium, UCF) gases only a much lower work fraction (approximately 4 %) can be attained than for non-dissociating

perfect gas [Kui89a, Dam89]), an effect that can only be explained partly by the fact that the cycle-averaged κ for Modelium and UCF (approximately 1.25) is lower than 1.40 (the value chosen for the calculations with perfect gas). However, from these calculations it can furthermore be concluded that Modelium approximates the behaviour of UCF quite well.

A final remark in this section concerns the very high so-called "basic pumping power" circulating in the magnetic coil system, which is modelled (in the "solid-piston" GCFR model) as the instantaneous working power P_{work} , which is given by:

$$P_{work} \equiv p \times \frac{dV_{fuel}}{dt} \quad (5.3.3)$$

(also see Eq. (5.2.3)). For a "solid piston" GCFR with $V_{tot} = 12.57 \text{ m}^3$, running at 50 Hz (harmonic cycle: Eq. (5.2.2)) with a compression ratio of $K = 2$, and assuming a pressure of approximately 15 bar, the maximum working power is approximately 1.48 GigaWatt. A small loss factor in the magnetic coil system (e.g. due to ohmic losses) will lead to a severe deterioration of the conversion efficiency. It might even render magnetic pumping useless, if the loss is of the same order as the MI energy extraction. A possible way of avoiding this problem is using autonomous gas density oscillations in a GCFR, driven by nuclear fissions. We investigated this possibility in the form of the "two-compartment" combined GCFR model, to be presented in Chapter 7.

5.4 Comparison with infinitesimal cycle

In order to gain a better understanding of the finite cycle calculation results (e.g. presented in the previous section), especially of the influence of the thermodynamic properties of the gas, we studied the so-called "infinitesimal Otto cycle", which was introduced in Section 4.5 (also see [Kui91a]). We can make a comparison between the results of a finite cycle calculation and those of the corresponding infinitesimal one by comparing the infinitesimal efficiency factor ζ with the so-called "efficiency factor" ζ^* (for finite cycles with completely externally controlled volume sequence, such as an Otto cycle), which is defined by:

$$\zeta^* \equiv \eta \frac{K}{K-1} \quad (5.4.1)$$

Results for finite and infinitesimal cycle calculations for a non-dissociating perfect gas are given in Figures 5.12 and 5.13. Figure 5.12 shows the (infinitesimal) efficiency factors as a function of the compression ratio K for the same cycles as in Figure 5.8. Figure 5.13 gives results as a function of the c_p/c_v -ratio κ . The factors increase with increasing K and κ . As expected, the ideal Otto cycle has a higher efficiency (see Eq. (4.5.1)) than the GCFR Otto cycle; the latter is more efficient than the GCFR harmonic cycle. The infinitesimal efficiency factor is somewhat smaller than the real efficiency factor for a finite ideal Otto cycle; for the other cycles it represents an overestimation. This is caused by the fact that, for the real GCFR cycles, fission energy is also generated in the fuel gas during other parts of the cycle than the isochoric heating phase (Otto cycle). This lowers the conversion efficiency. It is evident, however, that the infinitesimal efficiency

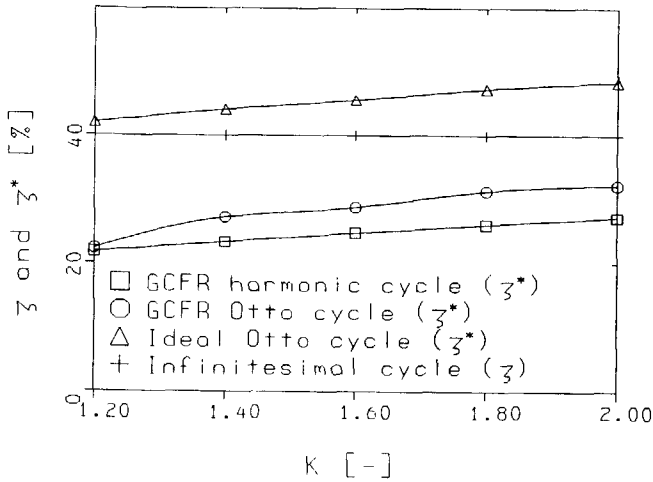


Figure 5.12 (Infinitesimal) efficiency factor as function of the compression ratio (perfect gas; $\kappa = 1.40$).

factor provides a reasonable estimate (of the upper limit) of the efficiency of finite cycles, without performing elaborate calculations as are needed for obtaining the exact efficiency.

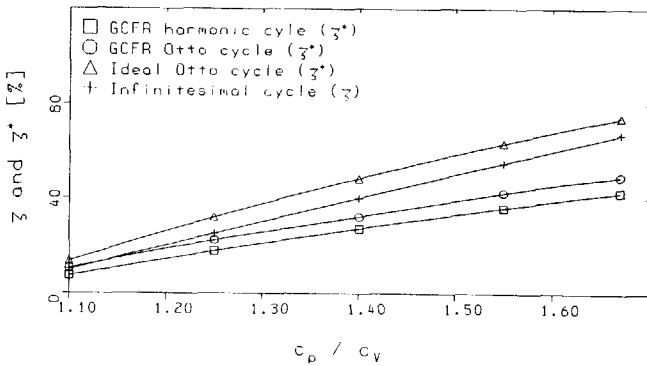


Figure 5.13 (Infinitesimal) efficiency factor as function of c_p/c_v -ratio (perfect gas; $K = 2.0$).

Efficiency factors for Modelium are shown in Figure 5.14 as a function of the BOC temperature. It is seen that the infinitesimal efficiency factor provides a good estimate for the actual cycle efficiency; there is no big difference between the infinitesimal efficiency factor calculated at average cycle pressure and temperature (denoted by " $\langle p \rangle, \langle T \rangle$ ") or at BOC temperature and pressure (denoted by " (p, T) at BOC"). An assessment of efficiency on the basis of

Eqs. (4.5.1), (4.5.10) and (5.4.1), using cycle-averaged values for c_v and κ (denoted by " $\langle c_v \rangle$ " and " $\langle c_p/c_v \rangle$ ", respectively), gives gross under- and overestimation, respectively. The figure shows clearly that ζ , evaluated at BOC conditions, provides a good accuracy, without the need of a lengthy cycle calculation. Obviously, the infinitesimal efficiency factor can also be used to estimate those BOC conditions (T_{BOC} and ρ_{BOC}), where a finite cycle can be expected to render an optimal work fraction. From Figure 4.7, which shows the infinitesimal efficiency factor (for Modelium) as a function of T , it can then be concluded that a high work fraction η can only be expected at high temperatures (far above the dissociation region) where the gas approximates a monatomic perfect gas.

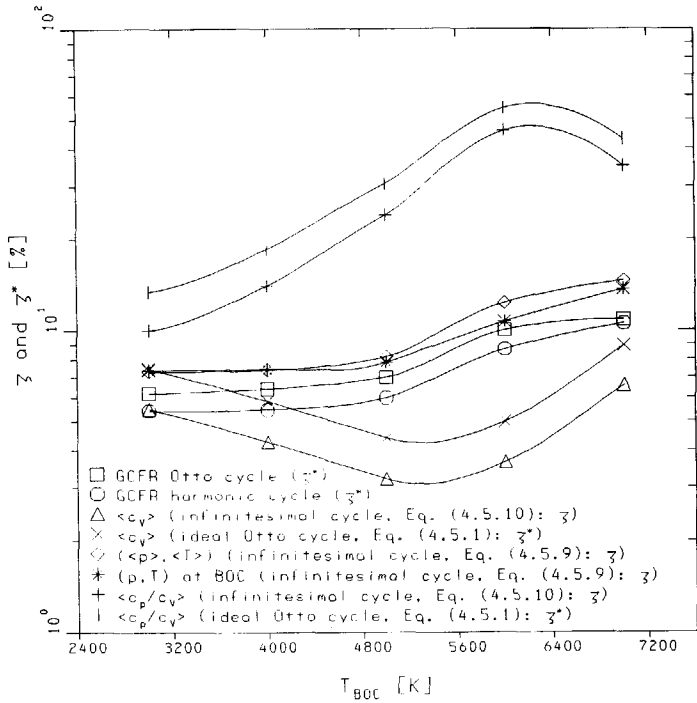


Figure 5.14 Comparison of several (infinitesimal) efficiency factor values for Modelium as function of T_{BOC} .

The results for Modelium show that, even in the case of a dissociating medium, ζ at T_{BOC} and ρ_{BOC} provides a reasonably accurate estimation η^* (by Eq. (4.5.11)) of the cycle efficiency η . It is therefore expected that the same is valid for UCF, where ζ can be calculated from EOS-data and the $U(p, T)$ -function, which are available in tabular form [Boe89a].

5.5 Conclusions

Neutron kinetic and (finite and infinitesimal) thermodynamic cycle calculations have been performed for the "solid piston" model of a -magnetically- pumped GCFR, in order to investigate the influence of several parameters on the reactor physical and thermodynamical behaviour of the system.

The neutron kinetics is highly non-linear, which is reflected in the fact that the cycle-averaged (prompt) reactivity is negative and decreases with increasing compression ratio (at constant cycle-averaged power). The non-linearity is enhanced by the synchronic but in anti-phase oscillation of the neutron generation time. From the safety point of view, however, it is important to note that stopping of pumping (i.e. compression ratio $K \rightarrow 1$) will lead to an immediate and strong power decrease.

From the finite cycle calculations it can be concluded that for a pumped GCFR with dissociating fuel gas a direct energy conversion efficiency η is attainable of only a few percent (in the investigated parameter range). Comparison of these finite cycle calculations with so-called infinitesimal Otto cycle calculations leads to the conclusion that it is possible, even in the case of non-ideal, dissociating gas, to obtain a reasonable estimation of the attainable conversion efficiency of a finite cycle from the so-called infinitesimal efficiency factor ζ of the fuel gas, evaluated at the BOC (beginning of the cycle) state. This infinitesimal efficiency factor is completely determined by the properties of the gas.

However, a big problem is posed by the very high so-called "basic pumping power", circulating in the magnetic coil system, which is modelled (in the "solid piston" GCFR model) as the instantaneous working power. A small loss factor in the magnetic coil system (e.g. due to ohmic losses) will lead to a severe deterioration of the conversion efficiency. It might even render magnetic pumping useless, if the loss is of the same order as the MI energy extraction. A possible way of avoiding this problem is using autonomous density oscillations in a GCFR, driven by nuclear fissions.

Chapter 6

GAS DYNAMICS

6.1 Introduction

One of the important parts of the combined "two-compartment" GCFR model -to be presented in Chapter 7- is the description of the dynamical behaviour of the fuel gas in the cylindrical GCFR gas space. In this chapter we will present two models for the description of the GCFR gas dynamics. In these models we assume that the length (L_{gas}) of the gas space is much larger than its radius (R_{gas}), so that we only need to consider one-dimensional gas dynamics in axial direction. Furthermore, we neglect friction effects (i.e. we assume zero viscosity of the gas), as is often done in -low velocity- gas dynamics studies [Roh85].

The most appropriate gas dynamics model from the fundamental, physical point of view is a model, based on the well-known conservation equations for mass (continuity equation), momentum (Navier-Stokes or Euler equation) and energy (first law of thermodynamics), and the equation of state (EOS) $V(\rho, T)$ and the internal energy $U(\rho, T)$ of the gas (see [Lan63, Bir63, Roh85]). Such a model renders the mass density distribution (ρ_m), the temperature (T), the pressure (p) and the velocity (v) as function of position (x) and time (t), given the local fission power density $Q_{fiss}(x, t)$ and the (radiative) heat loss to the wall (see Section 4.3). In a combined GCFR model, the fuel gas density distribution is then used as input for the neutronics part of the model. The neutronics part on its turn calculates the fission power density distribution and the circle is closed. In the case that a stationary solution is desired, an iterative procedure can be used, similar to the one applied in the "solid piston" model (see Chapters 3 and 5). In Section 6.2 we present the basic equations of this gas dynamics model (for the one-dimensional case) together with an -approximative- analytical treatment. In this analytical treatment we assume the variations of the variables (pressure, temperature, mass density) to be small ("acoustic" or "small signal" approximation), and the initial velocity distribution to be as in the Fundamental Acoustic Mode ("FAM").

However, the model mentioned above, which employs partial differential equations for position- and time-dependent (thermodynamical) quantities, is quite complicated. For use in the combined "two-compartment" GCFR model we therefore developed an alternative and more simple description of the GCFR gas dynamics. In this so-called "Two-Compartment" Model ("TCM") we imagine the gas space to be divided into two compartments, of which the thermodynamic variables (pressure p , temperature T , volume V) are described by ordinary differential equations. The parameters in this gas dynamics model are chosen such that -for small amplitudes- the natural oscillation frequency (f) and the momentary (total) kinetic energy ($E_{kin}(t)$) have the same values as in the fundamental acoustic mode (FAM). In Section 6.3 we introduce this description. We also give an -approximative- analytical treatment of this model, for a comparison with the acoustic gas dynamics model.

Furthermore, in Section 6.4 we estimate the attainable conversion efficiency (η), for the case that an energy extraction mechanism -modelled as a friction force,

proportional to the velocity- is present in such a way that the amplitude of the density (and velocity) oscillations is constant (i.e. in the "stationary" state).

6.2 Acoustic model

As mentioned above, the basis of the acoustic model consists of the well-known conservation equations for mass, momentum and energy, combined with the EOS and the internal energy function of the (fuel) gas [Lan63, Bir63, Roh85]. Assuming: (I) one-dimensional gas dynamics (axial position $-L_{gas}/2 \leq x \leq L_{gas}/2$; time t), (II) horizontal flow (i.e. no gravitation effects), (III) total gas space volume V_{tot} ($= \pi R_{gas}^2 L_{gas}$) and (IV) a total amount of fuel gas N_0 ($= m_{tot} / M_0$; M_0 = "original" molar mass; general, dissociating gas; see Chapter 4), these equations take the following form:

$$\frac{\partial \rho_m}{\partial t} + \rho_m \frac{\partial v}{\partial x} + v \frac{\partial \rho_m}{\partial x} = 0 \quad (6.2.1a)$$

(mass conservation: continuity equation)

$$\rho_m \left(\frac{\partial v}{\partial t} + v \frac{\partial v}{\partial x} \right) = - \frac{\partial p}{\partial x} \quad (6.2.1b)$$

(equation of motion: Navier-Stokes or Euler equation; no friction)

$$\frac{\rho_m}{m_{tot}} \left(\frac{\partial U}{\partial t} + v \frac{\partial U}{\partial x} \right) = -p \frac{\partial v}{\partial x} + Q_{net}(x,t) \quad (6.2.1c)$$

(energy balance: first law of thermodynamics)

$$\rho_m(x,t) = \frac{m_{tot}}{V[\rho(x,t), T(x,t)]} \quad (6.2.1d)$$

(EOS)

($V(\rho, T)$ is the volume and $U(\rho, T)$ is the internal energy of N_0 "original" moles of gas; see Chapter 4). For the net power density $Q_{net}(x,t)$ we assume: (I) a constant and spatially flat neutron flux, so that the fission power density $Q_{fiss}(x,t)$ is proportional to the mass density $\rho_m(x,t)$, (II) a constant (radiative) heat transport (to the wall) per unit volume, in such a way that the total radiated power is in balance with the (constant) total fission power P_{fiss} and (III) absence of heat transport in axial direction. We then obtain:

$$Q_{net}(x,t) = P_{fiss} \left(\frac{\rho_m(x,t)}{m_{tot}} - \frac{1}{V_{tot}} \right) \quad (6.2.2)$$

It must be noted, however, that assumption "(II)" has limited validity for the case that increasing density oscillations in the gas occur.

We also assume rigid walls at the boundaries ($x = \pm L_{gas}/2$), so that the boundary conditions on the velocity v read:

$$v(\pm \frac{1}{2} L_{gas}, t) = 0 \quad (6.2.3)$$

For the initial conditions (at $t = 0$) we assume:

$$\begin{aligned} \rho(x,0) &= \langle \rho \rangle & T(x,0) &= \langle T \rangle \\ \rho_m(x,0) &= \frac{m_{tot}}{V_{tot}} & Q_{net}(x,0) &= 0 \\ v(x,0) &= v_0 \cos \left[\frac{\pi x}{L_{gas}} \right] & \frac{\partial v}{\partial t}(x,0) &= 0 \end{aligned} \quad (6.2.4)$$

(fundamental acoustic mode (FAM); angle brackets " $\langle \dots \rangle$ " denote space- and time-averaged value of variable). Furthermore, it is obvious that:

$$V(\langle \rho \rangle, \langle T \rangle) = V_{tot} \quad \pi R_{gas}^2 \int_{-L_{gas}/2}^{L_{gas}/2} \rho_m(x,t) dx = m_{tot} \quad (6.2.5)$$

As mentioned, for the analytical treatment of this model, we assume the variations in the variables to be small, compared to the average value:

$$\begin{aligned} \rho &= \langle \rho \rangle + \tilde{\rho} & T &= \langle T \rangle + \tilde{T} \\ \rho_m &= \frac{m_{tot}}{V_{tot}} + \tilde{\rho}_m \equiv \langle \rho_m \rangle + \tilde{\rho}_m & v &= \tilde{v} \end{aligned} \quad (6.2.6)$$

(tilde "--" denotes varying component of the variable; $\langle v \rangle = 0$). Under this assumption, and using the partial derivatives A_U , B_U , A_V and B_V evaluated at $(\langle \rho \rangle, \langle T \rangle)$ (see Chapter 4, Eq. (4.5.4); N_0 "original" moles), the basic equations can -in first order approximation- be written as:

$$\frac{\partial \tilde{\rho}_m}{\partial t} + \langle \rho_m \rangle \frac{\partial \tilde{v}}{\partial x} = - \frac{\langle \rho_m \rangle}{V_{tot}} \left[A_V \frac{\partial \tilde{T}}{\partial t} + B_V \frac{\partial \tilde{\rho}}{\partial t} \right] + \langle \rho_m \rangle \frac{\partial \tilde{v}}{\partial x} = 0 \quad (6.2.7a)$$

$$\langle \rho_m \rangle \frac{\partial \tilde{v}}{\partial t} = - \frac{\partial \tilde{\rho}}{\partial x} \quad (6.2.7b)$$

$$\frac{1}{V_{tot}} \left[A_U \frac{\partial \tilde{T}}{\partial t} + B_U \frac{\partial \tilde{\rho}}{\partial t} \right] = - \langle \rho \rangle \frac{\partial \tilde{v}}{\partial x} + Q_{net}(x,t) \quad (6.2.7c)$$

$$\tilde{\rho}_m = - \frac{\langle \rho_m \rangle}{V_{tot}} (A_V \tilde{T} + B_V \tilde{\rho}) \quad (6.2.7d)$$

$$Q_{net}(x,t) = \frac{P_{fiss}}{m_{tot}} \tilde{\rho}_m \quad (6.2.7e)$$

Laplace-transformation (see e.g. [Spi65]) of these equations, using the initial conditions stated in Eq. (6.2.4), yields:

$$\frac{1}{V_{tot}} (A_V s \tilde{T} + B_V s \tilde{\rho}) = \frac{\partial \tilde{v}}{\partial x} \quad (6.2.8a)$$

$$\langle \rho_m \rangle \left[s\hat{v} - v_0 \cos \left(\frac{\pi x}{L_{gas}} \right) \right] = -\frac{\partial \hat{\rho}}{\partial x} \quad (6.2.8b)$$

$$\frac{1}{V_{tot}} (A_U s \hat{T} + B_U s \hat{\rho}) = -\langle \rho \rangle \frac{\partial \hat{v}}{\partial x} + \hat{Q}_{net}(x, s) \quad (6.2.8c)$$

$$\hat{\rho}_m = -\frac{\langle \rho_m \rangle}{V_{tot}} (A_V \hat{T} + B_V \hat{\rho}) \quad (6.2.8d)$$

$$\hat{Q}_{net}(x, s) = \frac{P_{fiss}}{m_{tot}} \hat{\rho}_m(x, s) \quad (6.2.8e)$$

(transformation: $t \rightarrow s$; circonflexe " $\hat{\quad}$ " denotes Laplace-transform of varying component of variable). From this set of equations we can derive an expression for the Laplace transform of the velocity v :

$$s^2 \hat{v} + \frac{V_{tot}^2 (A_U + A_V \langle \rho \rangle)}{N_0 M_0 (A_U B_V - B_U A_V)} \frac{\partial^2 \hat{v}}{\partial x^2} = s v_0 \cos \left(\frac{\pi x}{L_{gas}} \right) - \frac{1}{s} \frac{V_{tot} A_V P_{fiss}}{(A_U B_V - B_U A_V) N_0 M_0} \frac{\partial^2 \hat{v}}{\partial x^2} \quad (6.2.9)$$

Using the expression for the infinitesimal efficiency factor ζ (see Section 4.5, Eq. (4.5.6)), this can be written as:

$$s^2 \hat{v} - c^2 \frac{\partial^2 \hat{v}}{\partial x^2} = s v_0 \cos \left(\frac{\pi x}{L_{gas}} \right) + \frac{1}{s} \zeta \frac{P_{fiss}}{m_{tot}} \frac{\partial^2 \hat{v}}{\partial x^2} \quad (6.2.10)$$

In which the velocity of sound (c) in the gas is given by:

$$c^2 = -\frac{V_{tot}^2 (A_U + A_V \langle \rho \rangle)}{N_0 M_0 (A_U B_V - B_U A_V)} = -\frac{V_{tot}^2 \kappa}{N_0 M_0 B_V} = \frac{\kappa R \langle T \rangle}{\left[\frac{M_0}{g} \right] \left[1 - \frac{\langle \rho \rangle}{g} \frac{\partial g}{\partial \rho} \right]} \quad (6.2.11)$$

(g = dissociation factor of the gas at ($\langle \rho \rangle$, $\langle T \rangle$); see Chapter 4, Eqs. (4.2.1), (4.5.4) and (4.5.7c)). For a perfect, non-dissociating gas ($g \equiv 1$), this reduces to the well-known formula:

$$c^2 = \frac{\kappa R \langle T \rangle}{M_0} \quad (6.2.12)$$

If this "perfect gas"-formula is used for the calculation of the velocity of sound in a non-perfect dissociating gas (using an adapted value for the molar mass, viz. M_0 / g), the value found will usually be too high, as the derivative of g with respect to ρ will usually be negative (like in UCF and Modelium; see Chapter 4, Figure 4.3).

6.2.1 Adiabatic case

If we "switch off" the fission power production and the radiative heat transport to the wall ($Q_{net} \equiv 0$: adiabatic case), then Eq. (6.2.10) reduces to:

$$s^2 \hat{v} - c^2 \frac{\partial^2 \hat{v}}{\partial x^2} = s v_0 \cos \left[\frac{\pi x}{L_{gas}} \right] \quad (6.2.13)$$

From this we can conclude, by inverse Laplace transformation [Spi65]:

$$v(x,t) = v_0 \cos(2\pi ft) \cos \left[\frac{\pi x}{L_{gas}} \right] \quad (6.2.14)$$

This is the fundamental acoustic mode (FAM) standing wave, with oscillation frequency f , given by the well-known formula:

$$f = \frac{c}{2L_{gas}} \quad (6.2.15)$$

The mass density distribution $\rho_m(x,t)$ for the FAM can then be derived, using Eq. (6.2.7a), resulting in:

$$\rho_m(x,t) = \frac{m_{tot}}{V_{tot}} \left[1 + \frac{v_0}{c} \sin \left[\frac{\pi x}{L_{gas}} \right] \sin(2\pi ft) \right] \quad (6.2.16)$$

In the combined "two-compartment" GCFR model (Chapter 7) we assume the gas space to be subdivided into a core part ($-L_{gas}/2 \leq x \leq 0$) and an expander part ($0 \leq x \leq L_{gas}/2$) of equal volume $V_{core} = V_{exp} = V_{tot}/2$. In the fundamental acoustic mode (FAM) standing wave, the mass of the fuel gas in the core part is then given by:

$$m_{core}(t) = \frac{1}{2} m_{tot} \left[1 - \frac{2}{\pi} \frac{v_0}{c} \sin(2\pi ft) \right] \quad (6.2.17)$$

Using Eq. (2.4.1), we can now calculate the density distribution variable ε for the FAM:

$$\varepsilon = -\frac{2}{\pi} \frac{v_0}{c} \sin(2\pi ft) \quad (6.2.18)$$

The momentary kinetic energy $E_{kin}(t)$ of the gas can be calculated, using Eqs. (6.2.14) and (6.2.16). We find:

$$\begin{aligned} E_{kin}(t) &= \pi R_{gas}^2 \int_{-L_{gas}/2}^{L_{gas}/2} \frac{1}{2} \rho_m(x,t) [v(x,t)]^2 dx \\ &= \frac{1}{4} m_{tot} v_0^2 \cos^2(2\pi ft) \end{aligned} \quad (6.2.19)$$

6.2.2 Non-adiabatic case

Using the solution for $v(x,t)$ from the adiabatic case, viz. Eq. (6.2.14), we can also calculate an approximated solution of Eq. (6.2.10) (the general, non-adiabatic case), by means of (first order) perturbation theory. The term of Eq. (6.2.10), describing the fission power density and the radiative heat transfer, must then be considered as a (small) perturbation on the adiabatic case (Eq. (6.2.13)). The approximated solution then consists of an unperturbed contribution $v^{(0)}(x,t)$ (the solution for the adiabatic case: Eq. (6.2.14)), and a perturbed contribution

$\mu v^{(1)}(x,t)$:

$$s^2 \hat{v} - c^2 \frac{\partial^2 \hat{v}}{\partial x^2} = s v_0 \cos \left[\frac{\pi x}{L_{gas}} \right] + \mu \frac{1}{s} \zeta \frac{P_{fiss}}{m_{tot}} \frac{\partial^2 \hat{v}}{\partial x^2} \quad (6.2.20a)$$

$$\hat{v}(x,s) = \hat{v}^{(0)}(x,s) + \mu \hat{v}^{(1)}(x,s) \quad (6.2.20b)$$

(dimensionless perturbation parameter μ). Substitution of Eq. (6.2.20b) into Eq. (6.2.20a), dividing left hand side and right hand side by μ and putting μ to zero renders an ordinary differential equation for the Laplace transform of the perturbed component. The solution of this equation is given by:

$$\hat{v}^{(1)}(x,s) = -\zeta \frac{P_{fiss}}{m_{tot}} \left[\frac{\pi}{L_{gas}} \right]^2 \frac{v_0}{\left[s^2 + \left(\frac{\pi c}{L_{gas}} \right)^2 \right]^2} \cos \left[\frac{\pi x}{L_{gas}} \right] \quad (6.2.21)$$

From this we can obtain the approximated solution for the non-adiabatic case (inverse Laplace transformation; $\mu \rightarrow 1$ in Eq. (6.2.20b)):

$$v(x,t) = v_0 \cos \left[\frac{\pi x}{L_{gas}} \right] \left[\cos(2\pi ft) + \zeta \frac{P_{fiss}}{m_{tot}} \frac{2\pi ft \cos(2\pi ft) - \sin(2\pi ft)}{4\pi f c^2} \right] \quad (6.2.22)$$

Clearly, the amplitude of v (and consequently also the amplitudes of the other variables: p , T , ρ_m) increases with time, and this increase occurs more rapidly with larger values of the specific power P_{fiss} / m_{tot} and/or the infinitesimal efficiency factor ζ of the gas.

6.3 Two-compartment model

As mentioned in Section 6.1, for the combined "two-compartment" GCFR model, to be presented in Chapter 7, we developed a more simple description of the GCFR gas dynamics, the so-called "Two-Compartment" Model ("TCM"). As is shown in Figure 6.1, in the TCM the total gas space (volume V_{tot}) is divided, by a movable imaginary wall (area $S_{gas} = \pi R_{gas}^2$), into two compartments, containing equal amounts of fuel gas ($m_1 = m_2 = m_{tot}/2$; $N_{0,1} = N_{0,2} = N_0/2$). The momentary position of this imaginary wall is indicated by the variable x_w ($-L_{gas}/2 \leq x_w \leq L_{gas}/2$). The imaginary wall controls the volumes of the "core" (subscript "1" in TCM description: $V_1(t)$) and "expander" (subscript "2": $V_2(t)$; $V_1(t) + V_2(t) = V_{tot}$).

The gas in both compartments is considered to be homogeneous and characterized by the pressure (p_1, p_2), the temperature (T_1, T_2), the volume (V_1, V_2) and the "actual" amount of gas (N_1, N_2). In both compartments the "general" equation of state (EOS: see Chapter 4, Eq. (4.2.1); dissociating and non-dissociating gas) is assumed to apply:

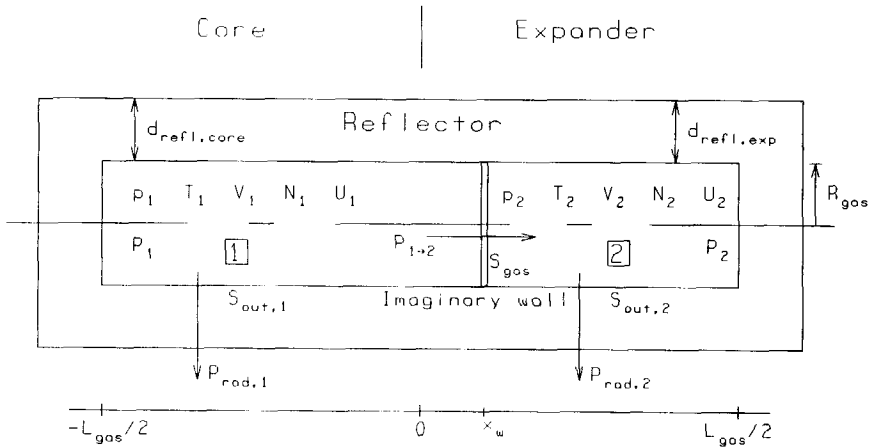


Figure 6.1 Two-compartment gas dynamics model.

$$V_1(\rho_1, T_1) = \frac{N_1(\rho_1, T_1)RT_1}{\rho_1} = \frac{N_{0,1}RT_1g(\rho_1, T_1)}{\rho_1} = \frac{\frac{1}{2}N_0RT_1g(\rho_1, T_1)}{\rho_1} \quad (6.3.1a)$$

$$V_2(\rho_2, T_2) = \frac{N_2(\rho_2, T_2)RT_2}{\rho_2} = \frac{N_{0,2}RT_2g(\rho_2, T_2)}{\rho_2} = \frac{\frac{1}{2}N_0RT_2g(\rho_2, T_2)}{\rho_2} \quad (6.3.1b)$$

The rates of change of the internal energy (U) of core ($j = 1$) and expander ($j = 2$) are given by:

$$\frac{dU_j}{dt} = \frac{d}{dt} \left[\frac{1}{2} U(\rho_j, T_j) \right] = P_{net,j} + (-1)^j \rho_j S_{gos} \frac{dx_w}{dt} \quad (6.3.2)$$

$U(\rho, T)$ = internal energy of N_0 "original" moles at (ρ, T) .

The net power supply $P_{net,j}$ to compartment j is given by:

$$P_{net,j} = P_j - P_{rad,j} + (-1)^j P_{1-2} \quad (6.3.3)$$

P_j is the fission power generated in compartment j (see Figure 6.1). In the combined "two-compartment" GCFR model this is, in general, a time-dependent quantity, which is calculated by the neutron kinetics part of the model (see Section 3.2). However, for the approximative analytical treatment presented in the remainder of this chapter, we assume a constant, spatially flat neutron flux, so that: $P_1 = P_2 = P_{fiss}/2$.

The axial heat transport P_{1-2} from core gas to expander gas (see Figure 6.1) is determined by photon diffusion and heat conduction (see Section 4.3,

Eq. (4.3.14)). This heat transport, however, is small compared to the transport to the surrounding wall. For the analytical treatment it is assumed to be zero.

In the combined "two-compartment" GCFR model (Chapter 7) we assume the (radial) heat transport $P_{rad,j}$ to the surrounding wall (see Figure 6.1: $P_{rad,j}$) to be determined by photon diffusion, according to Eq. (4.3.11) (substitute: $R_{core} = R_{gas}$; $S_{out} = S_{out,j}$; $T_{eff} = T_j$; $N = N_j$). For the analytical treatment in this chapter, however, we use two different models for the radiative heat transport to the surrounding wall. In the first model, like in the acoustic model (Section 6.2: Eq. (6.2.2)), we assume constant (radiative) heat transport per unit volume, in such a way that the total radiated power ($P_{rad,1} + P_{rad,2}$) is in balance with the (constant) total fission power $P_{fiss} (= P_1 + P_2)$, so that:

$$P_{rad,j} = P_{fiss} \frac{V_j}{V_{tot}} \quad (6.3.4a)$$

In the second model we assume the (radial) radiative heat transport to be given by Eq. (4.3.7) (substitute: $V = V_j$; $T_{eff} = T_j$; $N = N_j$), where the constant C_{rad} is chosen in such a way that the total radiated power at average temperature and pressure ($\langle p \rangle, \langle T \rangle$) is in balance with the (constant) total fission power P_{fiss} , so that:

$$P_{rad,j} = P_{fiss} \frac{\langle p \rangle}{V_{tot} \langle T \rangle^5} \frac{V_j T_j^5}{\rho_j} \quad (6.3.4b)$$

Like in the "acoustic model" (Section 6.2), however, it must be noted that the assumption of balance between the (constant) total fission power and the total radiated power (at average temperature and pressure) has limited validity for the case that increasing density oscillations in the gas occur.

For a complete description of the TCM gas dynamics, we furthermore need an equation of motion for the imaginary wall, separating the compartments. If we assume that a fraction α of the total mass m_{tot} of the fuel gas is attributed to the imaginary wall, we obtain:

$$\alpha m_{tot} \frac{d^2 x_w}{dt^2} = (\rho_1 - \rho_2) S_{gas} - 2 \Gamma m_{tot} \frac{dx_w}{dt} \quad (6.3.5)$$

The mass parameter α is chosen in such a way that, for small amplitude, the natural oscillation frequency in the TCM model is equal to the FAM value, given by Eq. (6.2.15). It therefore (see Section 6.3.1) has the value $(2/\pi)^2 (\approx 0.41)$.

The term containing Γ is a model for an energy extraction mechanism. In the numerical calculations with the combined "two-compartment" GCFR model (see Chapter 7) this term is assumed to be zero, because no energy extraction mechanism is taken into account there. However, in Section 6.4 we will present an analytical treatment of the effect of energy extraction, as described by the Γ -term.

For the set of equations, describing the dynamical behaviour of the gas in TCM description, we assume the following initial conditions:

$$\begin{aligned}
x_w(0) &= 0 & \varepsilon &= 0 \\
\rho_j(0) &= \langle \rho \rangle & T_j(0) &= \langle T \rangle \\
V_j(0) &= \frac{1}{2} V_{tot} & P_{net,j} &= 0 \\
v_w(0) &\equiv \frac{dx_w(0)}{dt} > 0 & \frac{dv_w(0)}{dt} &= 0
\end{aligned} \tag{6.3.6}$$

($v_w \equiv dx_w / dt =$ velocity of the imaginary wall). These initial conditions are consistent with the FAM initial conditions, stated in Eq. (6.2.4).

In the combined "two-compartment" GCFR model (see Chapter 7) it is necessary to make a connection from the gas dynamics part to the neutron kinetics part of the model. As was stated in Sections 2.4 and 3.2, the two-compartment point kinetics model expects information on the fuel gas density distribution in the form of the (FAM) density distribution variable ε , which is defined by Eq. (2.4.1). To establish the connection, we assume that the relationship between x_w (TCM-description of the gas) and ε (FAM-description of the gas) is given by:

$$\varepsilon = -\sigma \frac{x_w}{L_{gas}} \tag{6.3.7}$$

The parameter σ is chosen such in such a way that, for small amplitude, the momentary kinetic energy $E_{kin}(t)$ of the gas has the same value in both TCM and FAM description (Eq. (6.2.19)). It therefore (see Section 6.3.1) has the value $(4\sqrt{2})/\pi (\approx 1.80)$.

6.3.1 Adiabatic case

Like in the acoustic model (Section 6.2.1) we first "switch off" the fission power, the (radiative) heat transport (Eq. (6.3.2): $P_{net,j} = 0$) and the energy extraction mechanism (Eq. (6.3.5): $\Gamma = 0$). Following the same procedure as in Section 6.2 (small signal approximation; Laplace transformation) we can derive an expression for the Laplace transform of the position x_w of the imaginary wall:

$$s^2 \hat{x}_w + \frac{4 S_{gas}^2 (A_U + A_V \langle \rho \rangle)}{\alpha m_{tot} (B_U A_V - A_U B_V)} \hat{x}_w = v_w(0) \tag{6.3.8}$$

The natural oscillation frequency f of the system is given by:

$$f = \frac{1}{2\pi} \left[\frac{4 S_{gas}^2 (A_U + A_V \langle \rho \rangle)}{\alpha m_{tot} (B_U A_V - A_U B_V)} \right]^{1/2} = \frac{c}{\pi L_{gas} \sqrt{\alpha}} \tag{6.3.9}$$

(c given by Eq. (6.2.11)). The mass parameter α is chosen such that f has the same value in TCM and FAM description. So, using Eqs. (6.2.11), (6.2.15) and (6.3.9), we can calculate: $\alpha = (2/\pi)^2$.

From Eqs. (6.3.8) and (6.3.9) we can calculate, applying inverse Laplace transformation:

$$x_w(t) = \frac{v_w(0)}{2\pi f} \sin(2\pi f t) \tag{6.3.10}$$

Differentiation yields the velocity of the imaginary wall:

$$v_w(t) = v_w(0) \cos(2\pi ft) \quad (6.3.11)$$

And for the momentary kinetic energy of the gas we find:

$$E_{kin}(t) = \frac{1}{2} \alpha m_{tot} [v_w(t)]^2 = \frac{2}{\pi^2} m_{tot} [v_w(0)]^2 \cos^2(2\pi ft) \quad (6.3.12)$$

When we compare this with the FAM result, viz. Eq. (6.2.19), and assume equal momentary kinetic energy $E_{kin}(t)$ in both descriptions, we obtain:

$$v_o = \frac{2\sqrt{2}}{\pi} v_w(0) \quad (6.3.13)$$

($v_o, v_w(0) > 0$). Combination of Eqs. (6.2.15), (6.2.18), (6.3.10) and (6.3.13) then renders:

$$\varepsilon = -\frac{4\sqrt{2}}{\pi} \frac{x_w}{L_{gbs}} \quad (6.3.14)$$

So, the parameter σ in Eq. (6.3.7) has the value $(4\sqrt{2})/\pi$. We use this result in our numerical calculations with the combined "two-compartment" GCFR model (Chapter 7), where, however, the amplitude of the variables is not necessarily small.

6.3.2 Non-adiabatic case

In the same way as in the acoustic model (Section 6.2.2), we can use the solution of the adiabatic case, viz. Eqs. (6.3.10) and (6.3.11), to approximate the solution of the non-adiabatic case (Eq. (6.3.3): $P_1 + P_2 = P_{fiss} > 0$ and/or Eq. (6.3.5): $\Gamma > 0$), by applying first order perturbation theory. In the non-adiabatic cases, presented in this section, we keep $\Gamma = 0$ (i.e. no energy extraction), and we only consider the influence of fission energy production and (radiative) heat transport to the surrounding wall. For the first radiative heat transport model (Eq. (6.3.4a)) the first order perturbation procedure then yields:

$$v_w(t) = v_w(0) \left[\cos(2\pi ft) + \zeta \frac{P_{fiss}}{m_{tot}} \frac{2\pi ft \cos(2\pi ft) - \sin(2\pi ft)}{4\pi f c^2} \right] \quad (6.3.15)$$

This is consistent with the FAM result, viz. Eq. (6.2.22), which indicates that the two-compartment gas dynamics model is, also in the non-adiabatic case, a good approximation to the fundamental acoustic mode.

For the second radiative heat transport model (Eq. (6.3.4b)), we followed the same procedure, but, for the sake of simplicity, only for a non-dissociating perfect gas ($g \equiv 1$; $\zeta = \kappa - 1$; Eq. (4.5.10)). We obtained the following result:

$$v_w(t) = v_w(0) \left[\cos(2\pi ft) + \frac{P_{fiss}}{m_{tot}} 2(\kappa - 1)(3 - 2\kappa) \frac{2\pi ft \cos(2\pi ft) - \sin(2\pi ft)}{4\pi f c^2} \right] \quad (6.3.16)$$

The momentary kinetic energy $E_{kin}(t)$ is then given by:

$$\begin{aligned}
 E_{kin}(t) &= \frac{1}{2} a m_{tot} [v_w(t)]^2 \\
 &\approx \frac{2}{\pi^2} m_{tot} [v_w(0)]^2 \cos(2\pi f t) \\
 &\quad \times \left[\cos(2\pi f t) + \frac{P_{fiss}}{m_{tot}} 4(\kappa - 1)(3 - 2\kappa) \frac{2\pi f t \cos(2\pi f t) - \sin(2\pi f t)}{4\pi f c^2} \right]
 \end{aligned} \tag{6.3.17}$$

(square of perturbed contribution omitted).

The rate of change of the cycle-averaged kinetic energy $\langle E_{kin}(t) \rangle_\tau$, is small compared to the oscillation frequency f ($= 1/\tau$). Therefore, using $\langle \cos^2(2\pi f t) \rangle_\tau = 1/2$ and $\langle \cos(2\pi f t) \sin(2\pi f t) \rangle_\tau = 0$, the cycle-averaged kinetic energy can be approximated by:

$$\langle E_{kin}(t) \rangle_\tau \approx \frac{2}{\pi^2} m_{tot} [v_w(0)]^2 \left[\frac{1}{2} + \frac{P_{fiss}}{m_{tot}} \frac{(\kappa - 1)(3 - 2\kappa)}{c^2} t \right] \tag{6.3.18}$$

The relative rate of change of the cycle-averaged kinetic energy can then be approximated by:

$$\begin{aligned}
 \frac{1}{\langle E_{kin}(0) \rangle_\tau} \left(\frac{d \langle E_{kin}(t) \rangle_\tau}{dt} \right) &\approx \frac{P_{fiss}}{m_{tot}} \frac{2(\kappa - 1)(3 - 2\kappa)}{c^2} \\
 &= \frac{P_{fiss}}{N_0 R \langle T \rangle} \frac{2(\kappa - 1)(3 - 2\kappa)}{\kappa}
 \end{aligned} \tag{6.3.19}$$

From Eq. (6.3.19) it can be concluded that the maximum rate of change will be attained if $\kappa = \sqrt{3/2}$. For larger values of κ the variations of T_1 and T_2 will also be larger, which, for $\kappa > 3/2$, will render the net heat supply (Eqs. (6.3.3) and (6.3.4b)) to a compartment negative during compression. This leads to a decrease in amplitude, as the "direction" of the cycle in the $p(V)$ -diagrams (of both compartments) will be counter clockwise. For smaller κ , the variation of the temperatures will also be smaller and will be compensated by the variation of the volumes (V_1 and V_2) of the compartments. For $\kappa \rightarrow 1$ $\langle E_{kin}(t) \rangle_\tau$ is constant as all the extra heat (loss) is taken up (or supplied by) the gas, due to its large heat capacity (see Chapter 4, Eq. (4.5.10)). In Chapter 7 we will compare this result (Eq. (6.3.19)), which was obtained for small amplitude, with the numerical results of the combined "two-compartment" GCFR model calculations (constant, flat flux approximation: Section 7.3), for which, however, the amplitude of the oscillations is not necessarily small.

6.4 Energy extraction

In the TCM description of the gas dynamics, it is also possible to describe the effect of the presence of a "direct"- energy extraction mechanism (e.g. MHD). For this we assume that the (time-dependent) force, exerted by this mechanism on the imaginary wall, is proportional to the velocity $v_w(t)$, but has opposite sign (like a friction force): the Γ -term in Eq. (6.3.5) with $\Gamma > 0$. The momentary extracted power is then given by:

$$P_{ext}(t) = 2 \Gamma m_{tot} [v_w(t)]^2 \quad (6.4.1)$$

Again applying first order perturbation theory, we find for a general, dissociating gas, assuming the first radiative heat transport model (Eq. (6.3.4a)):

$$\begin{aligned} v_w(t) &= v_w(0) \cos(2\pi f t) \\ &+ v_w(0) \left[\zeta \frac{P_{fiss}}{m_{tot}} \frac{1}{4\pi f c^2} - \frac{\pi \Gamma}{8f} \right] 2\pi f t \cos(2\pi f t) \\ &- v_w(0) \left[\zeta \frac{P_{fiss}}{m_{tot}} \frac{1}{4\pi f c^2} + \frac{\pi \Gamma}{8f} \right] \sin(2\pi f t) \end{aligned} \quad (6.4.2)$$

If we now assume that the system is stationarily oscillating (i.e. the amplitude of the oscillations does not change with time), then the relationship between the (constant) total fission power P_{fiss} and the energy extraction parameter Γ is necessarily given by:

$$P_{fiss} = \frac{\pi^2 m_{tot} c^2 \Gamma}{2 \zeta} \quad (6.4.3)$$

From Eqs. (6.4.1) and (6.4.2) we find for the cycle-averaged extracted power:

$$\begin{aligned} \langle P_{ext}(t) \rangle_\tau &= \Gamma m_{tot} [v_w(0)]^2 \left[1 + \left(2 \zeta \frac{P_{fiss}}{m_{core}} \frac{1}{4\pi f c^2} \right)^2 \right] \\ &\approx \Gamma m_{tot} [v_w(0)]^2 \end{aligned} \quad (6.4.4)$$

(c^2 given by Eq. (6.2.11); the term containing ζ is small compared to 1 for "normal" values of P_{fiss}). Combining Eqs. (5.1.1), (6.4.3) and (6.4.4), we can calculate the conversion efficiency for the stationarily oscillating GCFR in TCM description (general, dissociating gas; radiative transport model according to Eq. (6.3.4a)):

$$\eta \equiv \frac{\langle P_{ext} \rangle_\tau}{P_{fiss}} = \frac{2 \zeta}{\pi^2} \left(\frac{v_w(0)}{c} \right)^2 \quad (6.4.5)$$

Using Eq. (6.3.13), we can also express the conversion efficiency in FAM quantities:

$$\eta = \frac{\zeta}{4} \left(\frac{v_0}{c} \right)^2 \quad (6.4.6)$$

Obviously, if the first radiative heat transport model (Eq. (6.3.4a)) is assumed to apply, high values for the conversion efficiency can only be attained with high values for the infinitesimal efficiency factor ζ and/or the velocity amplitude v_0 (FAM) or $v_w(0)$ (TCM), respectively. Colgate and Aamodt [Col57] e.g. assume $v_0 = 2c$.

For the second radiative transport model (Eq. (6.3.4b)) with perfect, non-dissociating gas, we can follow the same procedure, obtaining:

$$\begin{aligned} v_w(t) &= v_w(0) \cos(2\pi ft) \\ &+ v_w(0) \left[\frac{P_{fiss}}{m_{tot}} \frac{2(\kappa-1)(3-2\kappa)}{4\pi f c^2} - \frac{\pi\Gamma}{8f} \right] 2\pi ft \cos(2\pi ft) \\ &- v_w(0) \left[\frac{P_{fiss}}{m_{tot}} \frac{2(\kappa-1)(3-2\kappa)}{4\pi f c^2} + \frac{\pi\Gamma}{8f} \right] \sin(2\pi ft) \end{aligned} \quad (6.4.7)$$

For a stationarily oscillating GCFR, the relationship between the (constant) total fission power P_{fiss} and the energy extraction parameter Γ is then given by:

$$P_{fiss} = \frac{\pi^2 m_{tot} c^2 \Gamma}{4(\kappa-1)(3-2\kappa)} \quad (6.4.8)$$

And the cycle-averaged extracted power is given by:

$$\begin{aligned} \langle P_{ext} \rangle_\tau &= \Gamma m_{tot} [v_w(0)]^2 \left[1 + \left(\frac{P_{fiss}}{m_{tot}} \frac{(\kappa-1)(3-2\kappa)}{\pi f c^2} \right)^2 \right] \\ &\approx \Gamma m_{tot} [v_w(0)]^2 \end{aligned} \quad (6.4.9)$$

(c^2 given by Eq. (6.2.12)); the term containing κ is small compared to 1 for "normal" values of P_{fiss} . From Eqs. (6.3.13), (6.4.8) and (6.4.9) we can again calculate the conversion efficiency for a stationarily oscillating GCFR, expressed in FAM (v_0) or TCM ($v_w(0)$) quantities (perfect, non-dissociating gas; radiative transport model according to Eq. (6.3.4b)):

$$\begin{aligned} \eta &= \frac{4}{\pi^2} (\kappa-1)(3-2\kappa) \left(\frac{v_w(0)}{c} \right)^2 \\ &= \frac{1}{2} (\kappa-1)(3-2\kappa) \left(\frac{v_0}{c} \right)^2 \end{aligned} \quad (6.4.10)$$

When we compare Eqs. (6.4.10) and (6.3.19), we can conclude that, if the second radiative heat transport model (Eq. (6.3.4b)) is assumed to apply, η has a maximum for the value of κ , for which, in absence of an energy extraction mechanism, the rate of increase of the kinetic energy also has a maximum.

For both energy transport models (Eqs. (6.3.4a) and (6.3.4b)) it is clear that

a practical conversion efficiency can only be attained for velocity amplitudes (TCM: $v_w(0)$; FAM: v_0), which are higher than the velocity of sound c in the gas. However, for those cases the validity of the analytical treatment presented here is questionable.

Chapter 7

TWO-COMPARTMENT GCFR MODEL

7.1 Introduction

In Chapter 5 we stated that a possible way of avoiding the problem of the very high "basic pumping power" in an actively -magnetically- pumped GCFR, is using autonomous fuel gas density oscillations, driven by nuclear fissions. If the kinetic energy of the moving (ionized) fuel gas is to be directly extracted by magneto-hydrodynamical (MHD) or inductive (MI) means, then these oscillations should be increasing for the case that such an energy extraction mechanism is not present. In this way active compression of the fuel gas into the core region is not necessary anymore.

For the analysis of such a system, we developed a calculational model, combining neutron kinetics and gas dynamics, the so-called combined "two-compartment" GCFR model. In Section 7.2 we give a description of this calculational model. Its various parts (neutron statics, neutron kinetics, thermodynamics, heat transport, two-compartment gas dynamics) have already been introduced in the previous chapters.

In Section 7.3 some results of calculations are presented for the case of a constant, spatially flat neutron flux (i.e. neutron kinetics part "switched off"). We compare the numerical results obtained for this case with the results, obtained from an analytical treatment of the problem, applying first order perturbation theory, which was already presented in Section 6.3. It will be shown that, for velocity amplitudes which are not too high, the analytical approach yields values for the rate of increase of the cycle-averaged kinetic energy of the gas, which approximate quite well the numerical results.

Some results obtained from calculations with the "full" combined "two-compartment" GCFR model (neutron kinetics part "switched on" again) are presented in Section 7.4. In all our numerical calculations, we assume absence of an energy extraction mechanism, and therefore expect increasing density oscillations.

However, in Section 7.5 we give a qualitative description of the influence of the presence of a -direct- energy extraction mechanism on the behaviour of the GCFR, based on analytical considerations presented in Section 6.4.

7.2 Model description

For the construction of the combined "two-compartment" GCFR model we assume a symmetric, cylindrical GCFR (see Chapter 2, Figure 2.14, Case "I"), with a cylindrical gas space (volume V_{tot}) of length L_{gas} and radius R_{gas} . This gas space is assumed to be filled with an amount of N_0 moles of UCF gas (see Section 4.1), with total mass m_{tot} ($= N_0 M_0$; $M_0 = 0.277$ kg), which, however, is considered to behave as a non-dissociating, perfect gas (dissociation function $g(p, T) \equiv 1$; see Section 4.2). An overview of the most important parameters of this GCFR is listed

in Table 7.1

Table 7.1 General parameters of the "two-compartment" GCFR model.

Reactor geometry	Symmetric (case "1")
Gas space geometry	Cylinder
Length of gas space (L_{gas})	10.0 m
Radius of gas space (R_{gas})	1.0 m
Gas space cross section (S_{gas})	3.14 m ²
Total gas space volume (V_{tot})	31.4 m ³
Core wall thickness ($d_{refl,core}$)	1.0 m
Expander wall thickness ($d_{refl,exp}$)	1.0 m ($\delta_{th} = 0$)
Reactor gas composition (molar)	20.5 % CF ₄ 25.0 % UF ₄ 54.5 % UF ₆
Enrichment	50 % ²³⁵ U
c_p/c_v -ratio of the fuel gas (κ)	As specified
Total mass of the fuel gas at $\varepsilon = 0$ and $n_{RCD} = 1$ ($m_{tot,crit}$)	125.1 kg
Heat transfer coefficient (C_{rad})	4.90 · 10 ⁻⁹ W mole m ⁻⁶ K ⁻⁴
Axial photon diffusion heat transfer coefficient ($C_{rad,axial}$)	8.35 · 10 ⁻¹² W m ⁻¹ K ⁻⁴
Heat conductivity (λ_{th})	0.3 W m ⁻¹ K ⁻¹

The gas space is assumed to be subdivided into a core part and an expander part of equal, constant volume $V_{core} = V_{exp} = V_{tot}/2$ (FAM description of the fuel gas distribution; see Sections 2.4 and 6.2). The momentary distribution of the fuel gas over core and expander can be described in terms of the (FAM) density distribution variable ε , defined in Chapter 2 by Eq. (2.4.1), which for this case ($V_{core} = V_{exp}$) takes the form:

$$\varepsilon = 2 \frac{m_{core}}{m_{tot}} - 1 \quad (7.2.1)$$

(-1 < ε < 1; m_{core} = (time-dependent) mass of the fuel gas in the core part).

As indicated in Figure 7.1, the main components of the combined "two-compartment" GCFR model are neutron kinetics and gas dynamics. The (two-compartment) neutron (point-) kinetics model, which was introduced in Section 3.2, renders the momentary total fission power $P_{fiss}(t)$ and the distribution of the total fission power over core ($P_{core}(t)$) and expander ($P_{exp}(t)$):

$$\frac{dP_{fiss}}{dt} = \frac{\rho(\varepsilon) - \beta_{eff}}{\Lambda(\varepsilon)} P_{fiss} + \frac{Q_f}{v_f \Lambda(\varepsilon)} \sum_{i=1}^6 \lambda_i C_i \quad (7.2.2)$$

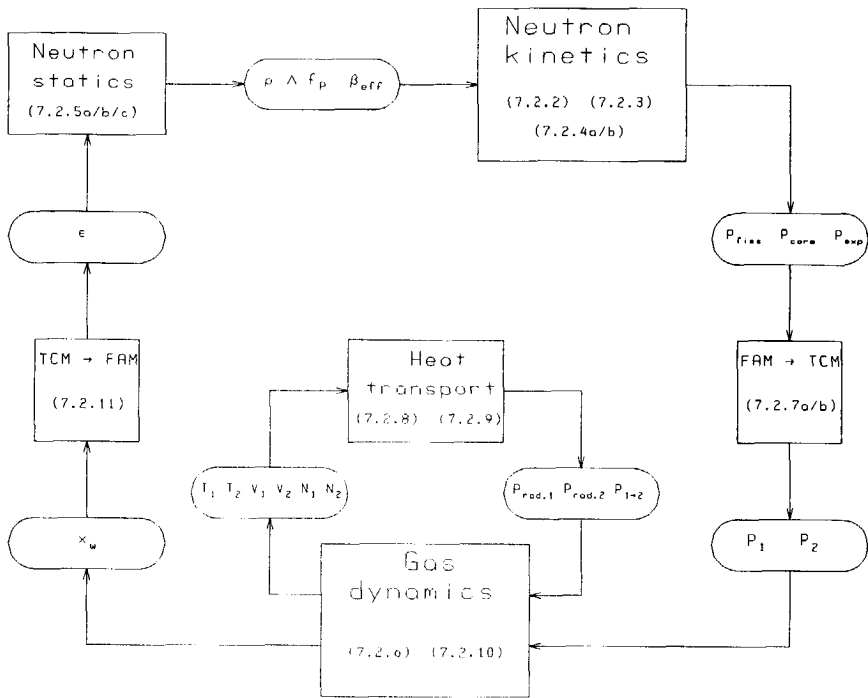


Figure 7.1 Structure of combined two-compartment GCFR model (corresponding equations indicated between brackets).

$$\frac{dC_i}{dt} = \frac{\nu_f \beta_{eff,i}}{Q_f} \langle P_{fiss} \rangle_\tau - \lambda_i C_i \quad i = 1, \dots, 6 \quad (7.2.3)$$

$$P_{core}(t) = f_p(\epsilon) P_{fiss}(t) \quad (7.2.4a)$$

$$P_{exp}(t) = [1 - f_p(\epsilon)] P_{fiss}(t) \quad (7.2.4b)$$

(see Section 3.2, Eqs. (3.2.10), (3.2.11), (3.2.12a) and (3.2.12b)). The delayed neutron contribution (Eq. (7.2.3)) is assumed to be dependent on the cycle-averaged total fission power $\langle P_{fiss} \rangle_\tau$ (oscillation period $\tau = 1/\lambda$) only, as the envisaged oscillation period ($\tau \approx 0.02$ s) is much shorter than the half life of the shortest living delayed neutron precursor ($T_{1/2} = 0.23$ s; see Appendix B, Table B.4).

The neutron kinetics part is controlled by the reactor physical quantities ρ (reactivity), Λ (neutron generation time), f_p (core power fraction) and $\beta_{eff,i}$ (effective delayed neutron fraction for delayed group i). These quantities are dependent upon the fuel gas distribution over core and expander, described by the variable ϵ , and also on the average (relative) density of the fuel gas (n_{RCD} ; relative to the critical

average density), which is proportional to the total mass (m_{tot}) of the fuel gas. For the symmetric, cylindrical GCFR (Section 2.4, Figure 2.14, case "I"), an average relative density $n_{RCD} = 1$ corresponds to $m_{tot} = 125.1$ kg (see Section 2.4, Table 2.8). This dependence can be described by relatively simple functional relations, obtained from a "multi-compartment" static GCFR neutronic model (see Section 2.2, Eqs. (2.2.31), (2.2.32) and (2.2.33), and Appendix A). The coefficients of these functional relations were obtained from two-dimensional static neutron diffusion calculations (see Section 2.4, Table 2.9). Assuming a symmetric, cylindrical GCFR (case "I") and a "rectangular" density distribution (see Section 2.4, Eq. (2.4.2)), the following expressions were found for the reactor physical quantities ρ , Λ and f_p :

$$\rho = -1.0466 \cdot 10^{-2} n_{RCD} + 0.30551 - 0.29345 n_{RCD}^{-1} - 5.063 \cdot 10^{-2} \varepsilon^2 \quad (7.2.5a)$$

$$\Lambda = 2.2733 \cdot 10^{-5} n_{RCD} + 6.0107 \cdot 10^{-4} + 3.0004 \cdot 10^{-3} n_{RCD}^{-1} + 4.556 \cdot 10^{-4} \varepsilon^2 \quad (7.2.5b)$$

$$f_p = 0.5000 + 0.459 \varepsilon \quad (7.2.5c)$$

For the effective delayed neutron fraction, we used: $\beta_{eff} = 0.00652$ (see Section 2.3).

For the gas dynamics part of the combined "two-compartment" GCFR model (Figure 7.1) we utilized the two-compartment gas dynamics model (TCM), which was introduced in Section 6.3. As is indicated in Figure 6.1, in this model the total gas space is assumed to be divided into two parts with equal mass (instead of equal volume, like in the FAM description; see Section 6.2), by a movable imaginary wall with momentary position x_w . Because we assume a non-dissociating, perfect gas, Eqs. (6.3.2) and (6.3.3), which describe the rate of change of the internal energy of the (TCM) compartments, can be written as:

$$N_j c_v \frac{dT_j}{dt} = \frac{dU_j}{dt} = P_j - P_{rad,j} + (-1)^j \left[P_{1 \rightarrow 2} + p_j S_{gas} \frac{dx_w}{dt} \right] \quad (7.2.6)$$

($j = 1$ denotes core; $j = 2$ denotes expander (TCM description)); c_v = specific heat at constant volume of the fuel gas; T_j = temperature in compartment j ; p_j = pressure in compartment j ; P_j = produced fission power in compartment j ; $P_{rad,j}$ = heat transport from compartment j to the surrounding graphite wall (areas $S_{out,1}$ and $S_{out,2}$, respectively); $P_{1 \rightarrow 2}$ = heat transport from core to expander by photon diffusion and conduction; see Figure 6.1).

The produced fission powers in core and expander in TCM description (Figures 6.1 and 7.1: P_1 and P_2 , respectively) are related to the produced fission powers in FAM description (Figure 7.1: P_{core} and P_{exp} , respectively) by the assumption that the ratio of the specific powers in core and expander is the same in both descriptions:

$$P_1 = \frac{(1 - \varepsilon)}{(1 - \varepsilon) f_p + (1 + \varepsilon) (1 - f_p)} P_{core} \quad (7.2.7a)$$

$$P_2 = \frac{(1 + \varepsilon)}{(1 - \varepsilon) f_p + (1 + \varepsilon) (1 - f_p)} P_{exp} \quad (7.2.7b)$$

In case of a constant, spatially flat neutron flux (for which $f_p = 0.5 (1 + \epsilon)$; Eq. (2.4.4)) we then obtain: $P_1 = P_2 = 0.5 P_{fiss}$.

As was stated in Section 4.3, the axial heat transport P_{1-2} from core to expander (in TCM description; see Figure 6.1 and Figure 7.1) is assumed to be determined by heat conduction and photon diffusion (heat conductivity λ_{th}), according to:

$$P_{1-2} = \frac{2 S_{gas}}{L_{gas}} [C_{rad,axial} (T_1^4 - T_2^4) + \lambda_{th} (T_1 - T_2)] \quad (7.2.8)$$

(also see Eq. (4.3.14)). For our calculations we assumed $C_{rad,axial} = 8.35 \cdot 10^{-13} \text{ W m}^{-1} \text{ K}^{-4}$ (see Section 4.3) and $\lambda_{th} = 0.3 \text{ W m}^{-1} \text{ K}^{-1}$ [Boe91b]. This heat transport, however, is small compared to the transport to the graphite wall surrounding the fuel gas. It was assumed to be zero in the analytical treatment, presented in Section 6.3.

The heat transport from core and expander to the surrounding graphite wall is assumed to be determined by photon diffusion, according to:

$$P_{rad,j} = C_{rad} \frac{V_j \left[\frac{1}{2} R_{gas} S_{out,j} \right] T_j^4}{N_j} \quad (7.2.9)$$

($N_j = N_0/2$; also see Section 4.3, Eq. (4.3.11)). However, for demonstration purposes, and to account for the effect of conduction and convection, we used a ten times larger value for C_{rad} than was given in Section 4.3, viz. $4.90 \cdot 10^{-9} \text{ W mole m}^{-6} \text{ K}^{-4}$.

Under the assumption of absence of an energy extraction mechanism, the equation of motion for the imaginary wall in the TCM description of the gas dynamics (Section 6.2, Eq. (6.3.5)) becomes:

$$a m_{tot} \frac{d^2 x_w}{dt^2} = (p_1 - p_2) S_{gas} \quad (7.2.10)$$

As mentioned in Section 6.3, the mass parameter a is chosen such that the natural oscillation frequency in the TCM description is equal to the frequency in the FAM description. It therefore has the value $(2/\pi)^2$ (see Section 6.3.1).

The relationship between the x_w -variable in the TCM description and the ϵ -variable in the FAM description is given by:

$$\epsilon = -\sigma \frac{x_w}{L_{gas}} \quad (7.2.11)$$

(see Eq. (6.3.7)). As stated in Section 6.3.1, the parameter σ is chosen such that, for small amplitude, the momentary kinetic energy E_{kin} of the gas has the same value in the TCM and FAM descriptions. It therefore has the value $(4\sqrt{2})/\pi$.

In Table 7.2 the initial conditions for our combined "two-compartment" GCFR model calculations are listed. These initial conditions are in agreement with those, used in the analytical treatment (Eq. (6.3.6)).

Table 7.2 Initial conditions and auxiliary parameters for combined "two-compartment" GCFR calculations.

Total mass of the fuel gas (m_{tot})	As specified
Initial core gas temperature (T_1)	10,000 K
Initial expander gas temperature (T_2)	10,000 K
Initial core gas pressure (p_1)	11.89 bar
Initial expander gas pressure (p_2)	11.89 bar
Initial "division wall" position ($x_w(0)$)	0
Initial "division wall" velocity ($v_w(0)$)	As specified (> 0)
Initial total fission power (P_{fiss})	118.83 MW

7.3 Constant flat flux approximation

Using the values given in Table 7.1 for the reactor parameters and assuming a constant, spatially flat neutron flux (i.e. constant P_{fiss} and $P_1 = P_2$; neutron kinetics part "switched off"), we calculated the behaviour of the system, starting from the initial conditions (and parameters) listed in Table 7.2. The total fission power P_{fiss} was given the value 118.83 MW, because this is approximately equal to the heat transported to and through the surrounding wall, when the gas temperature is 10,000 K.

In Figure 7.2 an example is shown of the behaviour of several system variables as a function of time (between 0.0 and 0.1 s). The oscillatory nature of the behaviour is clearly demonstrated. At the given parameter values the oscillation frequency is approximately 31 Hz. This is in agreement with the value found from analytical considerations (see Section 6.2, Eq. (6.2.15)). The oscillation frequency is not sensitively dependent upon the initial velocity, as long as this initial velocity is less than the sound velocity (approximately 613 m/s for the case presented in Figure 7.2; see Section 6.2, Eq. (6.2.12)).

Figure 7.3 demonstrates the influence of the c_p/c_v -ratio κ of the fuel gas on the rate of change of the cycle-averaged kinetic energy $\langle E_{kin}(t) \rangle_t$ (approximated by the relative change in 1 second). For κ -values higher than approximately 1.50, $\langle E_{kin}(t) \rangle_t$ decreases with time, which means that the density oscillations are damped out. This is caused by the fact that, at high κ , the variations of the temperatures T_1 and T_2 are also high, which renders the net heat supply (fission power minus heat leakage) to a compartment negative during compression. This leads to a decrease in amplitude (see Section 6.3.2). For smaller κ the variation in T_1 (and T_2) is smaller and is compensated by the variations in $S_{out,1}$ (and $S_{out,2}$) and V_1 (and V_2) and the net heat supply to the compartment during compression is positive. For $\kappa \rightarrow 1$, $\langle E_{kin} \rangle_t$ is constant as all the extra heat (loss) is taken up (or supplied by) the gas due to its large heat capacity. Figure 7.3 also shows that, at high (1000 m/s) velocity, increase of the amplitude, although smaller than for lower velocities, still occurs, provided that κ is in the correct range.

In the figure also the analytical results are shown, which were obtained from

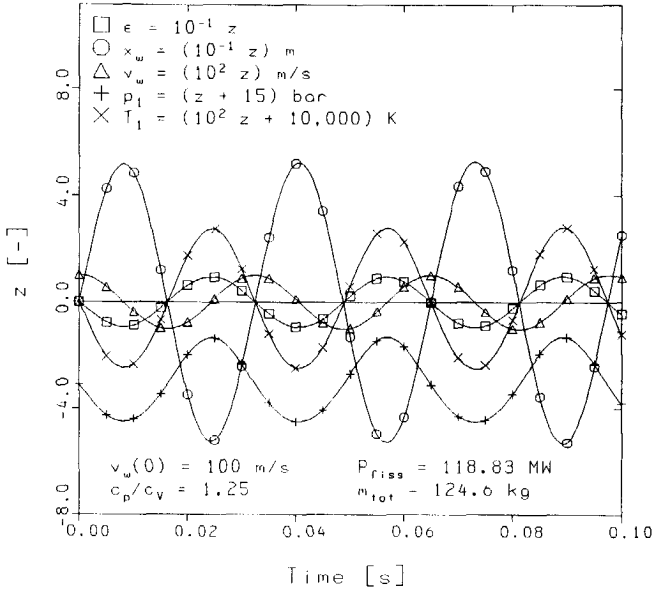


Figure 7.2 Constant, flat flux calculation results (z is a dimensionless vertical scale variable).

first order perturbation calculations (see Section 6.3.2, Eq. (6.3.19)). The analytical solution predicts that $\langle E_{kin}(t) \rangle$, decreases with time for $\kappa > 1.50$ (exactly). For the numerical calculations, the cycle-averaged kinetic energy already decreases for κ -values which are somewhat lower than 1.50. This is caused by the fact that, in the numerical treatment, axial heat transport ($P_{1 \rightarrow 2}$; Eq. (7.2.8)) has been taken into account, which decreases the net heat supply to a compartment during compression. This is not the case in the analytical treatment. The analytical solution also predicts a maximum rate of increase of $\langle E_{kin}(t) \rangle$, for $\kappa = \sqrt{3/2} \approx 1.22$. Altogether, from Figure 7.3 it can be concluded that the numerical results are approximated quite well by the results from first order perturbation theory, especially for initial velocities which are not too high.

7.4 Combined model calculation results

Having the neutron kinetics part of the combined "two-compartment" GCFR model "switched on" again, we performed calculations for the case of a symmetric GCFR. For this configuration the reactivity ρ and the neutron generation time Λ are even functions of ε (Eqs. (7.2.5a) and (7.2.5b)).

In Figure 7.4 an example is shown of the behaviour of several system variables as a function of time (between 0.0 and 0.1 s), starting from the initial conditions stated in Table 7.2. The total fuel mass m_{tot} (and consequently the

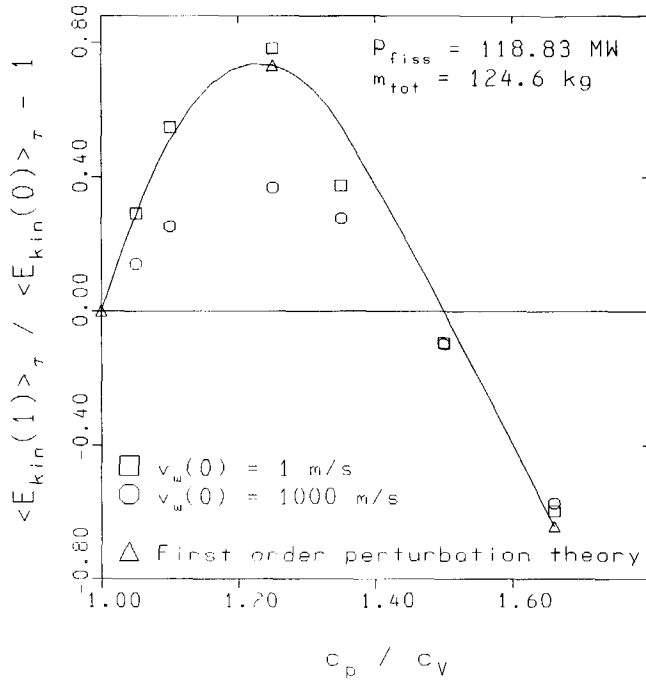


Figure 7.3 Influence of c_p/c_V -ratio κ on the kinetic energy behaviour for constant, flat flux.

average relative fuel gas density n_{RCD}) was chosen such that, for $\varepsilon = 0$ (i.e. spatially flat fuel gas density distribution), the reactivity $\rho(0)$ has the value $2 \cdot 10^{-4}$. Again the oscillatory behaviour of the variables is clearly demonstrated. The density distribution variable ε and the core fission power P_{core} oscillate at approximately 31 Hz and have the same phase, because, for the case of the symmetric GCFR, the neutron flux in the fuel gas is approximately spatially flat (see Section 2.4, Figure 2.15). The reactivity ρ , which is an even function of ε , oscillates at the double frequency. The total fission power P_{fiss} consists of a small oscillatory part superimposed on a trend function part. The oscillatory part, which is determined by the prompt neutrons (see Eqs. (7.2.2) and (7.2.3)), oscillates at the same frequency as the reactivity (phase lag of 90°). Its local minima and maxima correspond to the zero crossings of the reactivity. The trend function part is decreasing, as the cycle-averaged reactivity is more negative than is required for stationary operation [Akc58, Smi65].

We also studied the influence of the initial velocity $v_w(0)$, and the reactivity $\rho(0)$ at spatially flat ($\varepsilon = 0$) fuel gas density distribution, on the behaviour of the (cycle-averaged) kinetic energy of the fuel gas, for a c_p/c_V -ratio $\kappa = 1.25$ (other parameters and initial conditions as stated in Tables 7.1 and 7.2). Figure 7.5 presents the results of these calculations. In all cases shown the rate of change of

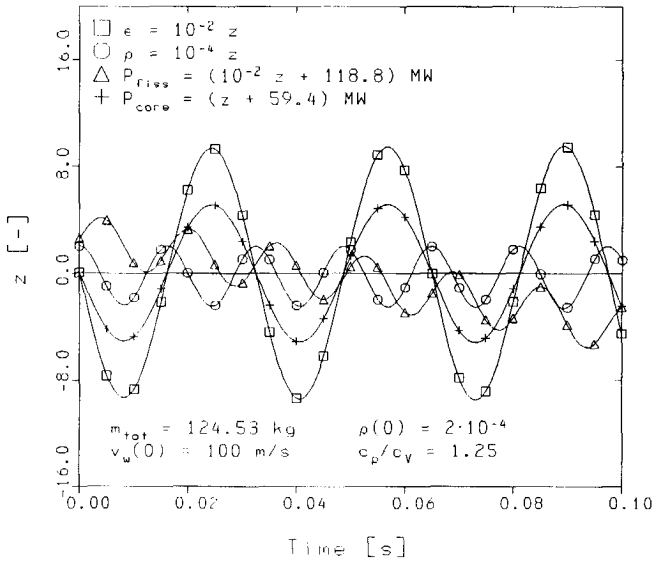


Figure 7.4 Combined "two-compartment" GCFR calculation results (symmetric GCFR; z is a dimensionless vertical scale variable).

the (cycle-averaged) kinetic energy decreases with increasing $v_w(0)$. For $v_w(0) = 1000$ m/s (which is higher than the sound velocity in the gas, given by Eq. (6.2.12)) the rate of change becomes rather small, but even in this case it stays positive.

The flat fuel density distribution reactivity $\rho(0)$ does not seem to have much influence on the rate of change, except for the case of $\rho(0) = 2 \cdot 10^{-2}$. In this case the reactor is initially prompt supercritical (because $\rho(0) > \beta_{eff} = 0.00652$) and even prompt supercritical on average (except for the case of $v_w(0) = 1000$ m/s) and the total fission power P_{fiss} increases rapidly, which also causes a rapid increase of the (cycle-averaged) kinetic energy. This can also be expected from analytical considerations (Eqs. (6.3.17) and (6.3.18)). For $v_w(0) = 1000$ m/s the reactor is -on average- not prompt supercritical and the increase of the total fission power and of the (cycle-averaged) kinetic energy takes place much more gradually.

For all cases shown (except for the case of $\rho(0) = 2 \cdot 10^{-2}$) the rate of change of the kinetic energy is somewhat smaller than for the reference case (constant, spatially flat neutron flux and, consequently, constant total fission power), which is also shown in the figure. This is caused by the fact that, in the combined model, the variation of the core fission power fraction f_p with ε (Eq. (7.2.5c); FAM description) is smaller than for the case of a constant, spatially flat flux (Section 2.4, Eq. (2.4.4)). In the TCM description of the gas dynamics, this causes the produced fission power in a compartment (Eqs. (7.2.7a) and (7.2.7b)) during compression to be smaller than in the case of a constant, spatially flat flux. This, on its turn, decreases the net heat supply to a compartment during compression, which again lowers the rate of increase of the cycle-averaged kinetic energy.

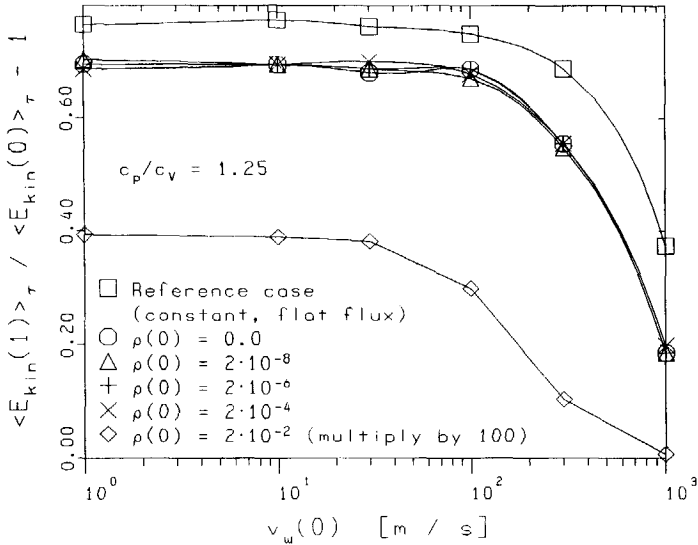


Figure 7.5 Influence of initial reactivity and initial velocity on the kinetic energy behaviour.

However, the behaviour with increasing initial velocity $v_w(0)$ is similar, and we expect that this also will be the case for other values of κ than 1.25.

For these cases ($\rho(0) \neq 2 \cdot 10^{-2}$) also the total fission power is limited, as, for increasing amplitude of v_w and ε , the cycle-averaged reactivity will become negative (Eq. (7.2.5a)). If, however, $\rho(0)$, and consequently m_{tot} , is too high (e.g. $2 \cdot 10^{-2}$), then the increase of the amplitude of ε , as ε is limited between -1 and 1, can not lower the reactivity below zero sufficiently and the reactor will be supercritical on average.

A remark must be made about the neutron point kinetics model, applied in the combined "two-compartment" GCFR model. In the neutron kinetics model, which was introduced in Section 3.2, it is assumed that the total number of neutrons in the system, required for a given total fission power, is independent of the fuel density distribution (variable ε). In Appendix D, however, it is shown that this is not exactly the case (see Eqs. (D.6), (D.7) and (D.8)), not even for the symmetric, cylindrical GCFR. The effect gives rise to an extra term in the equation for the total fission power (compare Eqs. (7.2.2) and (D.11)) and further investigation of the influence of this term on the neutron kinetical behaviour of the system is necessary. However, we expect that the influence of this extra term on the (cycle-averaged) total fission power will be small, so that the rate of increase of the oscillations will only slightly be altered.

7.5 Influence of energy extraction

Up till now we performed calculations for the case of absence of a -direct- energy extraction mechanism, which show that, provided that κ is in the correct range, increasing (density, velocity, kinetic energy) oscillations occur (assumed: perfect, non-dissociating gas). In Section 6.4 we presented an analytical treatment (first order perturbation theory) of the effect of the presence of an energy extraction mechanism, modelled as a friction force proportional to the velocity (Eq. (6.3.5): Γ -term; $\Gamma > 0$). An expression for the conversion efficiency η was derived for the case that the system is stationarily oscillating (Eq. (6.4.10); assumed: second radiative transport model: Eq. (6.3.4b); constant cycle-averaged fission power). In this case, the relationship between the constant (cycle-averaged) total fission power P_{fiss} and the energy extraction parameter Γ will be given by Eq. (6.4.8). The cycle-averaged reactivity will be slightly negative, as was the case for the "solid piston" GCFR (see Chapter 5, Figure 5.5; also see [Akc58, Smi65]).

If the demanded extracted power P_{ext} is increased (i.e. Γ increases: Eq. (6.4.9)) we expect the following behaviour. An increase of Γ will cause a decrease of the oscillation amplitude of the velocity v_w (Eq. (6.4.7)) and, consequently, of ϵ . For the symmetrical GCFR, this will cause an increase of the cycle-averaged reactivity (Eq. (7.2.5a)), which will cause the cycle-averaged total fission power to increase (Eq. (7.2.2)). This will again cause an increase in the oscillation amplitude until the cycle-averaged fission power is again in balance with Γ (Eq. (6.4.8)) and the cycle-averaged reactivity has again returned to its old value (i.e. the oscillation amplitude has returned to its old value). The latter is only possible if m_{tot} is not too high, because ϵ can only attain values between -1 and 1. If this condition is met, the (cycle-averaged) total fission power will follow the demanded extracted power.

7.6 Conclusions

Numerical model studies have been performed for a symmetric, cylindrical GCFR, using a "two-compartment" GCFR model, which combines neutron kinetics, thermodynamics and (two-compartment) gas dynamics. For these calculations we assumed absence of a -direct- energy extraction mechanism (such as MHD or MI), and we also assumed the fuel gas to behave as a non-dissociating, perfect gas. The calculations show that increasing autonomous density oscillations of the fuel gas are possible, provided that the c_p/c_v -ratio κ is in the correct range, viz. $1 < \kappa < 1.5$.

For velocities, which are not too high (less than the sound velocity c in the gas) it was found that rate of increase of the oscillations can be predicted quite well by an analytical formula, which was derived in Chapter 6 by applying first order perturbation theory to the two-compartment gas dynamics model.

On the basis of these analytical considerations it can be expected that, in the case that a -direct- energy extraction mechanism is present, the (cycle-averaged) total fission power will follow the demanded extracted power, provided that the total fuel mass m_{tot} is not too high.

EPILOGUE

In the investigation of a futuristic, conceptual system, such as the GCFR described in this thesis, usually a number of more or less questionable assumptions are made, and the investigation of the validity of all of these assumptions is a necessary condition for having even the slightest possibility of ever reaching the stage of a practical realization of such a system. Furthermore, it is inevitable that there are numerous questions and problems connected to the development of such a system, which haven't even been mentioned in the previous chapters. In this final section we will comment on some of these assumptions, questions and problems.

One of the main assumptions is that of chemical and thermodynamical equilibrium between the UCF fuel gas and the graphite container wall. However, the existence of this equilibrium has only been investigated for the case of a stationary (i.e. non-oscillating) GCFR and it is certainly not impossible on beforehand that, in an oscillating GCFR, serious corrosion of the wall will occur. This might not only be a problem for the GCFR with oscillating fuel gas, but also for a stationary GCFR, in which spontaneous convection of the fuel gas occurs.

In our investigations, the UCF gas is assumed to be "fresh", which means that we assume the absence of fission products in the gas and that we also do not take into account the effect of depletion of the fuel. However, except for the very first moment of operation, fission products (such as xenon and samarium) will be present in the gas, which necessitates the investigation of their influence on the neutron physical, chemical and thermodynamical behaviour of the GCFR. Continuous "on-line" reprocessing will reduce the amount of fission products in the fuel gas and will also supply the fresh fuel, necessary for operation.

In our numerical and analytical model calculations, it was assumed that the GCFR was already "running". However, a GCFR with oscillating fuel gas is not "born" that way, and it is important to investigate how a GCFR can be brought safely from the cold, stationary state to the hot, oscillating state.

From calculations using the "solid piston" GCFR model, we found that a conversion efficiency of only a few percent can be reached, if it is required that the thermodynamic cycle is closed by itself. It is also interesting to investigate whether a closed cycle with higher conversion efficiency is possible as well. This can possibly be achieved by maximizing the fission energy production during the compressed state, by careful selection of the volume sequence $V_{fuel}(t)$, combined with external reactivity control.

The gas dynamics model used in the combined "two-compartment" GCFR model is a quite crude, one-dimensional, two-compartment model. For a more detailed investigation of the GCFR gas dynamics it is necessary to use also a more detailed gas dynamics model, which is capable of calculating in more detail the space- and time-dependent distribution of the density (and other thermodynamic variables) in the fuel gas. This can also be connected to a more accurate neutron statics/kinetics model than the model based on the single density distribution variable ϵ , which was used in our model calculations.

We did not investigate in detail the interaction between the moving -ionized-fuel gas and the magnetic field generated by the coil system and it is not beyond doubt that magneto-inductive energy extraction is possible. An alternative for the magneto-inductive energy extraction scheme might be a system, which makes use

of the mechanical forces exerted by the oscillating (moving) gas on the graphite container.

It is clear that, concerning this highly unconventional but nevertheless promising nuclear reactor concept, still many problems remain unsolved and many questions unanswered. They present, however, a challenge for continued investigations.

Appendix A

MULTI-COMPARTMENT NEUTRON TRANSPORT

In order to obtain a better understanding of the numerical -static- neutron transport and neutron diffusion calculation results (see Chapter 2) and to derive (formal) functional relationships between several reactor physical properties of a GCFR (e.g. fit functions for the reactivity and the neutron generation time as function of the fuel gas density), so-called "multi-compartment" neutron transport models were developed and studied. Like in nodal methods (see e.g. Ronen [Ron86]), in these models the reactor is considered to consist of M compartments (index $m = 1, \dots, M$), in each of which the volume-averaged neutron flux $\varphi_m^{(g)}$ (G groups; index $g = 1, \dots, G$) is to be calculated. The (volume-averaged) neutron fluxes in all compartments and all energy groups are represented by the so-called flux vector $\underline{\varphi}$ with $(M \cdot G)$ elements:

$$\{\varphi\}_{[(G-1)m + g]} \equiv \varphi_m^{(g)} \quad (\text{A.1})$$

(curly brackets "{...}" denote element of matrix or vector). The volumes V_m of the M compartments are represented in the (diagonal) volume matrix \underline{V}_M (double underline "" denotes matrix) with $(M \cdot G) \times (M \cdot G)$ elements:

$$\{V_M\}_{[(G-1)m + g], [(G-1)m' + g']} \equiv \delta_{[(G-1)m + g], [(G-1)m' + g']} \times V_m \quad (\text{A.2})$$

($\delta_{i,j}$ is the Kronecker delta). The neutron group velocities $v^{(g)}$ are represented in the (also diagonal) velocity matrix $\underline{v}^{(G)}$ with $(M \cdot G) \times (M \cdot G)$ elements:

$$\{v^{(G)}\}_{[(G-1)m + g], [(G-1)m' + g']} \equiv \delta_{[(G-1)m + g], [(G-1)m' + g']} \times v^{(g)} \quad (\text{A.3})$$

We now introduce the multi-compartment representation of the time-dependent neutron transport equation:

$$\left(\underline{v}^{(G)}\right)^{-1} \cdot \underline{V}_M \cdot \frac{d\underline{\varphi}}{dt} = \underline{F} \cdot \underline{V}_M \cdot \underline{\varphi} + \underline{E} \cdot \underline{V}_M \cdot \underline{\varphi} + \underline{V}_M \cdot \underline{S} \quad (\text{A.4})$$

(exponent "-1" denotes inverse of the matrix; \underline{F} = fission matrix; \underline{E} = absorption-, scatter- and transport matrix; \underline{S} = external source density vector; assumed to be zero further on).

The fission matrix \underline{F} is also a $(M \cdot G) \times (M \cdot G)$ matrix in which each element:

$$\{F\}_{[(G-1)m + g], [(G-1)m' + g']} = w_{m' \rightarrow m}^{(g)} \eta_{m'}^{(g')} n_{rel, m'} \Sigma_{a, m'}^{(g')} \quad (\text{A.5})$$

represents the contribution of the group g' flux in compartment m' to the rate of increase of the the number of group g neutrons in compartment m by means of fission: $w_{m' \rightarrow m}^{(g)}$ is the fraction of the fission neutrons, born in compartment m' , which re-appear in group g in compartment m ; $\eta_{m'}^{(g')}$ is the number of fission neutrons produced per absorbed group g' neutron in compartment m' ; $n_{rel, m'}$ is the -dimensionless- relative density in compartment m' ; $\Sigma_{a, m'}^{(g')}$ is the macroscopic group g' absorption cross section (at the reference density) in compartment m' .

The absorption-, scatter- and transport matrix \underline{E} is a $(M \cdot G) \times (M \cdot G)$ matrix in which each element:

$$\{E\}_{((G-1)m + g), ((G-1)m' + g')} = +\delta_{m,m'} n_{rel,m} \sum_{s,m} \Sigma_{s,m}^{(g' \rightarrow g)} \quad (\text{A.6a})$$

(scattering from group g' to group g in compartment m)

$$+\delta_{g,g'} K_{m' \rightarrow m}^{(g)} \quad (\text{A.6b})$$

(transport of group g neutrons from compartment m' to m)

$$-\delta_{m,m'} \delta_{g,g'} n_{rel,m} \Sigma_{a,m}^{(g)} \quad (\text{A.6c})$$

(absorption of group g neutrons in compartment m)

$$-\delta_{m,m'} \delta_{g,g'} n_{rel,m} \sum_{g''=1}^G \Sigma_{s,m}^{(g \rightarrow g'')} \quad (\text{A.6d})$$

(scattering from group g in compartment m)

$$-\delta_{m,m'} \delta_{g,g'} \sum_{m''=0}^M K_{m \rightarrow m''}^{(g)} \quad (\text{A.6e})$$

(transport of group g neutrons from compartment m)

represents the contribution of the group g' flux in compartment m' to the rate of change of the number of group g neutrons in compartment m by means of absorption, scattering and transport: $K_{m \rightarrow m'}^{(g)}$ is the probability per unit path length that a group g neutron leaves compartment m and enters compartment m' ; $K_{m \rightarrow 0}^{(g)}$ is the probability per unit path length that a group g neutron will leak out of the system from compartment m ; $\Sigma_{s,m'}^{(g' \rightarrow g)}$ is the macroscopic scattering cross section (at the reference density) in compartment m' for scattering from group g' to group g .

Under the assumption that the net transport of group g neutrons from compartment m' to compartment m is zero if the group g neutron fluxes have the same value in both compartments, a reciprocity relation can be derived for the compartment-to-compartment transport coefficients $K_{m' \rightarrow m}^{(g)}$ and $K_{m \rightarrow m'}^{(g)}$, viz.:

$$V_m K_{m \rightarrow m'}^{(g)} = V_{m'} K_{m' \rightarrow m}^{(g)} \quad (\text{A.7})$$

The compartment-to-compartment transport coefficients $K_{m \rightarrow m'}^{(g)}$ are assumed to be independent of the relative densities $n_{rel,m}$. Furthermore, $K_{m \rightarrow m'}^{(g)}$ is assumed to be zero if compartment m' is not adjacent to compartment m , and $K_{m \rightarrow 0}^{(g)}$ is assumed to be zero if compartment m is not on the outer boundary of the system or if a reflective boundary condition is to be imposed.

In the same way as in the "normal" neutron transport equation (see e.g. [Dud76]), we can introduce the multiplication factor k_{eff} (or rather its inverse: λ) to obtain a (time-independent) eigenvalue equation (eigenvalue λ , eigenvector $\underline{\psi}$), the multi-compartment equivalent of the time-independent neutron transport equation:

$$\underline{H} \cdot \underline{\psi} \equiv \lambda \underline{F} \cdot \underline{V}_M \cdot \underline{\psi} + \underline{E} \cdot \underline{V}_M \cdot \underline{\psi} = \underline{0} \quad (\text{A.8})$$

In order for this equation to have a non-trivial solution (i.e. a non-zero eigenvector) the determinant of the system matrix \underline{H} , defined in Eq. (A.8), must be zero. Solving the equation:

$$\det \underline{H} = 0 \quad (\text{A.9})$$

renders the eigenvalue(s) λ and the corresponding eigenvector(s) \underline{u} in terms of all the system parameters mentioned above (group cross sections, relative densities, etc.). For simple models (e.g. one-group/one-compartment) a formal solution can be obtained by a "hand calculation" (see e.g. Section 2.2.2), but for the problems with more groups and/or more compartments we utilized the algebraic manipulation code package REDUCE [Ray87]. However, the results obtained by the built-in equation solver of REDUCE can be very complicated indeed and if M and/or G is/are too high, no solution is found at all.

But, as we are only interested in the fundamental eigenvalue (and the corresponding eigenvector), we can make use of the fact that $\det \underline{H}$ is a polynomial in λ and approximate the true solution for the eigenvalue λ (which does not differ very much from unity for the -approximately- critical reactor) by:

$$\lambda \approx 1 - \frac{(\det \underline{H})_{(\lambda=1)}}{\left[\frac{d(\det \underline{H})}{d\lambda} \right]_{(\lambda=1)}} \quad (\text{A.10})$$

which is a rational algebraic function of the relative densities $n_{rel,m}$ in the compartments ($m = 1, \dots, M$). The approximated value of the reactivity can then (see Eq. (2.2.5)) be written as:

$$\rho = 1 - \lambda \approx \frac{(\det \underline{H})_{(\lambda=1)}}{\left[\frac{d(\det \underline{H})}{d\lambda} \right]_{(\lambda=1)}} \quad (\text{A.11})$$

The corresponding approximation for the eigenvector \underline{u} can then be obtained by substituting the approximated eigenvalue into Eq. (A.8), removing one equation from the corresponding system of equations (retaining $(M \cdot G) - 1$ independent equations with $(M \cdot G)$ unknowns: $\varphi_m^{(g)}$), and solving the remaining system.

The total fission power produced in the system can then be calculated:

$$P_{fiss} = Q_f \sum_m \sum_g \frac{\eta_m^{(g)}}{\nu_f^{(g)}} V_m n_{rel,m} \Sigma_{a,m}^{(g)} \varphi_m^{(g)} \quad (\text{A.12})$$

And the fraction of the total fission power produced in compartment m is given by:

$$f_{P,m} = \frac{\sum_g \frac{\eta_m^{(g)}}{\nu_f^{(g)}} V_m n_{rel,m} \Sigma_{a,m}^{(g)} \varphi_m^{(g)}}{\sum_{m'} \sum_g \frac{\eta_{m'}^{(g)}}{\nu_f^{(g)}} V_{m'} n_{rel,m'} \Sigma_{a,m'}^{(g)} \varphi_{m'}^{(g)}} \quad (\text{A.13})$$

(Q_f = average thermal energy produced per fission event; $\nu_f^{(g)}$ = average number of neutrons released per fission event, caused by a group g neutron; we assume the same Q_f and $\nu_f^{(g)}$ in all compartments where fission occurs).

Another important reactor physical quantity, from the point of view of neutron kinetics (see Chapter 3 and Appendix D) is the neutron generation time, which can be defined as:

$$\Lambda \equiv \frac{\text{total number of neutrons}}{\text{fission neutron production rate}} \quad (\text{A.14})$$

(see e.g. [Dud76]). This quantity, too, can be calculated if the flux vector is known.

However, the computer codes DAC-I [NEA72] and CITATION [NEA79] calculate the neutron generation time Λ by also taking into account the neutron importance (or adjoint function), which is the (fundamental) eigenfunction of the (time-independent) adjoint neutron transport or adjoint neutron diffusion equation (see e.g. [Lew65, Bel70]). To be more in line with this way of calculation, we now introduce the multi-compartment analogue of the time-independent adjoint equation:

$$\underline{H}^T \cdot \underline{\psi}^* = \underline{Q} \quad (\text{A.15})$$

(superscript "T" denotes transposed matrix or vector; $\underline{\psi}^*$ = adjoint function (or neutron importance) vector). As this equation has the same eigenvalue(s) as the "forward" equation (Eq. (A.8)), we can approximate $\underline{\psi}^*$ in the same way as $\underline{\psi}$. Taking the neutron importance into account, the neutron generation time Λ is then given by:

$$\Lambda = \frac{(\underline{\psi}^*)^T \cdot (\underline{V}^{(0)})^{-1} \cdot \underline{V}_M \cdot \underline{\psi}}{(\underline{\psi}^*)^T \cdot \underline{E} \cdot \underline{V}_M \cdot \underline{\psi}} \quad (\text{A.16})$$

Furthermore, the reactivity can also be written as:

$$\rho = \frac{(\underline{\psi}^*)^T \cdot (\underline{E} + \underline{E}) \cdot \underline{V}_M \cdot \underline{\psi}}{(\underline{\psi}^*)^T \cdot \underline{E} \cdot \underline{V}_M \cdot \underline{\psi}} \quad (\text{A.17})$$

(fundamental eigenvectors $\underline{\psi}$ and $\underline{\psi}^*$). This expression for the reactivity was used in the derivation of the neutron point kinetics equations (see Chapter 3 and Appendix D).

We now have obtained (approximated) expressions for λ (and thus for k_{eff} and ρ), Λ and $f_{p,m}$, which are rational algebraic functions of the relative densities $n_{rel,m}$ in the compartments. In Chapter 2 (Section 2.2.2) some examples are given of multi-compartment neutron transport models.

Appendix B

NEUTRON GROUP CONSTANTS

All of the static neutron transport and neutron diffusion calculations, presented in Chapter 2, were performed by means of computer codes (viz. XSDRNPM [NEA87], ANISN [NEA86a], ANISN(E) [NEA79], CITATION [NEA89], DAC-I [NEA72]), which follow a multi-group approach for taking into account the dependence of neutron cross sections (and other quantities such as the fission spectrum and the neutron velocity) on the neutron energy (see e.g. [Dud76]). So, group constants (viz. neutron group cross sections, group fission spectrum, neutron group velocities) had to be calculated, starting from basic data (neutron point cross sections, resonance parameters), taken from the ENDF/B-IV [Gar75] (routes "A" and "C"; see Section 2.1, Figure 2.1) and JEF-1 [NEA85] (route "B") data libraries.

In the following, we will first describe the generation of so-called fine group constants (in fine group libraries), necessary for fine group (one-dimensional) neutron transport calculations by XSDRN (route "A") and XSDRNPM (routes "B" and "C"). Subsequently we will describe the generation of the so-called broad group constants (in broad group libraries), necessary for subsequent broad group neutron transport and neutron diffusion calculations. This generation was also performed by the codes XSDRN (route "A") and XSDRNPM (routes "B" and "C") by a so-called group condensation calculation (from 123 to 4 in routes "A" and "C"; 187 to 4 groups in route "B"). Finally, we will list some data on delayed neutrons, which is necessary for the calculation of the effective delayed neutron fractions $\beta_{eff,i}$ by the codes DAC-I and CITATION (see Chapter 2).

Following route "B" from the JEF-1 data library onward, we used the code system NSLINK [Lee91] to generate a fine group AMPX-Master library. The most important part of the NSLINK system is the code NJOY [NEA86b], which contains modules for data extraction (from ENDF/B and JEF data files), unresolved resonance energy self-shielding [Wil66, Bel70, Mas76], Doppler broadening [Bec62, Wil66, Bel70, Dud76, Mas76], group cross section generation, etc. Group cross sections are cross sections, which are averaged over an energy interval (the group), using the neutron flux as a weighting function [Dud76]. The resulting AMPX-Master library contains (microscopic) neutron group cross sections for selected nuclides at selected temperatures (see Table B.1) in the LANL 187 energy group structure [NEA86b], together with resolved resonance parameters (to be processed later by NITAWL). This 187-group structure has the advantage over the GAM-THERMOS 123-group structure [NEA78], used in routes "A" [Dam88, Dve88, Kui88] and "C", that its neutron energy range is wider ($1 \cdot 10^{-5}$ eV to 20.0 MeV for the LANL set; $5 \cdot 10^{-3}$ eV to 14.9 MeV for the GAM-THERMOS set). Furthermore, in the thermal energy range the LANL set has a finer energy group structure.

Subsequently, the code NITAWL [NEA87] was used for resolved resonance energy self-shielding treatment and Doppler broadening (resonance nuclides ^{235}U and ^{238}U - only) according to the Nordheim [Nor62] method and the generation of a 187-group AMPX-Working library, which contains (microscopic) neutron group cross sections only (no resonance parameters anymore) for the nuclides, present in the AMPX-Master library, at the same temperatures. This resonance treatment

Table B.1 Parameters for JEF-1 and ENDF/B-IV data extraction, fine group neutron cross section generation and resolved resonance treatment (routes "A" and "B").

Calculational route	"A" ("old")	"B" ("new")
Basic data library	ENDF/B-IV	JEF-1
Energy group structure	GAM-THERMOS	LANL
# fine energy groups	123	187
Energy range (eV)	$5 \cdot 10^{-3} - 14.9 \cdot 10^6$	$1 \cdot 10^{-5} - 20.0 \cdot 10^6$
# thermal groups	30	52
Upper energy of first thermal group (eV)	1.86	3.059
Weighting function	1/E	Fission spectrum- 1/E- Maxwellian
Core gas composition (molar %)	"old" 30 % CF ₄ 70 % UF ₄	"new" 20.5 % CF ₄ 25.0 % UF ₄ 54.5 % UF ₆
Enrichment	50 % ²³⁵ U	50 % ²³⁵ U
Core gas nuclide densities (10 ¹⁸ cm ⁻³)	¹² C 6.64 ¹⁹ F 88.5 ²³⁵ U 7.74 ²³⁸ U 7.74	¹² C 4.1977 ¹⁹ F 93.281 ²³⁵ U 8.1621 ²³⁸ U 8.1621
Core gas temperature(s) (K)	10,000	2000, 5000, 10,000, 20,000
Reflector material	graphite	graphite
Reflector bulk temperature(s) (K)	1000	1000, 2000
Resolved resonance treatment method	Nordheim	Nordheim
Resonance nuclides	²³⁵ U, ²³⁸ U	²³⁵ U, ²³⁸ U
"Absorber lump" geometry	sphere	sphere
"Absorber lump" radius (cm)	100.0	100.0
Dancoff factor C (0.0 = single fuel lump surrounded by infinite moderator)	0.0	0.0

is necessary, as the succeeding multigroup neutron transport code XSDRNPM can only use group cross sections as data and no parameters, describing the (resolved) resonance cross sections. NITAWL updates the group cross sections in the resolved resonance energy range so that the effect of these -sharply peaked- cross section resonances is taken into account in the succeeding neutron transport calculation by XSDRNPM. NITAWL only needs to process the resolved resonances, as the NSLINK system has already taken care of the unresolved ones. For the

resolved resonance treatment, the GCFR was considered as a single, spherical fuel (absorber) lump, surrounded by an infinite moderator (Dancoff factor in NITAWL = 0.0 [Nor62, Dud76, Mas76]), which is a close approximation for a spherical GCFR. In Table B.1 the most important parameters for these calculations are listed. Note that we used nuclide densities, based on the composition of UCF gas in chemical and thermodynamical equilibrium with a graphite wall at 2000 K, according to Klein (1987): 20.5 % CF₄, 25.0 % UF₄ and 54.5 % UF₅ (50 % enriched in ²³⁵U; RSG "new" gas composition: see Sections 2.3 and 4.1).

In route "A", the code XLACS [NEA73a] was used to create an ("old" format) AMPX-Master library, containing GAM-THERMOS 123 energy group neutron cross sections and resolved resonance parameters. The subsequent resolved resonance processing according to the Nordheim method was performed by a part of the XSDRN code [NEA73b], which also performs the fine group neutron transport calculation [Dve88, Kui88]. Consequently, no AMPX-Working library was generated. The important parameters for these calculations are listed in Table B.1 as well. Note that nuclide densities were used, based on a UCF gas composition of 70 % UF₄ (50 % enriched) and 30 % CF₄ ("old" gas composition) [Dam83, Dve88, Kui88].

In route "C" first the "old" format AMPX-Master library (route "A") was converted by the COMET code [NEA78], resulting in a ("new" format) AMPX-Master library, still containing GAM-THERMOS 123 energy group neutron cross sections and resolved resonance parameters. Subsequently an AMPX-Working library was produced by NITAWL, using the "new" gas composition. The remaining parameters were chosen as in route "A" (see Table B.1).

The fine group AMPX-Master and AMPX-Working libraries contain so-called microscopic cross section data (dimension [m²]). However, in the computer codes applied for the neutron transport and neutron diffusion calculations, so-called macroscopic cross sections (dimension [m⁻¹]) are used. In general, a macroscopic (group) cross section Σ_j (reaction type *j*: *t* = total, *a* = absorption, *s* = scattering, etc) for a mixture of nuclides is defined in terms of the microscopic (group) cross sections σ_{*j*,*i*} and the densities *n_i* of the nuclides (index *i*) in the mixture by:

$$\Sigma_j \equiv \sum_i n_i \sigma_{j,i} \quad (\text{B.1})$$

In Figure B.1 the macroscopic total (Σ_t) and absorption (Σ_a) neutron group cross sections of the fuel gas (Table B.1, route "B") are shown as function of the neutron energy, for a gas temperature of 10,000 K, the gas temperature at which most of our static neutronic calculations were performed. As expected [Dud76] for low energies both cross sections display a *E*^{-1/2}-behaviour. For these low energies (below approximately 0.1 eV), absorption is the largest contribution to the total cross section. For high energies (above approximately 1.0 keV) scattering is the main contribution (note the ¹⁹F scattering resonances between 2·10⁴ and 1·10⁶ eV). In the intermediate energy range (approximately 1.0 - 1·10³ eV) the resonances of ²³⁵U and ²³⁸U (e.g. the 6.7 eV resonance of ²³⁸U) are clearly present.

In general, the mean free path λ_{*j*} for a certain nuclear reaction *j* (scattering, absorption, total, etc.) is given by:

$$\lambda_j \equiv (\Sigma_j)^{-1} \quad (\text{B.2})$$

From Figure B.1 it can be concluded that, for neutron energies above approximately

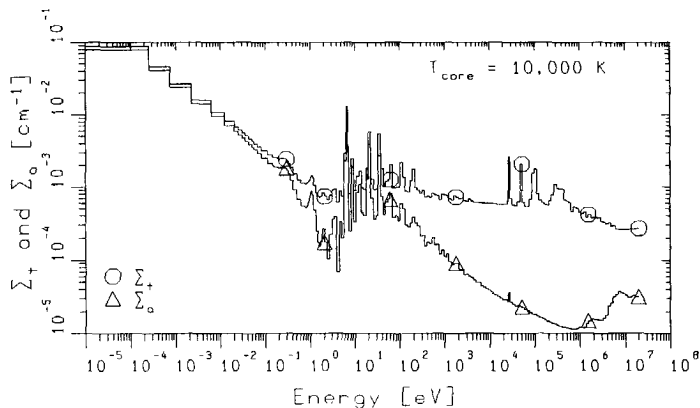


Figure B.1 Macroscopic total and absorption fine group cross sections for UCF gas ("new" gas composition; RSG gas density).

1 eV, both the total and the absorption mean free path are of the order of 10 (total) or 100 (absorption) metres, strongly dependent upon the neutron energy. This is -much- larger than the -assumed- dimensions of the gas space of our GCFR (see Chapter 2), which implies that criticality is based on multiple "reflections" of neutrons by the graphite wall, requiring a high reflection coefficient of that wall.

As mentioned above, XSDRNPM (routes "B" and "C"; main calculational parameters are listed in Chapter 2, Table 2.1) was also used to generate the broad group cross section libraries, necessary for subsequent neutron transport and neutron diffusion calculations by ANISN/DAC-1 [NEA86a, NEA72] and CITATION [NEA89], respectively. The broad group neutron cross sections are calculated (by XSDRN and XSDRNPM) by averaging the flux-weighted fine group cross sections over the broad group energy range and over the spatial zone to which the resulting broad group cross sections are to apply. In this way also spatial shielding is taken into account in the broad group cross sections, as these cross sections will depend on the spatial zone ("core" or "reflector" in the -spherical- GCFR; see Figure 2.2) for which they are calculated.

For the subsequent broad group calculations it is also necessary to know the broad group fission spectrum $\chi^{(g)}$ and the broad group neutron velocities $v^{(g)}$ (broad group index g). The latter are calculated by XSDRNPM by averaging the flux-weighted inverse of the neutron velocity $v(E)$ over the energy range of the broad group concerned, and by subsequently calculating the inverse of this average [Bel70]. In Table B.2 the results of these broad group averaging calculations (routes "B" and "C") are listed. We also show the results of Dveer [Dve88], who used XSDRN (route "A").

Note that there exists a discrepancy between the (group 3 and 4) velocities calculated by XSDRN (route "A") on one hand and those calculated by XSDRNPM (routes "B" and "C") on the other. We suspect that XSDRN does not calculate the broad group velocities in the correct way, like XSDRNPM, but unfortunately we used these velocities in our first ANISN(E)/DAC-1 calculations [Kui88], rendering

Table B.2 Results of XSDRNPM (and XSDRN) cross section condensation calculations.

Calculational route	Broad group index g	Broad group fission spectrum $\chi^{(g)}$	Broad group velocity $v^{(g)}$ (ms ⁻¹)
"A" ENDF/B-IV GAM-THERMOS 123 fine groups XSDRN	1	0.98286	1.054·10 ⁷
	2	1.7003·10 ⁻²	2.156·10 ⁶
	3	1.37·10 ⁻⁴	1.304·10 ⁵
	4	0.0	7.009·10 ³
"B" JEF-1 LANL 187 fine groups NITAWL XSDRNPM	1	0.984403	1.085·10 ⁷
	2	1.54733·10 ⁻²	1.916·10 ⁶
	3	1.23994·10 ⁻⁴	9.000·10 ⁴
	4	1.59074·10 ⁻⁹	4.761·10 ³
"C" ENDF/B-IV GAM-THERMOS 123 fine groups NITAWL XSDRNPM	1	0.982859	1.078·10 ⁷
	2	1.7003·10 ⁻²	1.916·10 ⁶
	3	9.102·10 ⁻⁴	9.102·10 ⁴
	4	1.102·10 ⁻⁹	4.837·10 ³

values of the neutron generation time Λ which are too low by a factor of approximately 1.5 (see Section 2.3). The values for $v^{(g)}$, calculated by XSDRNPM from LANL 187-group data ("B") and GAM-THERMOS 123-group data ("C") agree very well. The differences are less than 2 %. The wider energy range of the LANL 187 group set can be noticed in the $v^{(1)}$ being slightly higher and the $v^{(4)}$ being slightly lower than the corresponding values found with the GAM-THERMOS 123 group set. In all three cases presented, most of the fission neutrons (more than 98 %) appear in group 1.

Table B.3 Broad group (route "B") mean free paths and diffusion lengths in the RSG core fuel gas.

Broad group index	λ_t (m)	λ_a (m)	L (m)
1	18.6	696	78.8
2	12.5	330	40.9
3	8.62	11.7	6.24
4	3.72	4.88	2.43

In Table B.3 the broad group values of the (total and absorption) mean free path and the diffusion length (route "B") in the fuel gas (nuclide densities as listed in Table B.1) are listed. Note that for the higher energy groups (1 - 3) these values are again -much- larger than the -assumed- dimensions of the gas space of our GCFR (see Chapter 2).

Table B.4 Delayed neutron parameters for ^{235}U .

Delayed group index i	Yield β_i (%)	λ_i (s^{-1})	$T_{1/2}$ (s)	Broad group index g	$\chi_d^{(g)}$ (-)
1	0.021	0.0126	55	1	0.93
2	0.142	0.030	23	2	0.07
3	0.128	0.112	6.2	3	0.00
4	0.257	0.301	2.3	4	0.00
5	0.075	1.14	0.61		
6	0.027	3.01	0.23		
$\beta_{tot} = 0.650$ %					

For the calculation of the effective delayed neutron fractions $\beta_{eff,i}$ (delayed neutron precursor time group i ; $i = 1, \dots, 6$; sum β_{eff} , the total effective delayed neutron fraction), it is necessary to supply the spectrum $\chi_d^{(g)}$ of the delayed neutrons, the delayed neutron fractions β_i (sum: β_{tot}) and the delayed neutron precursor decay constants λ_i [Bel70, Mas76]. These quantities were taken from the JEF-1 library (delayed fractions β_i and decay constants λ_i for ^{235}U) and Stephenson [Step86] (delayed neutron spectrum $\chi_d^{(g)}$). The spectrum of delayed group 2 was assumed for all delayed groups, as is often done [Mas76]. In Table B.4 the necessary information on delayed neutrons is listed.

Appendix C

TEMPERATURE INFLUENCE

The neutron transport and neutron diffusion calculations, by the codes XSDRN [NEA73b], XSDRNPM [NEA87], ANISN(E) [NEA79], ANISN [NEA86a], DAC-I [NEA72] and CITATION [NEA89], on spherical and cylindrical GCFRs (reported in Chapter 2) were all performed using group cross sections for a fuel gas temperature of 10,000 K and a reflector temperature of 1000 K. However, as indicated in Appendix B (Table B.1), in the 187-group AMPW-Working library (route "B"; see Chapter 2, Figure 2.1) microscopic neutron group cross sections are available for fuel gas temperatures of 2000, 5000, 10,000 and 20,000 K, and for reflector (bulk) temperatures of 1000 and 2000 K. This gives the opportunity to show the effect of a temperature change on these group cross sections.

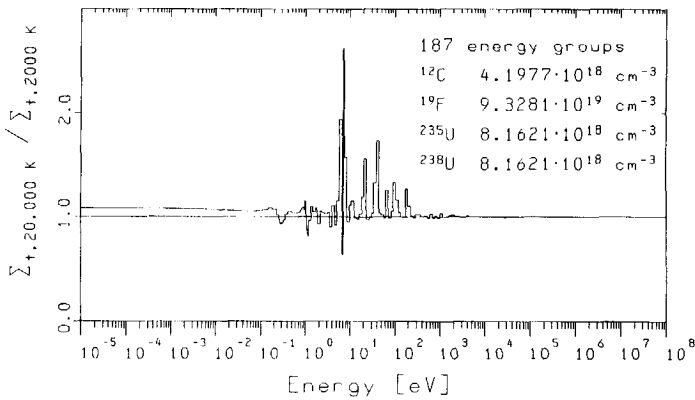


Figure C.1 Influence of a temperature increase of the core fuel gas from 2000 to 20,000 K on the macroscopic total group cross sections.

Figure C.1 demonstrates the influence of the core gas temperature on the macroscopic total group cross section Σ_t (see Appendix B, Eq. (B.1) for the definition) of the fuel gas mixture ("new" composition: see Appendix B, Table B.1), when its temperature is increased from 2000 to 20,000 K. Clearly, at high neutron energies (far above the resolved resonance energy and thus much higher than kT ; T = temperature, k = Boltzmann's constant = $0.861735 \cdot 10^{-4} \text{ eV K}^{-1}$) the temperature change from 2000 to 20,000 K has no influence on the total cross section, as the neutrons have a much higher velocity than the core gas nuclei. At low neutron energies (below approximately 0.1 eV) the cross section increases with temperature. In the resonance region of ^{235}U and ^{238}U (approximately between 1.0 and 10^4 eV) the ratio of the total group cross sections varies around 1.0. This is due to Doppler broadening [Bec64, Wil66, Bel70] of the resonances, which causes some group cross sections to be decreased and other -neighbouring- group

cross sections to be increased by the NITAWL [NEA87] resonance treatment (see Appendix B).

The influence of a (bulk) temperature increase of the graphite reflector on its macroscopic total group cross sections is demonstrated in Figure C.2 (nuclide density $8.55 \cdot 10^{22} \text{ cm}^{-3}$). Again for high neutron energies no changes can be seen, but for low energies (below approximately 1 eV) the macroscopic total group cross section increases with temperature.

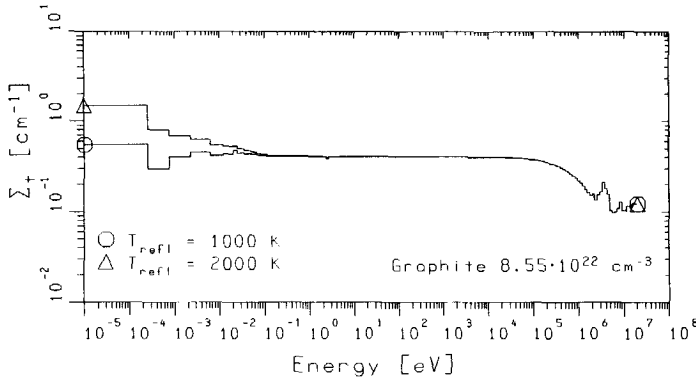


Figure C.2 Influence of a temperature increase of the reflector from 1000 to 2000 K on the macroscopic total group cross sections.

As the temperatures of the core fuel gas (T_{core}) and reflector (T_{refl}) influence the group cross sections, it can be expected that they also influence the neutron spectrum and the multiplication factor. The influence of core and reflector temperature on the neutron spectrum in the GCFR core (RSG geometry; 187-group XSDRNPM calculation, route "B"; see Chapter 2) is demonstrated in Figure C.3. At high energies, no change of the spectrum with T_{core} or T_{refl} can be detected, which is expected as the neutron energies are much larger than kT . Also at low (thermal) energies the influence of T_{core} on the spectrum is very small: in Figure C.3 the influence of a change from 10,000 K (RSG) to 20,000 K can only be noticed as slightly thicker graph lines in the low energy region. The influence of the reflector (bulk) temperature T_{refl} on the neutron spectrum (in the core) is much greater. An increase of from 1000 K (RSG) to 2000 K causes an easily detectable shift of the local maximum in the thermal region from approximately 0.20 eV to 0.40 eV. So the thermal part of neutron spectrum in the core is mainly determined by the reflector temperature.

The influence of the core and reflector temperature on the effective multiplication factor k_{eff} (of the RSG) is demonstrated in Figure C.4 (187-group XSDRNPM calculation, route "B"). As expected [Dam83], an increase of the reflector (bulk) temperature causes a decrease in k_{eff} , which can be explained by the fact that an increase of the reflector temperature causes a hardening of the thermal part of the spectrum (see above), which on its turn lowers the effective absorption cross section of the fuel gas (see Appendix B, Figure B.1). An increase of the core temperature causes a decrease in k_{eff} as well, but the influence of the

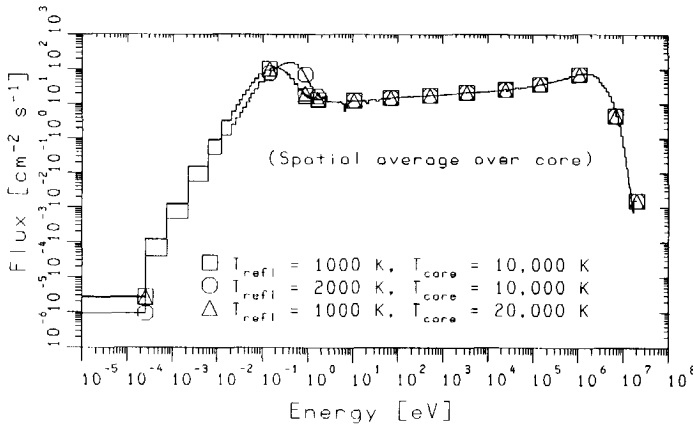


Figure C.3 Influence of the core temperature (T_{core}) and reflector temperature (T_{refl}) on the neutron spectrum (flux per unit lethargy) in the RSG core.

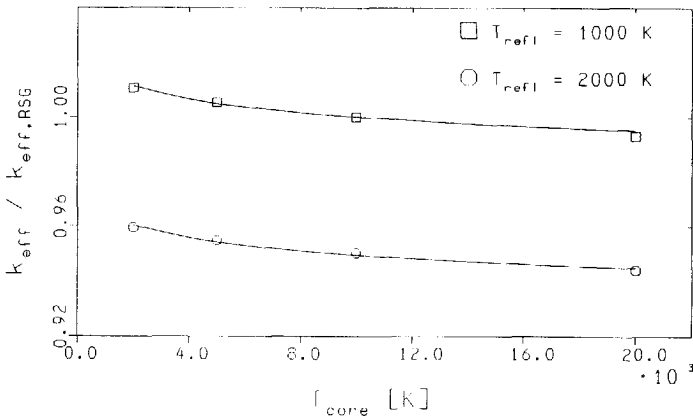


Figure C.4 Influence of core temperature and reflector temperature on k_{eff} .

core temperature is much smaller than that of the reflector temperature, because the (thermal part of the) neutron spectrum is hardly influenced by a change of T_{core} (see above). Following van Dam and Hoogenboom [Dam83] we used a fit function to describe this temperature influence, but we also included the influence of the core temperature:

$$\frac{k_{eff}}{k_{eff,RSG}} = \left(\frac{T_{core}}{T_{core,RSG}} \right)^{a_{TC}} \times \left(\frac{T_{refl}}{T_{refl,RSG}} \right)^{a_{TR}} \quad (C.1)$$

We found: $a_{TC} = -7.06 \cdot 10^{-3}$ and $a_{TR} = -7.48 \cdot 10^{-2}$. Clearly, Eq. (C.1) gives a good description of the influence of T_{core} and T_{refl} on the multiplication factor, which is

also demonstrated quantitatively by the low value of Δ (defined in Chapter 2 by Eq. (2.3.1)): $\Delta = 0.08$. This indicates a good fit. Van Dam and Hoogenboom [Dam83] found a somewhat different value for α_{TR} , viz. $-9.0 \cdot 10^{-2}$, but their calculations were performed for a core radius of $R_{core} = 2$ m and a lower density of the fuel gas. However, the variations of k_{eff} , due to variations of the core gas temperature, are small compared to variations of k_{eff} , caused by the expected variations of fuel gas density and density distribution in the "solid piston" (Chapter 5) and "two-compartment" (Chapter 7) model calculations. Furthermore, in those calculations the reflector temperature is assumed to be kept constant at 1000 K. Therefore, temperature feedback is not taken into account in the neutronics parts of those models.

Appendix D

TWO-COMPARTMENT NEUTRON KINETICS

In Chapter 3, two neutron kinetics models were derived to be used in the "solid piston" (Chapter 5) and the "two-compartment" (Chapter 7) combined GCFR model, respectively. It is also possible to derive both models from a more general description of two-compartment neutron kinetics. Starting from the multi-compartment time-dependent neutron transport equation (Appendix A, Eq. (A.4)), we can derive a one-group/two-compartment ($G = 1$, $M = 2$; group index g omitted further on) neutron transport equation, including delayed neutrons:

$$\underline{V}_M \cdot \frac{1}{v} \frac{d\underline{\psi}}{dt} = \underline{F}_p \cdot \underline{V}_M \cdot \underline{\psi} + \underline{E} \cdot \underline{V}_M \cdot \underline{\psi} + \underline{V}_M \cdot \underline{f}_d S_d \quad (\text{D.1})$$

(v = neutron velocity; $\underline{F}_p \equiv (1 - \beta_{eff}) \underline{E}$ = prompt fission matrix; β_{eff} = effective delayed neutron fraction; $\underline{\psi} \equiv (\psi_1, \psi_2)^T$ = time-dependent neutron flux vector; S_d = average delayed neutron precursor density; \underline{f}_d = distribution of delayed neutron precursors over the two compartments; all matrices are 2×2 ; see Appendix A). The average delayed neutron precursor density is given by:

$$S_d = \frac{1}{V_{tot}} \sum_{i=1}^6 \lambda_i C_i \quad (\text{D.2})$$

($V_{tot} = V_1 + V_2$ = total volume; C_i = number of delayed neutron precursors of delayed time group i ; λ_i = decay constant of delayed neutron precursors of delayed time group i ; 6 delayed neutron precursor time groups; see Appendix B, Table B.4). The balance equation for the delayed neutron precursors of delayed group i reads:

$$\frac{dC_i}{dt} = \beta_{eff,i} \eta \Sigma_a \sum_{m=1}^2 n_{rel,m} V_m \psi_m - \lambda_i C_i \quad (\text{D.3})$$

($\beta_{eff,i}$ = effective delayed neutron fraction for delayed time group i ; $i = 1, \dots, 6$; η = number of fission neutrons per absorbed neutron; Σ_a = macroscopic absorption cross section at the reference density; η and Σ_a are assumed to have the same value for both compartments; $n_{rel,m}$ = relative density in compartment m (dimensionless); see Appendix A).

The corresponding time-independent one-group/two-compartment neutron transport equation reads:

$$\lambda \underline{E} \cdot \underline{V}_M \cdot \underline{\psi}_0 + \underline{E} \cdot \underline{V}_M \cdot \underline{\psi}_0 = \underline{Q} \quad (\text{D.4})$$

(see Appendix A, Eq. (A.8)). Solving Eq. (D.4) renders the -fundamental-eigenvalue λ and corresponding eigenvector $\underline{\psi}_0 \equiv (\psi_{0,1}, \psi_{0,2})^T$ (static neutron flux vector). From this equation the time-independent two-compartment adjoint equation can be derived (see Appendix A, Eq. (A.15)), with -the same- eigenvalue λ and eigenvector $\underline{\psi}_0^+ \equiv (\psi_{0,1}^+, \psi_{0,2}^+)^T$ (adjoint function vector).

We now assume that, at any moment, the higher order mode components of the neutron flux are negligible to the fundamental mode (see Section 3.3), so that the time-dependent neutron flux vector can be written as:

$$\underline{\varphi} = \underline{\varphi}_0 \Omega(t) \quad (\text{D.5})$$

(Ω = dimensionless function of time). The relative densities ($n_{rel,m}$; $m = 1$ or 2) in the compartments are assumed to be functions of the density distribution variable ε (e.g. see Section 2.2.2), which is time-dependent in our combined GCFR models (Chapters 5 and 7). Because the relative densities are functions of ε , also the static flux vector $\underline{\varphi}_0$ and the adjoint function vector $\underline{\varphi}_0^+$ are functions of ε . We can also write:

$$\frac{d\underline{\varphi}}{dt} = \underline{\varphi}_0 \frac{d\Omega(t)}{dt} + \Omega(t) \frac{d\underline{\varphi}_0}{d\varepsilon} \frac{d\varepsilon}{dt} \quad (\text{D.6})$$

By multiplying both sides of Eq. (D.1) by $(\underline{\varphi}_0^+)^T$, substituting the expressions for the reactivity ρ and the neutron generation time Λ from Appendix A (Eqs. (A.16) and (A.17); fundamental eigenvectors $\underline{\varphi}_0$ and $\underline{\varphi}_0^+$) and applying Eq. (D.6) we obtain:

$$\frac{d\Omega}{dt} = \left[\frac{\rho - \beta_{eff}}{\Lambda} + Z(\varepsilon) \frac{d\varepsilon}{dt} \right] \Omega + \frac{1}{\Lambda} \frac{(\underline{\varphi}_0^+)^T \cdot \underline{V}_M \cdot \underline{f}_d}{(\underline{\varphi}_0^+)^T \cdot \underline{F} \cdot \underline{V}_M \cdot \underline{\varphi}_0} S_d \quad (\text{D.7})$$

with:

$$Z(\varepsilon) \equiv - \frac{(\underline{\varphi}_0^+)^T \cdot \underline{V}_M \cdot \frac{d\underline{\varphi}_0}{d\varepsilon}}{(\underline{\varphi}_0^+)^T \cdot \underline{V}_M \cdot \underline{\varphi}_0} \quad (\text{D.8})$$

The Z-function takes into account the fact that, for a given fission neutron production rate (or total fission power) in the system, the total number of neutrons in the system to obtain this production rate is dependent upon the density distribution (ε).

According to Eq. (A.12) the total fission power produced in the system is given by:

$$P_{fiss} = \frac{Q_f \eta \Sigma_a}{V_f} [n_{rel,1}(\varepsilon) V_1 \varphi_{0,1}(\varepsilon) + n_{rel,2}(\varepsilon) V_2 \varphi_{0,2}(\varepsilon)] \Omega(t) \quad (\text{D.9})$$

The normalization of the static flux vector is assumed to be chosen in such a way that the term between square brackets ("[...]") is independent of the density distribution variable ε , and -therefore- independent of time. This means that, in the static calculation, the total fission neutron production rate in the system is assumed to be constant. This is e.g. the case in the numerical static neutronic calculations by XSDRN, ANISN(E), ANISN and CITATION, presented in Chapter 2.

We now assume that, at any moment, the relative source strength distributions of prompt and delayed neutrons are equal, so that:

$$\frac{1}{V_{tot}} \underline{V}_M \cdot \underline{f}_d = \frac{\underline{F} \cdot \underline{V}_M \cdot \underline{\varphi}_0}{\eta \Sigma_a [n_{rel,1} V_1 \varphi_{0,1} + n_{rel,2} V_2 \varphi_{0,2}]} \quad (\text{D.10})$$

For a spatially flat flux (i.e. $\varphi_{0,1} = \varphi_{0,2}$) this is equivalent to the assumption of homogeneously mixed delayed neutron precursors.

Combining Eqs. (D.3), (D.7), (D.9) and (D.10), we can now derive:

$$\frac{dP_{fiss}}{dt} = \left[\frac{\rho - \beta_{eff}}{\Lambda} + Z(\varepsilon) \frac{d\varepsilon}{dt} \right] P_{fiss} + \frac{Q_f}{v_f \Lambda} \sum_{i=1}^6 \lambda_i C_i \quad (D.11)$$

And:

$$\frac{dC_i}{dt} = \frac{v_f \beta_{eff,i}}{Q_f} P_{fiss} - \lambda_i C_i \quad i = 1, \dots, 6 \quad (D.12)$$

From this general description of one-group/two-compartment neutron kinetics it is possible to derive the neutron kinetics models, presented in Chapter 3, by applying certain approximations.

For the case of the "solid piston" model (see Section 3.1) we assume that the GCFR is asymmetric and that all the fission power P_{fiss} is produced in the core ($m = 1$; see Sections 2.4 and 3.1). So the core fission power fraction $f_p = 1$ (see Appendix A, Eq. (A.13)). The relative density (n_{rel}) in the core is given by:

$$n_{rel} = n_{rel,0} (1 + \varepsilon) \quad (D.13)$$

(also see Section 3.1, Eq. (3.1.4)). Consequently, the flux in the expander ($m = 2$) is given by $\varphi_2 = 0$ and the static flux in the core is given by:

$$\varphi_{0,1} = X \frac{1}{1 + \varepsilon} \quad (D.14)$$

(normalization constant X). In the same way the adjoint function can be calculated and, applying Eq. (D.8), we find:

$$Z(\varepsilon) = \frac{1}{1 + \varepsilon} \quad (D.15)$$

Substitution into Eq. (D.11) and applying Eq. (D.13) renders:

$$\frac{dP_{fiss}}{dt} = \left[\frac{\rho - \beta_{eff}}{\Lambda} + \frac{1}{n_{rel}} \frac{dn_{rel}}{dt} \right] P_{fiss} + \frac{Q_f}{v_f \Lambda} \sum_{i=1}^6 \lambda_i C_i \quad (D.16)$$

This is the same expression as was found in Section 3.1 for use in the "solid piston" GCFR model (Eq. (3.1.10)), except for the delayed neutron term on the right hand side. The difference can be explained by the fact that in the derivation presented here, all delayed neutron precursors are assumed to be in the core, because the relative source strength distributions of prompt and delayed neutrons are assumed to be the same (see Eq. (D.10)). On the other hand, in Section 3.1 it was assumed that the delayed neutron precursors are distributed homogeneously over the entire (time-dependent) fuel gas volume, so that a factor (V_{core} / V_{fuel}) appears in the delayed neutron term of Eq. (3.1.10).

For the case of the "two-compartment" model (see Section 3.2), we assume that the static flux vector $\underline{\varphi}_0$ (and also the adjoint function vector $\underline{\varphi}_0^+$) is strictly time-independent, so that Eq. (D.6) reduces to:

$$\frac{d\underline{\varphi}}{dt} = \underline{\varphi}_0 \frac{d\Omega}{dt} \quad (D.17)$$

In this case it can be derived that $Z(\varepsilon) = 0$, which is equivalent to the assumption that the total number of neutrons in the system, required for a given total fission neutron production rate, is independent of ε . Under this assumption Eq. (D.11) reduces to Eq. (3.2.10) (Section 3.2). However, even for the symmetric, cylindrical

GCFR (see Section 2.4, case "I", and Chapter 7) this is not exactly the case. This is demonstrated in Figure D.1, in which a comparison is made, for the symmetric, cylindrical GCFR (Section 2.4, case "I", and Chapter 7; "rectangular" axial density distribution), between the $(\rho - \beta_{eff})/\Lambda$ -term and the $Z(\epsilon) \cdot d\epsilon/dt$ -term of Eq. (D.11). In the figure also the $Z(\epsilon)$ -function for this case is shown. For low frequencies (e.g. $f = 2$ Hz) the $(\rho - \beta_{eff})/\Lambda$ -term is dominant: the sum of both terms (indicated by "Sum") is largely determined by the $(\rho - \beta_{eff})/\Lambda$ -term. This means that at low frequencies the assumption stated above is valid. However, at higher frequencies (e.g. $f = 30$ Hz) the $Z(\epsilon) \cdot d\epsilon/dt$ -term becomes more important. This means that the oscillating component of the total fission power P_{fiss} (see Section 7.4, Figure 7.4) will become more and more determined by the $Z(\epsilon) \cdot d\epsilon/dt$ -term, which was also the case for the "solid piston" GCFR model (see Section 5.3; $f = 30 - 50$ Hz). For a frequency of 30 Hz the amplitude of the variation of both terms is of the same order of magnitude and therefore we expect that the amplitude of the oscillating component of the total fission power will not be very much different from the amplitude for the case that $Z(\epsilon) = 0$ (see Section 7.4). Furthermore, we expect that the cycle-averaged total fission power will still be determined by the $(\rho - \beta_{eff})/\Lambda$ -term, because for the symmetric, cylindrical GCFR the cycle-averaged value of the $Z(\epsilon) \cdot d\epsilon/dt$ -term will always be zero. Altogether we therefore expect that the influence of the $Z(\epsilon) \cdot d\epsilon/dt$ -term on the gas dynamics, and especially on the rate of increase of the density oscillations, will be small. Further investigations, however, remain desirable.

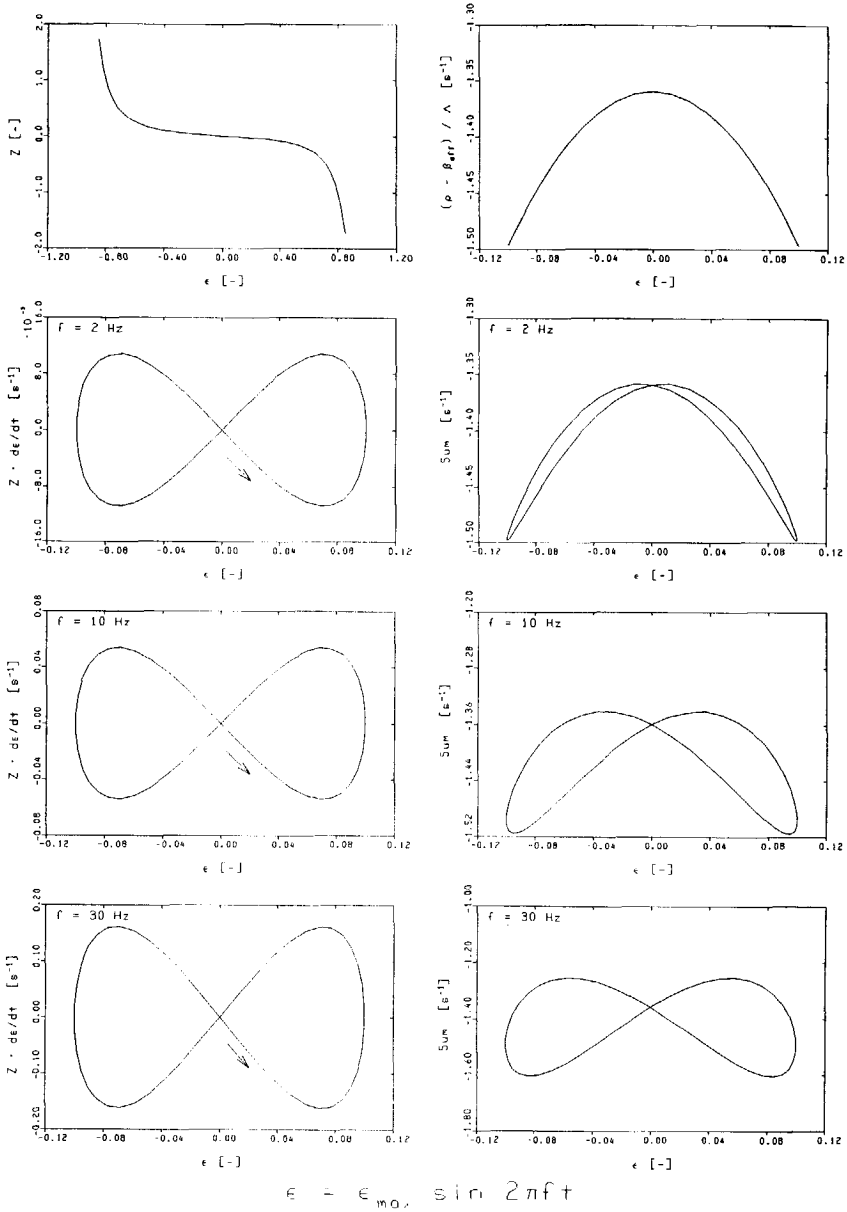


Figure D.1 Comparison between the $(\rho - \beta_{eff})/\Lambda$ -term and the $Z(\epsilon) \cdot de/dt$ -term of Eq. (D.11) for the symmetric, cylindrical GCFR (case "I").

REFERENCES

- Akcasu, A.Z. (1958), "General solution of the reactor kinetic equations without feedback", *Nuclear Science and Engineering*, Vol. 3, 456 - 467.
- Alesso, P.M., *et al.* (1991), "Inherently safe nuclear-driven internal combustion engines", *Proc. 6th International Conference on Emerging Nuclear Energy Systems*, June 16-21, Monterey, California, USA (published in: *Fusion Technology*, Vol. 20, No. 4, Part 2, December, 1001 - 1005).
- Beckurts, K.M. & Wirtz, K. (1964), "Neutron physics", Springer Verlag, Berlin (translated from German by L. Dresner, Oak Ridge National Laboratory, Oak Ridge, Tennessee, USA).
- Bell, G.I. & Glasstone, S. (1970), "Nuclear reactor theory", Van Nostrand Reinhold Company, New York.
- Bird, R.B., Stewart, W.E. & Lightfoot, N.E. (1963), "Transport phenomena", John Wiley & Sons, New York.
- Boersma-Klein, W. (1989a), FOM-Institute for Atomic and Molecular Physics, Amsterdam, the Netherlands, UCF thermodynamics tables, private communication.
- Boersma-Klein, W., Kistemaker, J. & Stein, H.N. (1989b), "Use of thermochemical modelling for the analysis of energy extraction in gas-core fission reactors", *Journal of Nuclear Materials*, Vol. 167, 135-144.
- Boersma-Klein, W. & Kistemaker, J. (1990a), "The behaviour of a mixture of uranium- and carbon fluorides in contact with a graphite wall between 1000 and 2000 K", *High Temperature Science*, Vol. 28, 1-13.
- Boersma-Klein, W., Kistemaker, J. & Stein, H.N. (1990b), "Equation of state and specific heats of U-C-F gas mixtures at high temperatures and pressures", *High Temperature Science*, Vol. 29, 63-88.
- Boersma-Klein, W. & Kistemaker, J. (1991a), "Transport phenomena in a dissociating U-C-F gas mixture", *Journal of Nuclear Materials*, Vol. 182, 24-35.
- Boersma-Klein, W. & Kistemaker, J. (1991b), "Physical processes in the boundary layer of a gas core fission reactor", *Proc. 6th International Conference on Emerging Nuclear Energy Systems*, June 16-21, Monterey, California, USA (published in: *Fusion Technology*, Vol. 20, No. 4, Part 2, December, 610 - 614).
- Callen, H.B. (1960), "Thermodynamics", John Wiley & Sons, New York.
- Case, K.M., de Hoffmann, F. & Placzek, G. (1953), "Introduction to the theory of neutron diffusion", Vol. 1, U.S. A.E.C. report, Los Alamos National Laboratory, Los Alamos, New Mexico, USA.
- Colgate, S.A. & Aamodt, R.L. (1957), "Plasma reactor promises direct electric power", *Nucleonics*, Vol. 15, August, 50-55.
- Cramer, K.R. & Pai, S.I. (1973), "Magnetofluid dynamics for engineers and applied physicists", McGraw-Hill, New York.
- van Dam, H. & Hoogenboom, J.E. (1983), "Physics of a gaseous core reactor", *Nuclear Technology*, Vol. 63, 359-368.
- van Dam, H. (1987), "Time dependence of neutron reflection by the graphite wall of a gaseous core reactor", Report IRI-131-87-009, Interfacultair Reactor Instituut, Delft, The Netherlands (available on request).

- van Dam, H. (1988), "Neutron kinetics of a pumped gaseous-core reactor", *Annals of Nuclear Energy*, Vol. 15, No. 2, 85-93.
- van Dam, H. *et al.* (1989), "Neutron and thermal dynamics of a gaseous core fission reactor", *Proc. 5th International Conference on Emerging Nuclear Energy Systems*, Singapore Science Publishers, 39-44.
- Diaz, N.J. & Dugan, E.T. (1980), "Gaseous reactors for electrical power generation", *Atomkernenergie-Kerntechnik*, Vol. 36, 188.
- Diaz, N.J., Dugan, E.T. & Oliver, C.C. (1980), "Cycling gas power reactor systems", *Atomkernenergie-Kerntechnik*, Vol. 36, 191.
- Duderstadt, J.J. & Hamilton, L.J. (1976), "Nuclear reactor analysis", John Wiley & Sons, New York.
- Dugan, E.T. & Diaz, N.J. (1988), "Heterogeneous gas core reactor for space nuclear power", *SPIE*, Vol. 871, Space Structures, Power and Power Conditioning, 25-30.
- Dugan, E.T., Lear, W.E. & Welch, G.E. (1988), "Pulsed gas core reactor for burst power", *SPIE*, Vol. 871, Space Structures, Power and Power Conditioning, 42-47.
- Dveer, S. (1988), Interfacultair Reactor Instituut, Delft, the Netherlands, private communication/concept report.
- Eriksson, G. (1970), "Thermodynamic studies of high temperature equilibria VIII: General equations for the calculation of equilibria in multiphase systems", *Chemical Scripta*, Vol. 8, 100 - 103.
- Eriksson, G. & Hack, K. (1989), "SAGE - SOLGASMIX based Advanced Gibbs Energy minimizer", Computer code under private contract, Gesellschaft für Thermochemie und Physik mbH, Aachen, Germany.
- Garber, D. *et al.* (1975), Report BNL-NCS-50496.
- Glasstone, S. & Eddlund, M.C. (1960), "The elements of nuclear reactor theory", D. Van Nostrand Company, New York.
- Hatsopoulos, G.N. & Gyftopoulos, E.P. (1979), "Thermionic energy conversion - Volume II", The MIT Press, Cambridge, Massachusetts, USA.
- Hoogenboom, J.E. *et al.* (1991), "The temperature distribution in a gas core fission reactor", *Annals of Nuclear Energy*, Vol. 18, No.4, 183-195.
- Iyevlev, V.M. (1977), "Some results of investigation of the gas-phase cavity type reactor", *Moscow Izvestiya Akademii Nauk SSSR: Energetiki i Transport*, No. 6, 24-31.
- IMSL (1987), Fortran subroutines for mathematical applications, version 1.0, Users' manual, April.
- Kerkdijk, C.B.W. & Kistemaker, J. (1978), "Energy transport in gas core reactors", Report AMOLF 78/284, FOM-Institute for Atomic and Molecular Physics, Amsterdam, the Netherlands.
- Kistemaker, J. (1978a), "Some aspects of a fission based plasma engine", *Proc. 1st International Symposium on Nuclear Induced Plasmas and Nuclear Pumped Lasers*, Les Editions de Physique, Paris-Orsay.
- Kistemaker, J. & Nieskens, M.J.P.C. (1978b), "Wall stabilization in a possible high-temperature gas-core fission reactor", *Energy Conversion*, Vol. 18, 67-71.
- Kistemaker, J. *et al.* (1986), "Gas-core fission reactor aspects", *Proc. 4th International Conference on Emerging Nuclear Energy Systems*, Singapore Science Publishers, 258.
- Kistemaker, J. & Boersma-Klein, W. (1987), "Corrosion processes in a high

- temperature gas core fission reactor", *High Temperature Science*, Vol. 24, 37.
- Kistemaker, J. & Boersma-Klein, W. (1989), "The gas blanket in a gas core fission reactor", *Proc. 5th International Conference on Emerging Nuclear Energy Systems*, Singapore Science Publishers, 45-50.
- Klein, W. (1987), "Thermodynamic performance of a gas-core fission reactor", Ph.D thesis, Eindhoven University of Technology, Eindhoven, the Netherlands.
- Kuijper, J.C. (1988), "Parametric study of reactivity and neutron generation time of gaseous core fission reactors", Report IRI-131-88-018, Interfacultair Reactor Instituut, Delft, the Netherlands (available on request).
- Kuijper, J.C. *et al.* (1989a), "Thermodynamic cycle calculations for a gaseous core fission reactor", Report IRI-131-89-010, Interfacultair Reactor Instituut, Delft, the Netherlands (available on request).
- Kuijper, J.C. *et al.* (1989b), "Simulator studies of a gaseous core fission reactor", *Proc. 5th International Conference on Emerging Nuclear Energy Systems*, Singapore Science Publishers, 51-55.
- Kuijper, J.C. *et al.* (1990), "Reactor physics and thermodynamics of a gaseous core fission reactor", *Proc. PHYSOR-90*, P III, 157-166.
- Kuijper, J.C. & van Dam, H. (1991a), "Thermodynamic cycle calculations for a pumped gaseous core fission reactor", *Journal of Nuclear Science and Technology*, Vol. 28, No. 2, January, 95-106.
- Kuijper, J.C. & van Dam, H. (1991b), "A gaseous core fission reactor with autonomously oscillating fuel gas", *Proc. 6th International Conference on Emerging Nuclear Energy Systems*, June 16-21, Monterey, California, USA (published in: *Fusion Technology*, Vol. 20, No. 4, Part 2, December, 545 - 549).
- Landau, L.D. & Lifschitz, E.M. (1963), "Fluid mechanics", Pergamon Press, Oxford (translated from Russian by J.B. Sykes and W.H. Reid).
- de Leege, P.F.A. (1990), Interfacultair Reactor Instituut, Delft, the Netherlands, private communication.
- de Leege, P.F.A. (1991), "NSLINK", *Proc. Int. Topical Meeting: Advances in Mathematics, Computations, and Reactor Physics*, April 28 - May 2, Green Tree Marriot, Pittsburg, Pennsylvania, USA, 30.5 5, 1-3.
- Lewins, J. (1965), "Importance - the adjoint function", Pergamon Press, Oxford.
- Massimo, L. (1976), "Physics of high temperature reactors", Pergamon Press, Oxford.
- NEA (1972), Report DAC-1, NESC-0455, Computer Code Library, Nuclear Energy Agency Data Bank.
- NEA (1973a), Report XLACS, NESC-0572, Computer Code Library, Nuclear Energy Agency Data Bank.
- NEA (1973b), Report XSDRN, NESC-0393, Computer Code Library, Nuclear Energy Agency Data Bank.
- NEA (1978), Report AMPX-2 (COMET, CONTAC, OCTAGN), PSR-0063/AMPX-II, Computer Code Library, Nuclear Energy Agency Data Bank.
- NEA (1979), Report ANISN(E), CCC-0082, Computer Code Library, Nuclear Energy Agency Data Bank.
- NEA (1985), "Index to the JEF-1 nuclear data library", JEF Report 1, September.
- NEA (1986a), Report ANISN, CCC-0254/7, Computer Code Library, Nuclear Energy

- Agency Data Bank.
- NEA (1986b), Report NJOY, PSR-0171, Computer Code Library, Nuclear Energy Agency Data Bank.
- NEA (1987), Report SCALE-3 (NITAWL, XSDRNPM), CCC-0466, Computer Code Library, Nuclear Energy Agency Data Bank.
- NEA (1989), Report CITATION, NESC-0387, Computer Code Library, Nuclear Energy Agency Data Bank.
- Nieskens, M.J.P.C., Stein, H.N. & Kistemaker, J. (1978), "Thermodynamic equilibrium calculations in the system uranium-carbon-fluorine", *Ind. Eng. Chem. Fund.*, Vol. 17, No. 4.
- Nordheim, L.W. (1962), "A new calculation of resonance integrals", *Nuclear Science and Engineering*, Vol. 12, 457-463.
- Panicker, M.M., Dugan, E.T. & Anghaie, S. (1988), "Neutronics of a coupled multiple chamber gaseous core reactor power system", *SPIE*, Vol. 871, Space Structures, Power and Power Conditioning, 31-42.
- Panicker, M.M. & Dugan, E.T. (1991a), "Identification and implementation of variance reduction methods for efficient Monte Carlo criticality calculations of gaseous core reactors", *Proc. Int. Topical Meeting: Advances in Mathematics, Computations, and Reactor Physics*, April 28 - May 2, Green Tree Marriot, Pittsburg, Pennsylvania, USA, 23.1 2, 1-11.
- Panicker, M.M. & Dugan, E.T. (1991b), "Coupled core kinetics of pulsed and burst power multiple cavity gaseous core reactor system", *Proc. Int. Topical Meeting: Advances in Mathematics, Computations, and Reactor Physics*, April 28 - May 2, Green Tree Marriot, Pittsburg, Pennsylvania, USA, 23.2 5, 1-12.
- Parks, D.E. *et al.* (1969), "Optical constants of uranium plasma", Report NASA CR-72348, U.S. National Technical Information Service.
- Rayna, G. (1987), "REDUCE: Software for algebraic computation", Springer Verlag Inc., New York.
- REACTOR RESEARCH (1988), "RRGRAPH for IBM-PC and compatible computers using MS/PC DOS", Code manual, Reactor Research Foundation, Delft, The Netherlands.
- Rohsenov, W.M., Hartnett, J.P. & Ganić, E.N. (1985), "Handbook of heat transfer fundamentals", McGraw-Hill, New York.
- Ronen, Y. (1986), "Handbook of nuclear reactor calculations - Volume I", CRC Press Inc., Boca Raton, Florida, USA.
- Schneider, R.T. & Thom, K.H. (1975), "Fissioning uranium plasmas and nuclear-pumped lasers", *Nuclear Technology*, Vol. 27, September, 34-50.
- Smith, H.P. (1965), "Divergence of the mean power level during an oscillation experiment", *Nuclear Science and Engineering*, Vol. 22, 253 - 269.
- Spiegel, M.R. (1965), "Laplace transforms", Schaum's outline series in mathematics, McGraw-Hill, New York.
- Stekelenburg, A.J.C. (1988), "Een simulator voor een gaskernreactor met een oscillerende brandstofmassa" (= "A simulator for a gaseous core reactor with oscillating fuel mass"), Report IRI-131-88-021, Interfacultair Reactor Instituut, Delft, The Netherlands (available on request).
- Stekelenburg, A.J.C. (1990), "A computer simulator for a pumped gaseous-core fission reactor", Report IRI-131-90-001, Interfacultair Reactor Instituut, Delft, The Netherlands (available on request).

- Stephenson, J.M. (1986), "Delayed neutron parameter requirements for reactor physics purposes", *Proc. Specialists' Meeting on Delayed Neutron Properties*, September 15-19, Birmingham, England (Editor: D.R. Weaver).
- Thom, K. (1979), "Der Gasphasenreaktor", Urheber Verlag, Bonn.
- Uleman, R.M. (1982), "The influence of the core temperature distribution on the reactivity of a gas core reactor", M.Sc thesis, Delft University of Technology, Delft, the Netherlands (available on request).
- UNION CARBIDE (1959), "The industrial graphite engineering handbook", Union Carbide International Corporation.
- Welch, G.E., Dugan, E.T. & Lear, W.E. (1988), "Disk MHD generator for a burst power gas core reactor", *SPIE*, Vol. 871, Space Structures, Power and Power Conditioning, 15-24.
- Williams, M.R.R. (1966), "The slowing down and thermalization of neutrons", North Holland Publishing Company, Amsterdam.
- Wolff, L.R. (1990), Centre for Technical Ceramics, Eindhoven University of Technology, Eindhoven, the Netherlands, private communication.

SUMMARY

In this thesis we present a -numerical and analytical- investigation of the static and dynamic properties of a -conceptual- gaseous core fission reactor (GCFR) with oscillating (moving) fuel gas. In Chapter 1 we give a description of such a GCFR concept. It consists of a graphite cylinder of, say, 2 m diameter and 10 m length, filled with a mixture of uranium- and carbon fluorides (UCF) at high temperature (several thousands of K) in ionized state, in chemical and thermodynamical equilibrium with the graphite cylinder wall. The cylindrical gas space is divided into an active "core" region, surrounded by an effective (thick) neutron reflector, and a so-called "expander" region, surrounded by a much less effective neutron reflector. In operation, part of the fuel gas oscillates back and forth between core and expander region. With homogeneously distributed fuel over core and expander, the reactor is approximately critical. As the fuel gas is ionized, and therefore electrically conductive, it can interact with the magnetic field, generated by a current in the coil surrounding the expander. In this way plasma dynamic compression of the fuel gas from the expander into the core (rendering the reactor supercritical) and magneto-inductive energy extraction are possible. The investigation of such a system requires the study of neutron statics, neutron kinetics, reactor gas thermodynamics and gas dynamics. We develop two calculational models combining (some of) these aspects: (I) the "solid piston" model presented in Chapter 5 (combining neutron statics/kinetics and thermodynamics; no gas dynamics) and (II) the "two-compartment" model presented in Chapter 7 (combining neutron statics/kinetics, thermodynamics and gas dynamics). In the development of these models we follow a step-by-step approach.

A study of the static neutronic properties of spherical and cylindrical GCFRs is presented in Chapter 2. We investigate the influence of the fuel gas average density and the fuel gas density distribution on the reactivity, the neutron generation time and the core fission power fraction (cylindrical GCFR) by means of one- and two-dimensional static neutron transport and neutron diffusion calculations. The dependence of these quantities on the fuel density (and the density distribution) is used in the description of the neutron kinetics of the GCFR (Chapter 3). It is shown that this dependence can be adequately described by relatively simple functions of the (average) fuel gas density and/or a single variable ϵ , describing the distribution of the fuel gas over the gas space. The forms of these functions are obtained from "chord" and "multi-compartment" GCFR models, also presented in Chapter 2 (and Appendix A). We also investigate the influence of the temperatures of the fuel gas and the reflector on the reactivity of the GCFR and it is shown that an increase of either one of these temperatures causes a decrease of the reactivity (Appendix C). This is favourable from the safety point of view. The influence of the reflector temperature is much larger than that of the gas temperature.

The neutron kinetics parts of the combined GCFR models are introduced in Chapter 3. We assume the applicability of point kinetics (fundamental neutronic mode) and we use the expressions for reactivity, neutron generation time and core fission power fraction obtained from the static neutronic calculations, presented in Chapter 2. In order to check the applicability of point kinetics we also estimate

the difference in rate constant between the fundamental and the first higher order neutronic mode (for the case of a critical, symmetric cylindrical GCFR). The value we find for this difference is an order of magnitude larger than the characteristic density oscillation frequency in our GCFR (about 30 Hz), which is an indication that we may indeed neglect the higher order neutronic modes.

The thermodynamic properties of the GCFR, and of the fuel gas in particular, are treated in Chapter 4. One of the main characteristics of "our" GCFR concept is that the graphite reflector wall is part of the chemical system. This means that this wall, in order to stay intact (at least on average), must be in chemical and thermodynamical equilibrium with the reactor gas mixture (uranium, carbon, fluorine: UCF). At 2000 K and 25 bar the wall will be in equilibrium with a UCF gas mixture, consisting of 20.5 % CF_4 , 54.5 % UF_5 and 25.0 % UF_4 (molar) (i.e. $[\text{U}]:[\text{C}]:[\text{F}] = 0.70 : 0.18 : 4.00$). This equilibrium composition is (at a temperature of approximately 2000 K) not sensitively dependent upon the pressure. In all our investigations we assume that the temperature at the gas-wall interface is 2000 K. However, the temperature in the centre of the gas will be much higher (say 10,000 K) and at this temperature the "original" CF_4 , UF_5 and UF_4 will have dissociated into lower valent uranium- and carbon fluorides (and even single atoms, ions and electrons). This behaviour is also reflected in the dependence of the specific heat of the UCF gas (at constant pressure or constant volume) on the temperature and the pressure.

Because of this complexity we introduce a model gas "Modelium" with an artificial, analytical equation of state (EOS), as an approximation for the "real" EOS of the UCF gas, which is only available in tabular form. From the postulated EOS of Modelium we derive expressions for other thermodynamic quantities (such as the enthalpy H), using general thermodynamic relationships. It is shown that these quantities for Modelium and UCF gas show a similar behaviour with temperature and pressure.

In Chapter 4 we also introduce the concepts of the "infinitesimal Otto cycle" and the so-called "infinitesimal efficiency factor" ζ . This quantity can be directly calculated from the thermodynamical properties of the gas (for Modelium it is possible to derive a -quite complicated- analytical expression for ζ) and it can be used to estimate, with reasonable accuracy, the efficiency η of a finite thermodynamic cycle. We demonstrate this in Chapter 5.

In Chapter 5 we present the combined model of a so-called "solid piston" GCFR. In this model the interaction of the ionized fuel gas with the magnetic field generated by the coil is represented by a solid piston, which controls the total volume occupied by the fuel gas. The extracted energy is then modelled as the mechanical work performed by the gas on the piston. The model combines neutron kinetics and thermodynamics. However, no gas dynamics is taken into account, as the fuel gas, occupying the space controlled by the piston, is assumed to be massless and homogeneous.

Using this model, we investigate the influence of several parameters, such as volume sequence type (harmonic or Otto cycle), compression ratio K , pumping frequency f , gas type (non-dissociating, perfect gas; Modelium; UCF), c_p/c_v -ratio κ (in the case of a perfect gas), cycle-averaged fission power $\langle P_{fiss} \rangle_r$, heat leakage (on/off), on the thermodynamic cycle behaviour of the GCFR and on the attainable efficiency in particular. In general, a harmonic cycle is less efficient than an Otto cycle. Also the use of a dissociating gas (UCF or Modelium) lowers the

efficiency, because of the "damping" influence of the dissociation- and recombination processes on the temperature- and pressure variations. Modelium turns out to approximate the behaviour of UCF gas quite well. It is also shown that the actual efficiency rendered by this kind of thermodynamic cycle calculations indeed can be estimated, with reasonable accuracy, from the infinitesimal efficiency factor ζ of the gas (for both perfect and dissociating gas), evaluated at the BOC (beginning of the cycle) state.

A big problem is posed by the very high so-called "basic pumping power" circulating in the magnetic coil system, which is modelled (in the "solid piston" GCFR model) as the instantaneous working power. A small loss factor in the magnetic coil system (e.g. due to ohmic losses) will lead to a severe deterioration of the conversion efficiency. It might even render magnetic pumping useless, if the loss is of the same order as the energy extracted by induction. A possible way of avoiding this problem is using autonomous gas density oscillations, driven by nuclear fissions.

For the investigation of such a system it is necessary to introduce a gas dynamics model. In Chapter 6 we discuss two different (one-dimensional) gas dynamics models. The first model, the "acoustic model", is based on the well known conservation equations for mass (continuity equation), momentum (Navier-Stokes or Euler equation) and energy (first law of thermodynamics) and the equation of state and the internal energy of the gas. The second model, which was developed especially for use in the "two-compartment" GCFR model (Chapter 7), assumes the cylindrical gas space to be subdivided into two compartments, containing the same amount (mass) of fuel gas, by a movable imaginary wall (position x_w), to which a fraction α of the total fuel gas mass is attributed. The parameters of this two-compartment gas dynamics model are chosen such that, in absence of fission energy production in the gas and heat transport to or from the gas (adiabatic case), the natural oscillation frequency and the momentary kinetic energy of the fuel gas are the same as in the fundamental acoustic mode (acoustic model). In case of presence of fission energy production and heat transport, the rate of increase of the cycle-averaged kinetic energy of the gas is then also the same in both gas dynamics models. One of the determining factors of this rate of increase is again the so-called "infinitesimal efficiency factor" ζ of the gas, which is equal to $\kappa - 1$ for a non-dissociating, perfect gas.

With the two-compartment gas dynamics model we also perform an -analytical- investigation on the influence of the presence of an energy extraction mechanism -such as MHD or induction- of the behaviour of the system. It is found that a practical conversion efficiency can only be obtained with very high (supersonic) velocities of the gas.

A model for a GCFR with autonomously oscillating fuel gas, combining neutron statics/kinetics, thermodynamics and (two-compartment) gas dynamics is presented in Chapter 7. In this calculational model we assume the absence of an energy extraction mechanism and it is shown that, provided that the c_p/c_v -ratio κ (assuming a perfect, non-dissociating gas) is in the correct range, increasing (density, velocity, kinetic energy) oscillations occur. For velocities, which are not too high (less than the sound velocity c in the gas), it is shown that the rate of increase of the oscillations can be predicted quite well by an analytical formula, which was derived in Chapter 6 by applying first order perturbation theory to the two-compartment gas dynamics model. The presence of an energy extraction

mechanism (such as MHD or induction) will render the oscillations stationary and, provided that certain conditions are met, the (cycle-averaged) total fission power will follow the demanded extracted power.

SAMENVATTING

Dit proefschrift beschrijft een numerieke en analytische studie naar de statische en dynamische eigenschappen van een -conceptuele- gaskernreactor (GCFR: "Gaseous Core Fission Reactor") met oscillerend splijstofgas. In Hoofdstuk 1 wordt een beschrijving gegeven van zo'n GCFR concept. Het bestaat uit een grafiet cilinder (afmetingen: diameter ongeveer 2 m, lengte ongeveer 10 m), gevuld met een mengsel van uranium- en koolstoffluoriden (UCF: Uranium, Carbon, Fluorine). Dit gasmengsel heeft een hoge temperatuur (enkele duizenden K) en bevindt zich derhalve in een geheel of gedeeltelijk geïoniseerde toestand. Aangenomen wordt dat het gas in chemisch en thermodynamisch evenwicht is met de omringende grafietwand. De cilindrische ruimte, waarin het splijstofgas zich bevindt, is onderverdeeld in een "kern"- en een "expansie"-gedeelte. Het kerngedeelte is omringd door een effectieve (dikke) neutronenreflector, terwijl het expansiegedeelte omringd is door een -veel- minder effectieve (dunnere) reflector. Bij homogene verdeling van het splijstofgas over de kern en het expansiegedeelte is de reactor ongeveer kritiek. Het splijstofgas is geïoniseerd, en derhalve elektrisch geleidend. Hierdoor is interactie mogelijk met een magnetisch veld, gegenereerd door een stroom door de spoel om het expansiegedeelte. Op deze wijze (plasmadynamische compressie) kan het splijstofgas van het expansie- naar het kerngedeelte worden bewogen, waardoor de reactor superkritiek wordt. Verder is hierdoor ook magneto-inductieve energie-extractie mogelijk. In het onderzoek komen diverse aspecten van de GCFR aan de orde: neutronenstatica, neutronenkinetica, thermodynamica van het splijstofgas en gasdynamica. Er werden twee GCFR modellen ontwikkeld, die ieder (enkele van deze) aspecten combineren: (I) het "zuiger" model (neutronenstatica/kinetica en thermodynamica; geen gasdynamica) and (II) het "twee-compartimenten" model (neutronenkinetica/statica, thermodynamica en gasdynamica).

Een onderzoek naar de statische reactorfysische eigenschappen van bolvormige en cilindrische GCFR's wordt beschreven in Hoofdstuk 2. Door middel van statische één- en twee-dimensionale neutronentransport- en neutronendiffusieberekeningen werd de invloed onderzocht van de dichtheid en de dichtheidsverdeling van het splijstofgas op de reactiviteit, de neutronengeneratietijd en de fractie van het totale vermogen dat in het kerngedeelte geproduceerd wordt (voor de cilindrische GCFR). Informatie over deze verbanden is noodzakelijk voor de beschrijving van de neutronenkinetica van de GCFR (Hoofdstuk 3). Het blijkt dat deze verbanden op adequate wijze kunnen worden beschreven met relatief eenvoudige functies van de gemiddelde gasdichtheid en de dichtheidsverdelingsvariabele ϵ . De vorm van deze functies kan worden afgeleid m.b.v. zogenaamde "koorden"- en "multi-compartiment" GCFR modellen, welke eveneens beschreven staan in hoofdstuk 2 (en Appendix A). Verder werd de invloed onderzocht van de temperatuur van het splijstofgas en de reflector op de reactiviteit van de GCFR (Appendix C). Een verhoging van deze temperaturen blijkt te resulteren in een afname van de reactiviteit, hetgeen gunstig is vanuit het oogpunt van veiligheid. Verder is de invloed van de reflectortemperatuur veel groter dan die van de gastemperatuur.

Het neutronenkineticamodel van de beide GCFR modellen staat beschreven in Hoofdstuk 3 (en Appendix D). Er wordt verondersteld dat de reactor zich op

ieder moment in de fundamentele neutronische mode bevindt (puntkinetica) en er wordt gebruik gemaakt van de uitdrukkingen voor de reactiviteit, de neutronengeneratietijd en de vermogensfractie in de kern, die waren afgeleid in Hoofdstuk 2. Ter controle van de toepasbaarheid van het puntkineticamodel wordt een schatting gemaakt van het verschil in tijdconstante tussen de fundamentele neutronische mode en de eerste hogere orde mode. Dit verschil blijkt een orde van grootte kleiner te zijn dan de karakteristieke periode van de dichtheidsoscillaties in de GCFR (ongeveer 0,03 s). Dit is een indicatie dat de hogere orde neutronische modes inderdaad verwaarloosd mogen worden.

De thermodynamische eigenschappen van de GCFR -in het bijzonder die van het splijstofgas- worden behandeld in Hoofdstuk 4. Een van de voornaamste eigenschappen van "ons" GCFR concept is dat de reflectorwand van grafiet een onderdeel is van het chemische systeem. Dit betekent dat deze wand, om (tenminste gemiddeld) intact te blijven, in chemisch en thermodynamisch evenwicht moet zijn met het splijstofgasmengsel (UCF). Bij een temperatuur van 2000 K en een druk van 25 bar is de wand in evenwicht met een UCF gasmengsel, bestaande uit 20,5 % CF_4 , 54,5 % UF_5 and 25,0 % UF_4 (molair) (d.w.z. $[\text{U}]:[\text{C}]:[\text{F}] = 0,70 : 0,18 : 4,00$). Deze evenwichtssamenstelling is, althans bij een temperatuur van ongeveer 2000 K, niet erg gevoelig voor de druk. In alle berekeningen is bij het gas-wand grensvlak een temperatuur van 2000 K verondersteld. De temperatuur in de bulk van het gas zal echter veel hoger zijn (in de orde van 10.000 K) en bij deze temperatuur zullen de "originele" UF_5 -, UF_4 - en CF_4 -moleculen zijn gedissociëerd tot lager valente uranium- en koolstoffluoriden en zelfs tot losse atomen, ionen en electronen. Dit gedrag is ook terug te vinden in het verband tussen de soortelijke warmte van het UCF gas (bij constant volume of constante druk) en de druk en de temperatuur.

Vanwege dit complexe gedrag wordt, eveneens in Hoofdstuk 4, het modelgas "Modelium" geïntroduceerd, als een benadering van het "echte" UCF gas. Modelium heeft een analytische toestandsvergelijking (Equation Of State: "EOS"), terwijl de EOS van UCF gas alleen beschikbaar is in tabelvorm. M.b.v. algemene thermodynamische relaties worden uit de analytische EOS van Modelium andere thermodynamische grootheden afgeleid, zoals de interne energie U en de enthalpie H . Uit vergelijking blijkt dat deze grootheden voor UCF en Modelium een zelfde soort gedrag vertonen als functie van druk en temperatuur.

In Hoofdstuk 4 worden ook de zogenaamde "infinitesimale Otto cyclus" en de daarmee samenhangende "infinitesimale efficiëntiefactor" ζ geïntroduceerd. Deze grootheid kan rechtstreeks worden afgeleid uit de thermodynamische eigenschappen van het gas en kan worden gebruikt voor de schatting, met redelijke nauwkeurigheid, van het rendement η van een eindige thermodynamische cyclus. Dit wordt gedemonstreerd in Hoofdstuk 5. Voor Modelium is het mogelijk een -tamelijk ingewikkelde- analytische uitdrukking af te leiden voor ζ .

In Hoofdstuk 5 wordt het "zuiger" model voor een -magnetisch- gepompte GCFR behandeld. In dit model wordt de interactie tussen het geïoniseerde splijstofgas en het magnetische veld, opgewekt door de spoel, gerepresenteerd door een zuiger, die het volume van het splijstofgas bepaalt. De geëxtraheerde energie wordt dan gerepresenteerd door de mechanische arbeid, die door het gas op de zuiger wordt verricht. In het model worden neutronenkinetica en thermodynamica gecombineerd. Er wordt echter geen rekening gehouden met gasdynamica: het splijstofgas wordt massaloos en homogeen verondersteld.

Met dit model wordt de invloed onderzocht van diverse parameters, zoals de wijze van volumeverandering (harmonische of Otto-cyclus), de compressieverhouding K , de pompfrequentie f , het soort gas (niet-dissociërend, ideaal gas; Modelium; UCF), de c_p/c_v -verhouding κ , het cyclus-gemiddelde nucleaire vermogen $\langle P_{fiss} \rangle$, en de warmtelek (aan/uit), op het thermodynamisch cyclusgedrag van deze GCFR, en op het bereikbare rendement in het bijzonder. Het blijkt dat, in het algemeen, een harmonische cyclus minder efficiënt is dan een Otto-cyclus. Ook het gebruik van een dissociërend gas (UCF of Modelium) heeft een negatieve invloed op het bereikbare rendement, vanwege de "dempende" invloed van de dissociatie- en recombinatieprocessen op de temperatuur- en drukvariaties. Het blijkt verder dat Modelium het gedrag van UCF gas goed benadert. Ook blijkt het mogelijk om, met redelijke nauwkeurigheid, het rendement van een eindige thermodynamische GCFR cyclus te schatten uit de infinitesimale efficiëntiefactor van het gas, berekend bij de thermodynamische condities aan het begin van de cyclus.

Een groot probleem vormt het zogenaamde "basis pompvermogen" ("basic pumping power"), dat circuleert in het magnetische spoelsysteem, en welke (in het "zuiger" GCFR model) wordt gerepresenteerd door het momentane arbeidsvermogen. Een kleine verliesfactor in het spoelsysteem (bijvoorbeeld door ohmse verliezen) zal leiden tot een zeer grote vermindering van het rendement. Magnetisch pompen zal zelfs volkomen zinloos zijn als de verliezen van dezelfde orde van grootte zijn als de energie, geëxtraheerd door middel van inductie. Een mogelijke manier om dit probleem te omzeilen, is het gebruik van autonome dichtheidsoscillaties in het gas, die worden aangedreven door kernsplijting.

Voor het onderzoek naar zo'n systeem is een gasdynamicamodel nodig. In Hoofdstuk 6 worden twee gasdynamicamodellen behandeld. Het eerste model, het zogenaamde "acoustische model", is gebaseerd op de bekende behoudswetten voor massa (continuïteitsvergelijking), impuls (Navier-Stokes of Euler-vergelijking) en energie (eerste hoofdwet van de thermodynamica), en de toestandsvergelijking en de vergelijking voor de interne energie van het gas. Het tweede model, dat speciaal werd ontwikkeld voor het gebruik in het "twee-compartimenten" GCFR model (Hoofdstuk 7), neemt aan dat de cilindervormige ruimte, waarin het gas zich bevindt, is onderverdeeld in twee compartimenten, die ieder dezelfde hoeveelheid (massa) gas bevatten). De scheiding tussen deze twee compartimenten wordt gevormd door een denkbeeldige, beweegbare wand, waaraan een fractie α van de totale massa van het gas wordt toegekend. De parameters van dit twee-compartimenten gasdynamicamodel zijn zo gekozen, dat in het adiabatische geval (d.w.z. geen energieproductie in het gas en geen warmtelek van of naar de buitenwereld) de natuurlijke oscillatiefrequentie dezelfde is als in de fundamentele acoustische mode (acoustisch model). In het geval dat er energieproductie in het gas is en warmtelek, is dan ook het tempo van toename van de cyclus-gemiddelde kinetische energie voor beide gasdynamicamodellen gelijk. Eén van de bepalende factoren voor dit tempo is wederom de zogenaamde "infinitesimale efficiëntiefactor" ζ van het gas, die voor een niet-dissociërend, ideaal gas, gelijk is aan $\kappa - 1$.

M.b.v. dit twee-compartimenten gasdynamicamodel werd een analytische studie verricht naar de invloed van de aanwezigheid van een energie-extractiemechanisme -zoals MHD of inductie- op het gedrag van het systeem. Het blijkt dat een praktisch bruikbaar rendement slechts kan worden verkregen bij zeer

hoge (supersone) snelheden van het gas.

In Hoofdstuk 7, tenslotte, wordt het gecombineerde "twee-compartimenten" GCFR model behandeld. In dit model worden neutronenstatica/kinetica, thermodynamica en (twee-compartimenten) gasdynamica gecombineerd. Een energie-extractiemechanisme wordt niet aanwezig verondersteld en het blijkt dat aangroeiende (dichtheids-, snelheids-, kinetische energie-) oscillaties optreden, mits de c_p/c_v -verhouding κ , in het juiste bereik ligt, bij aanname van een niet-dissociërend, ideaal gas. Voor snelheden kleiner dan de geluidssnelheid c in het gas blijkt het aangroei tempo van de oscillaties goed te voorspellen te zijn door middel van een analytische formule, welke werd afgeleid in Hoofdstuk 6 door het toepassen van eerste orde storingsrekening in het twee-compartimenten gasdynamicamodel. Bij aanwezigheid van een energie-extractiemechanisme (zoals MHD of inductie) worden de oscillaties stationair. Het cyclus-gemiddelde totale nucleaire vermogen zal, vooropgesteld dat aan enkele voorwaarden is voldaan, het gevraagde (geëxtraheerde) vermogen volgen.

ACKNOWLEDGEMENT

Many people contributed, in one way or another, to the work described in this thesis. First of all, I would like to thank my project leader and supervisor, Prof. Dr. Ir. Hugo van Dam, for introducing me into the field of nuclear reactor physics, for giving me the opportunity of taking part in the "Gaseous Core Fission Reactor"-project within the Department of Reactor Physics of the Interfacultair Reactor Instituut of the Delft University of Technology, and for his guidance, criticisms and suggestions. Also the other participants in the project in the past four years are greatly acknowledged for the pleasant cooperation and for many valuable discussions: Prof. Dr. J. Kistemaker (FOM-AMOLF, Amsterdam, the Netherlands), former project leader and initiator of the project, Dr. Witza Boersma-Klein (FOM-AMOLF), who was in charge of the investigation of the chemical and heat transport aspects of the project, Dr. Ir. Eduard Hoogenboom (IRI), who also investigated the heat transport and temperature profile in gaseous core fission reactors, and Ir. Armand Stekelenburg, who designed and implemented the "all-software" GCFR-simulators. Thanks are also due to Ir. Piet de Leege (IRI) for introducing me into the computer code system, using which most of the reactor physical calculations, presented in this thesis, were performed, and to all other members of the Department of Reactor Physics, and of the IRI in general, for the friendly and stimulating atmosphere.

I wish to express my gratitude to the Netherlands Technology Foundation ("Stichting Technische Wetenschappen"), for their financial support, and also to the members of the "STW-begeleidingscommissie" for their interest in the project.

Thanks are also due to Prof. Dr. H.L. Dodds (Oak Ridge National Laboratory, Oak Ridge, Tennessee, USA), Prof. Dr. V.M. Novikov (I.V. Kurchatov Atomic Energy Institute, Moscow) and Dr. Ir. L.R. Wolff (Eindhoven University of Technology) for their valuable ideas and suggestions.

Finally, I wish to thank my wife, Wilma C.M. Leermakers, for her patience, understanding and support, and also for her organizational talents.

* * *

Vele mensen hebben, op de een of andere manier, bijgedragen aan het in dit proefschrift beschreven werk. Op de eerste plaats wil ik mijn promotor en projectleider, Prof. Dr. Ir. Hugo van Dam, bedanken voor de introductie in het vakgebied der reactorfysica, voor de gelegenheid die hij mij gaf deel te nemen aan het gaskernreactorproject in de afdeling Reactorfysica van het Interfacultair Reactor Instituut van de Technische Universiteit Delft, voor zijn wijze van begeleiden, voor zijn kritiek en suggesties. Mijn dank gaat verder uit naar de andere deelnemers aan het project in de afgelopen vier jaar, voor de prettige samenwerking en de waardevolle discussies: Prof. Dr. J. Kistemaker (FOM-AMOLF), voormalig projectleider en initiatiefnemer, Dr. Witza Boersma-Klein (FOM-AMOLF), die verantwoordelijk was voor het onderzoek naar de chemische en warmtetransport aspecten van het project, Dr. Ir. Eduard Hoogenboom, die eveneens onderzoek verrichtte naar warmtetransport en temperatuurprofielen in gaskernreactoren, en

Ir. Armand Stekelenburg, die de "all-software" GCFR-simulatoren heeft ontworpen en geïmplementeerd. Verder wil ik Ir. Piet de Leege (IRI) bedanken, die mij wegwijs maakte in de programmatuur, waarmee een groot deel van de reactorfysische berekeningen, gepresenteerd in dit proefschrift, is uitgevoerd, alsmede alle andere leden van de afdeling Reactorfysica en van het IRI in het algemeen, voor de prettige en stimulerende werkomgeving.

Tevens gaat mijn dank uit naar de Stichting Technische Wetenschappen, voor hun financiële steun aan het project, en naar de leden van de begeleidingscommissie, voor hun interesse in het project.

Verder wil ik Prof. Dr. H.L. Dodds (Oak Ridge National Laboratory, Oak Ridge, Tennessee, USA), Prof. Dr. V.M. Novikov (I.V. Kurchatov Atomic Energy Institute, Moskou) en Dr. Ir. L.R. Wolff (Technische Universiteit Eindhoven) bedanken voor hun waardevolle ideeën en suggesties.

Tenslotte wil ik mijn vrouw, Wilma C.M. Leermakers, bedanken voor haar geduld, begrip en steun, en tevens voor de inzet van haar organisatorische talenten.

James C. Kuijper

CURRICULUM VITAE

James C. Kuijper was born on April 7, 1961, in Hengelo (Ov.), the Netherlands. In that town he also received primary and secondary education. After graduation from highschool in 1979 ("Gymnasium β " certificate), he studied Applied Physics at the Twente University of Technology ("Technische Hogeschool Twente"; nowadays "Universiteit Twente") in Enschede, the Netherlands. In the summer of 1983 he spent three months at the Berkeley Nuclear Laboratories in Berkeley, Gloucestershire, U.K., where he took part in the development of a system for the detection and quantification of radioactive aerosol particles on air filters. His third year project was the development of a calibration system for platinum resistance thermometers for district heating applications. His final year project was the development of a system for so-called "gated" Raman spectroscopy on biological particles (cells, chromosomes) in streaming liquid (supervisors: Dr. Ir. F.F.M. de Mul and Prof. Dr. J. Greve, Biophysics Group, Department of Applied Physics). On March 18, 1986, he received the Master of Science degree ("Ir."). For the fulfilment of his military duties he was stationed, by the Royal Netherlands Navy, at the "Fysisch en Electronisch Laboratorium TNO" in The Hague, where he worked on passive towed-array sonar signal processing. The next four years, from January 1, 1988, onward, he spent at the Department of Reactor Physics of the Interfacultair Reactor Instituut of the Delft University of Technology in Delft, taking part in the "Gaseous Core Fission Reactor"-project (project leaders: Prof. Dr. J. Kistemaker and Prof. Dr. Ir. H. van Dam). Since May 1, 1992, he has accepted a position with the Netherlands Energy Research Foundation ("Energieonderzoek Centrum Nederland") in Petten.

* * *

James C. Kuijper werd geboren op 7 april 1961 in Hengelo (Ov.). Na het doorlopen van de lagere en de middelbare school (Gymnasium β) begon hij in 1979 met de studie Technische Natuurkunde aan de toenmalige Technische Hogeschool Twente in Enschede (heden ten dage Universiteit Twente). In de zomer van 1983 liep hij gedurende drie maanden stage bij de Berkeley Nuclear Laboratories in Berkeley, Gloucestershire, Engeland. Daar werkte hij aan de ontwikkeling van een systeem voor de detectie en kwantificatie van radioactieve aerosoldeeltjes op luchtfilters. Zijn derdejaarsproject was de ontwikkeling van een calibratie-installatie voor platina-weerstandsthermometers voor afstandsverwarmingstoepassingen. Zijn afstudeerproject was de ontwikkeling van een systeem voor zogenaamde "gated" Raman spectroscopie aan biologische deeltjes (cellen, chromosomen) in stromende vloeistof (onder leiding van Dr. Ir. F.F.M. de Mul en Prof. Dr. J. Greve van de vakgroep Biofysische Techniek, Afdeling der Technische Natuurkunde). Op 18 maart 1986 behaalde hij de ingenieurstitel ("oude stijl"). Ter vervulling van zijn militaire verplichtingen werd hij door de Koninklijke Marine gedetacheerd bij het Fysisch en Electronisch Laboratorium TNO in Den Haag, waar hij onderzoek deed naar signaalverwerkingsmethoden voor passieve "towed-array" sonar toepassingen. Vanaf 1 januari 1988 was hij werkzaam bij de afdeling Reactorfysica van het

Interfacultair Reactor Instituut van de Technische Universiteit Delft, waar hij deelnam aan het gaskernreactorproject (projectleiders: Prof. Dr. J. Kistemaker en Prof. Dr. Ir. H. van Dam). Met ingang van 1 mei 1992 is hij verbonden aan het Energieonderzoek Centrum Nederland in Petten.